TECHNISCHE UNIVERSITÄT MÜNCHEN

Lehrstuhl Entwicklungsgenetik

The effect of mitochondrial dysfunction on astrocytes and radial glia like stem cells in the adult hippocampus

Birgit Ebert

Vollständiger Abdruck der von der Fakultät Wissenschaftszentrum Weihenstephan für Ernährung, Landnutzung und Umwelt der Technischen Universität München zur Erlangung des akademischen Grades eines

Doktors der Naturwissenschaften

genehmigten Dissertation.

Vorsitzender: Univ.-Prof. Dr. E. Grill

Prüfer der Dissertation: 1. Univ.-Prof. Dr. W. Wurst

2. Univ.-Prof. Dr. D. C. Lie
(Friedrich-Alexander Universität Erlangen-Nürnberg)

Die Dissertation wurde am 25.02.2013 bei der Technischen Universität München eingereicht und durch die Fakultät Wissenschaftszentrum Weihenstephan für Ernährung, Landnutzung und Umwelt am 30.04.2013 angenommen.

TABLE OF CONTENT

1 ZUSAMMENFASSUNG

Astrozyten, sternförmige Zellen des Zentralnervensystems, die Neurone im Säugetiergehirn zahlenmäßig übertreffen, sind von essentieller Bedeutung für die Homöostase im Gehirn. Sie versorgen Nervenzellen mit Nährstoffen, regulieren neuronale Homöostase und das Überleben der Neurone und unterstützen zudem die synaptische Plastizität. Radiale Gliazellen in der Subgranulärzone des adulten Hippocampus sind spezialisierte Astrozyten, welche als neurale Stammzellen dienen und kontinuierlich neue Nervenzellen generieren. Dieser Prozess wird adulte Neurogenese genannt und erzeugt funktional integrierte neue Neurone über die gesamte Lebendauer. Adulte Neurogenese ist wichtig für kognitive Funktionen und beruht auf dem Zusammenspiel von Erhaltung, Proliferation und Differenzierung der adulten neuralen Stammzellen. Die Rate der adulten Neurogenese verringert sich während des Alterungsprozesses und konnte teilweise mit einer parallelen Abnahme kognitiver Funktionen korreliert werden. Die zugrundeliegenden zellulären und molekularen Mechanismen sind jedoch noch nicht vollständig verstanden. Beide Astrozytenpopulationen - protoplasmatische Astrozyten wie auch radiale Gliazellen - könnten im Alterungsprozess involviert sein. Unter Zuhilfenahme von Mitochondrien, Zellorganellen, deren gestörte Integrität und reduzierte oxidative Phosphorylierungsaktivität bereits mit dem Alterungsprozess in Verbindung gebracht werden konnten, ist es möglich die Verknüpfung mitochondrialer Fehlfunktion in Astrozyten und der Alterung zu analysieren.

Die Verwendung eines Mausmodells für mitochondriale Fehlfunktion ermöglichte es, den mitochondrialen Transkriptionsfaktor A (TFAM) speziell in Astrozyten und neuralen Stammzellen konditional zu entfernen (cko). Entgegen der Erwartungen waren keine offensichtlichen Veränderungen des Verhaltens und der äußeren Erscheinung der TFAM defizienten Mäuse zu beobachten. Im Detail bedeutet das, dass weder die Bewegungskoordination, die Lern- und Erinnerungsfähigkeit, der Geruchssinn oder das Angstverhalten, noch die Verarbeitung sensorischer Signale sichtbar verändert waren.

Zudem wiesen die TFAM mutanten Tiere keine Effekte auf die generelle Lebensfähigkeit neuronaler Zellen auf. Erste Anzeichen einer reaktiven Gliose konnten im Hippocampus und Neocortex anhand einer verstärkten Expression von Glial fibrillary acidic protein nachgewiesen werden, wobei das Fehlen weiterer Reaktivitätscharakteristika, wie ein Anschwellen der Astrozyten oder die Hochregulation anderer Zellmarker wie Vimentin, auf eine schwache Gliose hindeuten. Diese *in vivo* Ergebnisse liefern fundierte Belege für die Annahme, dass Astrozyten Atmungskettendefekte kompensieren können.

Weiterhin wurden die Auswirkungen mitochondrialer Fehlfunktionen auf neurale Stammzellen und ihre Nachkommen hinsichtlich Proliferation, Überleben und Entwicklung der zellulären Morphologie untersucht. Thymidin-Analogon basierte Ansätze und Expressionsanalysen von Proliferationsmarkern (z.B. Ki67) ergaben eine deutlich reduzierte Teilungsfähigkeit hippocampaler neuraler Stammzellen 3 ½ Monate nach Rekombination des *Tfam* locus, sowie eine verringerte Überlebensfähigkeit der TFAM defizienten Nachkommenschaft. Die Anzahl der radialen Glia-ähnlichen Stammzellen war im Vergleich mit Kontrollmäusen nicht verändert, allerdings zeigten die *Tfam* cko Mäuse eine beeinträchtigte neuronale Differenzierung derselben. Der Einsatz retroviraler Methoden zur Kennzeichnung und Visualisierung neugeborener Neurone im adulten Hippocampus deutete auf Morphologiedefekte während des Reifungsprozesses hin. Eine reduzierte Zelllänge und Komplexität des Dendritenbaumes konnten sowohl in Neuronen, generiert von TFAM defizienten Stammzellen, als auch in Cre-Virus-injizierten akut TFAM depletierten Neuronen nachgewiesen werden. Allerdings wurden in chronisch TFAM defizienten Nervenzellen bereits im Zellalter von 21 Tagen Morphologiedefekte festgestellt, im Gegensatz zu der akuten TFAM-Defizienz, welche erst nach 90 Tagen sichtbare Auswirkungen zeigte. Spines, dendritische Ausstülpungen, die meist das morphologische Korrelat der Synapsen darstellen, waren unverändert hinsichtlich ihrer Anzahl und Morphologie. Weiterführende Untersuchungen TFAM defizienter Nervenzellen werden zeigen, ob es Unterschiede der synaptischen Plastizität entlang des Dendritenbaumes und speziell innerhalb der Domänen verschiedener Astrozyten gibt. Erstaunlicherweise war der Mitochondriengehalt in TFAM defizienten Neuronen nur minimal verändert. Weiterhin können Neurone in Wildtyp-Mäusen als Reaktion auf körperliche Aktivität ihren Mitochondriengehalt steigern, wohingegen TFAM defiziente Nervenzellen ihren Bestand an Mitochondrien nicht anpassen können.

Die Ergebnisse dieser Studie deuten daraufhin, dass neurale Stammzellen, um sich zu teilen und funktionell integrierte Nervenzellen zu generieren, abhängig sind von einer effizienten ATP-Produktion durch mitochondriale oxidative Phosphorylierung, während Astrozyten anscheinend eine gestörte Atmungskettenaktivität kompensieren können. Die vorliegende Arbeit ermöglicht neue Einblicke in die Rolle der Astrozyten und Mitochondrien in der Plastizität des Gehirns und während des Alterungsprozesses.

2 SUMMARY

Astrocytes, star shaped cells that outnumber neurons by five fold in the mammalian brain, are known to be important for brain homeostasis. They provide neurons with energy metabolites, regulate neuronal homeostasis, survival, and synaptic plasticity. Radial glia-like cells in the subgranular zone of the adult hippocampus are specialized astrocytes which serve as neural stem cells and continuously generate new neurons. This process is called adult neurogenesis and produces functionally integrated new neurons throughout the lifetime. Adult neurogenesis is important for cognitive functions and relies on maintenance, proliferation and differentiation of adult neural stem cells. The rate of adult neurogenesis declines with age and is partly correlated with a decrease in cognitive function, while the cellular and molecular mechanisms underlying impaired neurogenesis in the ageing brain are not fully understood. Both protoplasmic astrocytes as well as radial glial cells might be involved in the process of ageing. Impaired mitochondrial integrity and reduced activity of the oxidative phosphorylation have been implicated in ageing as well and is therefore an interesting tool to analyze the connection between mitochondrial dysfunction in astrocytes and ageing.

Here, a mouse model for mitochondrial dysfunction, which enables conditional ablation of mitochondrial transcription factor A (TFAM) especially in adult astrocytes and neural stem cells, was studied. It was first noted that TFAM mutant mice did not display any obvious alterations in behavior and outer appearance. There were no detected changes in their motor coordination, learning and memory, smelling, anxiety, and sensory gating. Furthermore, mutant mice did not show major effects of TFAM depletion on overall neural cell viability and reactive gliosis. A significant increase in Glial fibrillary acidic protein expressing astrocytes was found in the hippocampus and the neocortex, but no hypertrophy or up-regulation of Vimentin could be detected. These *in vivo* findings provide strong evidence for the capability of astrocytes to compensate for respiratory chain deficiencies.

Moreover, the effects of mitochondrial dysfunction on neural stem cells and their progeny regarding proliferation, survival and development of cellular morphology, were examined. Thymidine-analogue based birthdating paradigms and analyses of marker expression (e.g. Ki67) revealed greatly impaired proliferation of neural stem cells detectable 3 ½ months after induction of TFAM depletion. There were also survival deficits of TFAM-deficient neuronal progeny in particular from 3 ½ to 6 months after recombination of the *Tfam* locus. In line with decreased proliferation and survival, *Tfam* cko mice revealed impaired fate decisions of neural stem cells, while the radial glial population was maintained comparable to control mice. The analyses of retroviral based birthdating and visualization of newly generated neurons in the adult hippocampus implied an impaired neuronal maturation process with regard to dendritic length and complexity. This was already evident in 21 days old neurons that originated from TFAM-deficient neural stem cells and in 90 days old neurons

lacking TFAM only upon Cre virus injection. Spines, i.e. the morphological correlate of excitatory glutamatergic synapses, were unchanged with respect to their general amount and morphology. Further investigation of TFAM-deficient neurons will clarify whether there are neuronal-section or astrocytic-domain differences in synaptic plasticity. Moreover, the mitochondrial content was only slightly changed in TFAM-depleted neurons. In contrast to WT mice, the amount of mitochondria could not be adjusted to increasing energy consumption rates as induced by physical activity.

The findings of this study indicate that neural stem cells depend on an efficient generation of ATP via mitochondrial oxidative phosphorylation to further proliferate and generate new functionally integrated neurons, while adult astrocytes seem to be able to compensate for an impaired respiratory chain. This study will provide new insights into the role of astrocytes and mitochondria in the process of brain ageing and plasticity.

3 INTRODUCTION

3.1 Adult neurogenesis

Neurogenesis in the brain of adult mammals was first discovered in rats in 1965 by Altman and Das (Altman and Das, 1965). This discovery was largely neglected for several decades but since the early 90s it has become well accepted that neurogenesis takes place in two distinct regions of the adult mammalian brain, namely the subventricular zone (SVZ)/olfactory bulb and the subgranular zone of the hippocampal dentate gyrus (DG) (Figure 1 a) (Zhao et al., 2008).

New neurons are produced by neural stem cells, which are characterized by the potential of self-renewal, proliferation, and differentiation. Under physiological circumstances the majority of NSCs, however, are in a resting or so-called quiescent state. The different cellular stages need to be balanced to ensure maintenance of the stem cell pool without lacking the functionality of newborn neurons throughout the entire lifetime (Faigle and Song, 2012; Imayoshi et al., 2008). Stem cells are embedded in a cellular and molecular microenvironment, which enables/controls stem cells to proliferate, self-renew and differentiate in particular into new neurons, and which has been termed neurogenic niche (Seri et al., 2001; Filippov et al., 2003; Ahn and Joyner, 2005).

Neural stem cells, Type 1 or radial glial cells, have a radial morphology and share some characteristics with astrocytes such as expression of marker proteins like the transcription factor sex determining region Y box 2 (Sox2), glial fibrillary acidic protein (GFAP), and brain lipid binding protein (BLBP) (Steiner et al., 2006; Filippov et al., 2003). As illustrated in Figure 1 b, adult neurogenesis is a complex sequence of several developmental stages. It starts from activation of the quiescent stem cells; division into transit amplifying Type 2 cells; proliferation and neuronal fate determination linked to cell cycle exit becoming postmitotic Type 3 cells. This is followed by maturation, migration and integration of the cells into the preexisting neuronal circuits (Lugert et al., 2010; Suh et al., 2007; Ming and Song, 2005; Filippov et al., 2003). Immature neurons in the DG migrate only a short distance within the granular cell layer in the direction of the molecular layer. This is in contrast to newly generated neurons from the SVZ that migrate from the walls of the lateral ventricle through the rostral migratory stream, which is ensheathed by astrocytes, all the way towards the olfactory bulb where they finally integrate as mature granular- and periglomerular interneurons (Kuhn et al., 2005b; Belluzzi et al., 2003; Alvarez-Buylla and Garcia-Verdugo, 2002; Mason et al., 2001; Peretto et al., 1997). Adult neurogenesis is modulated by complex behavior, for example, enriched environment or running itself was shown to increase proliferation resulting in generation of more DG neurons (Lugert et al., 2010; Kronenberg et al., 2006; Kempermann et al., 2002). In addition, physical activity accelerates functional integration of newly generated neurons (Piatti et al., 2011).

A crucial step during the development of a newborn DG neuron is the functional integration into the pre-existing neural network. Within the first two weeks of differentiation only a small portion of the hippocampal newborn neurons survives. They integrate by forming axonal connections towards hilar interneurons and pyramidal neurons in the CA3 region and developing a complex dendritic arborization and connections in the molecular layer over the first six to eight weeks (Ge et al., 2008; Zhao et al., 2006; Ge et al., 2006; Kuhn et al., 2005a; van Praag et al., 2002; Hastings and Gould, 1999). Newborn cells get their first tonic input via ambient γ-aminobutyric acid (GABA) released from local interneurons as early as one week after neuronal birth (Ge et al., 2006; Ge et al., 2008; Tozuka et al., 2005; Owens and Kriegstein, 2002). The first glutamatergic synaptic input is morphologically and electrophysiologically evident at two weeks after neuronal birth (Espósito et al., 2005; Zhao et al., 2006; Ge et al., 2006). In parallel, mossy fiber synaptic outputs to hilar and CA3 neurons are generated (Toni et al., 2008). The first dendritic protrusions, the so-called spines, are the morphological correlates and a sign of excitatory glutamatergic input (Zhao et al., 2006; Nimchinsky et al., 2002). As depicted in Figure 2, there are different kinds of dendritic protrusions. On the one hand there are filopodia which are long, thin and very motile, reaching for possible new connections. On the other hand there are established spines which can be still modified. These are classified into three main types: the short and stubby spines, mushroom like spines and thin spines (McKinney, 2010). Initially the spine density increases significantly until approximately two months of cellular age, when only the percentage of mushroom spines continues to rise (Song et al., 2005).

Less than 1000 new granule neurons are established in young adult mice (Kempermann et al., 1997), which seems to be negligible compared to approximately 3×10^5 overall DG neurons. Nevertheless, recent work has proven the importance of newborn neurons and mature DG neurons for hippocampal-dependent tasks, such as spatial learning (Garthe et al., 2009), pattern separation (Clelland et al., 2009), and pattern completion (Nakashiba et al., 2012). Examining functional intrinsic properties of newly generated granule neurons revealed a deeper insight into the role of these neurons during hippocampal function. These new DG neurons are not restricted to introducing new synaptic connections, but rather modify pre-existing ones by competing with mature DG neurons for the pre- and/or postsynaptic contact (Toni et al., 2007; Toni et al., 2008). Moreover, hippocampal immature neurons exhibit a transient (four to eight weeks after birth) lower threshold of long-term potentiation (LTP) and a low input specificity. In combination with their high intrinsic excitability this makes them unique in processing information compared to early postnatally generated mature DG neurons (Marín-Burgin et al., 2012; Ge et al., 2006; Tozuka et al., 2005; Schmidt-Hieber et al., 2004; Snyder et al., 2001). The resulting heterogeneous population of immature granule neurons is characterized by the expression of NR2B-containing N-Methyl-D-aspartate (NMDA) receptors (Snyder et al., 2001; Ge et al., 2007), and the protracted innervation by inhibitory GABAergic synaptic

inputs (Li et al., 2012; Marín-Burgin et al., 2012; Ge et al., 2006) leading to an increased firing probability due to an enhanced excitation/inhibition balance. The functional relevance of newborn neurons with distinct properties was examined in loss-of-function studies impairing or abolishing hippocampal neurogenesis, which revealed deficits in performance in contextual and spatial memory tasks (Sahay et al., 2011; Clelland et al., 2009; Deng et al., 2009; Garthe et al., 2009; Kitamura et al., 2009; Imayoshi et al., 2008; Zhang et al., 2008; Dupret et al., 2008; Saxe et al., 2006; Shors et al., 2001). It was shown that adult neurogenesis is involved in memory and learning tasks (Revest et al., 2009; Zhang et al., 2008; Dupret et al., 2008); that it is required for the acquisition of new learning subjects tested in the Morris Water Maze (Kempermann and Gage, 2002), and that impaired adult neurogenesis results in an increased anxiety-related behavior in transgenic mouse models (Revest et al., 2009; Saxe et al., 2006). Furthermore, the cognitive decline during ageing correlates with the decrease of adult neurogenesis observed in adult rodents (Schouten et al., 2012; Drapeau et al., 2003). Interestingly, this decreased rate of adult neurogenesis could be rescued by physical exercise in rodents (van Praag, 2005).

Adult neurogenesis appears to be limited to the SVZ/OB and the SGZ/DG neurogenic niches (Gould, 2007; Kazanis, 2012; Kohman and Rhodes, 2012; Saaltink et al., 2012). The reason is most likely the specialized microenvironment in those regions that enables proliferation, fate commitment, and neuronal differentiation of the local stem cell population (Lie et al., 2002; Shihabuddin et al., 2000; Suhonen et al., 1996). A balanced maintenance and differentiation of the stem cell pool is very important to ensure a continuous generation of newborn neurons throughout lifetime and to keep the rate of neurogenesis space- and time-regulated, since new granule neurons are capable of modulating the hippocampal network. Hippocampus-dependent behavior can be impaired, for instance, by uncontrolled enhancement of adult neurogenesis via decrease of programmed cell death through pharmacological inhibitors (Dupret et al., 2007). Even though many extrinsic and intrinsic signaling regulators modulating adult neurogenesis, such as neurotransmitter, hormones, growth factors, cytokines, small non-coding RNAs, morphogens, transcription factors (e.g. Sox2), and the canonical Wnt/β-catenin pathway or the canonical Notch signaling have been unraveled (for review see Zhao et al., 2008; Schwarz et al., 2012), the role of subcellular compartments like mitochondria remains elusive, although, for example, the influence of accumulated mitochondrial DNA mutations on neural stem cell fate decision has been described previously (Wang et al., 2011a).

This work focuses on mitochondria within adult hippocampal neural stem cells and their progeny as well as astrocytes, which fulfill an important regulatory function in the control of stem cell behavior in the neurogenic niche (Christopherson et al., 2005; Hughes et al., 2010; Höke and Silver, 1994; Mauch et al., 2001; Goritz et al., 2005).
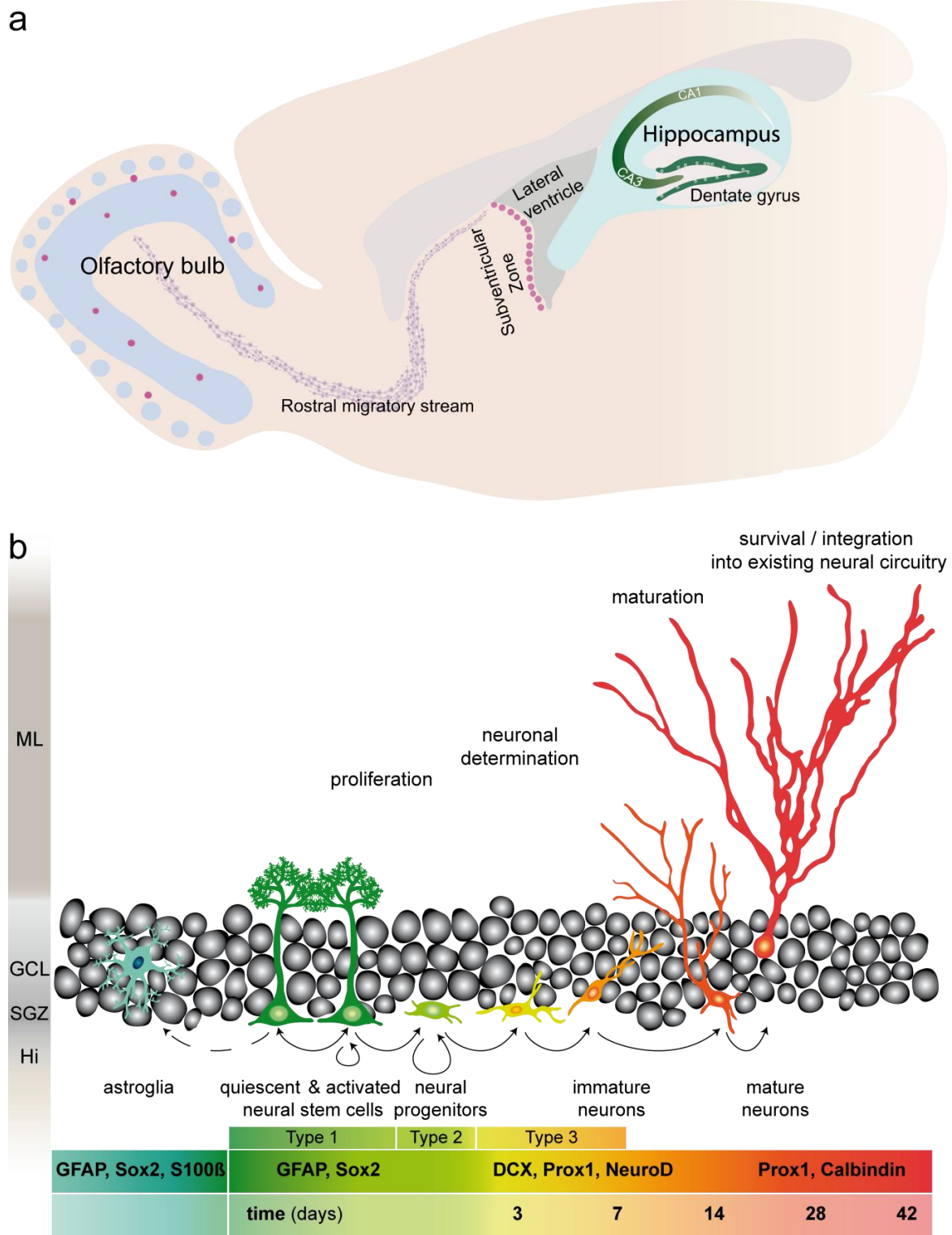
Figure 1 Neurogenic niches in the adult rodent brain. (a) There are two neurogenic regions, one is the subventricular zone next to the lateral ventricle, generating cells that are migrating via the rostral migratory stream towards the olfactory bulb. The other one is the hippocampal dentate gyrus (DG). (b) Schematic close up of DG adult neurogenesis, including timeline and exemplary marker expression. Type 1: quiescent and activated neural stem cells, Type 2: transient amplifying neural progenitors, Type 3: immature neurons/neuroblasts Type I and Type II. ML: molecular layer, GCL: granular cell layer, SGZ: subgranular zone, Hi: hilus. (Bonaguidi et al., 2011; Karalay et al., 2011; Encinas et al., 2011a; Suh et al., 2007; Lie et al., 2004; Alvarez-Buylla and Garcia-Verdugo, 2002; Kempermann and Gage, 2000; Pleasure et al., 2000; Kuhn et al., 1996)
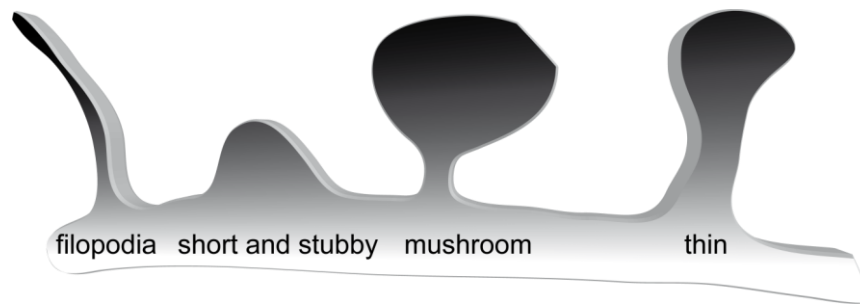
Figure 2 Different types of dendritic spines. Cartoon showing various shapes of dendritic protrusions that are the morphological equivalent of synapses. Filopodia are long and flexible reaching out for existing synapses to compete for connections, short (less than 0.5 µm) and stubby spines, mushroom-like spines (head more than 0.6 µm diameter), and thin spines with an elongated neck and small head (McKinney, 2010).

3.2 Mitochondria

3.2.1 Morphology and function

According to the endosymbiosis theory, mitochondria were once free living bacteria that were taken up by eukaryotic cells without being digested. This resulted in a symbiosis of mitochondria with their host cells; the mutual dependence evolved evolutionarily (Kutschera and Niklas, 2005; Margulis, 1975). Mitochondria are essential components of eukaryotic cells. They are not isolated within the cell but are rather in a continuous communication with the cell to regulate cellular processes like metabolism, cell cycle, cellular development, and cell death (McBride et al., 2006).

As depicted in Figure 3 mitochondria contain two membranes: an outer and an inner membrane. The latter folds into cristae providing membrane surface for the respiratory chain complexes (McBride et al., 2006; Wallace, 2005). This is crucial since one of the main functions of mitochondria is the cellular energy supply in the form of adenosine triphosphate (ATP), which is generated via oxidative phosphorylation (Forner et al., 2006). Mitochondria reveal the same basic morphological organization in different cell types. Nevertheless, highly folded lamellar cristae, to increase the surface for increased oxidative phosphorylation activity, are typical for neurons, liver and muscle cells, as these cell types have a very high energy demand and require especially high respiratory rates (Forner et al., 2006). Since mitochondria serve as a calcium storage and buffer (Werth and Thayer, 1994), there are granules of calcium, and in addition, both ribosomes and mitochondrial DNA (mtDNA) localized in the matrix. Furthermore, processes like β-oxidation and the citrate cycle are taking place within the mitochondrial matrix (Sherratt, 1991). Moreover, mitochondria play an essential role in the biogenesis of iron sulfur clusters integrated in proteins catalyzing electron transfer and metabolic reactions (Lill, 2009; Rouault and Tong, 2005; Kispal et al., 1999). Finally, mitochondria are essential during apoptosis, releasing cytochrome c as well as serving as activators

of caspases (SMAC: second mitochondria-derived activator of caspase) in the cytosol (Du et al., 2000). Besides the numerous functions of mitochondria, they represent both the main source and the detoxifier of reactive oxygen species (ROS), which are thought to contribute to mtDNA mutations (Trifunovic et al., 2005). Considering the plentitude of mitochondrial functions the role of mitochondria in disease and ageing is of great interest. Indeed, it was found that mitochondrial dysfunction is associated with human disorders such as cancer, heart failure, diabetes mellitus, neurodegeneration, and aging (Park and Larsson, 2011; Hebert et al., 2010; Kujoth et al., 2006; Chan, 2006; Wang et al., 2001).

Mitochondria contain their own maternally inherited genome in their matrix in the form of thousands of copies per cell. The mammalian mitochondrial genome is composed of approximately 16600 base pairs (bp) in humans and 16300 bp in mice (Holt et al., 2000; Solá et al., 2013) (Figure 3 b). Most mitochondrial proteins are nuclear-encoded and imported into mitochondria, except for two ribosomal RNAs, 22 transfer RNAs, and 13 essential subunits of respiratory chain complexes (Bibb et al., 1981; Anderson et al., 1981).
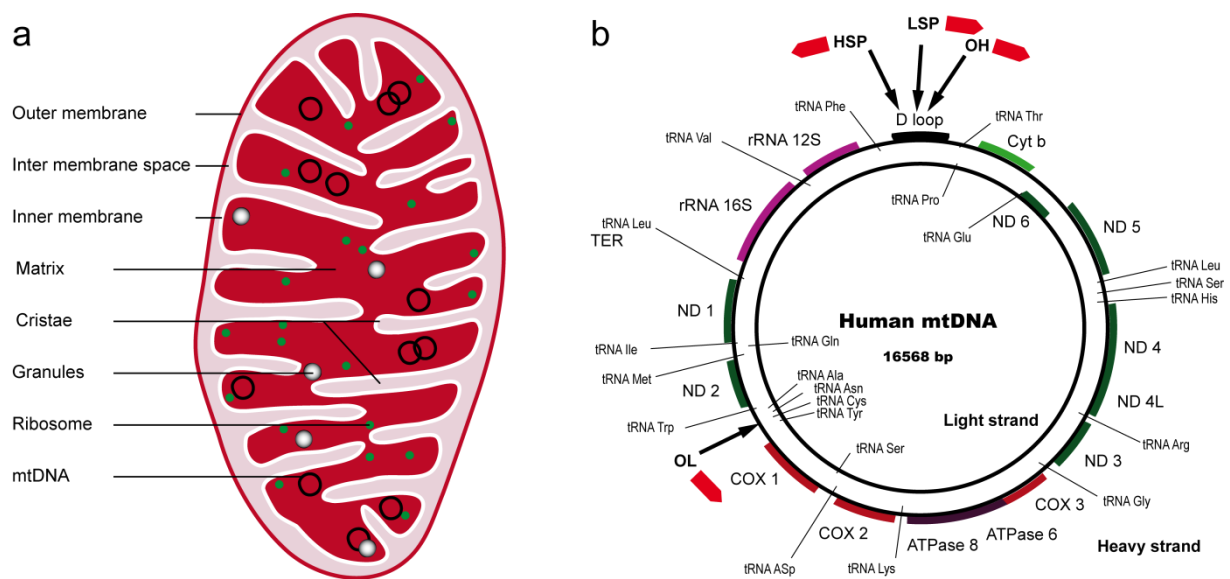
Figure 3 Mitochondrial structure and mtDNA. (a) Schematic illustration of a mitochondrium. (b) Human mtDNA, polycistronically transcribed: depicted are the mtDNA-encoded 12 S and 16 S rRNA, 22 tRNAs, 13 essential subunits of the respiratory chain complexes, and the non coding regulatory region (D loop). The D loop includes the promoters of the heavy (HSP) and light strand (LSP), and the origion of replication on the heavy strand (OH). Replication starts at the OH and asynchronously proceeds counterclockwise from the light strand origin of replication (OL). Cyt b: Cytochrome b, ND 1-6: NADH dehydrogenase subunits, COX 1-3: Cytochrome c oxidase subunits, ATPase 6 and ATPase 8: ATP synthase subunits (Nadege et al., 2009; Sherratt, 1991).

Rather than being static individual cellular organelles, mitochondria constantly undergo fusion and fission processes and are thought to form a large communicating network (Youle and van der Bliek,

2012; Csordás, 2006; Youle and Karbowski, 2005) (Figure 4). Fusion of the outer membrane of two mitochondria in close proximity is mediated by mitofusins, while fusion of the inner membrane is enabled by optic atrophy 1 (OPA1) (Belenguer and Pellegrini, 2012; Ehses et al., 2009). During fission, which is the process of dividing mitochondria, the fission 1 protein (Fis1) recruits the large GTPase and dynamin related protein Drp1, which subsequently causes constriction and scission of mitochondria. Both processes need to be balanced to keep cells in a healthy state (Chan, 2012).

To avoid mitochondrial deficiency, in particular a dysfunctional respiratory chain, a quality control is applied that leads, for instance, to degradation of misfolded proteins (Tatsuta and Langer, 2008). Furthermore, mitochondrial fusion enables the mixture of mtDNA, proteins, lipids, and metabolites to ensure homogeneity of mitochondrial membrane potential and respiration throughout the cell (Legros et al., 2004; Chen et al., 2005). If mitochondria are severely damaged, they either undergo fission followed by mitophagy (Figure 4 d) or they induce apoptosis to abolish the affected cell (Tatsuta and Langer, 2008).

Mitochondria are not only dynamic regarding their morphological changes, but also with regard to their distribution. Mitochondria move along both microtubule and actin tracks. Their transport is paused and changes in direction as requested since mitochondrial movement is defined by physiological signals (Hollenbeck and Saxton, 2005; Boldogh and Pon, 2007). Mitochondrial transport is especially required in neurons to ensure adapted energy supply even in cellular fractions far away from the soma, since diffusion of ATP is not sufficient (Hollenbeck and Saxton, 2005). Anterograde transport towards the cellular periphery relies on kinesin motors, while retrograde transfer is enabled by dynein motors (Chada and Hollenbeck, 2003; Hollenbeck and Saxton, 2005; Kang et al., 2008; Morris and Hollenbeck, 1995). The coordination of different motors is not fully understood. Nevertheless, regarding the calcium-dependent mitochondrial motility, there is one model for anterograde transport that involves an outer mitochondrial membrane protein, Miro, which senses Calcium via EF hands (Wang and Schwarz, 2009). During transport Miro interacts with kinesin-1 via milton, an adaptor protein, while upon Calcium binding Miro directly interacts with the motor domain of kinesin-1 thereby releasing the kinesin-1 microtubule contact (Wang and Schwarz, 2009; Schon and Przedborski, 2011). This allows stopping of mitochondria at ATP-requiring locations upon increased Calcium signaling (Wang and Schwarz, 2009).
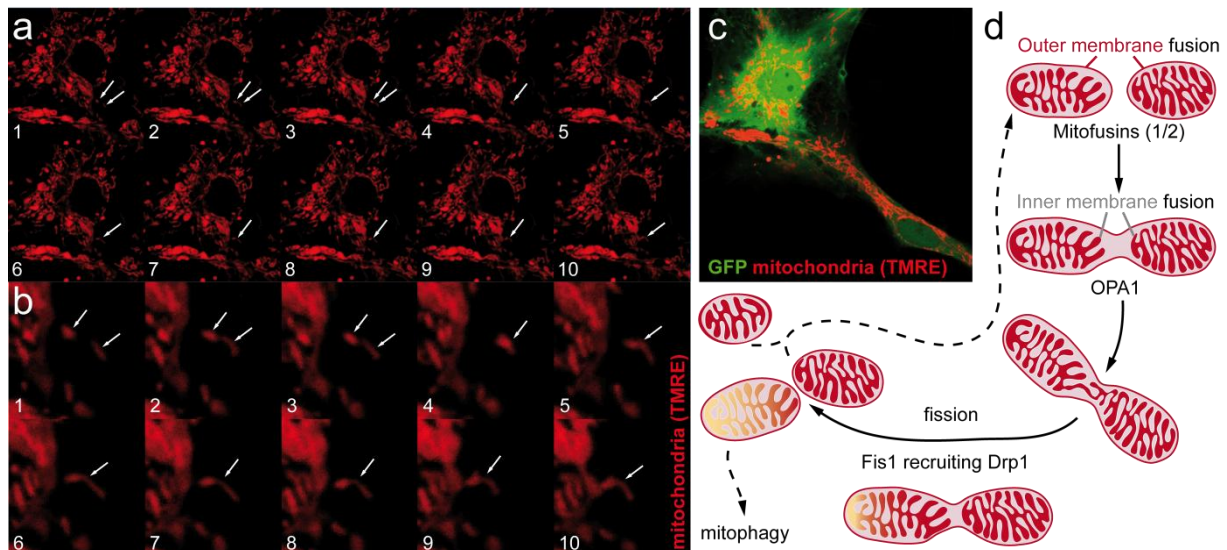
Figure 4 Mitochondrial dynamics and distribution. (a) Live imaging (2 min in total) of a mitochondrial fusion event. SVZ neurospheres were treated with 0.5 µM HTNCre for 20 h, to induce EGFP reporter expression, and were differentiated for 7 d. Differentiated cells including cells with astrocytic morphology were incubated with 50 nM TMRE (fluorescent mitochondrial membrane potential-dependent indicator) for 30 min prior imaging. (b) Enlarged view of the same live imaging series as in (a). Arrows indicate single mitochondria. (c) Mitochondrial distribution throughout the cell. Cell morphology was visualized by the recombined EGFP reporter. Confocal pictures were taken with a 63 times objective with 1.5 times additional zoom. (d) Schematic description of mitochondrial fusion and fission events including proteins that are involved at sequential stages: Mitofusin 1 and 2, OPA1 (optic atrophy 1), Fis1 (fission 1), and Drp1 (dynamin-related protein). If mitochondria accumulate a high load of mutations they can get abolished by mitophagy following fission (Chan, 2012; Galindo et al., 2012; Gottlieb and Gustafsson, 2011).

3.2.2 Oxidative Phosphorylation

The electron transport chain, located in the inner mitochondrial membrane, generates a proton motive force enabling oxidative phosphorylation of adenosine diphosphate (ADP) to ATP, representing the main source of cellular ATP (MITCHELL, 1961; Hatefi, 1985). As illustrated in Figure 5 the respiratory chain consists of five enzyme complexes that are mainly nuclear-encoded. Only 13 subunits of Complex I, III, IV, and V are mtDNA-encoded, leaving Complex II completely nuclear-encoded (Divakaruni and Brand, 2011).

Loaded electron carriers (Nicotinamide Adenine Dinucleotide Hydrogen/NADH+H$^+$, flavin-adenine dinucleotide/FADH$_2$) generated by substrate oxidation during the citric acid cycle transfer their electrons to Complex I or II, the NADH dehydrogenase or succinate dehydrogenase (Divakaruni and Brand, 2011). Electrons continue through Complex III and IV until they reach their final acceptor oxygen, which, in an electrolytical reaction, leads to H$_2$O. Protons are pumped from the matrix to the intermembrane space via Complex I, III, and IV. This results in an electrochemical proton gradient, with the intermembrane space being more acidic than the matrix, and a generated membrane

potential of 150 to 180 mV (Trifunovic and Larsson, 2008). Complex V, the ATP synthase, uses this gradient to transfer protons back into the matrix using the resulting energy to phosphorylate ADP (Sherratt, 1991). Uncoupling proteins (UCPs) like UCP1, found in brown fat tissue, uncouple oxygen consumption and ATP production to generate heat. UCPs are also found in skeletal muscle and brain tissue indicating further functions besides thermogenesis for the regulation of the efficiency of ATP synthesis by the respiratory chain (Fleury et al., 1997; Ledesma et al., 2002; Echtay et al., 2002).
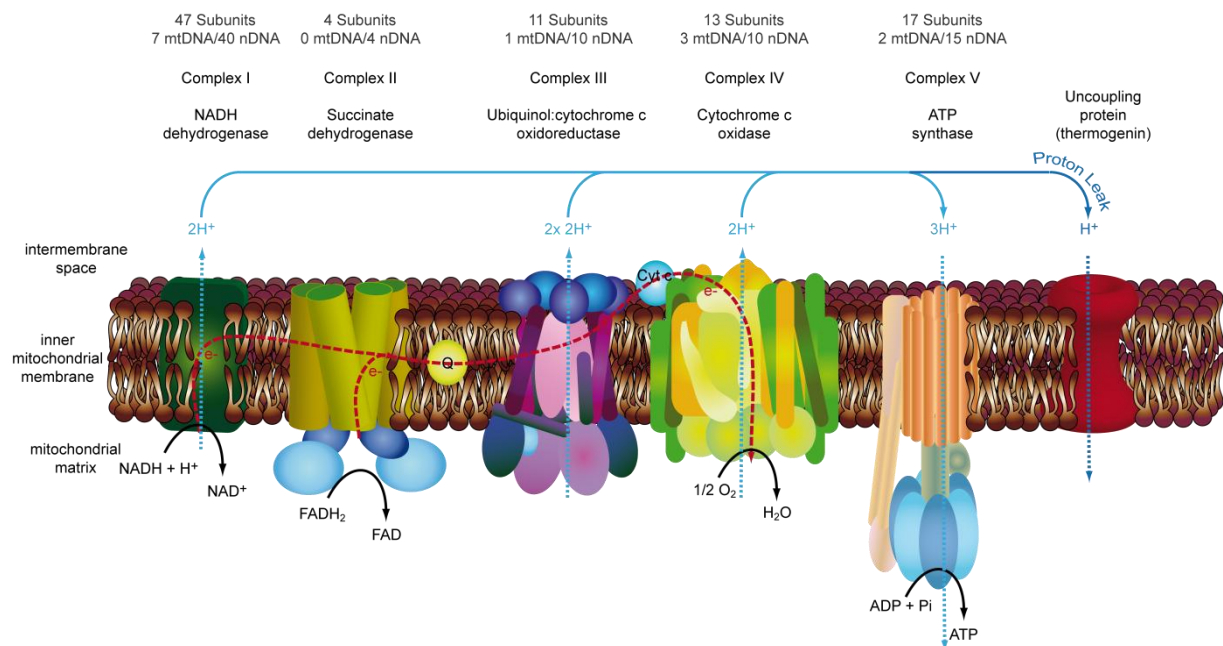
Figure 5 Oxidative Phosphorylation. Schematic overview of the respiratory chain complexes and the uncoupling protein located in the inner mitochondrial membrane. Complexes I to IV are generating a proton motiv force across the inner mitochondrial membrane that is used by the F_0/F_1 ATP synthase to phosphorylate ADP. A proton leak via the uncoupling protein allows regulation of the coupling of oxygen consumption and ATP synthesis (Divakaruni and Brand, 2011).

3.2.3   Mitochondrial transcription factor A - TFAM

The transcription of mtDNA-encoded genes is initiated by a basal machinery (Falkenberg et al., 2002), consisting of the mitochondrial RNA polymerase (POLRMT) and the essential mitochondrial transcription factors A (TFAM) and B2 (TFBM2) (Shi et al., 2012). In addition to transcription initiation, TFAM was shown to modulate the rate of mtDNA transcription depending on the different TFAM protein concentrations, e.g., low protein levels result in a low transcription rate, which increases at the same time as the protein concentration (Litonin et al., 2010). Nevertheless, high TFAM protein levels lead to a high compaction of mtDNA and thereby impede transcription (Kaufman et al., 2007; Campbell et al., 2012).

The *Tfam* gene is located on chromosome 10 in human and mouse and encodes a protein with a molecular weight of approximately 25 kDa (D'Errico et al., 2005; Siciliano et al., 2000). TFAM is a member of the high-mobility group (HMG) of proteins binding DNA (Parisi and Clayton, 1991). The protein contains a HMG domain at the amino terminus followed by a basic linker region, another HMG domain and a basic carboxy terminus (see Hallberg and Larsson, 2011 for the structure of TFAM in complex with mtDNA). TFAM is nuclear-encoded and harbors a mitochondrial target sequence that is cleaved after import into the mitochondrial matrix (Rantanen et al., 2001; Parisi and Clayton, 1991). The HMG domain enables TFAM to unwind and bend DNA to promote accurate promoter recognition and transcription. As depicted in Figure 6 TFAM binds immediately upstream of the transcriptional start sites of the light and heavy strand promoters initiating transcription by recruiting POLRMT (Lodeiro et al., 2012). mtDNA transcription is polygenic and results in three types of RNA (rRNA, mRNA, tRNA), which are processed thereafter. The fraction of rRNA is increased by looping out the part of mtDNA for the HSP1 transcript (12S and 16S rRNAs) by simultaneous binding of mitochondrial transcription termination factor mTERF to HSP1 and TERM. Thereby, the transcription complexes are efficiently reused, which ensures a high rRNA ratio for the mitochondrial translation machinery (Figure 6 b) (Scarpulla, 2008).

Even though TFAM is named a transcription factor it is also required for mtDNA replication, maintenance, and packaging (Ekstrand et al., 2004; Larsson et al., 1998; Kaufman et al., 2007; Campbell et al., 2012). Replication of mtDNA is conducted from the heavy strand origin of replication (OH) and asynchronously proceeds counterclockwise from the light strand origin of replication (OL) (Nadege et al., 2009; Sherratt, 1991). Short RNA primers generated by POLRMT are required for replication initiation at both the OH and OL (Clayton, 1991; Fusté et al., 2010). Replication is then carried out by the mitochondrial DNA polymerase (Falkenberg and Larsson, 2009), the winkle DNA helicase (Spelbrink et al., 2001), and the single stranded DNA binding protein (Falkenberg et al., 2007). Replication of the mitochondrial genome appears to be independent of nuclear DNA replication (Bogenhagen and Clayton, 1977). Which mtDNA molecules of a mitochondrion are subject to replication, as well as when and how often replication takes place, remains to be clarified.
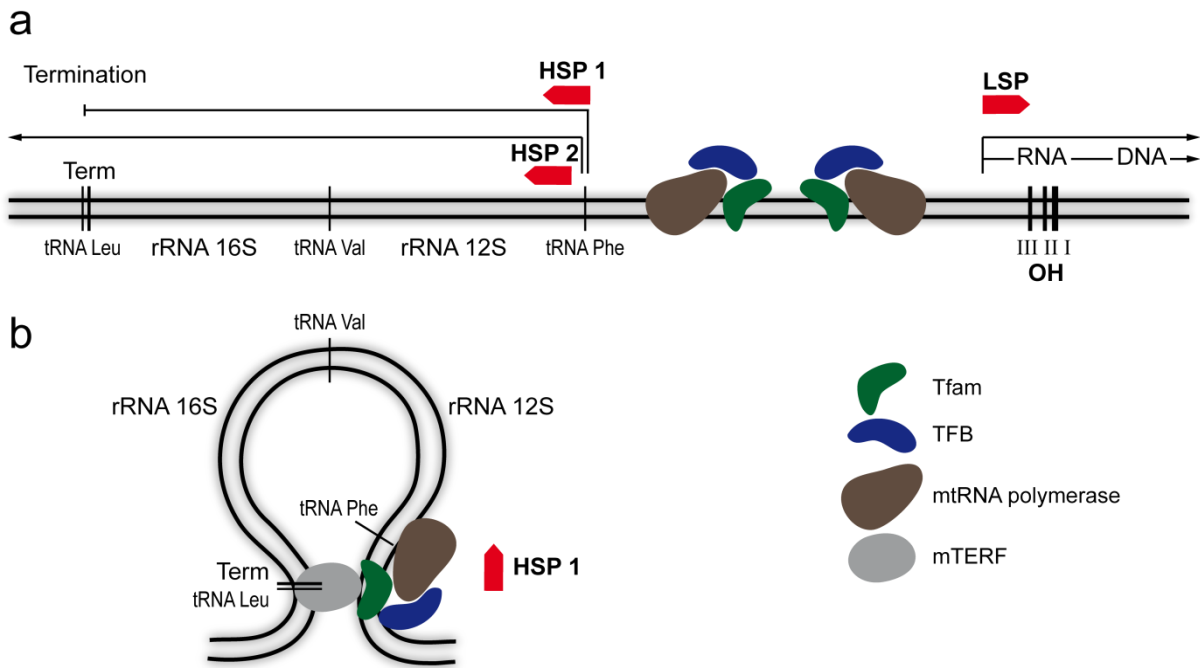
Figure 6 TFAM-dependent mtDNA transcription. Cartoon illustrating mtDNA transcription within the D loop (compare Figure 3 b). (a) Bidirectional promoters: Mitochondrial transcription initiation complex consisting of mitochondrial RNA polymerase (POLRMT), TFBM2, and TFAM. TFBM2 melts and stabilizes the open promoter and simultaneously contacts POLRMT, TFAM, the priming substrate, and the DNA template (Sologub et al., 2009). TFAM, an HMG protein, binds and bends the mtDNA and assists the initiation complex assembly (Litonin et al., 2010). OH heavy strand replication origin: Conserved sequence blocks I, II, and III serve as termination for transcription starting at LSP resulting in short transcripts used as primers for DNA replication (Scarpulla, 2008; Falkenberg et al., 2007). Transcripts initiated at the heavy strand promoter 2 (HSP2) can contain the entire mitochondrial genome, whereas (b) transcripts starting at HSP1 are terminated at the transcription terminator (TERM). (b) HSP1 initiated transcripts generate 12S and 16S rRNAs. Efficient reuse of the transcription complexes by looping out the rRNA DNA template is achieved by simultaneous binding of the mitochondrial transcription termination factor mTERF to HSP1 and TERM which ensures a high rRNA ratio for the mitochondrial translation machinery (Scarpulla, 2008).

TFAM is associated with mtDNA forming nucleoid-like structures (Kaufman et al., 2007; Gilkerson, 2009; Campbell et al., 2012; Farge et al., 2012). The relation of the concentration of TFAM protein and the grade of mtDNA compaction is illustrated in Figure 7. On average, one copy of TFAM binds per 15 to 20 bp mtDNA (Hallberg and Larsson, 2011). The respiratory chain generates the main portion of cellular ROS; one cause of mtDNA mutations. Within the mitochondrial matrix, a shield of TFAM protein protects mtDNA from damage by ROS. However, it remains under discussion whether this close proximity of mtDNA and the respiratory chain causes mtDNA mutations resulting in disease phenotypes (Pamplona, 2011; Xie et al., 2008; Kukat and Trifunovic, 2009; Yakes and van Houten, 1997).
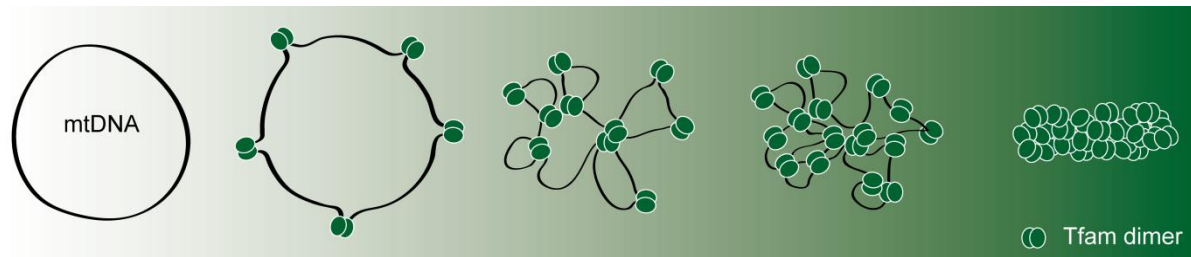
Figure 7 mtDNA compaction. TFAM dimer form loops by binding and linking mtDNA. With increasing concentration of TFAM (depicted from left to right) mtDNA is increasingly compacted. Already bound TFAM cooperatively facilitates binding of new TFAM proteins. At high TFAM concentrations formed nucleoid like structures impede with transcription and replication processes (Kaufman et al., 2007; Campbell et al., 2012).

Expression of *Tfam* is regulated by PGC1α; the coactivator 1α of the peroxisome proliferator-activated receptor gamma (PPARγ). PGC1α belongs to the family of transcriptional coactivators of PPARγ and interacts with the nuclear respiratory factor 2 (NRF-2) coactivating NRF-1. NRFs regulate transcription of all nuclear-encoded genes that are necessary for mitochondrial structure, protein import machinery, assembly of the respiratory chain, heme biosynthesis, as well as mitochondrial DNA transcription, translation, and replication, including TFAM (Gottlieb and Gustafsson, 2011; Scarpulla, 2008). PGC1α appears to be the key player in regulation of mitochondrial biogenesis as its up-regulation increases mitochondriogenesis and its suppression by acetylation leads to the opposite effect (Gottlieb and Gustafsson, 2011). The histone deacetlyase sirtuin 1 activates PGC1α on the protein level by deacetylation (Iwabu et al., 2010). Transcription of PGC1α is stimulated via different signaling pathways in distinct tissues by exercise, cytokines, cold, glucagon, and insulin (Fernandez-Marcos and Auwerx, 2011). Therefore, mitochondrial biogenesis can be adjusted to certain conditions and environmental changes, which might even involve mitochondrial removal or replacement (Gottlieb and Gustafsson, 2011).

3.2.4   TFAM-deficient mouse models

The first *Tfam* conditional knockout (cko) mice (*Tfam*^loxP/loxP^) were generated by Larsson and colleagues (1998). *Tfam*^loxP/loxP^ mice were generated by flanking exon VI and VII with directional loxP recognition sites. This would allow a Cre recombinase-mediated excision of the DNA part encoding for the protein domain that is required for promoter binding and activation of mitochondrial transcription (Trifunovic and Larsson, 2002). In the first description of these mice ubiquitous recombination was induced via a β-actin promoter driven bacteriophage P1 recombinase (Cre). These mice developed severe respiratory chain deficiency, aberrant mitochondrial morphology and early lethality between embryonic day 8.5 and 10.5 (Larsson et al., 1998). Heterozygous TFAM-deficient mice showed a gene dosage effect including reduction of the amount of mtDNA and mtDNA

transcripts as well as of mtDNA-encoded respiratory chain complex activity. In particular heart tissue was affected, while liver, kidney, and skeletal muscles appeared to be less sensitive to a reduced amount of TFAM protein (Larsson et al., 1998).

Tfam^loxP/loxP mice were used in various tissue to examine different aspects of mitochondrial dysfunction (Larsson et al., 1998; Wang et al., 1999; Silva et al., 2000; Sörensen et al., 2001; Ekstrand et al., 2007).

Restriction of the TFAM cko to cardiomyocytes resulted in a dilated cardiomyopathy (Wang et al., 1999). Among other TFAM depletion mouse models, this model of mitochondrial cardiomyopathy features an increase of mitochondrial fragmentation due to disturbed OPA1 processing caused by impaired mitochondrial membrane potential (Duvezin-Caubet et al., 2006). Mitochondrial diabetes evolved after loss of TFAM in pancreatic β cells (Silva et al., 2000). Reports regarding brain-specific disruption of the *Tfam* gene in dopaminergic and forebrain neurons (Sörensen et al., 2001; Ekstrand et al., 2007) will be discussed in the following paragraph.

The so-called Mitopark mice are characterized by a Parkinson's disease (PD) phenotype caused by a *Tfam* cko in dopaminergic neurons using a Cre under the control of the dopamine transporter (DAT-Cre) (Ekstrand et al., 2007). At the age of six weeks, these mice have a reduced level of the mitochondrially encoded mRNA (Cytochrome c oxidase subunit 1, COX1) and develop small cytoplasmic aggregates in dopaminergic midbrain neurons. Mitochondria seem to be part of the inclusions while α-synuclein, which is a component of Lewy bodies in human PD patients, was not detectable. Neuronal loss became evident at 12 weeks of age. First behavioral effects such as decreased locomotion and exploration behavior were seen at the age of 14 to 15 weeks. At the age of 20 weeks severe effects became visible: continuous neurodegeneration, a significantly decreased respiratory chain activity complex IV, and PD symptoms, e.g., tremor and twitching. At 45 weeks mice were dead or needed to be sacrificed due to their bad constitution (Ekstrand et al., 2007).

Postnatal disruption of TFAM in hippocampal and neocortical forebrain neurons also shows a progressive neurodegenerative phenotype as indicated by the name "mitochondrial late-onset neurodegeneration" (MILON) mice. These mice harbor a heterozygous calmodulin kinase II promoter driven Cre recombinase (CaMKII-Cre) crossed to the *Tfam*^loxP/loxP mice (Sörensen et al., 2001). The maximal recombination of the *Tfam* locus was reached at the age of one month. Nevertheless, the first effects; like reduction of mtDNA, mtRNA and TFAM protein, were only seen at two months of age. After another two months, respiratory chain deficiency (more precisely decreased activity of Complex I and IV) was measurable in forebrain neurons. Prolonged mitochondrial dysfunction was required for neurodegeneration with the first signs of disease becoming detectable at the age of five

months. Half a month later neurons were rapidly dying in the hippocampus and neocortex accompanied by an inflammatory response and gliosis, which was determined by measuring GFAP levels. GFAP up-regulation was only detected in the hippocampus and the corpus callosum, but not in the neocortex. With six months of age MILON mice were deteriorating physically and died shortly after. Interestingly, MILON mice did not exhibit an increase of glycolysis as analyzed by northern blot of glyceraldehyd-3-phosphate dehydrogenase (GAPDH), these data in combination with the massive neurodegeneration implies that neurons in this model cannot switch from oxidative phosphorylation to glycolysis (Sörensen et al., 2001). This goes hand in hand with the *in vitro* finding of Almeida et al. (2001): neurons in contrast to astrocytes cannot up-regulate glycolysis in response to inhibition of cellular respiration upon nitric oxide treatment (Almeida et al., 2001; Almeida et al., 2005).

3.2.5   Mitochondria in ageing and mitochondrial diseases

The most obvious effects of ageing in humans and in mice are degeneration of muscles, loss of hair, reduced weight and subcutaneous fat, a shrinking body in association with a curvature of the spine (kyphosis). There are also the less obvious phenotypes like osteoporosis, anemia, increased activation of apoptosis, cardiac enlargement and decreased fertility (Trifunovic et al., 2004; Kujoth et al., 2006). In addition to these physiological dysfunctions there is a higher risk of disease and death correlated with increasing age (Lee and Wei, 2012).

Ageing is a complex multifactorial process that is influenced by many factors such as the genetic background of an organism, the environment, nutrition, and the physical as well as the psychological constitution. Since the human population is ageing and new therapeutic approaches are required to facilitate old age, it is of high scientific interest to determine, what contributes to an ageing phenotype on the molecular level. Besides mechanisms such as the shortening of telomeres in somatic cells (Tümpel and Rudolph, 2012; Rajaraman et al., 2007; Miura et al., 2001) dysfunctional mitochondria have been causally linked to the process of ageing (Trifunovic et al., 2004; Fayet et al., 2002) Cottrell 2001 #278}(Müller-Höcker, 1989).

Increased amounts of random point mutations and deletions of mtDNA are associated with ageing that result in a mosaic pattern of mitochondrial dysfunction levels in different tissues like heart (Müller-Höcker, 1989), skeletal muscle (Fayet et al., 2002), and brain (Cottrell et al., 2001a; Cottrell et al., 2001b). The connection between mtDNA mutations and ageing was proven by the generation of the so-called mtDNA-mutator mouse (Trifunovic et al., 2004), which have a proof-reading-deficient mtDNA polymerase γ (PolgA, D257A). These mice accumulated three to five times more point mutations and a higher amount of mtDNA deletions. This caused a premature ageing phenotype

characterized by loss of hair and curvature of the spine already evident at 25 weeks of age as well as a reduced life span (median 48 weeks) (Trifunovic et al., 2004). Trifunovic et al. and others found that the reason for premature ageing in these mice is rather due to the dysfunctional respiratory chain activity than to an increased production of ROS (Trifunovic et al., 2005; Kujoth et al., 2006). Accumulated mtDNA mutations may also lead to enhanced ROS production, which in turn may result in an increase of mtDNA mutations. This could result in a vicious circle (Harman, 1972), contributing to the process of ageing just like impaired mitochondrial dynamics, reduced oxidative phosphorylation and membrane potential, as well as calcium regulation (Lee and Wei, 2012; Seo et al., 2010).

Mitochondria are the key player in efficient ATP production throughout different tissues (Newsholme et al., 2012). Besides mutations in mtDNA, mutations in nuclear-encoded mitochondrial enzymes can also provoke mitochondrial diseases (Larsson and Clayton, 1995; Larsson and Luft, 1999; Melov et al., 1999). Mitochondrial dysfunction due to disturbed mitochondrial integrity, distribution, transport, or mitochondrial dynamics is implicated in very common human neurodegenerative diseases such as amyotrophic lateral sclerosis (ALS) (Pratt et al., 2012; Martin, 2012), Alzheimer's disease (AD) (Rubio-Perez and Morillas-Ruiz, 2012; Weiner et al., 2012), Parkinson's disease (PD) (Marques and Outeiro, 2012), Charcot-Marie-Tooth (Patzko and Shy, 2012), and Huntington's disease (HD) (Oliveira, 2010; Schon and Przedborski, 2011).

In the motor neuron disease ALS; a multifactorial and neurodegenerative disorder characterized by a progressive atrophy of muscles, which finally results in paralysis and death of the patients, deficiencies in enzymes of the electron transport chain as well as mitochondrial apoptosis-related proteins were reported (Martin, 2012; Pratt et al., 2012; Shi et al., 2010). In particular one gene, the mitochondrial Cu/Zn superoxide dismutase 1 (SOD1), was found to be mutated in ALS patients causing an increase in oxidative stress and promoting inflammatory processes via glia cells (Bocci et al., 2011; Marchetto et al., 2008; Nagai et al., 2007). Furthermore, there are indications for impaired mitochondrial dynamics and transport in connection with ALS pathology (Magrané et al., 2012; Shi et al., 2010).

Another mitochondrial-related disease is the hereditary autosomal recessive spastic ataxia of Charlevoix-Saguenay (ARSACS) (Girard et al., 2012). The trigger for the disease is a mutation in the SACS gene, resulting in a protein that is supposed to interact with Drp1 in a way that proper mitochondrial fission is impaired. Hence, mitochondria start to aggregate and cannot reach the fine processes of cerebellar purkinje neurons, where they are crucial for the energy supply of synapses. Loss of this energy supply is detrimental for purkinje cells and their loss causes motor coordination defects in ARSACS patients (Girard et al., 2012).

There are two other prominent examples that directly link aberrant mitochondrial dynamics with human disease phenotypes. One is the autosomal dominant optic atrophy, a neuropathy of retinal ganglion cells, caused by mutations in the fusion associated GTPase OPA1 (Olichon et al., 2006; Ban et al., 2010). The other one indicated to be a mitochondrial disease is rather a group of heterogeneous peripheral neuropathies named Charcot-Marie-Tooth (Patzko and Shy, 2012). Mutations in two mitochondrial genes, Mitofusin 2 (MFN2) and ganglioside-induced differentiation-associated-protein 1 (GDAP1), which have been shown to play a role in either mitochondrial fusion (MFN2) or fission (GDAP1), could be causally linked with the disease phenotype (Cassereau et al., 2011; Kijima et al., 2005).

Friedreich's ataxia, an autosomal recessive degenerative disorder of nervous and muscle tissue, that involves a dysfunctional Frataxine gene, caused by expansion of GAA repeats therein (Rajeswari, 2012; Delatycki and Corben, 2012), is also linked to mitochondria. As a consequence of the loss of function of the Frataxine gene, there is an impairment in the regulation of the iron homeostasis, which affects the functionality of iron sulfur cluster-containing enzymes like the respiratory chain complexes I, II and III. Along with this, reduced oxidative phosphorylation contributes to the disease (Rötig et al., 1997).

AD is an adult onset disorder marked by β-amyloid plaques (originated from cleaved amyloid precursor protein) (Strooper and Voet, 2012; Jonsson et al., 2012), and neurofibrillary tangles of aggregated tau protein (Israel et al., 2012; Nakamura et al., 2012). Both are thought to cause brain inflammation involving reactive astrocytes and microglia (Rubio-Perez and Morillas-Ruiz, 2012). This cellular inflammatory process is progressively destroying adjacent cells and thereby impairing cognitive functions. Mitochondrial dysfunction might be a risk factor for and a contributor to AD (Lakatos et al., 2010). A TFAM S12T polymorphism was found to be only a moderate risk factor for late onset AD (Alvarez et al., 2008; Xu et al., 2009).

The other most common neurodegenerative disease, PD, is characterized by motor symptoms like resting tremor, bradykinesia, rigidity and postural instability as well as non-motor symptoms such as loss of sense of smell, sleep, and mood disorders (Uitti et al., 2005; Higginson et al., 2012; Latoo et al., 2012; Fernandez, 2012). A hallmark of PD is the progressive degeneration of nigrostriatal dopaminergic neurons as mimicked by the Mitopark mice described in section 3.2.4. Pathophysiology of sporadic and inherited PD forms might be associated with mitochondrial dysfunction caused by mtDNA mutations in the disease (Martin, 2012). Moreover, the genes encoding for mitochondrial associated PTEN-induced kinase 1 (PINK1) and the E3 ubiquitin ligase Parkin were found to be mutated in many cases of early-onset familial PD (Jin and Youle, 2012; Jones, 2010; Wang et al., 2011b). PINK1 is imported into healthy mitochondria and becomes localized to the

outer mitochondrial membrane upon damage and depolarization to recruit Parkin, which induces mitophagy (Deas et al., 2011; Jin et al., 2010). In Neurons lacking functional PINK1 and Parkin, damaged mitochondria are not removed (Geisler et al., 2010; Narendra et al., 2008) finally leading to neurodegeneration (Surmeier et al., 2010). Dopaminergic neurons in PD patients contain characteristic inclusions, the so-called Lewy bodies (Ekstrand et al., 2007). The major component of Lewy bodies is misfolded, and aggregated α-synuclein, which is either secreted by neurons or released after cell death and thereby activating adjacent astro- and microglia (Marques and Outeiro, 2012). Inclusions found in the Mitopark mouse model contained mitochondrial proteins, possibly implicating mitochondria in contributing to the generation of the inclusions (Ekstrand et al., 2007; Wang et al., 2011b).

 Further diseases are at least partly due to mutations in mtDNA, e.g., Kearns-Sayre syndrome (Zeviani et al., 1998; Comte et al., 2012), and Leber's Hereditary Optic Neuropathy (LHON) (Wallace et al., 1988; Yen et al., 2006; Kumar et al., 2012), or they are associated with general mitochondrial dysfunction like diabetes (Newsholme et al., 2012), Leigh syndrome (Terkawi et al., 2012), myoclonus epilepsy with ragged-red fibers (MERRF) (Monden et al., 2012; Bindoff and Engelsen, 2012), as well as mitochondrial myopathy, encephalopathy, lactic acidosis, and stroke-like episodes (MELAS) (Fukuyama et al., 2012; Koga et al., 2010).

3.3 Astrocytes

3.3.1 Morphology and Function

For decades astrocytes have been considered the glue or supporters for neurons, neglecting their vast important functions in maintaining a healthy central nervous system (CNS) (Sofroniew and Vinters, 2010). Astrocytes outnumber neurons by multiple fold in the mammalian brain (Figley and Stroman, 2011; Sofroniew and Vinters, 2010). They represent precursor cells with respect to the process of adult neurogenesis, as newborn neurons originate from astroglial cells (Belluzzi et al., 2003; Carleton et al., 2003; Seri et al., 2001). Astrocytes are in contact with blood vessels via their endfeet, thereby being part of the blood brain barrier as well as modulating cerebral blood flow and angiogenesis itself, which might be crucial for brain development and repair (Attwell et al., 2010; Gordon et al., 2007; Iadecola and Nedergaard, 2007). Within their territory, astrocytes supply neurons by taking up nutrients from the blood; more precisely, they resorb glucose and deliver lactate to the neurons. Glycogen is almost exclusively localized to astrocytes in adult rodents and serves as energy storage (Magistretti, 2009). Upon brain injury, astroglia are thought to be involved in the repair and wound healing process. Additionally, astrocytes support synaptogenesis (Christopherson et al., 2005; Hughes et al., 2010) and synaptic transmission (Christopherson et al.,

2005; Höke and Silver, 1994; Mauch et al., 2001; Goritz et al., 2005), accordingly, regulating ion and glutamate homeostasis. Together with the pre- and postsynapse they form the tripartite synapse, which is illustrated in Figure 8. Finally, astroglia can change the environmental content of small molecules including ATP, glutamate, and glucose as they express pannexins and connexins forming membrane hemichannels that allow release and uptake of these molecules. If this process becomes disturbed microglial cells are activated and restore the normal brain function. Reactive microglia may, via phagocytosis, clear cellular debris caused by apoptosis (Cerbai et al., 2012), other possible ways to exert their neuroprotective functions were reported (Boscia et al., 2009; Lauro et al., 2010; Vinet et al., 2012), but are not fully elucidated yet. Nevertheless, if the homeostatic imbalance is detrimental this results in overactivation of microglia and endothelia cells, both releasing molecules, which enhance astroglial hemichannel activity, finally causing astrocytes to release neurotoxic molecules leading to certain disease phenotypes (e.g. neurodegeneration) (Orellana et al., 2012).

Astroglia are not a homogenous population but are regionally specified and show distinct morphological and molecular characteristics. They can have (1) a protoplasmic pancake-like shape with many short branched processes, and many organelles, mainly found in the grey matter, (2) a fibrous shape with long, few branches and organelles, in the white matter, or (3) a radial shape with basal branches, and one long radial process with bushy apical branches, as found, e.g., in the DG, cerebellum (Bergmann glia), or the retina (Muller glia) (Molofsky et al., 2012; Gulbransen and Sharkey, 2012; Robel et al., 2011; Sofroniew and Vinters, 2010; Miller and Raff, 1984). It is noteworthy that human astrocytes are larger and more complex than rodent astrocytes (Oberheim et al., 2009). Several subsets of astrocytes are described in the literature determined by different cellular function, localization, and marker expression.

There is not yet a perfect marker for adult astrocytes, since many markers used until now are only expressed in subsets of astroglial cells or are not specific, but stain other cell types like oligodendrocyte precursors, or become up-regulated under pathological conditions (Molofsky et al., 2012). Nevertheless, the marker protein, which is used most in published studies, is GFAP, a structural component of many astrocytes (Molofsky et al., 2012). GFAP comes with the drawback of being poorly expressed in protoplasmic astrocytes and being an indicator for reactivity (Heinrich et al., 2010; Sofroniew and Vinters, 2010). GFAP is thought to control cell shape and enable cell movement (Duffy et al., 1982; Sofroniew and Vinters, 2010). Like GFAP, Vimentin and Nestin are intermediate filament proteins, which are eventually up-regulated during reactive gliosis (Sofroniew and Vinters, 2010).

S100β is another astrocytic marker protein, which is expressed by many astrocytes, but also by NG2 oligodendrocyte precursor cells weakening the specificity of this marker protein (Karram et al., 2008; Braun et al., 2009; Okabe et al., 2012).

Finally, GLAST, or alternatively named SLC1A3 or excitatory amino acid transporter 1 (EAAT1), is broadly expressed within the astrocytic population and therefore a good candidate locus to direct expression of transgenes towards astrocytes (Mori et al., 2006) as used in the present work. GLAST is a member of the solute carrier family 1 (glial high affinity glutamate transporter). The *Glast* gene is located on chromosome 15 in mice and encodes for a glutamate aspartate transporter. Glutamate is a major excitatory neurotransmitter of the brain, which is released by neurons into the synaptic cleft and is taken up by receptors localized on the corresponding postsynapse. Excessive glutamate is cleared by astrocytes to prevent neurotoxicity and to convert glutamate into glutamine, which is shuttled back to the neuron (Figure 8) (Allen and Barres, 2009; Eroglu and Barres, 2010; Perea et al., 2009). Glutamine synthetase (GS), which is mainly expressed in astrocytes, and facilitates the conversion of glutamate to glutamine, is one of the key players in astrocytic glutamate metabolism (Sofroniew and Vinters, 2010).

Each astrocyte in the CNS has its own territory and is only connected by hemichannels at the most distant fine processes with adjacent astrocytes. One astrocyte in the forebrain covers more than 100.000 synapses (Sofroniew and Vinters, 2010; Halassa et al., 2007b) therefore being able to transmit excitation from one synapse to another via waves of Ca^{2+} increase even within an astrocytic network (Araque et al., 1999a, 1999b; Scemes and Giaume, 2006; Halassa et al., 2007a). Illustrated in Figure 8 are a stabilized and nurtured pre- and postsynapse that are enwrapped by astrocytic processes. Perisynaptic glia regulate extracellular pH and ensure potassium ion homeostasis as K^{+} ions are cleared via astrocytic gap junctions after being released from neurons (Allen and Barres, 2009; Eroglu and Barres, 2010). Astrocytes express neurotransmitter receptors and release transmitter/signaling molecules such as ATP and D-serine (Allen and Barres, 2009; Eroglu and Barres, 2010). However, astroglia not only stabilize synapses, but they also take part in the elimination of synapses together with microglia (Eroglu and Barres, 2010).

Astroglia in the hippocampal and the SVZ neurogenic niche are distinct with regard to their potential to generate new cells; while cortical astrocytes are postmitotic under physiological conditions and can only proliferate or migrate upon CNS damage (Song et al., 2002).
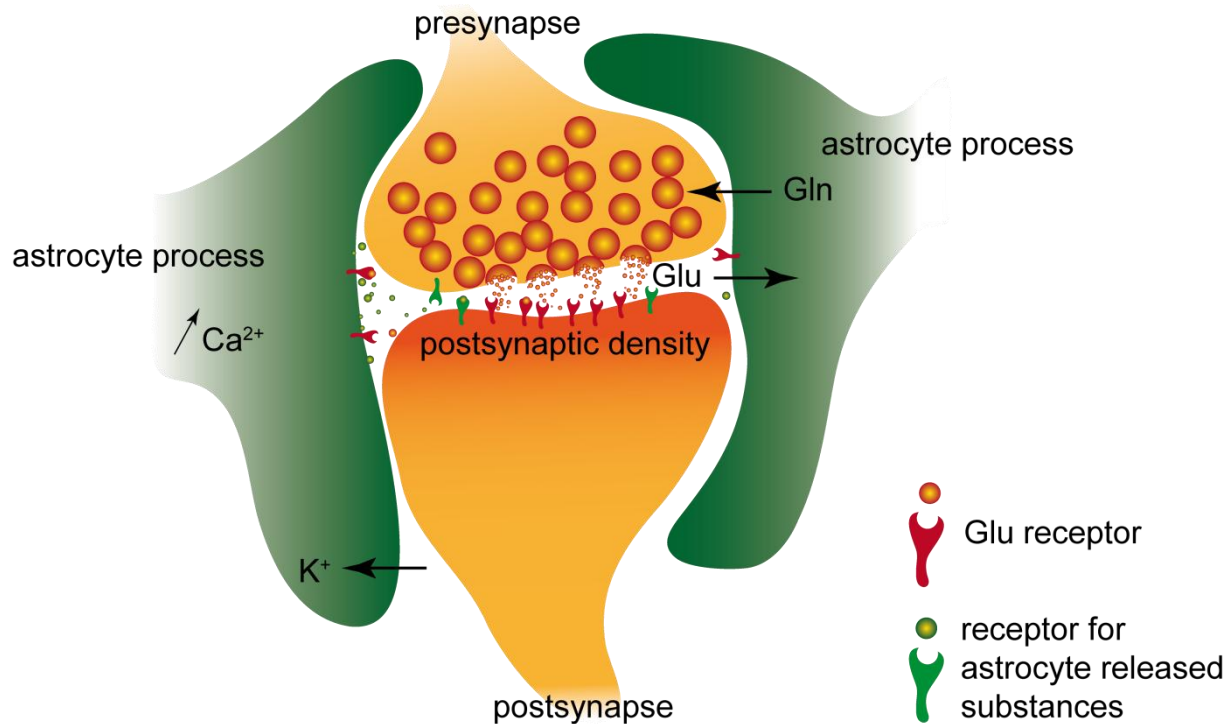
Figure 8 Tripartite synapse. Many neuronal synapses are ensheathed by astrocyte processes ensuring main functions as stabilizing, spatial buffering and neurotransmitter uptake. Glutamate is released from vesicles of the presynapse (Axon, orange) into the synaptic cleft. A network of structural proteins and receptors such as the glutamate receptor is defining the postsynaptic density (tip of dendritic spine, red). Binding of glutamate to its receptors on astrocytes results in an increase in intracellular Calcium concentrations - sensing an excitation of the synapse. This excitation can be modulated by astrocyte released substances that bind to receptors on pre- and post synapse acting either as stimulus or inhibitor. Clearing glutamate from the synaptic cleft astrocytes convert it into glutamine returning this to the neurons. Clearing of glutamate from the synaptic cleft is also important to allow future synaptic activity and to prevent neuronal death. Perisynaptic glia maintain ion homeostasis as shown for potassium and pH. (Allen and Barres, 2009; Eroglu and Barres, 2010; Perea et al., 2009; Araque et al., 1999a)

3.3.2 Reactive gliosis and astrocytic diseases

Reactive gliosis describes the activation of glial cells, mainly astrocytes (astrogliosis), upon brain injury, inflammation or during ageing (Bernal and Peterson, 2011). This reactivity is determined by molecular and structural changes, including increased expression of structural components (e.g. GFAP) (Höke and Silver, 1994; Pekny and Nilsson, 2005; Buffo et al., 2008; Sofroniew, 2009). Astrogliosis is paralleled by up-regulation of GFAP and other markers like Vimentin or Nestin, hypertrophy/cell swelling or - in severe cases by hyperplasticity/proliferation, cell migration, and the generation of a glial scar, which on the one hand impedes repair processes like axonal growth and remyelination, but is on the other hand important to restore tissue integrity and limit neuronal death and inflammation processes (Neary et al., 2003; Buffo et al., 2008; Sofroniew, 2009; Sofroniew and Vinters, 2010).

However, astrocytes are not alone in responding to injuries; there are glial precursor cells expressing NG2 and activated microglia involved in the repair process (Buffo et al., 2008). Reactive gliosis is a context specific combination of molecular, functional and cellular changes modulated by different signaling events (Sofroniew and Vinters, 2010). Triggers for such an astrogliosis might be intercellular signaling molecules like pro- and anti-inflammatory cytokines (e.g. TNFα, IL-6, TGFβ), Toll-like receptor ligands, neurotransmitter, ATP, ROS, toxic amounts of ammonia and other disease associated molecules like β-amyloid, or even conditions such as hypoxia, or food deprivation (Sofroniew and Vinters, 2010). One of the tasks of astrocytes would be the removal of β-amyloid and shielding neurons from β-amyloid aggregates (Rubio-Perez and Morillas-Ruiz, 2012) - a function that might be impaired in AD. Astrogliosis was also reported to be involved in PD progression, however, it is still under debate whether it has a positive or negative effect on the survival of dopaminergic neurons.

Astrocytes are involved in several human diseases such as hepatic encephalopathy or episodic ataxia type 6. Hepatic encephalopathy is initiated by liver damage resulting in toxic amounts of ammonia that needs to be disposed in the brain by astrocytes using glutamine synthetase, which is quite ATP consuming (Lemberg and Fernández, 2009). The disease is characterized by coma, brain edema, which are both promoted by high concentrations of glutamine, intracranial hypertension, and disturbance of neuronal function by increased load of glutamate due to transporter alterations, and additionally, mitochondrial-generated ROS (Lemberg and Fernández, 2009). A mutation leading to an amino acid substitution (Pro290Arg) in the SLC1A3 gene, i.e. the gene encoding for GLAST, results in an impaired glutamate uptake and hyperexcitation of certain neurons correlates with episodic uncoordinated movement found in patients with episodic ataxia type 6 (Winter et al., 2012). Alexander disease represents a progressive astrogliopathy based on dominant mutations in the *Gfap* gene (78 unique mutations are known) (Prust et al., 2011). The disorder shows different grades of symptoms including seizure, motor and cognitive impairment depending on the mutation and the age of the onset of the disease (Prust et al., 2011).

3.4 Aim of this study

Cognitive decline and memory impairment occur to an increasing degree in our ageing population (Broglio et al., 2012). The cellular and molecular mechanisms underlying age-related neurodegeneration and dysfunction of the brain are not fully understood. It is well established that astrocytes are important for neuronal homeostasis, survival, and synaptic plasticity (Sofroniew and Vinters, 2010; Figley and Stroman, 2011). Therefore, it is surprising how little attention has been paid to the contribution of astrocytes to brain dysfunction during ageing and to the impact of age-related mitochondrial dysfunction in astrocytes on brain function. This study aimed to detect ageing-associated effects of impaired oxidative phosphorylation in mature astrocytes and specialized astroglia cells in the dentate gyrus in the adult brain. To this end a genetic mouse model (GLAST::CreERT2 x $Tfam^{loxP/loxP}$ x CAG-CAT-EGFP) was generated, which allows the conditional induction of mitochondrial dysfunction specifically in adult astrocytes through deletion of the mitochondrial transcription factor A (TFAM). First, the effect of impaired mitochondrial integrity on the neuronal progeny of radial glia-like stem cells in the adult hippocampus was examined, regarding proliferation, survival and development of cellular morphology. Secondly, the response of adult astrocytes on mitochondrial dysfunction was studied. Finally, TFAM mutant mice were analyzed for behavioural alterations in motor coordination, learning and memory, smelling, anxiety, and sensory gating.

4   RESULTS

4.1   The GLAST::CreERT2 system - a tool to target distinct brain regions

Conditional ablation of *Tfam* has previously been used to study mitochondrial dysfunction in neuronal subpopulations as described in chapter 3.2.4. Here, the GLAST::CreERT2 mouse line was applied to investigate the effect of TFAM deficiency in astrocytes and in adult-born neurons.
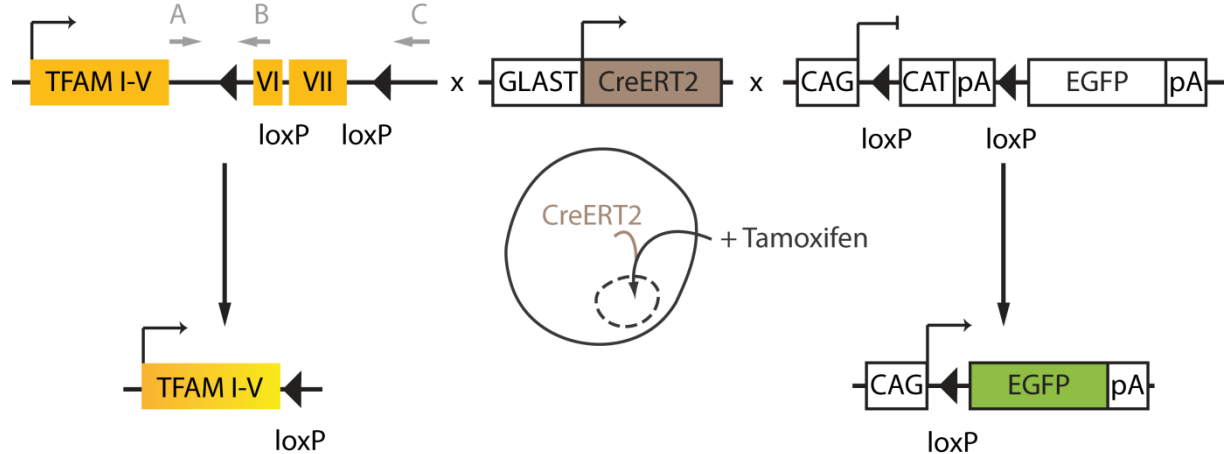
Figure 9 Recombination of the *Tfam* locus using the CreERT2 system under the control of the GLAST promoter. Exon VI and VII of the *Tfam* gene are flanked by loxP sites. Arrows A, B and C (light grey) mark the location of the TFAM-A, -B and -C genotyping primer. The reporter enhanced green fluorescent protein (EGFP) under control of the modified chicken β-actin promoter with a cytomegalovirus (CMV) enhancer (CAG) is not expressed until excision of the chloramphenicol acetyltransferase (CAT) (Kawamoto et al., 2000). The Cre recombinase fused to an artificial estrogen receptor (CreERT2) is constantly expressed under the activity of the glutamate aspartate transporter promoter (GLAST) (Mori et al., 2006). CreERT2 is translocated from the cytoplasm into the nucleus upon Tamoxifen administration. In the nucleus Cre recombinase interacts with the directly repeated loxP recognition sites and excises the flanked DNA (Feil et al., 1997). pA = polyadenylationsignal.

In the case of the GLAST::CreERT2 mouse model the expression of CreERT2, a fusion protein of Cre and the artificial estrogen receptor ERT2, is restricted to the glutamate aspartate transporter (GLAST) expressing cell population. This includes adult astrocytes and astrocytic radial glia-like cells of the neurogenic niches in the adult brain (Mori et al., 2006). In addition to the tissue-specific expression of Cre, a time-specific recombination is possible, since the CreERT2 recombinase can only translocate into the nucleus upon binding of the ERT2-ligand Tamoxifen, an artificial estrogen. Thus, Tamoxifen is applied to induce recombination in the nucleus of cells with an active GLAST promoter (Figure 9) (Feil et al., 1997). This time-specific restriction of recombination of adult astrocytes is particularly important to circumvent an impairment of embryonic development. This is because, in the developing brain, radial glial stem cells already bear characteristics of adult brain astrocytes like expression of GLAST (Mori et al., 2005). Consequently, many cells would be targeted at early developmental stages resulting in a high amount of side effects. This would prevent the study of mitochondrial dysfunction in adult astrocytes. Next to other astrocytic markers, such as the

intermediate filaments Nestin and GFAP, the calcium binding protein S100β, glutamine synthetase (GS) and others (Mori et al., 2005), GLAST is the one characterizing a subpopulation of approximately 60 % to 80 % of astrocytes in the brain (Mori et al., 2006). Hence, the targeted cell population is larger compared with other astrocytic markers for example the GFAP promoter (Nolte et al., 2001) or more cell type specific than the S100β promoter (Vives et al., 2003).

To have an indicator of successful recombination of the *Tfam* locus, GLAST::CreERT2 can be paired with a reporter mouse line like the CAG-CAT-EGFP or R26R mice. Only if Cre is active in the nucleus the conditional EGFP (Kawamoto et al., 2000) or β-galactosidase (Soriano, 1999) loci will be recombined and expressed and can be used as markers to identify cells in which recombination took place.

First, an *in vitro* approach was employed to analyze the recombination of *Tfam* at the protein and mRNA level. Recombination of the *Tfam* locus in EGFP reporter positive astrocytes was induced by transduction of the His-TAT-NLS-Cre (HTNCre) protein (Peitz et al., 2002).

As can be seen in Figure 10 a, TFAM-depleted astrocytes maintain their mitochondria as visualized by the mitochondrial marker Cytochrome C (light grey), while they show a nearly complete reduction of the TFAM protein (red) in comparison with non-recombined GFP negative astrocytes. 4 µm HTNCre led to an efficient DNA recombination (Figure 10 b) and five times less *Tfam* mRNA as revealed by qRTPCR (Figure 10 c).

These results indicate that the conditional *Tfam* locus can be efficiently recombined in astrocytes by Cre recombinase and that the recombination of the *Tfam* locus is correlated with expression of the EGFP reporter.
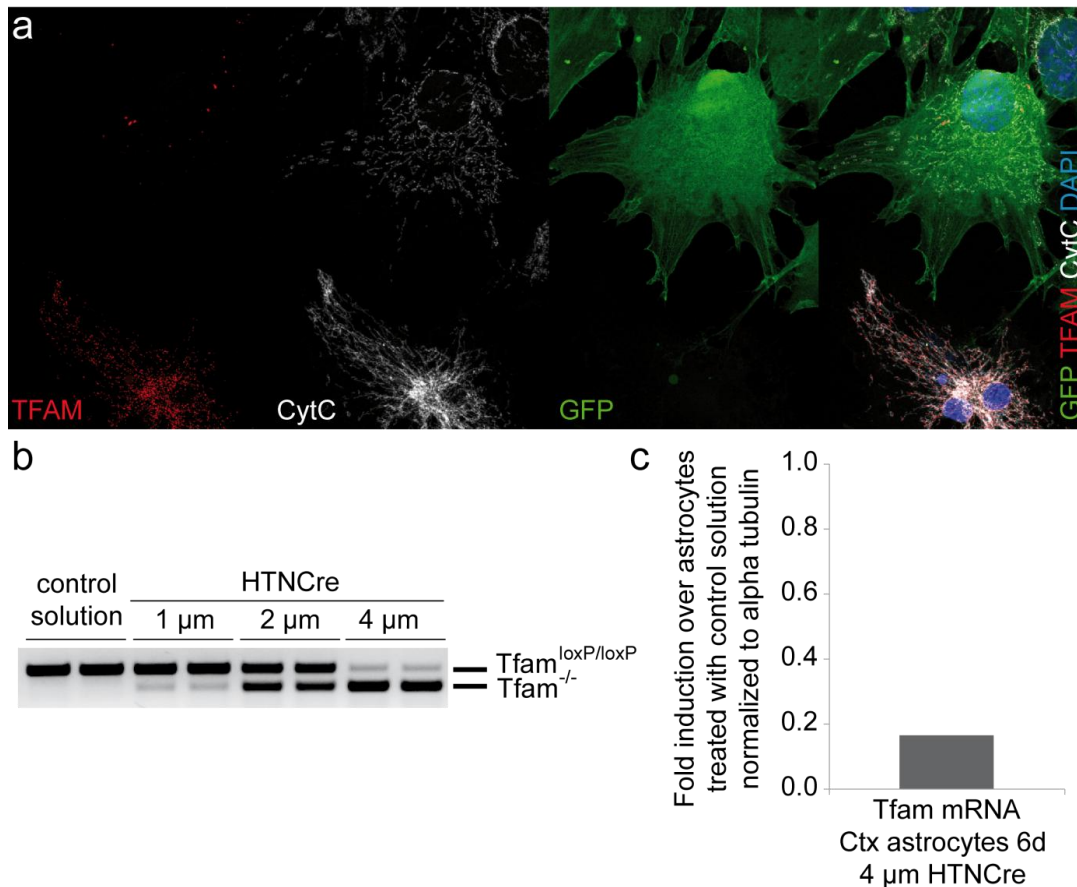
Figure 10 Cell-permeant Cre protein (HTNCre) as a tool for TFAM and EGFP recombination in cortical astrocytes. Primary astrocytes isolated from the cortex (Ctx) of P3 CAG-CAT-EGFP x *Tfam*^loxP/loxP^ mice were treated with HTNCre or control solution and were analyzed 6 d later. (a) Immunostaining of HTNCre transduced astrocytes. Recombined astrocytes expressed EGFP, co-stained with TFAM (red) and Cytochrome C (CytC, light grey), a mitochondrial marker, and DAPI, a nuclear marker. Note that the recombined GFP cell has a strongly reduced TFAM signal compared to the non-recombined only CytC positive cells. Confocal pictures were taken with a 63 times objective with 1.5 times additional zoom. (b) Genotyping PCR of cortical astrocytes that were transduced with different concentrations of HTNCre or control solution. Note that 4 μm HTNCre resulted in a high fraction of transduced cells having a recombined *Tfam* locus (329 bp). (c) qRTPCR of downregulated *Tfam* mRNA in primary cortical astrocytes 6 d after treatment with 4 μm HTNCre normalized to astrocytes treated with control solution and normalized to alpha tubulin, a microtubuli marker. Data were obtained together with Sarah M. Ehses and Germán D. Camargo Ortega.

As the available TFAM antibodies do not give a reliable signal *in vivo*, the EGFP reporter was used as a proxy to estimate the recombination efficiency. GLAST x *Tfam*^loxP/loxP^ x EGFP or R26R were Tamoxifen-treated at the age of two weeks and analyzed at the age of six months. Reporter recombination was taking place in astrocytic cells distributed throughout the brain (Figure 11 a). Highest rates of recombination were observed in Bergman glia of the cerebellum, in the thalamus and the striatum (Figure 11 b). The isocortex, especially the orbital, somatomotor and somatosensory areas, feature a high proportion of recombined cells. High recombination efficiency was also detected in regions where specialized astrocytes serve as stem cells and generate neuronal progeny i.e. the

SVZ/olfactory areas and the hippocampal region. The hind- and the midbrain show a few reporter positive cells.

To determine recombination of the conditional *Tfam* locus *in vivo*, genotyping PCR was performed. Genotyping PCR in unsorted dissected tissue did not result in *Tfam* ko bands (329 bp) in every isolated tissue (Figure 11 c). Recombination of the *Tfam* locus was only detectable in the isolated olfactory bulb (OB) and subventricular zone (SVZ), where a high proportion of recombined cells is located as shown in Figure 11 a. In tissue from cerebellum (Cb) and cortex (Ctx) only very faint ko bands could be detected. The bands of the PCR products for the non-recombined allele were far stronger, potentially due to the high number of neurons in the tissue.

Given the high number of non-recombined GFP negative cells, it was sought to determine whether EGFP reporter-positive cells also had recombination of the *Tfam* locus. Therefore, EGFP-positive cells were FACSorted from dissected brain regions. As shown in Figure 11 d, DNA was isolated to perform genotyping PCRs. The size of the PCR product is for $Tfam^{+/+}$ 404 bp, for $Tfam^{loxP/loxP}$ 437 bp, and for $Tfam^{-/-}$ 329 bp. Genotyping PCRs from DNA isolated from WT mice resulted in single bands around 400 bp. In case of the ko mice two bands were detectable, one around 440 bp and the other at 330 bp; the latter reflects a successful recombination. Thereby, Cre-mediated recombination of the *Tfam* locus after Tamoxifen treatment could be visualized on DNA level.

In conclusion, *Tfam* recombination could be demonstrated in astrocytes using both the HTNCre system and the GLAST::CreERT2 indicating that the $Tfam^{loxP/loxP}$ mouse is a powerful model system to study the effects of TFAM-dependent mitochondrial dysfunction in astrocytes.

GFP DAPI

a' GFP

a" DAPI
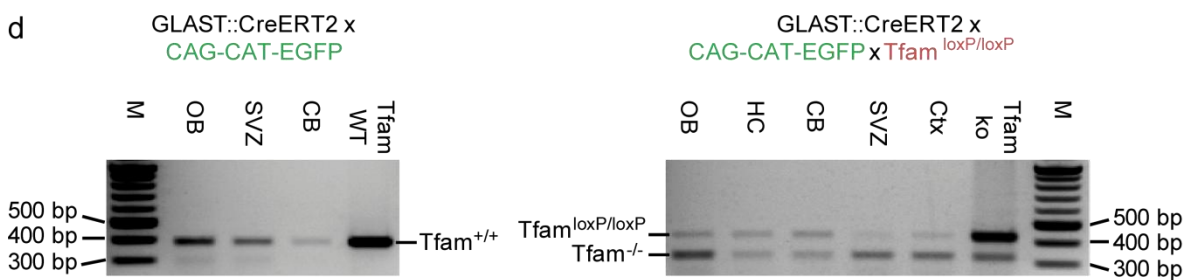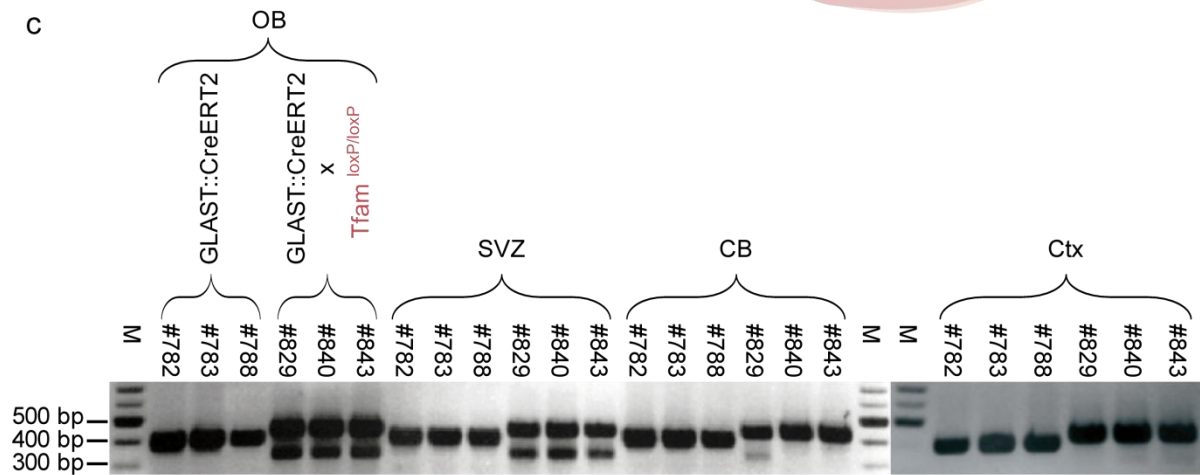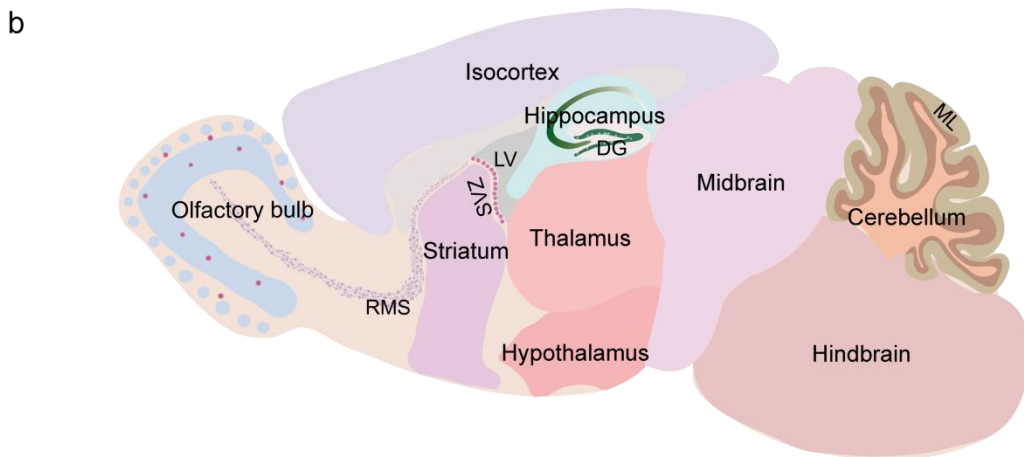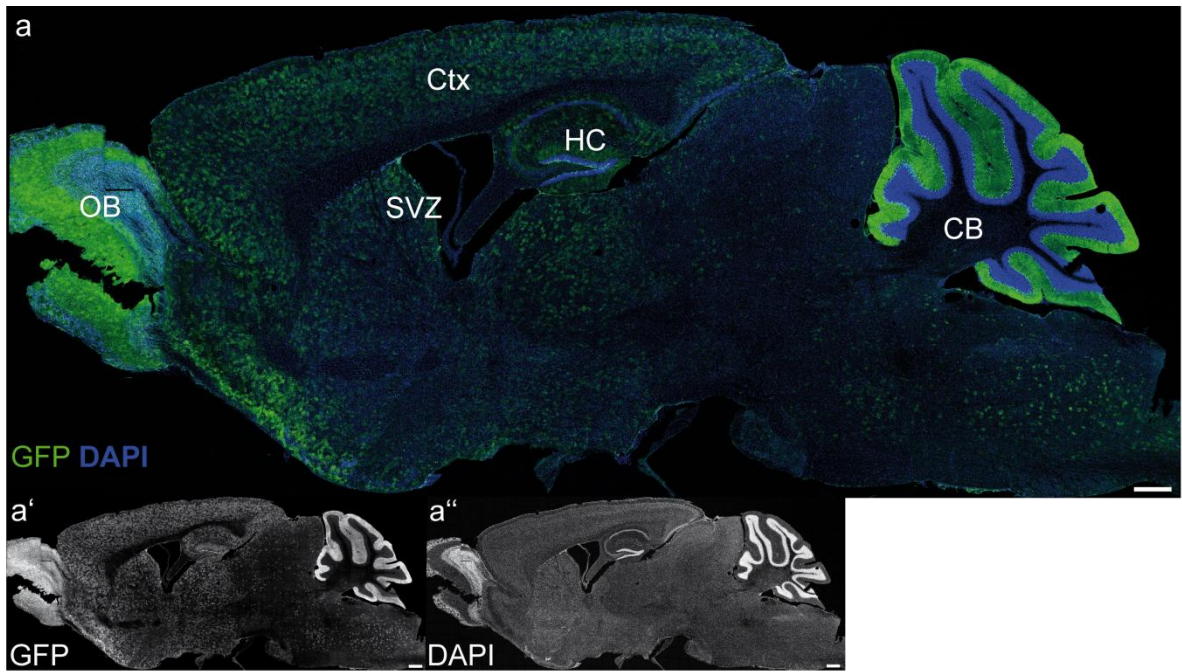
Figure 11 The *Tfam* locus is recombined in EGFP positive FACSorted and unsorted cells of mutant mouse brain tissue. (a) Tile scan confocal microscopy picture demonstrating exemplary recombined EGFP-positive cells in analyzed brain regions, in this case a WT mouse treated with Tamoxifen at P14/16/18 and sacrificed at the age of 6 months. The GFP signal is used to visualize recombined EGFP-positive cells, counterstained with DAPI (blue), a nuclear marker. (a') GFP signal in white. (a'') DAPI signal in white. (b) Schematic overview of an adult sagittal mouse brain showing all the regions where recombination is taking place. (c) Genotyping PCR of the *Tfam* locus in FACSorted recombined cells of CAG-CAT-EGFP x GLAST::CreERT2 x (*Tfam*$^{loxP/loxP}$) mice. Animals were treated with Tamoxifen at 2 weeks and sacrificed at the age of 2 months. In *Tfam* WT and *Tfam* ko lanes DNA originated from mousetails. (d) Genotyping PCR of the *Tfam* locus in distinct isolated brain regions of 10 months old young Tamoxifen-treated mice (WT: #782, 783, 788; cko: #829, 840, 843) giving a clear cko band only in tissue containing a high proportion of recombined cells (OB, SVZ). CB: cerebellum; Ctx: cortex; DG: dentate gyrus; HC: Hippocampus; ML: cerebellar molecular layer; OB: olfactory bulb; RMS: rostral migratory stream; SVZ: subventricular zone; M: 100 bp DNA ladder. Scale bars 500 μm.

4.2 Analyzing the effect of TFAM depletion in the hippocampal neurogenic niche

4.2.1 Reduced proliferation and survival of newborn neurons in the DG of young recombined TFAM-depleted CAG-CAT-EGFP x GLAST::CreERT2 x (*Tfam*$^{loxP/loxP}$) mice

Rodent hippocampal neurogenesis declines with age (Jinno, 2011; Kuhn et al., 1996). To determine whether *Tfam* depletion generated an ageing-like phenotype and compromised the function of adult hippocampal radial glia-like stem cells, the proliferation capacity was analyzed. The incorporation of the thymidine analogue 5-bromo-2-deoxyuridine (BrdU), which gets incorporated during the S-phase of proliferating cells, is a widely used tool to detect cells undergoing division (Ming and Song, 2005; Kempermann et al., 2003).

Tfam cko mice and control mice were treated with Tamoxifen at the age of two weeks to induce Cre activity and recombination. To examine proliferation and survival, mice received BrdU injections at the age of two months and were sacrificed either three hours, two, or four months after the last injection.

As depicted in Figure 12 a, there is no significant decrease in the number of BrdU positive cells in the SGZ after a three hours BrdU pulse in two months old cko mice compared to WT mice. This indicates that proliferation was unaltered. In contrast, staining for the proliferation marker Ki67 revealed strong proliferation defects in four months old *Tfam* cko mice (Figure 12 b). At this age, the number of proliferating cells in the SGZ of *Tfam* cko mice was reduced to 17 % compared to control mice, demonstrating that precursor proliferation was impaired by TFAM depletion.

To further analyze the survival, the number of BrdU-labeled newborn cells in the DG was determined two or four months after the final BrdU injection. As shown in Figure 12 c', the cko mice contained significantly less BrdU positive cells at the age of four (p = 0.005) and six (p = 0.01) months compared to the control mice.

Figure 12 d visualizes the time course of BrdU positive cells from two to six months of age. The total amount of BrdU positive cells at the two months time point (Figure 12 a) was set to a hundred percent. In the WT mice there were still approximately 80 % BrdU maintaining cells at four months of age and a significantly decreased percentage of 45 % (p = 0.045) at the age of six months. In the case of the TFAM-depleted mice, there was already a drop of BrdU maintaining cells at the age of four months (37 %), which was even more reduced at the age of six months (16 %, p = 0.003).

Free access to a running wheel leads to an increase in SGZ-proliferation in the DG, even in adult mice (van Praag, 2005). In addition, running was shown to rescue proliferation deficits caused by inducible Notch1 depletion (Ables et al., 2010). To investigate whether physical activity can counteract the decrease in proliferation in *Tfam* cko mice, they were recombined during postnatal week three and were housed either with or without running wheel for seven days at four months of age. To measure proliferation, mice received daily BrdU injections during the running wheel period and were sacrificed on day eight.

Depicted in Figure 13, the significant diminution of the proliferation rate (non-runner/runner; WT: 14.87 ± 2.38 cells per 1000000 µm³/ 18 ± 1.33 cells per 1000000 µm³; cko: 5.71 ± 0.88 cells per 1000000 µm ³/ 8.01 ± 1.15 cells per 1000000 µm³; p = 0.014/ p = 0.0002) in the hippocampus of *Tfam* cko mice could be demonstrated as was already shown in Figure 12. However, there was no proliferation deficit recovery in the mutants after one week of running. Using this BrdU paradigm, it was not possible to repeat the positive effect of running on proliferation in WT mice; several standard housed control mice showed inexplicably high rates of BrdU incorporation. A trend towards increased BrdU counts was observed in running cko mice. However, the average number of BrdU cells did not reach the basal level of BrdU positive cells in WT mice.

In summary, an increasing proliferation deficit could be observed for the first time at the age of four months in TFAM-depleted mice, implicating an impaired stem cell function. Moreover, the number of surviving newly generated BrdU maintaining cells was strongly reduced in TFAM-deficient mice after six months compared to four months. Finally, it appears that running might not be sufficient to recover the proliferation deficit at this age. A definite statement on the effects of running, however, is currently not possible as running did not significantly increase cell generation in controls.
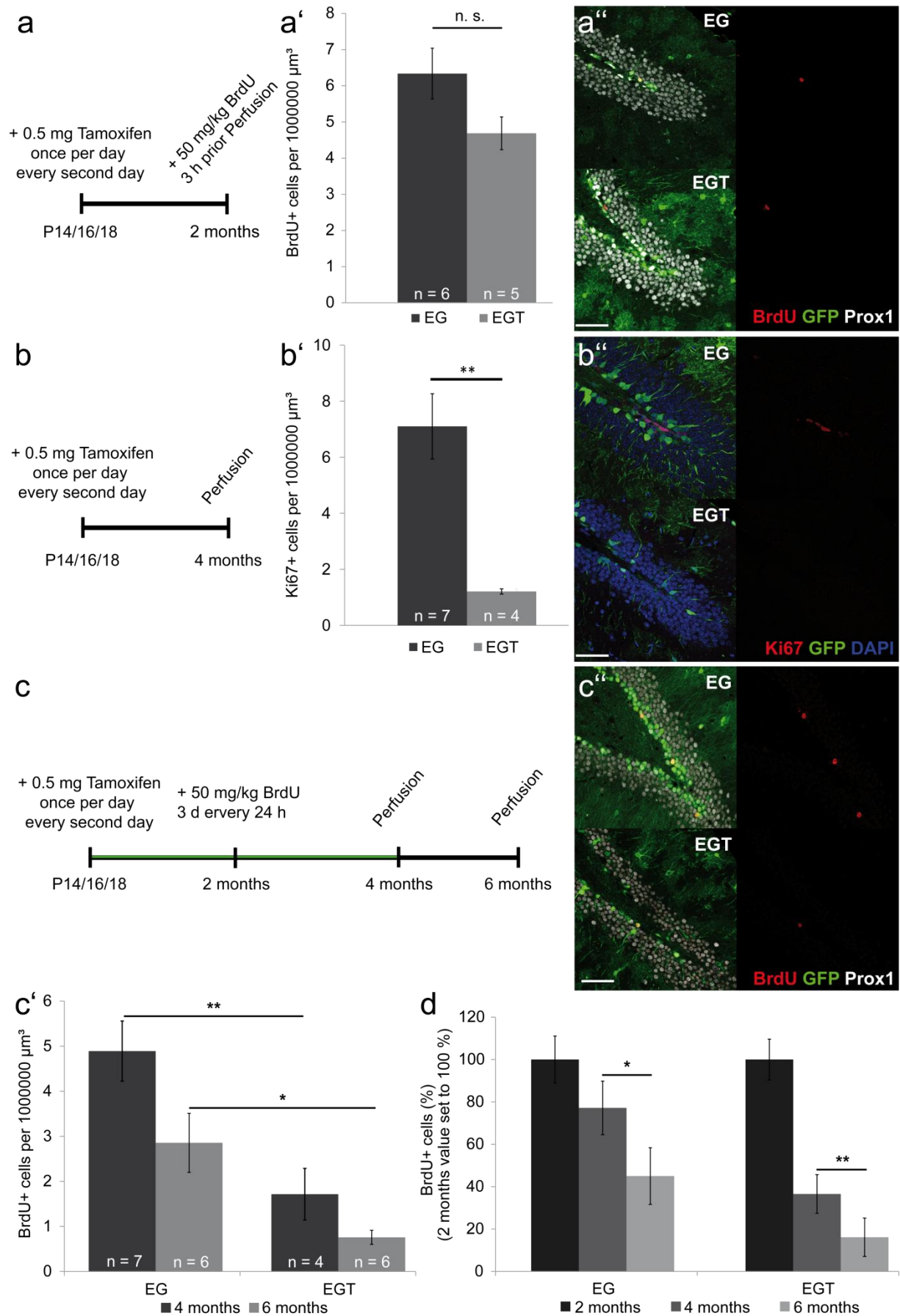
Figure 12 TFAM depletion in radial glial stem cells and astrocytes in the adult hippocampus leads to proliferation and survival deficits from 6 weeks onwards after induction of recombination.

Schematic depiction of experimental paradigm (a, b, c) and representative single plane confocal images of immunofluorescent stainings of brain sections from Tamoxifen-treated CAG-CAT-EGFP x GLAST::CreERT2 x (*Tfam*^loxP/loxP^) mice (a'', b'', c''). Corresponding images of the tip of the dentate gyrus were taken with the same confocal microscopy settings. BrdU (red) or Ki67 (red) counterstained with GFP to visualize recombined EGFP-positive cells, DAPI (blue), a nuclear marker, or Prox1 (grey), a neuronal marker. (a) 6 weeks after Cre-mediated recombination of the *Tfam* loci (*Tfam*$^{-/-}$) mutant mice showed no significantly reduced BrdU incorporation after a 3 h 50 mg/kg BrdU pulse compared to TFAM WT mice, in which only the EGFP reporter was recombined. (b) 3 and a half months after recombination the proliferation rate in *Tfam* cko animals was strikingly decreased as measured using the proliferation marker Ki67. (c) Furthermore TFAM deficiency resulted in pronounced decline of BrdU maintaining cells that were marked 6 weeks after recombination and analyzed 2 (see confocal images c'') and 4 months after BrdU injections (c'). BrdU was IP injected at the age of 2 months once a day for three consecutive days 50 mg/kg body weight. (d) The decrease of BrdU retaining cells over time from 2 to 6 months was significant in mutant mice, in contrast to control mice where there was only a tendency from two to four that gets significant from four to six months of age. Mean ± s.e.m.; *p < 0.05, **p < 0.01, ***p < 0.001, n. s. = not significant. Scale bars 50 µm.
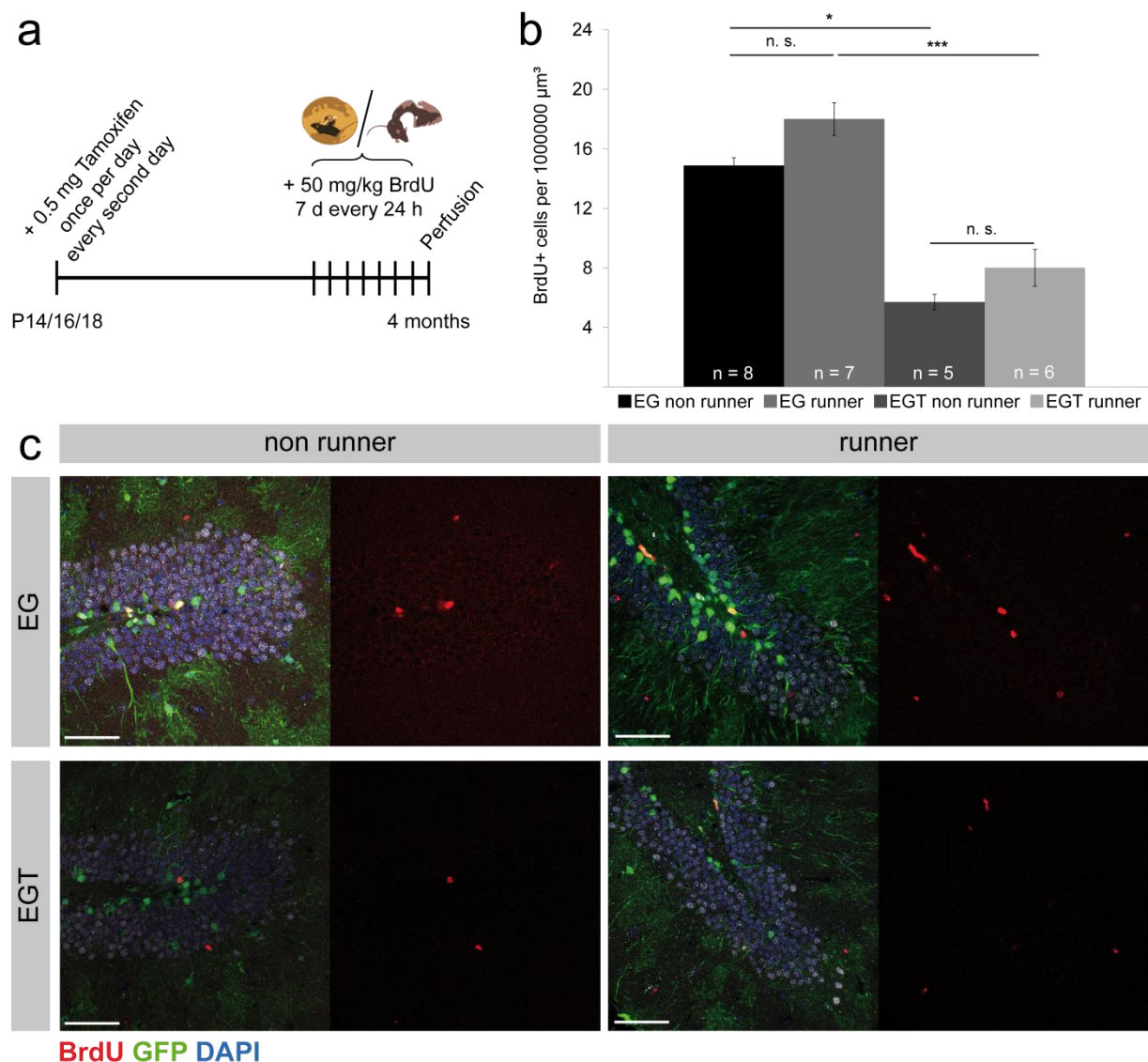
Figure 13 Physical activity does not considerably improve the proliferation rate in a TFAM-depleted neurogenic niche background. (a) Schematic description of experimental set up. (b) Mutant mice at the age of four months showed, under running or non-running conditions, significantly less proliferation compared to WT controls. (c) Representative single plane confocal images of immunofluorescent stainings of brain sections from P14/16/18 Tamoxifen-treated CAG-CAT-EGFP x GLAST::CreERT2 x (*Tfam*^loxP/loxP^) mice. Corresponding images of the tip of the dentate gyrus were taken with the same confocal microscopy settings. BrdU (red) counterstained

for recombined EGFP-positive cells, DAPI (blue), a nuclear marker, or Prox1 (grey), a neuronal marker. Mean ± s.e.m.; *p < 0.05, ***p < 0.001, n. s. = not significant. Scale bars 50 μm.

4.2.2   Fate decisions are impaired in adult hippocampal stem cells in TFAM-depleted mice

Under physiological conditions, a high proportion of new cells in the adult DG develops into fully functional granule neurons (Rao and Shetty, 2004; Kempermann and Gage, 2000); only a small fraction will adopt an astrocytic phenotype. To examine whether TFAM depletion in astrocytes and radial glia-like stem cells influenced the fate of newly generated cells, BrdU labeled cells were phenotyped.

To investigate the fate of newborn cells in the SGZ of young recombined four months old mice, S100β, an astrocytic marker, and Prox1, a dentate granule neuron marker, were employed to determine the respective fractions of astrocytes and neurons among all BrdU labeled newly generated cells and within the BrdU and GFP double positive population.

The total fraction of cells showing a neuronal fate (Prox1+) was significantly reduced by half in TFAM-deficient mice (p = 0.007) compared to control mice (Figure 14 e). Furthermore, a significant increase of BrdU+ only cells was observed in mutant mice (WT: 11 ± 1 % versus cko: 40 ± 8 %, p = 0.025; Figure 14 f: black bars). This indicates that overall differentiation of new cells into neurons was impaired. This effect was most likely the result of decreased neuronal production from recombined cells as the fraction of recombined GFP+ neurons in *Tfam* cko mice was decreased (WT: 65 ± 4 % versus 30 ± 6 %, p = 0.011; Figure 14 e: green bars). Whereas, the neuronal fraction among non-recombined newborn cells was unaltered (Figure 14 e: light grey bars).

Analyzing the total fraction of recombined GFP+ cells revealed a slight reduction within the total counted BrdU+ population in both countings (Figure 14 f: WT: 73 ± 2 % versus cko: 47 ± 14 %, p = 0.13; Figure 14 h: WT: 73 ± 6 % versus cko: 40 ± 12 %, p = 0.07; combined light and dark green bars). This suggests, a decreased differentiation of the recombined cell population in *Tfam* cko mice.

Next, the differentiation into astrocytes was determined using the astrocyte marker S100β. Overall the proportion of S100β+ cells among all BrdU+ cells appeared to be slightly increased, indicating an increased astrocytic differentiation. Intriguingly, the fraction of non-recombined S100β+ cells was significantly increased in mutant mice (WT: 17 ± 3 % versus cko: 44 ± 9 %, p = 0.048), while the fraction of recombined S100β+ cells appeared slightly reduced (WT: 31 ± 4.5 % versus cko: 14.4 ± 4.4 % , p = 0.06), as depicted in Figure 14 g. Thus recombined and non-recombined populations showed differences in their differentiation potential.

No changes were found in the BrdU+ only fraction comparing WT mice and mutant mice (Figure 14 h, black bars). This indicates, that the increased fraction of non-recombined only BrdU+ cells in the Prox1-counting (Figure 14 f, black bars) might reflect the increased portion of non-recombined S100β+ BrdU+ cells (Figure 14 h, on the right: light grey bars).

To conclude, the portion of astrocytes and neurons was altered in *Tfam* cko mice. The percentage of newly generated neurons was significantly reduced, mainly due to a reduced fraction of recombined neuronal cells. The trend towards less newborn astrocytes in the recombined cell population was masked by a significant increase of non-recombined, non neuronal S100β positive cells. These results suggest that there is some change in the differentiation of neural stem cells. The portion of non-recombined neurons was unaltered, while the proportion of non-recombined astrocytes was increased. This observation might indicate a niche effect where the compromised niche tries to compensate for TFAM-depleted astrocytes by recruiting TFAM positive neural stem cells into the astrocytic lineage.
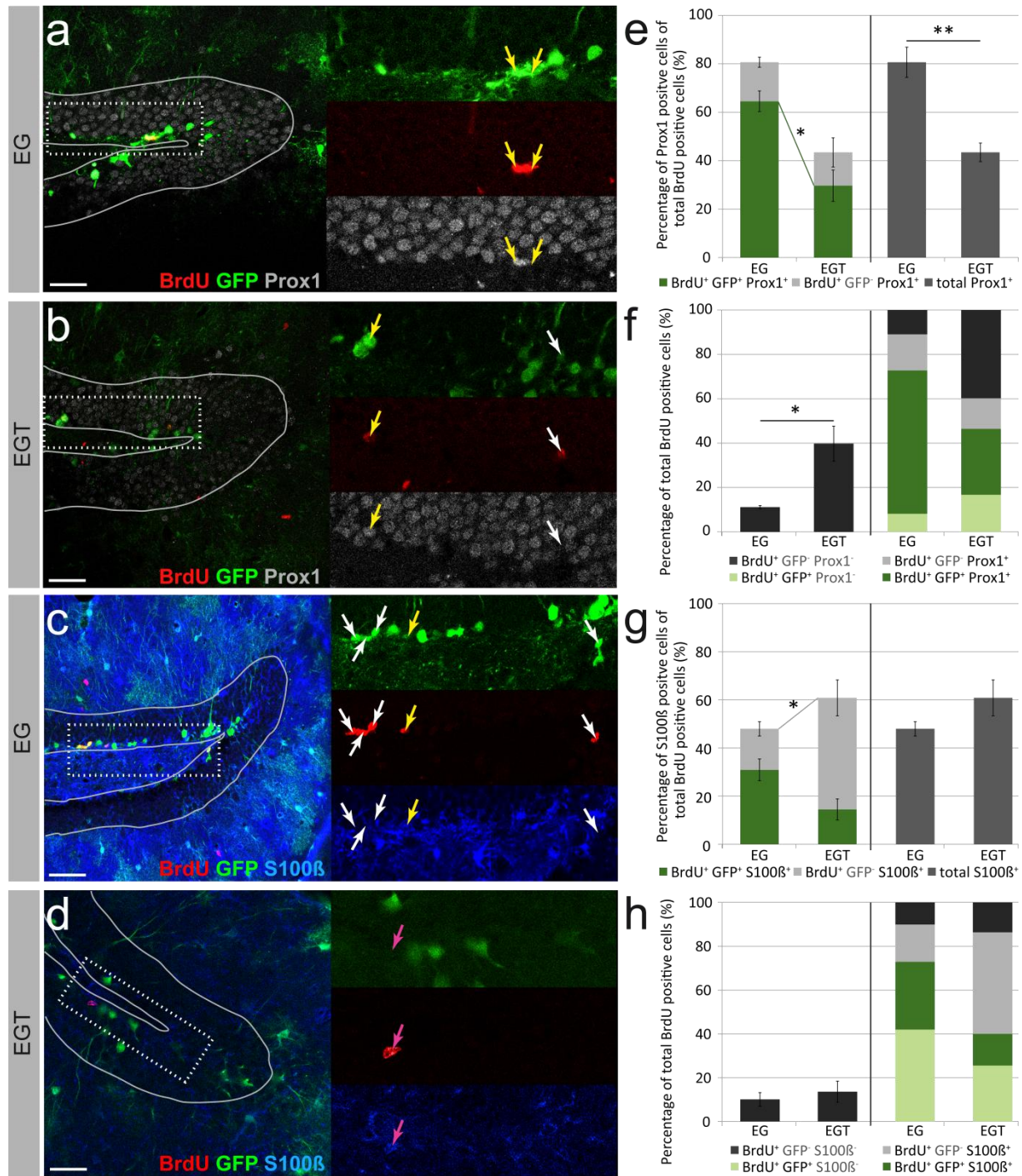
Figure 14 Neuronal differentiation is impaired in young recombined 4 months old CAG-CAT-EGFP x GLAST::CreERT2 (x *Tfam*^{loxP/loxP}) mice. Four months old mice were recombined at the age of two weeks, got daily BrdU injections for seven consecutive days and were sacrificed on day eight. (a-d) Representative single plane confocal images of immunofluorescent stainings of brain sections from P14/16/18 Tamoxifen-treated CAG-CAT-EGFP x GLAST::CreERT2 x (*Tfam*^{loxP/loxP}) mice. Corresponding images of the tip of the dentate gyrus (marked by thin grey line) were taken with the same confocal microscopy settings. BrdU (red) counterstained for recombined EGFP-positive cells. WT (a) and *Tfam* cko (b) counterstained with Prox1 (grey), a neuronal marker. Inset (dashed line): White arrows indicate GFP+/BrdU+ cells while yellow arrows highlight GFP+/BrdU+/Prox1+ cells. WT (c) and *Tfam* cko (d) sections additionally stained for S100β (blue), an astrocytic marker. Inset (dashed line): White arrows mark GFP+/BrdU+ cells, yellow arrows highlight GFP+/BrdU+/S100β+ cells, and purple arrow indicates a BrdU+/S100β+ cell. (e) Percentage distribution of Prox1+ cells positive for BrdU, and GFP within the total BrdU+ cell population. On the right hand side the total fraction of Prox1+ cells is depicted. For visualization purposes graphs of GFP+ cells are highlighted in green. (f) Proportion of only BrdU+,

Prox1 and GFP negative cells within the total BrdU count. Note the percentage distribution of all counted cell populations within the total BrdU count on the right hand side. (g) Proportions of cells being positive for BrdU+, GFP+ and S100β+, an astrocytic marker, within the total counted BrdU+ cell population. The dark grey bars on the right hand side depict the total S100β+ population. (h) Percentage distribution of BrdU+ only, S100β and GFP negative cells within the total BrdU count. Note the percentage distribution of all counted cell populations within the total BrdU count on the right hand side. Mean ± s.e.m.; *p < 0.05, **p < 0.01. Scale bars 50 μm.

4.2.3 TFAM-deficient mice maintain a glial population with radial morphology

The reduced proliferation described in chapter 4.2.1 may be the result of decreased numbers of neural stem cells or of a reduced neural stem cell function. To investigate this question, brain sections of four months old young recombined CAG-CAT-EGFP x GLAST::CreERT2 x ($Tfam^{loxP/loxP}$) animals were analyzed using the stem cell markers GFAP and Sox2 (Kriegstein and Alvarez-Buylla, 2009) along with the radial glial morphology to detect changes in the stem cell population. The total amount of GFAP, and Sox2 positive radial glial-shaped cells in the SGZ of *Tfam* cko brains was not significantly reduced in comparison to control mice (Figure 15). In addition, there was no difference in the proportion of GFP-positive cells among the radial glial population. Hence, TFAM depletion did not affect radial glia numbers indicating that reduced stem cell function rather than loss of radial glia cells underlied proliferation defects in TFAM-depleted mice. Figure 15 b' and c' show a divergent intensity of GFAP-expression, which will be discussed in section 4.4.
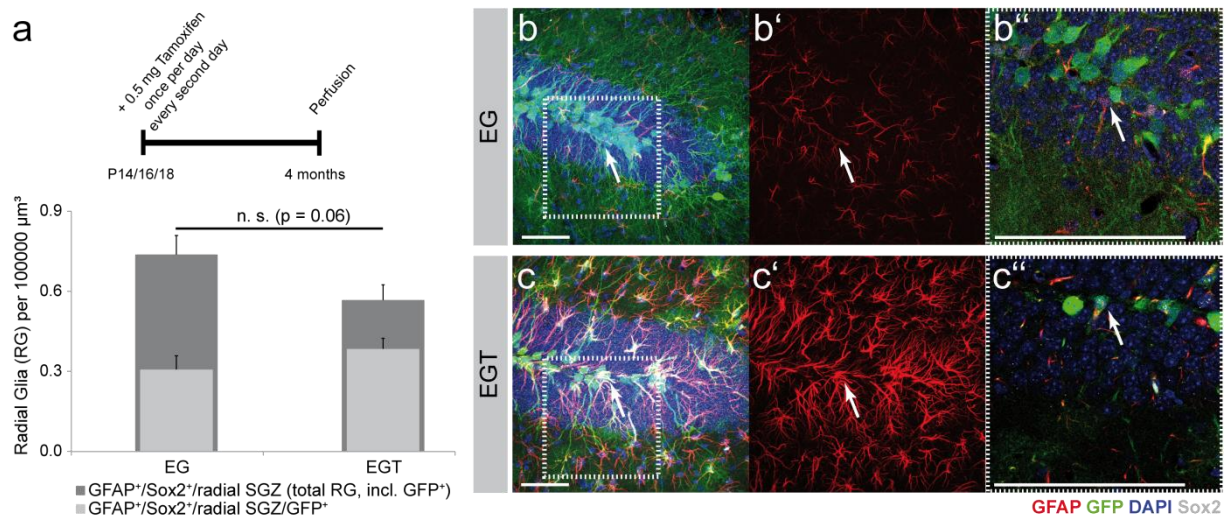
Figure 15 There is no effect on the stem cell population in 4 months old young Tamoxifen-treated CAG-CAT-EGFP x GLAST::CreERT2 x *Tfam*^{loxP/loxP} mice. (a) Schematic description of the used paradigm. Three and a half months after Cre-mediated recombination of the *Tfam* loci (*Tfam*^{-/-}) the sum of GFAP, and Sox2 positive radial glia-like cells in the SGZ is slightly reduced compared to equivalent Tamoxifen-treated CAG-CAT-EGFP x GLAST::CreERT2 mice. The amount of EGFP-positive recombined cells contained in the total population of counted radial glial remained the same. (b-b'', c-c'') Representative confocal images of immunofluorescent stainings of brain sections from P14/16/18 Tamoxifen-treated CAG-CAT-EGFP x GLAST::CreERT2 x (*Tfam*^{loxP/loxP}) mice. Corresponding confocal images were taken with the same microscopy settings. GFAP (red) and Sox2 (grey) were used as radial glial marker in addition with radial glial morphology to detect neural stem cells in the SGZ; counterstaining for recombined EGFP-positive cells, and DAPI (blue), a nuclear marker. Maximum projection of several stacks including the whole cell, merge (b, c) and GFAP only (b', c'). The arrows in the insets

show the soma of a GFAP, Sox2 (b'') and in case of the cko (c'') the soma of a GFP-positive radial glial cell in a single plane confocal image. Mean ± s.e.m.; n. s. = not significant. Scale bars 50 µm.

4.3 Morphological analyses of TFAM-deficient newborn neurons in the adult DG
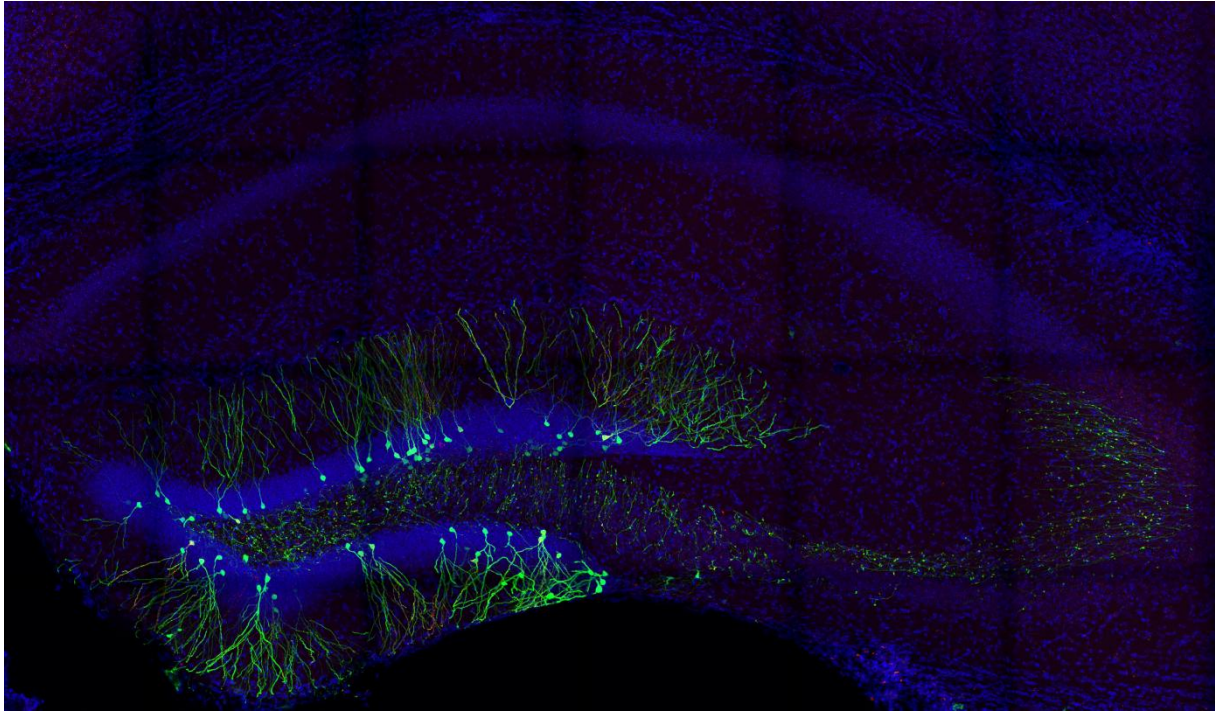
Figure 16 Retroviral injection into the adult hippocampal DG using CAG GFP and CAG IRES mDsRed (42 dpi). Overview of a virus injectionsite accumulated z-stack. The tile-scan was taken with a confocal microscope and a 40 times objective. Mitochondria are labeled in red with a retrovirus expressing mitoDsRed. The whole cell morphology, including the axons, is labeled by a GFP expressing retrovirus, co-staining with DAPI (blue, nuclear marker).

4.3.1 TFAM-depleted neural stem cells generate morphologically distinct developing neurons in GLAST::CreERT2 x *Tfam*^{-/-} mice - morphology analyses

Maturation and integration are important factors for the survival of a newborn neuron (Tashiro et al., 2006). The survival of newly generated neurons was strongly impaired in TFAM mutant mice. To gain better insight into the development and maturation process of newborn neurons derived from recombined TFAM-deficient neural stem cells in the DG, a cell morphology approach was applied.

MMLV retroviruses permit birthdating and thus the examination of newborn cells at defined developmental stages (Tashiro et al., 2006). Here, MMLV retroviruses encoding bicistronically for GFP and mitoDsRed (mDsRed) were employed. These viruses permit visualization of whole cell morphology including dendritic length and arborisation complexity and analyses of mitochondrial

volume and number. Since GFP was used it was necessary to cross the GLAST::CreERT2 x ($Tfam^{loxP/loxP}$) to the R26R instead of the EGFP reporter to label recombined cells.

As explained in section 3.1, adult-born neurons in the DG already develop an elaborated dendritic arborisation within the first three weeks following retroviral labeling/birthdating (Zhao et al., 2006). To analyze the effect of mitochondrial dysfunction on the dendritic development of maturing newborn neurons, a three weeks time point was chosen that also allowed analyses of spine formation which starts during week three (Toni et al., 2007) (compare section 4.3.3).

To follow the retroviral approach, young, two weeks old, Tamoxifen-treated mice harboring a recombined R26R β-gal expressing locus or in case of the cko mice an additionally recombined *Tfam* locus were kept under non-running or running conditions and received CAG GFP IRES mDsRed injections at the age of two months.

To examine the dendritic growth of WT and *Tfam* cko mice in a quantitative way the maximal extension of their dendritic trees was measured. Therefore, the ratio of the distance between the soma and the most distant dendritic endpoint with respect to the distance between the soma and the hippocampal fissure was determined. The graphs depicted in Figure 17 e-e''' visualize the proportion of cells spanning the molecular layer to a distinct level. The smaller the calculated ratio is the shorter the cells. The maximal extension analysis can be used to determine the maturation state of a newborn cell regarding its extension into the molecular layer. A fully mature cell is reaching the predefined boundary; the so-called hippocampal fissure (Krzisch et al., 2013).

Under non-running conditions there was no significantly different percentage distribution of the ratio of cell extension between WT and cko animals (Figure 17 e). In WT and mutant mice the percentage distribution of cells differentially spanning the molecular layer was significantly changed comparing non-running versus running conditions (non-running vs. running; WT: p = 0.025, cko: p = 0.04). These significant differences in the cell size distribution demonstrate the increased dendritic length due to physical activity in WT as well as in TFAM-depleted mice (Figure 17 e'', e'''). The direct comparison of the maximal extension analysis of WT and cko running animals showed a significantly (p = 0.007, Figure 17 e') higher proportion of small cells in the cko running mice.

Taken together, the maximal cell extension analysis revealed no differences under standard non-running conditions, while physical activity increased the portion of cells spanning further into the molecular layer in WT mice and cko mice. Running conditions resulted in a significantly higher fraction of short cells in TFAM-deficient mice compared to WT animals.
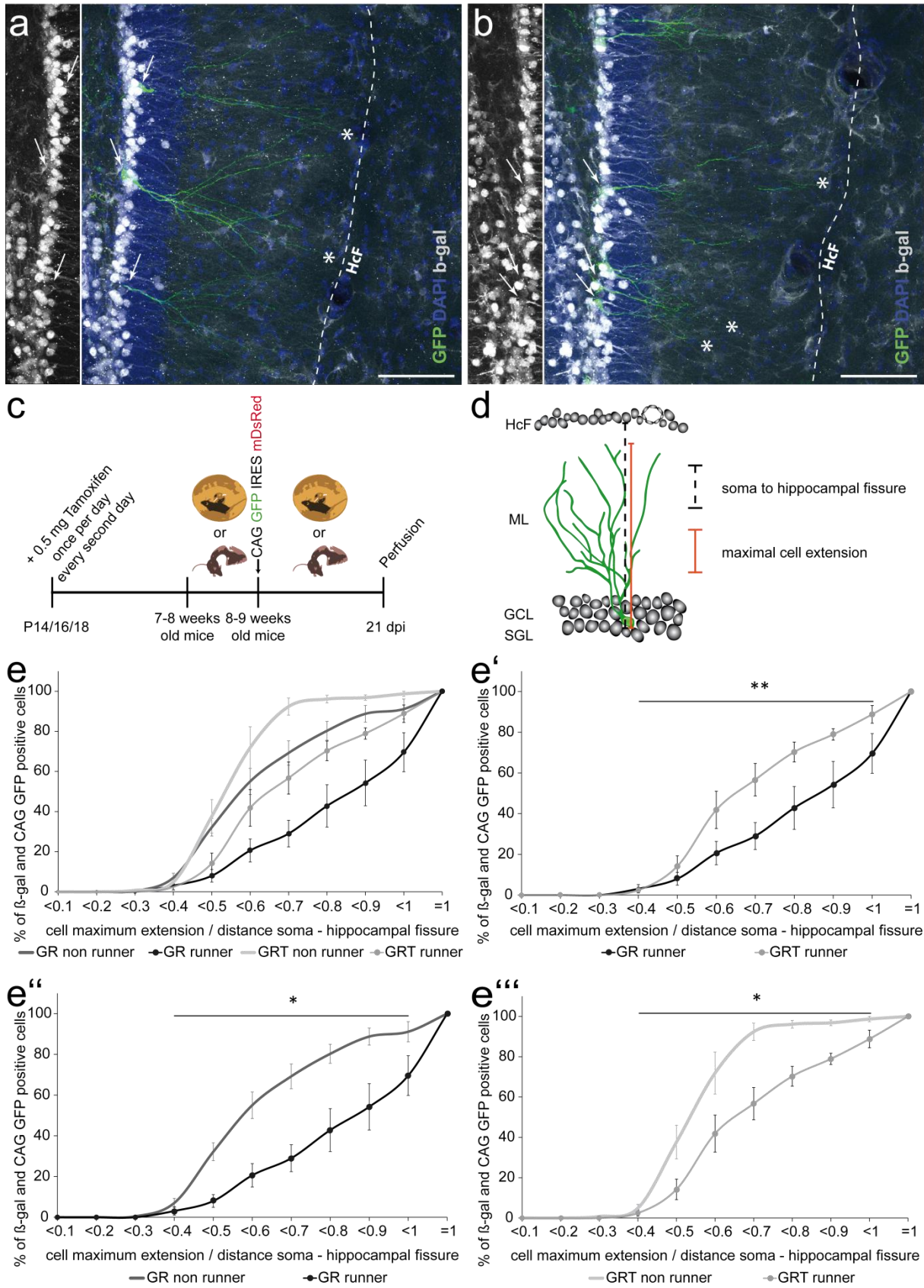
Figure 17 Maximal extension analysis of virus targeted 21 d old cells in young recombined GLAST::CreERT2 (x *Tfam*^loxP/loxP^) x R26R 2 months old mice under non-running or running conditions. Representative confocal images of the DG of (a) WT (GR) or (b) mutant (GRT) running mice. Immunostaining of virus transduced GFP expressing cells co-stained with DAPI (blue) and β-gal (light grey). Arrows indicate soma of recombined virus

targeted cells. The dashed line is highlighting the hippocampal fissure (HcF). Asterisks indicate the most distant dendritic endpoint. (c) Experimental paradigm. (d) Index calculation background. (e) Size-distribution of β-gal/CAG GFP-positive cells shown in percentage versus the ratio of the maximal cell extension and the distance soma to hippocampal fissure (maximal possible extension). 19 to 65 cells were analyzed per animal (n = 4). (e') WT and mutant mice under running conditions. (e'') WT runner versus non runner mice. (e''') Mutant runner versus non runner mice. Mean ± s.e.m.; *p < 0.05, **p < 0.01. Scale bars 50 μm.

To further investigate the effect of TFAM depletion on dendritic morphology Imaris 7.5 morphology analysis was employed as a very precise tool, which allows reconstruction and exact investigation of a limited amount of cells.

Tfam cko cells under standard housing conditions displayed more numerous but shorter dendritic segments, more basal branches, and an overall shorter appearance (Figure 18 a and b). The dendritic complexity can be further visualized by Scholl analyses, measuring the crossings of dendrites with imaginary circles moving away from the soma, depicted as Scholl intersections as shown in Figure 18 e. Scholl analyses revealed more dendritic branch points in combination with an unchanged total dendritic length (Figure 18 c, d) and a decreased amount of Scholl intersections (Figure 18 e).

Another interesting aspect was the effect of physical exercise on dendritic development, which could be shown to increase total dendritic length, spine density and mitochondrial content in 16 dpi cells of C57 BL6 mice (Kathrin Steib, unpublished data), and is known to improve neuronal maturation (Piatti et al., 2011). Here, this experimental paradigm allows investigating whether the running effect is still visible in 21 dpi cells and if it can be used as a challenger or rescue attempt for morphology impairments due to TFAM depletion.

As can be seen in Figure 18 c, at 21 dpi the total dendritic length was increased by running in WT runner 1227 ± 73 μm versus WT non runner 866 ± 85 μm (p = 0.003) and cko mice runner 937 ± 66 μm versus non runner 704 ± 53 μm (p = 0.008). As already mentioned, there was no significant difference in dendritic length between WT and cko non runner mice. However, running resulted in pronounced differences between cko and control neurons and the total length of the dendritic tree in neurons of cko mice runner was decreased by 24 % (937 ± 66 μm versus 1227 ± 73 μm, p = 0.005).

The dendritic arborisation is not only determined by dendritic length but also by the degree of branching, which is expressed by the number of branch points. There were fewer branch points in the WT running mice (11 ± 1) compared with the non-running mice (14 ± 1, p = 0.006) (Figure 18 d). *Tfam* cko running and non-running mice showed comparable numbers of branch points. Furthermore, TFAM-depleted neurons in the cko mice showed more branch points as compared to the WT mice in either non-running (18 ± 2 to 14 ± 1, p = 0.04) or under running conditions (16 ± 1 to 11 ± 1, p = 0.00002) (Figure 18 d).

The typical arborisation complexity of an immature neuron at 21 dpi that does not get any stimuli caused by physical exercise is shown by the WT (GR) non-running mice (Figure 18 a, e) revealing a dendritic tree which is mostly marked by some leftovers of basal dendrites, several branch points and short dendritic segments. Neurons that were generated under running conditions exhibit, in WT animals as well as in cko mice, a more mature dendritic arborisation compared with cells in non-running animals (Figure 18 e'', e'''). Nonetheless, TFAM-deficient newborn neurons failed under both conditions to develop a dendritic tree that reaches the WT complexity level (Figure 18 e, e').

In summary, under non-running conditions, three weeks old TFAM-deficient cells were already different compared to their corresponding control mice cells. The overall appearance of neurons generated in cko mice was less mature than WT cells with neurons showing multiple short dendrites. Remarkably, the morphology differences between WT mice and cko mice adult-born neurons became more prominent in the context of a physiological maturation stimulus i.e. voluntary wheel running. Neurons of cko mice displayed morphological deficits compared to WT mice as they had a reduced total dendritic length and arborisation as well as an increased amount of branch points. In general, physical activity can significantly increase dendritic length and arborisation complexity in newborn neurons of WT mice and cko animals. Interestingly, running conditions can improve the morphology of TFAM-deficient neurons at least to the level of WT non-running mice. Therefore, physical activity was demonstrated to partly rescue the TFAM depletion phenotype.
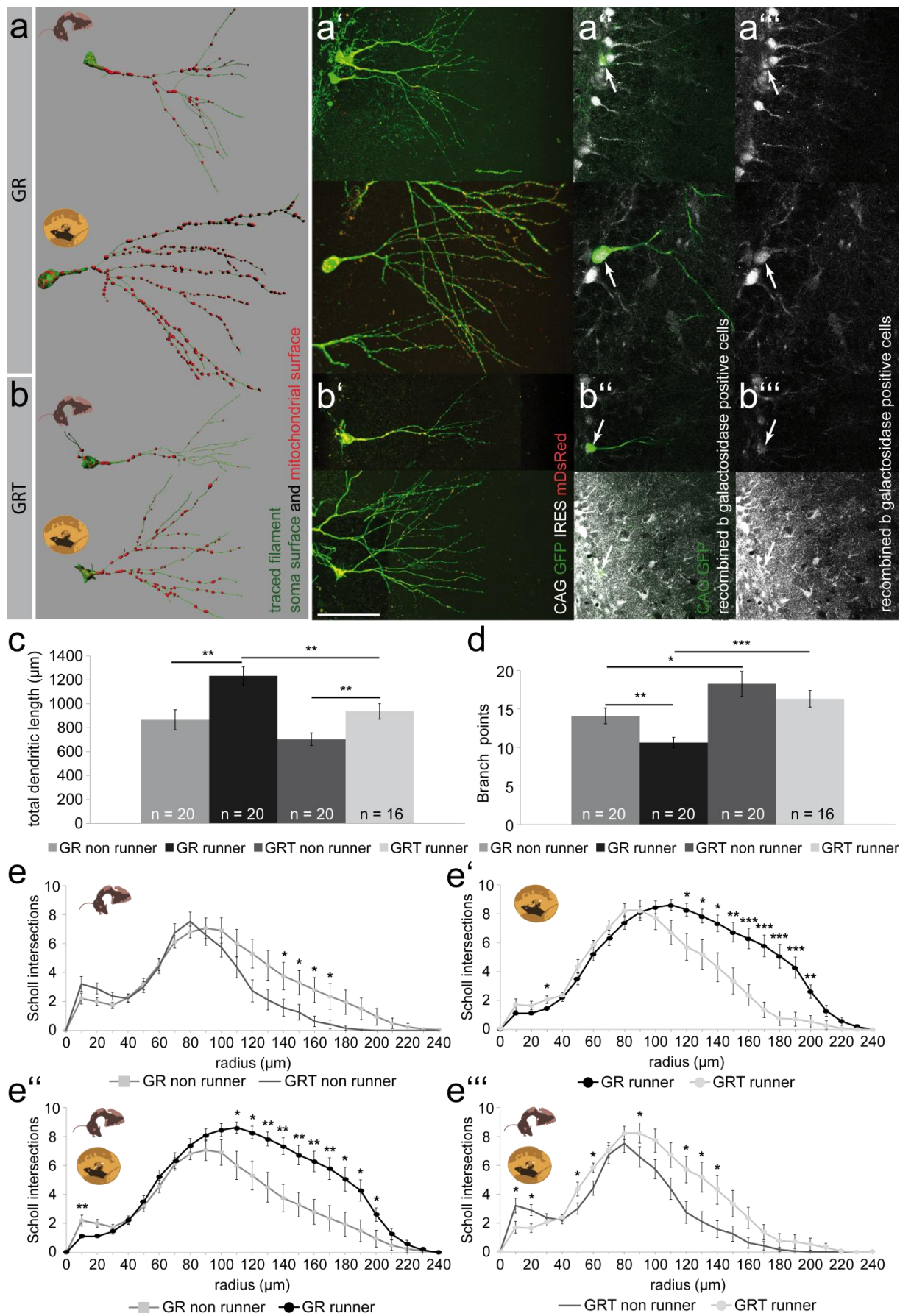
Figure 18 Neurons generated by TFAM-depleted neuronal stem cells evolve morphological deficits during maturation that can be improved but not rescued by stimulation through physical activity. GLAST::CreERT2 x

R26R x *Tfam*^loxP/loxP (GRT) and GLAST::CreERT2 x R26R (GR) mice were either housed under standard conditions or with an additional running wheel, for one week prior CAG GFP IRES mDsRed virus transduction and afterwards until the animals were sacrificed. (a, b) Whole cell morphology of (a) non-running and running GR mice, and (b) non-running and running GRT mice recreated using the GFP signal and the mitochondrial integrated DsRed signal applying Imaris 7.5 software analyses. (a', b') Confocal microscopy images of exemplary retroviral (CAG GFP IRES mDsRed) targeted cells that were used for analyses. (a'', b'') Co-staining with β-gal to detect recombined virus transduced cells. Single plane images merged and only β-gal staining (a''', b'''). White arrows are indicating the soma of the recombined exemplary cells. Corresponding images were taken with same microscopy settings. Intensity differences in β-gal are due to antibody penetration. (c) Mutant mice showed relatively less cell length compared with controls under running or non-running conditions. Running increased total dendritic cell length in WT and cko mice. (d) TFAM-deficient cells have more branch points than WT cells, while in cko as well as in WT running decreased the number of branch points, leading to a more mature morphology. (e) Enhanced arborisation complexity due to physical exercise as visualized by the number of Scholl intersections at distinct distances from the soma was also obvious in TFAM-depleted cells, however not as much as regarding the controls. (e'-e''') Depicted is the comparison between Scholl analyses of control or mutant non-running and running mice. n = 16-20; x = 4-5. Mean ± s.e.m.; *p < 0.05, **p < 0.01, ***p < 0.001. Scale bar 50 µm.

4.3.2 Physical activity can increase mitochondrial content in WT newborn neurons but fails to do so in TFAM-deficient mice

Physical exercise is known to increase mitochondrial biogenesis in murine heart tissue (Viña et al., 2009) and in two weeks old C57 BL6 hippocampal adult-born neurons (Dietrich et al., 2008; Steiner et al., 2011, Kathrin Steib, unpublished data). Therefore, the question arose if TFAM deficiency in three weeks old newborn SGZ neurons alters mitochondriogenesis triggered by running.

To this end the mitochondrial surface was analyzed along the dendrites and within the soma according to the fluorescent signal of the incorporated mDsRed in retrovirally labeled neurons at 21 dpi. For normalization of the mitochondrial number and volume per dendritic length or soma volume the reconstruction of the whole cell morphology was used. The following data are normalized, unless otherwise stated as total volume or total number. In contrast to the significantly altered total dendritic length (Figure 18), the total soma volume was not significantly changed between WT and *Tfam* cko mice, neither under running nor non-running conditions (data not shown).

Mitochondria were analyzed in two different compartments of the neurons: either along the whole dendritic filament or in the area of the soma and shaft.

Under standard housing conditions, there was no change detectable in mitochondrial number between neurons of WT mice or *Tfam* cko mice (Figure 19 b, c). There was also no difference regarding total mitochondrial number (WT non-running: 150 ± 28 versus cko non-running: 106 ± 15, p = 0.2, n = 17-18) or total mitochondrial volume (WT non-running: 849 ± 222 µm³ versus cko non-running: 871 ± 162 µm³, p = 0.9, n = 17-18) between WT and Tfam cko neurons in non-running mice.

However, the mitochondrial volume normalized to the soma size in neurons of cko mice was significantly raised with respect to neurons of WT animals (p = 0.048, Figure 19 b').

Upon physical exercise, newborn cells of control mice revealed a significant increase in mitochondrial number (p = 0.0003, Figure 19 c) as well as mitochondrial volume per dendritic length (p = 0.003, Figure 19 c'). Whereas, in the soma/shaft area of WT DG newborn neurons there were no differences observed in mitochondrial number or volume upon voluntary wheel running (Figure 19 b, b'). TFAM mutant neurons showed, upon running, no alterations in mitochondrial number or volume in the dendrites (Figure 19 c, c'), but a decreased mitochondrial volume in the soma/shaft area (p = 0.024, Figure 19 b') compared to neurons of non-running *Tfam* cko mice. Comparing WT neurons and TFAM mutant neurons under running conditions revealed significantly less mitochondria in the dendrites (number: p = 0.003, volume: p = 0.014, Figure 19 c, c') and soma (number: p = 0.003, Figure 19 b, b') of TFAM-depleted neurons.

The total mitochondrial content, as determined by the total number of mitochondria throughout the neurons, was significantly increased in WT mice by running conditions (WT non-running: 150 ± 28 versus WT running: 268 ± 24, p = 0.005, n = 13-18), while the running effect did not reach statistical significance regarding total mitochondrial volume (WT non-running: $849 \pm 222 \mu m^3$ versus WT running: $1357 \pm 228 \mu m^3$, p = 0.13, n = 13-18). This increase of mitochondrial content upon physical activity was not observed in *Tfam* cko mice, which maintained a total mitochondrial number (cko non-running: 106 ± 15 versus cko running: 153 ± 25, p = 0.1, n = 10-17) and total mitochondrial volume (cko non-running: $871 \pm 162 \mu m^3$ versus cko running: $861 \pm 196 \mu m^3$, p = 0.97, n = 10-17) comparable to the one in newborn neurons in the non-running TFAM mutant group.

In summary, physical activity increased mitochondrial content in newborn DG neurons of WT animals. As the mitochondrial density was particularly increased in the dendritic tree, but not in the soma/shaft area of WT neurons, it is likely that additionally produced mitochondria are distributed to the periphery to provide, e.g., energy for neuronal activity and plasticity along the dendrites. Concerning the TFAM mutant adult-born neurons there was no increased mitochondrial content detectable in the dendritic filament or the soma/shaft area after running. In contrast, there was a decreased mitochondrial volume density in the soma region. This suggests that the cell already contains its maximum of mitochondria and running induces a redistribution of the existing mitochondria. Thus, TFAM deficiency affects the capability of newborn neurons to increase their mitochondrial content according to their functional needs.

Mitochondrial dysfunction can impair mitochondrial dynamics which causes unbalanced fractions of fragmented or elongated mitochondria (Youle and van der Bliek, 2012). Thus, mitochondrial morphology was investigated in the following.

CAG GFP IRES mDsRed virally targeted TFAM-deficient and control adult-born neurons under non-running or running conditions were analyzed at 21 dpi. Dendritic filaments in the middle part of the dendritic trees were used to manually examine mitochondrial length. The classification of the measured mitochondrial length into fragmented, medium sized, medium large or even tubular did not reveal any significant shift of the mitochondrial size distribution (Figure 20 a).

Taken together, physical activity is increasing mitochondrial density in WT mice but is not affecting mitochondrial morphology in 21 dpi newborn neurons of WT mice or cko mice.
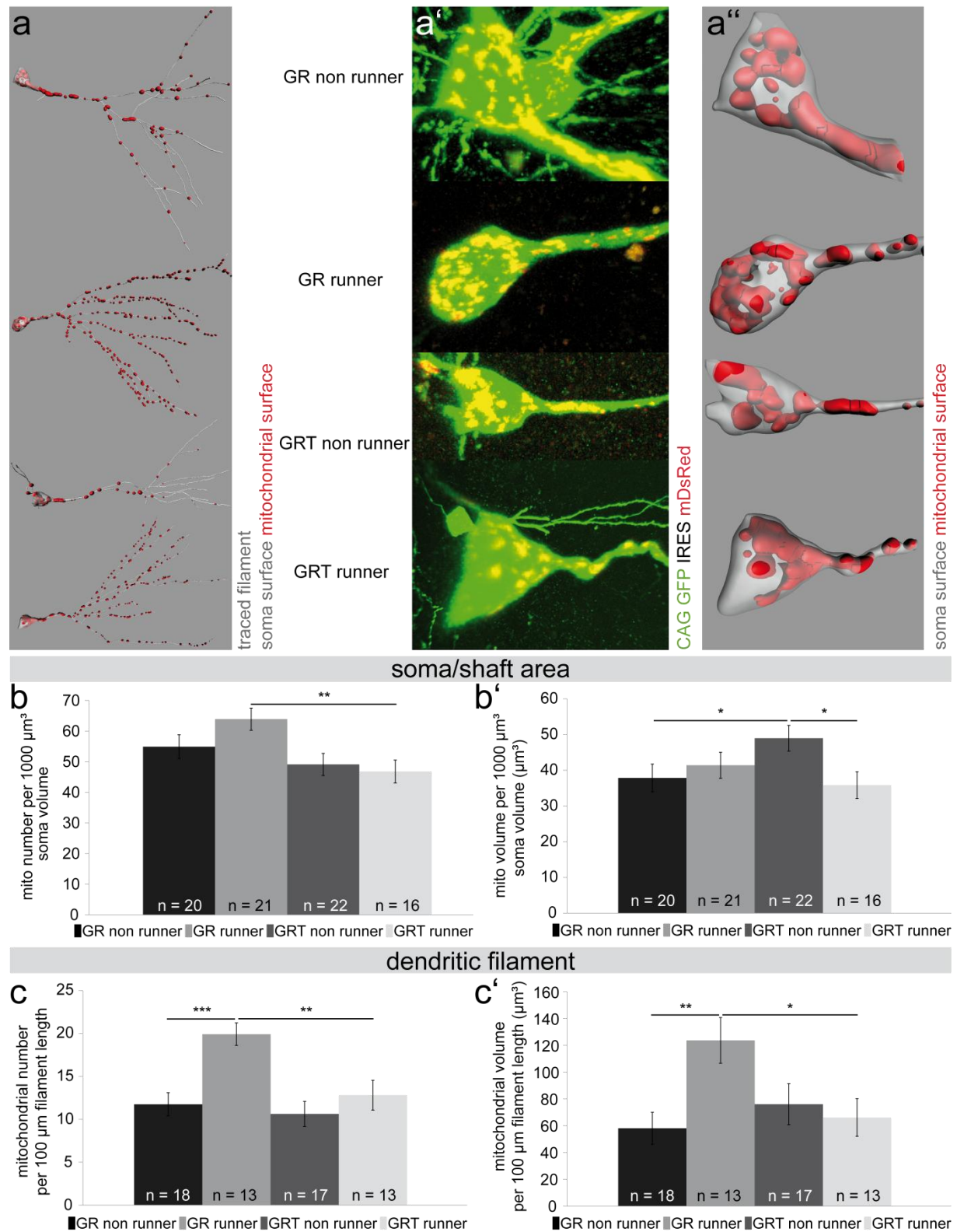
Figure 19 Mitochondrial volume and number per dendritic filament are increased by physical activity in WT but not in TFAM-depleted newborn neurons. Analysis of mitochondrial content in virally transduced (CAG GFP IRES mDsRed) 21 dpi newborn neurons. GLAST::CreERT2 x R26R x *Tfam*^loxP/loxP (GRT) and GLAST::CreERT2 x R26R (GR) mice were housed under standard or running conditions. (a) Mitochondrial distribution and content in the whole cell of the experimental groups recreated using the GFP signal and the mitochondrial integrated DsRed signal applying Imaris 7.5 software analyses. The whole cell morphology is depicted in light grey to highlight the mitochondrial surfaces (red). (a') Confocal microscopy images of exemplary soma that were used for analyses.

Corresponding images were taken with same microscopy settings. (a'') Imaris 7.5 reconstruction of virally transduced cell soma as depicted in a'. (b) The mitochondrial number per 1000 µm³ soma volume was significantly higher in neurons of WT running mice than in cko running mice. (b') Note that the mitochondrial volume per 1000 µm³ soma volume was highest in cells of cko non-running animals. (c) Mitochondrial number and (c') mitochondrial volume per 100 µm dendritic length, analyzed in the whole dendritic tree/filament, was increased in neurons of WT running animals. n = 13-22; x = 4-5. Mean ± s.e.m.; *p < 0.05, **p < 0.01, ***p < 0.001. There are no scale bars, as cell and soma sizes were adjusted for visualization purposes. Note that the total soma volume was not altered between the four groups.
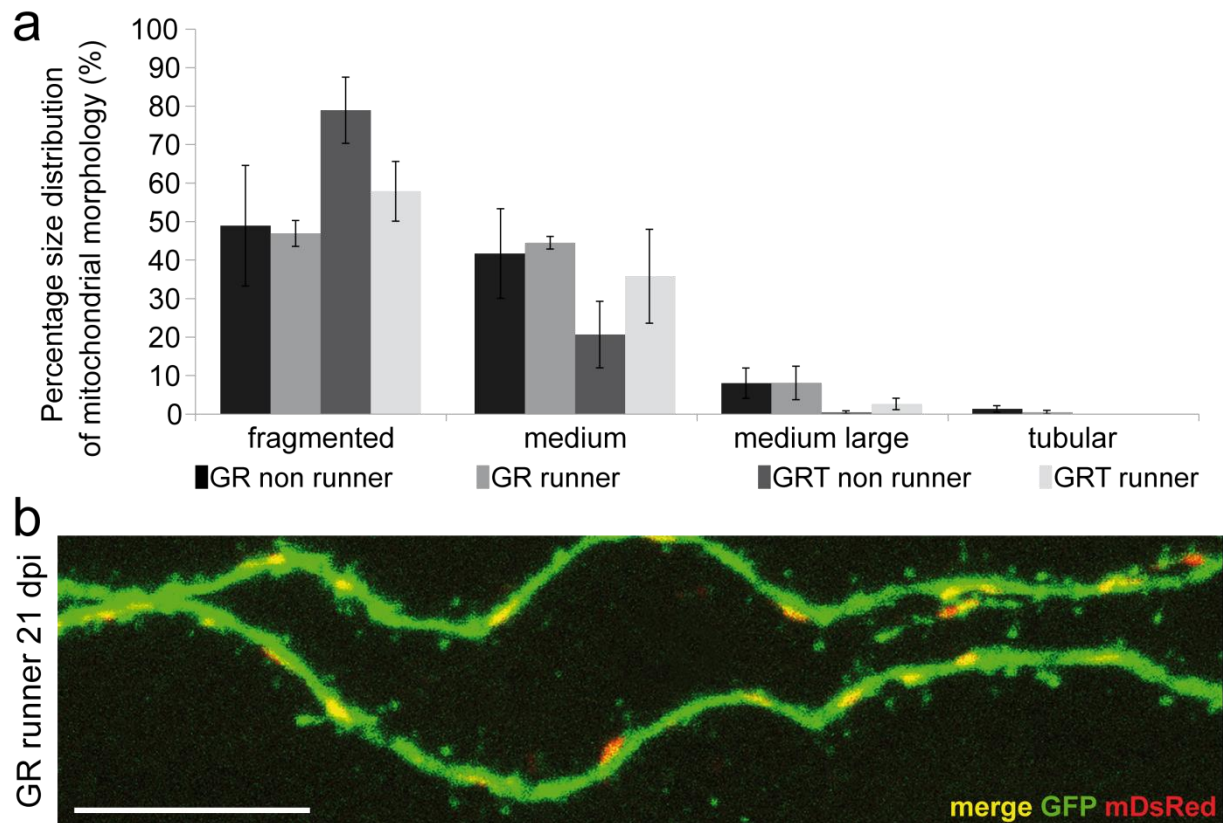
Figure 20 TFAM-depleted neurons do not show significant changes in mitochondrial morphology under running or non-running conditions at 3 weeks of age. Leica Application Suite AF analyses of mitochondria on dendritic filaments in 2/3 of the hippocampal molecular layer. Confocal microscopy pictures of GFP and mitoDsRed positive cells were taken with a 63 times glycerol objective and an additional 5 times zoom. (a) Mitochondria classified into different groups according to their longest diameter were not significantly different distributed therein. fragmented: < 1 µm, medium: 1 - 2 µm, medium large: 2 - 3 µm, tubular: > 3 µm. (b) Exemplary confocal image of a 21 dpi running WT animal filament, showing the expression of GFP and the mitochondrial localized mDsRed. 7 to 10 cells per animal and 3 to 4 mice per group were analyzed. Mean ± s.e.m.; **p < 0.01, ***p < 0.001. Scale bar 10 µm.

4.3.3   TFAM deficiency does not alter spine density in adult-born neurons

Spines are the morphological correlates of excitatory glutamatergic synapses (McKinney, 2010). They develop as protrusions along the dendritic filaments (Yuste and Bonhoeffer, 2004). The formation of dendritic spines in adult-born DG neurons starts in week three and increases during further maturation of the cell (Toni et al., 2007; Zhao et al., 2006). Spine density is extending during neuronal

maturation (Piatti et al., 2011). Spines can be classified into different categories as filopodia, thin, stubby or mushroom spines according to their stability, morphology and maturation level (Petrak et al., 2005).

To investigate whether TFAM deficiency affects formation or maintenance of dendritic spines CAG GFP IRES mDsRed virally targeted adult-born neurons of WT mice or cko mice were analyzed at 21 dpi. Dendritic filaments in the middle part of the molecular layer were used to determine spine density and the percentage of mushroom morphology.

Newly generated neurons of WT mice show no increase of spine density upon voluntary wheel running (Figure 21 b). A trend towards increased spine density was detectable in neurons of non-running versus running TFAM mutant mice (non-running: 2 ± 0.2 versus running: 4 ± 0.9, $p = 0.06$, Figure 21 b). The fraction of spines with mature mushroom-like morphology was comparable between all groups (Figure 21 b), although WT neurons showed a trend towards more mushroom-like spines under running conditions (non-running: 2 ± 0.8 % versus running: 4 ± 0.4 %, $p = 0.07$).

In summary, comparing non-running versus running mice within the WT or the *Tfam* cko mice group, physical activity did not significantly affect spine density and morphology in 21 dpi adult-born neurons. Nevertheless, in WT neurons the maturation level of spines, but not the density, is slightly increased. Additionally, TFAM depletion did not induce significant differences in spine content and morphology. However, physical activity appeared to enhance spine density, but not morphology maturation, in TFAM-depleted neurons.
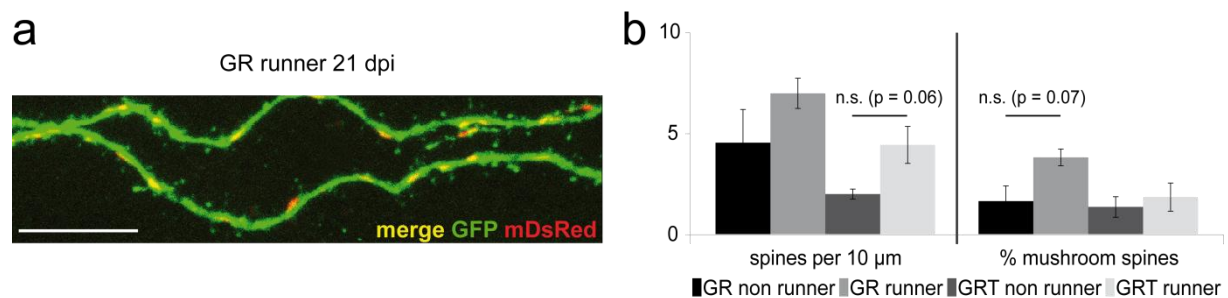
Figure 21 TFAM-depleted neurons do not show significant changes in spine density and morphology under non-running or running conditions at 3 weeks of age. Leica Application Suite AF analyses of dendritic spines on dendritic filaments in 2/3 of the hippocampal molecular layer. Confocal microscopy pictures of GFP-positive cells were taken with a 63 times glycerol objective and an additional 5 times zoom. (a) Representative confocal image of 21 dpi running WT mice filaments, showing the merge of the expression of GFP and mDsRed. (b) At 21 dpi the density of spines per 10 µm dendritic filament and the percentage of mushroom spines (diameter > 0.6 µm) was not significantly increased between non-running or running mice in either *Tfam* cko mice or WT animals. The average size of an examined dendritic filament was 39 µm in 21 dpi neurons. 7 to 10 cells per animal and 3 to 4 mice per group were analyzed. Mean ± s.e.m.; n.s. = not significant. Scale bar 10 µm.

4.3.4 TFAM depletion in neural stem cells leads to morphologically different mature neurons in running GLAST::CreERT2 x *Tfam*^{-/-} mice

Physical activity increases dendritic growth at 21 dpi (4.3.1). Newborn neurons become fully mature around six weeks of age (Tashiro et al., 2006), but the bulk of dendritic growth occurs during the first four weeks. To determine whether slower growing TFAM-deficient cells may reach full dendritic complexity over time or whether TFAM-depleted adult-born neurons show a permanent growth defect or delay or if they even start to degenerate, an additional later time point (42 dpi) was analyzed.

As described in chapter 4.3.1, the most prominent effect of TFAM deficiency on neuronal morphology was detected in 21 dpi adult-born neurons, which were generated under running conditions. Therefore, morphological analyses of six weeks old β-gal positive virally transduced cells (42 dpi time point) were conducted using the Imaris 7.5 software in cko and WT running mice.

Reconstruction of the dendritic filaments revealed a persisting deficit in total dendritic length and dendritic complexity of TFAM-deficient neurons. The dendritic length was significantly decreased in cko mice adult-born neurons compared to control neurons (WT: $1375 \pm 51\,\mu m$ versus cko: $1133 \pm 67\,\mu m$, p = 0.006). Hence, although there was a visible increase in cell length from 21 to 42 dpi in WT as well as in mutant animals (WT: 21 dpi $1227 \pm 73\,\mu m$ versus 42 dpi $1375 \pm 51\,\mu m$, cko: 21 dpi $937 \pm 66\,\mu m$ versus 42 dpi $1133 \pm 67\,\mu m$, Figure 18 c and Figure 22 d) the difference in dendritic length persisted between WT and TFAM mutant animals.

The number of branch points in neurons of running WT and cko mice was approximately 10 as shown in Figure 22 c. Thus, WT neurons had roughly the same amount of branch points at 21 (11) and 42 dpi (10), whereas neurons in cko mice diminished their branch points by one third from 16 at 21 dpi to 10 at 42 dpi (compare section 4.3.1).

The Scholl analyses, as depicted in Figure 22 f, showed a significantly reduced arborisation complexity in TFAM-deficient cells. Interestingly, the dendritic complexity is not changed in TFAM-depleted dendrites until approximately 150 μm from the soma, which could indicate that there were less branches built more distant from the soma or they were already degenerated.

Mitochondrial parameter such as volume and number per dendritic filament or soma shaft region did not differ between experimental groups (data not shown). In addition, the analysis of a dendritic segment in the range of two third of the molecular layer did not reveal any differences in mitochondrial size distribution (data not shown). This means that, compared with WT neurons, there were no alterations in the percentage distribution of fragmented, medium-sized, or tubular mitochondria within the examined dendritic segment.

To summarize, the dendritic morphology complexity remains significantly reduced in TFAM-deficient adult-born neurons under running conditions even at a time point of full maturation (Piatti et al., 2011; Espósito et al., 2005; Laplagne et al., 2006; Piatti et al., 2006; Zhao et al., 2006; Morgenstern et al., 2008). This is reflected in a decreased total dendritic length and a lower arborisation complexity. In contrast to these parameters the mitochondrial density and content is not altered. This is interesting, since in 21 dpi adult-born DG neurons there was a significant lower mitochondrial density and content detectable in running *Tfam* cko mice compared to WT neurons, suggesting less mitochondrial content in 42 dpi TFAM mutant neurons as well. This indicates an increasing mitochondrial biogenesis in maturing neurons even after TFAM depletion. In conclusion, TFAM-deficient adult-born neurons cannot compensate the growth defects with regard to total dendritic length, at least not until 42 dpi, but are somehow able to generate mitochondria in an amount comparable to WT neurons.
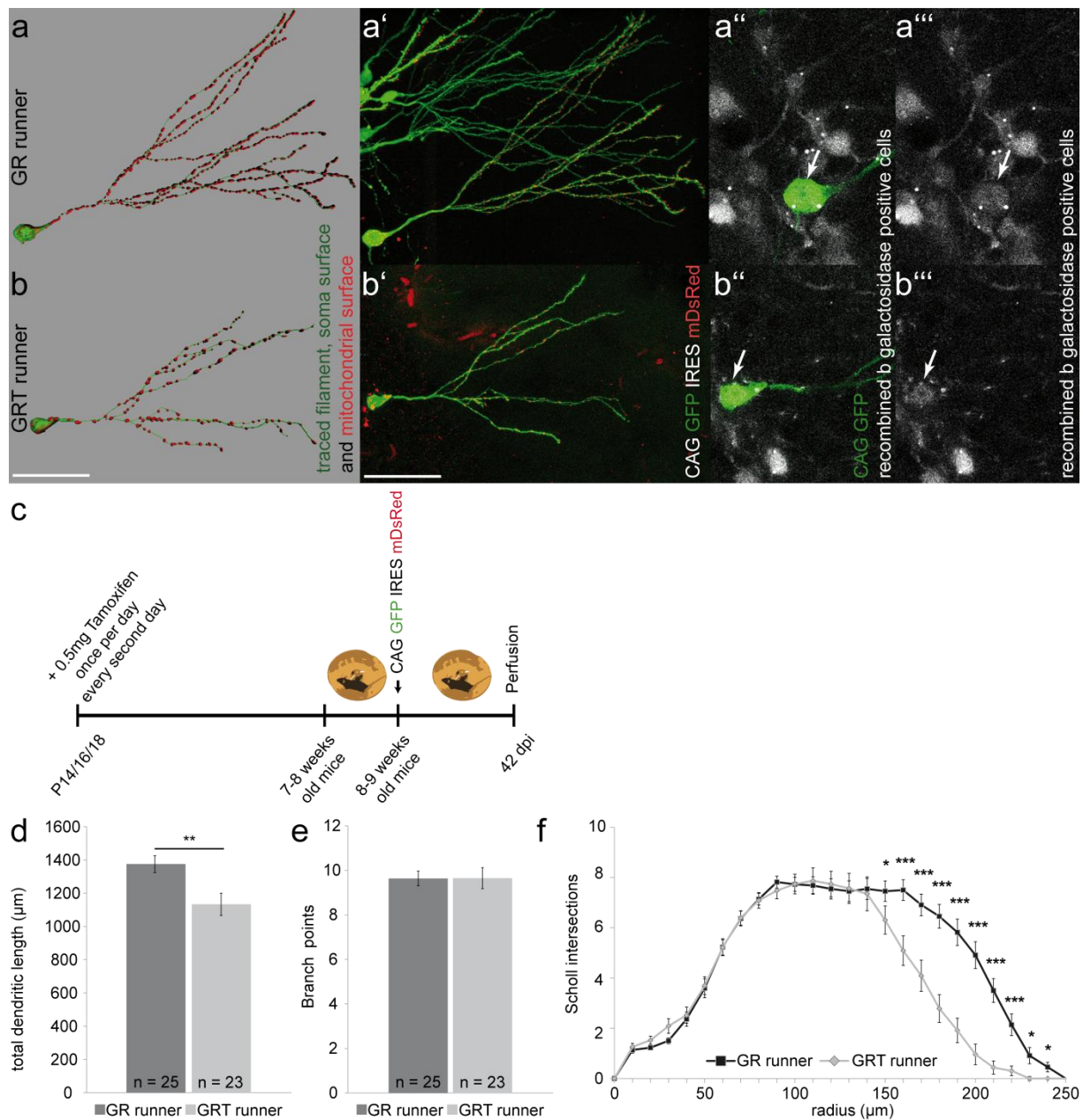
Figure 22 TFAM deficiency leads to neuronal impairment even in six weeks old cells under running conditions.

GLAST::CreERT2 x R26R (x $Tfam^{loxP/loxP}$) mice had free access to a running wheel one week before and 6 weeks after virus injection (CAG-GFP-IRES-mDsRed). Whole cell morphology analysis using Imaris 7.5 software to trace filaments and surfaces of (a) GR runner cells and (b) GRT runner cells. Confocal microscopy pictures of GFP and mitoDsRed positive cells that were also positive for β-gal. (a'-a''') Representative WT animal cell. Arrows are indicating β-gal signal (light grey) and therefore reporter recombination. (b'-b''') Representative mutant cell with a recombined *Tfam* and R26R locus. The arrows are highlighting the reporter positive soma. Corresponding images were taken with same microscopy settings. (c) Schematic experimental design. (d) Physical activity cannot compensate for the TFAM deficiency as six weeks old mutant cells showed a significantly reduced total dendritic cell length. (e) Branch point numbers were the same in mutant and control mice. (f) Scholl analyses revealed reduced arborisation complexity in TFAM mutant cells getting significant from 150 to 250 µm distance from the soma. n = 23-25; x = 4. Mean ± s.e.m.; *p < 0.05, **p < 0.01, ***p < 0.001. Scale bars 50 µm.

Since spine density extends during neuronal maturation (Piatti et al., 2011), it was investigated whether TFAM deficiency in mature adult-born neurons affects formation or maintenance of dendritic spines in CAG GFP IRES mDsRed virally targeted cells of WT mice or *Tfam* cko.

Interestingly, there was no difference in spine density and percentage of mushroom-like morphology detectable along dendritic segments in the middle part of the molecular layer comparing WT or TFAM mutant mice after physical exercise (Figure 23 b). Both, *Tfam* cko and control cells showed similarly increased spine density at the 42 dpi time point compared to the immature 21 dpi neurons (WT: 21 dpi 7 ± 0.7 versus 42 dpi 18 ± 0.9, p = 0.0002; or cko: 21 dpi 4.4 ± 0.9 versus 42 dpi 18.3 ± 0.9, p = 0.0001).

In summary, TFAM depletion does not induce significant differences in spine content and morphology even in mature neurons. Moreover, there is a constant increase in spine number during neuronal maturation in *Tfam* cko mice as well as in WT mice. This is an indication for a spine formation mechanism that might be largely independent of mitochondrial ATP in immature and mature neurons.
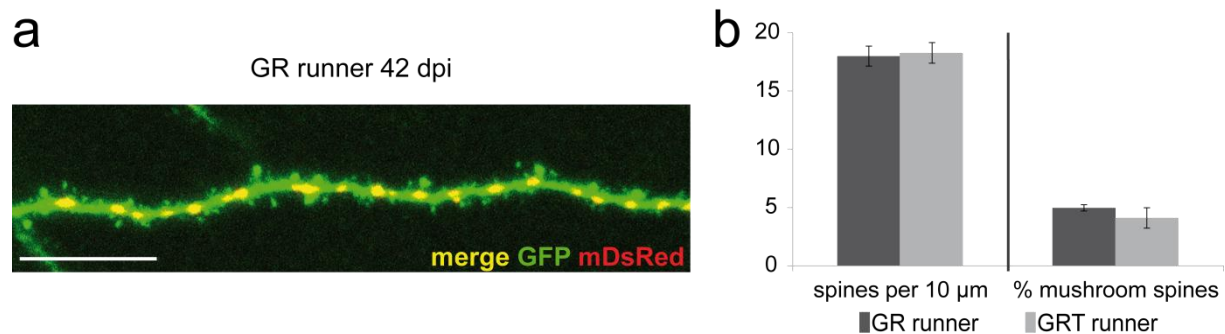
Figure 23 TFAM-depleted neurons do not show significant changes in spine density and morphology under running conditions at 6 weeks of age. Leica Application Suite AF analyses of dendritic spines on dendritic filaments in 2/3 of the hippocampal molecular layer. Confocal microscopy pictures of GFP-positive cells were taken with a 63 times glycerol objective and an additional 5 times zoom. (a) Representative confocal image of 42 dpi running WT mice filaments, showing the merge of the expression of GFP and mDsRed. (b) 42 dpi neurons of WT mice and *Tfam* cko mice reveal no differences in spine density or morphology (percentage of mushroom spines) under running conditions. The average size of an examined dendritic filament was 45 µm. 8 to 10 cells per animal and 4 mice per group were analyzed. Mean ± s.e.m. Scale bars 10 µm.

4.3.5 Acute TFAM depletion by retroviral targeting of newborn neurons in the DG led to impaired morphological development in 90 days old TFAM-deficient cells, but not in 28 and 42 dpi

New neurons in *Tfam* cko mice develop from TFAM-deficient stem cells and in a neurogenic nice that is partly formed by TFAM-deficient astrocytes.

To investigate the effect of acute TFAM deficiency in single cells during adult neurogenesis transgenic homozygous *Tfam*$^{loxP/loxP}$ mice were injected with retroviruses in the hippocampus at the age of two months. These retroviruses were encoding for GFP to visualize the morphology of the whole neuron and mDsRed to detect mitochondria. Additionally, in the case of TFAM depletion the virus was bicistronically encoding for GFP and Cre recombinase. The main advantage of the Cre virus approach is the ability to study the cell-autonomous effect of TFAM depletion in a healthy unaffected neurogenic niche. To increase the amount of transducable cells mice were running for one week prior to injection. Animals were sacrificed at 28, 42 or 90 dpi.

No significant morphology impairments were detected in four weeks old (28 dpi) adult-born neurons, as measured by total cell length, number of branch points and Scholl analyses (Figure 24 a-c). Furthermore, no reduction of dendritic cell length or increase of branch points was observed at 42 dpi (Figure 24 d, e). However, Cre transduction, and therefore TFAM depletion in 42 dpi neurons led to a slight increase of arborisation complexity (Figure 24 f). Significant differences between experimental groups became apparent at 90 dpi, with a significant reduction in dendritic length (GFP: 1441 ± 55 µm versus Cre: 1234 ± 47 µm, p = 0.002, Figure 24 g), a trend towards a lower amount of branch points and decreased dendritic complexity (Figure 24 h, j).

As can be seen in Figure 24 l to m' the mitochondrial content as determined by number (Figure 24 n) or volume (Figure 24 o) per 100 µm cell length (including soma to dendritic ends) was not changed in TFAM-deficient 90 dpi neurons.

Taken together, acute TFAM depletion leads to a significant impairment of neuronal growth after three months of age without affecting the mitochondrial content, but most probably impairing mitochondrial function. There was no membrane blebbing, nuclear fragmentation, or beading of processes detectable. Moreover, a continual increase was measured as total dendritic length in TFAM-deficient neurons from 28 to 90 dpi (Figure 24 a, d, g). This implies that the difference in dendritic length was most likely caused by impaired growth rather than dying back of dendrites or neurodegenerative processes.
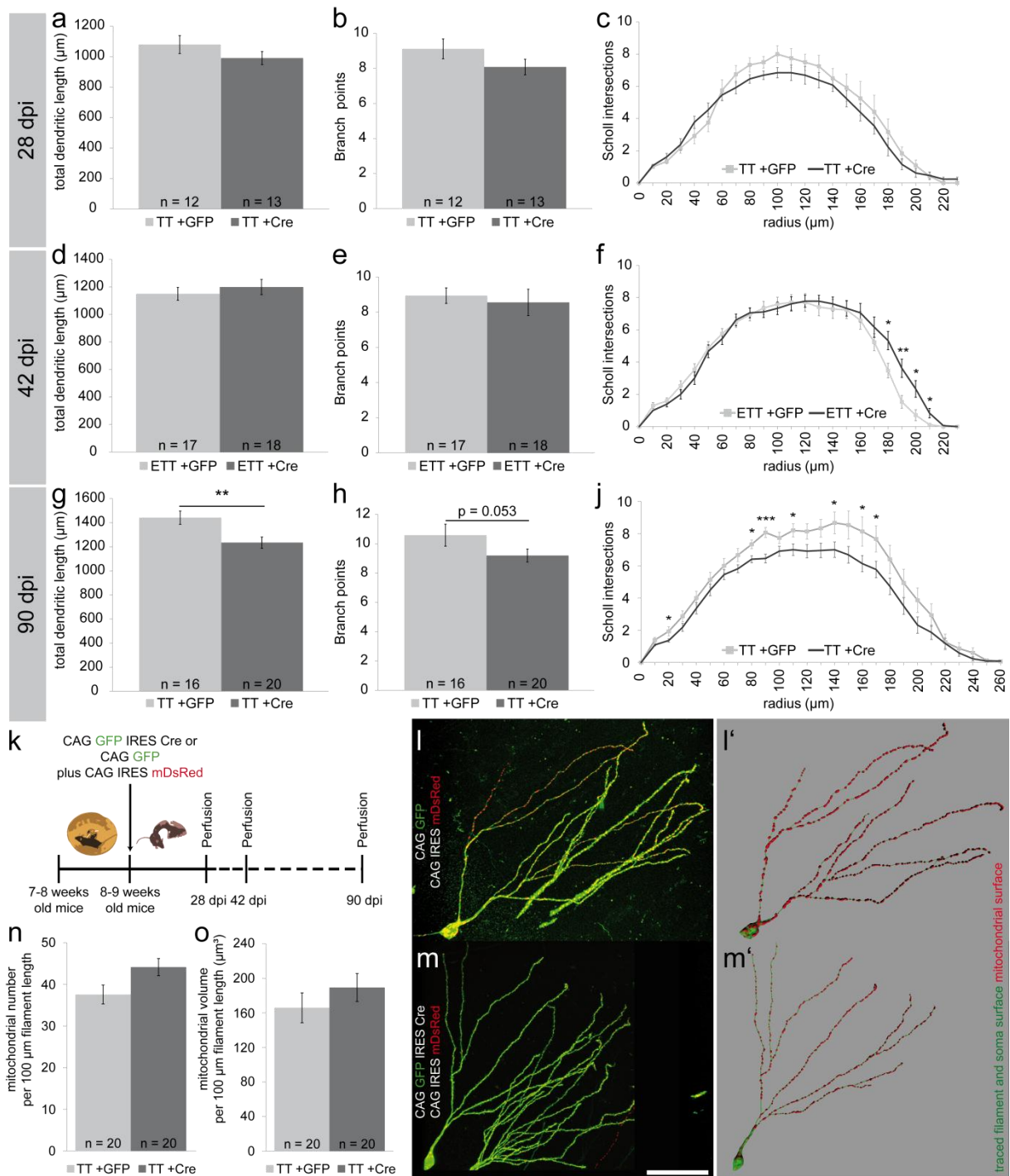
Figure 24 Transduction of *Tfam*[loxP/loxP] mice with a Cre expressing retrovirus leads to a delayed reduction or inhibition of dendritic growth in adult-born neurons. Imaris 7.5 morphology analyses of CAG GFP IRES Cre or control (CAG GFP) virus targeted DG neurons at 28, 42 and 90 dpi of *Tfam*[loxP/loxP] mice. CAG IRES mDsRed was used to visualize mitochondria. At 28 dpi there were no changes in (a) total dendritic length, (b) the number of branch points, or (c) the arborisation complexity depicted as Scholl analyses. (d-f) At 42 dpi analyzed cells were additionally EGFP reporter positive to determine differences in the intensity of both viruses used. This did not result in a strongly distinguishable GFP signal. No significant changes were detectable in (d) total dendritic length or (e) the amount of branch points. (f) Note that there was a significant increase in dendritic complexity in Cre transduced cells from 180 to 210 µm from the soma. At 90 dpi there was (g) a significant decrease of the total dendritic length in the TFAM-depleted adult-born neurons, while (h) the number of branch points was only slightly reduced. (j) The arborisation complexity in 90 dpi TFAM-deficient neurons was significantly

reduced. (k) Schematic overview of the experimental paradigm. (l, m) Confocal microscopy pictures of GFP and mitoDsRed positive cells. (l', m') Filament and surface tracing of exemplary cells. (l, l') Exemplary 90 dpi cell transduced with CAG GFP control virus and CAG IRES mDsRed. (m, m') 90 dpi TFAM-depleted neuron recombined and birthdated by CAG GFP IRES Cre and CAG IRES mDsRed. Non-significantly changed (n) mitochondrial number or (o) volume per 100 µm dendritic length of 90 dpi newborn neurons. Corresponding images were taken with same microscopy settings. n = 12-20; x = 4-5. Mean ± s.e.m.; *p < 0.05, **p < 0.01, ***p < 0.001. Scale bar 50 µm.

4.4   Up-regulation of glial fibrillary acidic protein caused by a TFAM-deficient astrocytic population

The recombination of Tamoxifen-treated GLAST x $Tfam^{loxP/loxP}$ x EGFP or R26R mice takes place in nearly all radial glial cells and a large part of the astrocytic population (Mori et al., 2006). In the following section the focus was on the recombined astrocytes.

Analyzing brain sections from young recombined TFAM-deficient mice at the age of two, four or six months did not reveal signs of astrocytic cell death (data not shown). However, astrocytes appeared to have an increased expression of the intermediate filament and reactive gliosis marker GFAP. To further investigate the effect of TFAM depletion in astrocytes, young recombined TFAM-deficient reporter positive mice were analyzed by immunohistochemistry at the age of four months. The regions that were analyzed are the hippocampus and the cortex. The cortex was included as one of the regions with a high amount of GFP-positive cells showing an astrocytic morphology and a region of nearly no GFAP-expression under physiological conditions (Hinkle et al., 1997).

As illustrated in Figure 25 a, $Tfam$ cko mice show significantly more GFP-positive cells with an astrocytic morphology in the molecular layer of the hippocampus than control mice (WT: 0.85 ± 0.08 cells per 100000 µm³ versus cko: 2.12 ± 0.38 cells per 100000 µm³, p = 0.017), suggesting an increased proliferation of recombined astrocytes in the molecular layer. In four months old young recombined $Tfam$ cko mice, which received daily BrdU injections for seven consecutive days and were sacrificed on day eight (compare section 4.2.1), there were no GFP and BrdU double positive astroglial cells detectable in the molecular layer (data not shown). Indicating that expansion of the astroglial population took place at earlier stages and was not the result of permanent gliogenesis. To analyze whether these GFP-positive cells were additionally remarkable regarding their reactivity potential, their GFAP-expression was examined. Many hippocampal astrocytes in control mice already express GFAP (Hinkle et al., 1997). However, there was a significant increase in GFP/GFAP double positive astrocytes in mutant mice (WT: 0.76 ± 0.07 cells per 100000 µm³ versus cko: 1.98 ± 0.41 cells per 100000 µm³, p = 0.027; Figure 25 a).

In contrast to the hippocampus there was virtually no GFAP-expression in the cortex of WT mice, only 10 % of all counted astrocytes (composed of all GFP, GS, and GFAP astroglial cells) contained GFAP. Whereas a strong increase of GFAP-positive astrocytes could be observed in the cortex of mutant animals (cko: 74.9 ± 6.1 % versus WT: 9.7 ± 2.4 %, p = 0.001, Figure 25 b). Not only the total amount of GFAP-positive cells, but also the proportion of GFAP/GFP double positive cells was significantly increased from 2 % to 37 % of all counted astrocytes (p = 0.00003, Figure 25 b), while the density of the GFP population remained unchanged.

GS, a general marker for astrocytes (Kozlova et al., 1993), was included to detect the non-recombined GFAP negative astrocytes in particular in the cortex of WT animals. The total amount of all included astrocytes in this analysis was determined by summing up all counted GS, GFP, and GFAP-positive cells in the cortex and each astrocytic subpopulation was normalized to the total amount of counted astrocytic cells. More than 90 % of all counted astrocytes in the cortex were positive for GS (Figure 25 b), and more than 96 % of all counted astrocytes in the molecular layer expressed GS (data not shown). The GS counterstaining was also used to examine whether there was a general increase in the astrocytic population in the hippocampal molecular layer or the isocortex, what could be denied (Figure 25 b, e-h'), since the total numbers of astrocytic cells were not altered (data not shown).

During inflammation or seizure astrocytes react with a change in properties resulting in a reactive gliosis, which gives an indication of a change in the healthy environment (Pekny and Nilsson, 2005). The observed increase in GFAP up-regulating cells is one characteristic of reactive gliosis, which is usually accompanied by hypertrophic cell morphology (Komitova et al., 2011) and reduced expression of GS (Ortinski et al., 2010). Neither hypertrophy nor changes in GS expression were detectable in TFAM mutant brain tissue (Figure 25 b, c-h').

To analyze whether an additional gliosis marker like Vimentin or inflammation marker like CD68 (reactive microglia) were up-regulated, quantitative RT PCR (qRTPCR) was conducted in ten months old GLAST::CreERT2 (x *Tfam*$^{loxP/loxP}$) mice in which recombination was induced at the age of two weeks. Figure 26 visualizes the results of the qRTPCR as fold induction mutant over control mouse hippocampal and cortical tissue normalized to the housekeeping gene RNaseP. None of the examined targets showed significant changes. *Tfam* was included to investigate *Tfam* mRNA reduction. No difference was detected, but as the non-recombined cells outnumber the TFAM-deficient cells this was not expected to show a significant reduction. Porin was used to check for the mitochondrial content, as it translates into a mitochondrial outer membrane pore protein. According to the Porin levels, the mitochondrial content was maintained at a constant level. CD68 and Vimentin, were used as gliosis marker as they are known to be up-regulated during reactive gliosis and inflammation

(Ortinski et al., 2010; Macauley et al., 2011). However, they were not significantly up-regulated in ten months old TFAM-deficient mice. The *in vivo* immunohistochemistry data suggested an up-regulation of GFAP in hippocampal and cortical astrocytes, as there were more GFAP-positive cells detectable in *Tfam* cko mice. No increase of GFAP mRNA was observed in cortical tissue, but, in hippocampal tissue there was a trend towards a doubling of GFAP mRNA (Figure 26).

In conclusion, TFAM deficiency in mice causes a strong up-regulation of GFAP in hippocampal and cortical astrocytes as measured by the increased amount of GFAP-positive cells. Interestingly, in the hippocampus there was not only GFAP but also the amount of recombined GFP-positive cells raised upon TFAM depletion. This suggests an increase in proliferation of recombined astrocytes; however, the period when such putative proliferation may take place remains unclear.
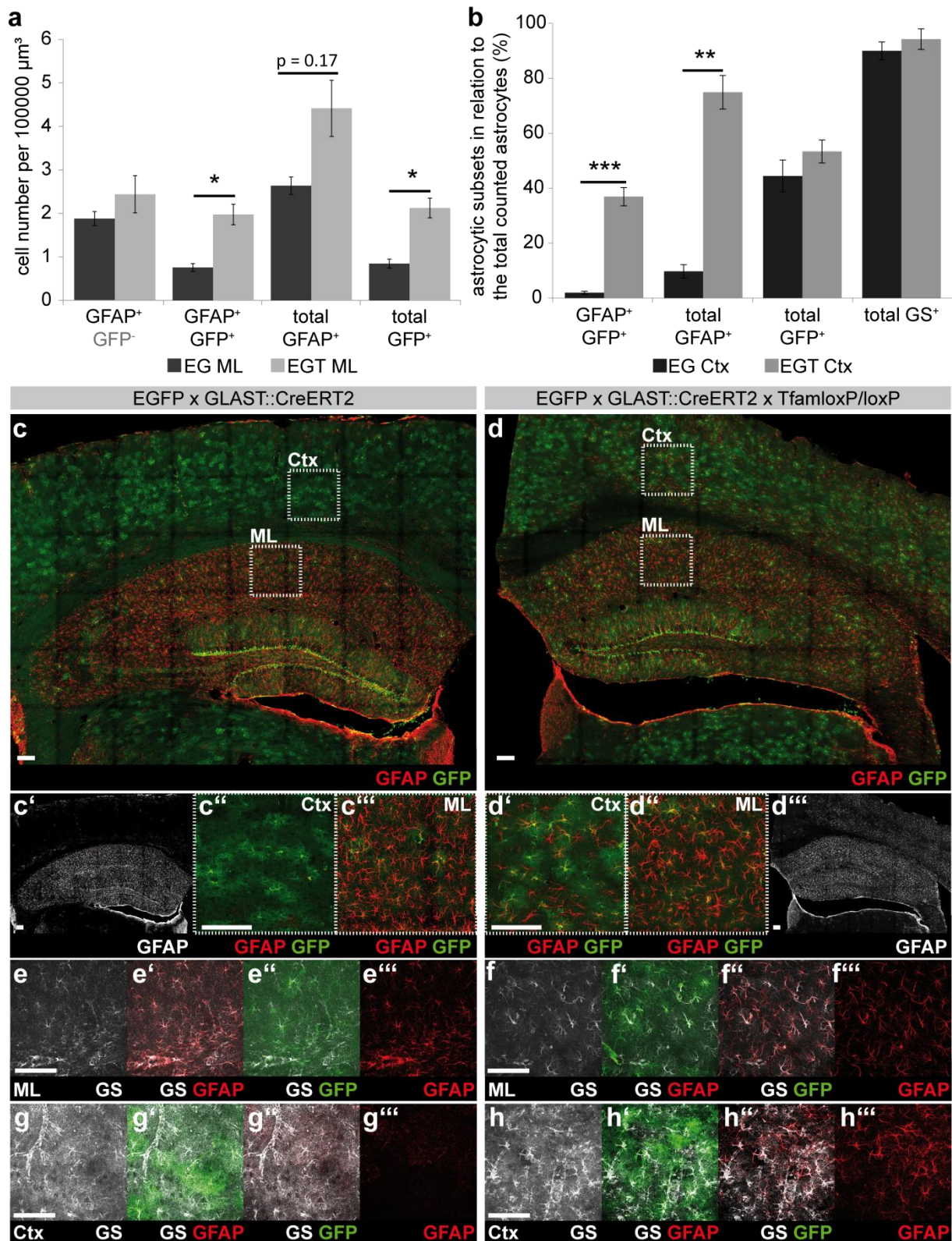
Figure 25 GFAP up-regulation in the cortex and hippocampus of 4 months old young recombined CAG-CAT-EGFP x GLAST::CreERT2 x (*Tfam*^loxP/loxP) mice. (a) Increased amount of GFP (reporter positive recombined cells) and GFAP/GFP double positive cells in the molecular layer of 4 months old mutant versus control mice (n = 4). Area that was used to count is illustrated by a dotted square in (c, d). Cell numbers were normalized to the volume of analyzed sections. (b) Percentage of astrocytic subpopulations based on total cell counts for GFAP, astrocyte-like GFP-positive cells, and GS (n = 3). (c) Exemplary picture of the forebrain region including the cortex showing a few GFAP-positive cells in WT mice in contrast to a strong up-regulation in the mutant cortex (d). (c') GFAP-expression in the control and mutant (d''') forebrain. (c'', c''') Close-up of the examined region in

the WT cortex and hippocampus as well as the mutant mice (d', d'') showing GFAP and GFP expressing cells. Representative confocal microscopy pictures of regions used for astrocytic subset percentage calculations: GS positive cells in the WT (e-e''') and mutant (f-f''') cortex co-stained for GFAP and GFP as well as in the WT (g-g''') and mutant (h-h''') hippocampus (ML). Ctx: cortex; ML: hippocampal molecular layer. Mean ± s.e.m.; *p < 0.05, ***p < 0.001. Scale bars 100 μm.
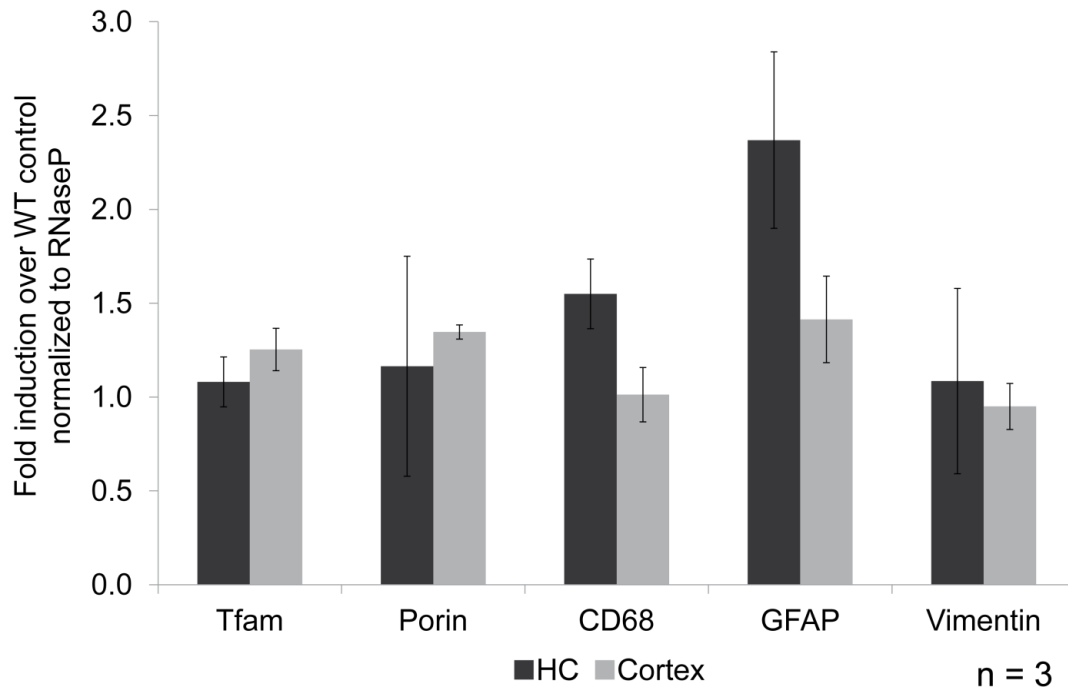
Figure 26 qPCR analysis of 10 months old young recombined GLAST::CreERT2 x (*Tfam*[loxP/loxP]) mice Quantitative real-time PCR analysis showing the fold induction of different targets over WT control normalized to the housekeeping gene RNaseP. *Tfam* mRNA is not reduced in *Tfam* cko mice tissue. *Porin* mRNA is not changed suggesting a constant mitochondrial content. CD68 is not increased in *Tfam* cko mice, which implies that there is no activation of microglia cells. The two reactive gliosis marker GFAP and Vimentin are also not up-regulated. However, a tendency towards an up-regulation of GFAP mRNA in the HC of *Tfam* cko mice was detected. Ctx: cortex; HC: Hippocampus. Mean ± s.e.m.

4.5 Behavioral phenotyping of the CAG-CAT-EGFP x GLAST::CreERT2 x (*Tfam*[loxP/loxP]) mice

In the following sections several behavioral aspects of the TFAM-deficient mice were investigated according to the brain regions with a high fraction of recombined GFP-positive cells (Figure 11). The rotarod (RR) examines putative deficiencies in motor coordination, balance and learning (Hamm et al., 1994) and is therefore particularly interesting because of the highly recombined Bergmann glia population in the cerebellum (Sausbier et al., 2004). Another way of assessing locomotor behavior is the open field (OF), which in addition allows interpretation of anxiety and exploration behavior of the examined TFAM-depleted mice (Prut and Belzung, 2003; Karl et al., 2003). Many TFAM-deficient cells were also accumulating in the OB (Figure 11) as there are constantly new neurons immigrating being generated by recombined SVZ stem cells (Alvarez-Buylla and Garcia-Verdugo, 2002). Therefore, the

sense of smell and the olfactory learning and recognition capability could be impaired. This aspect is addressed via the social discrimination (SD) test (Engelmann et al., 2011). Astrocytes throughout the brain and neurons in the neurogenic niches are affected by TFAM depletion. As astrocytes participate in the regulation of synaptic transmission basic nerve functions are possibly impaired, which are involved in pre-pulse inhibition (PPI) (Crawley et al., 2001). Therefore, the effect of TFAM deficiency on sensory gating was investigated by PPI. TFAM-deficient mice showed many defects in proliferation (4.2.1), and maturation (4.3.1) of adult-born hippocampal neurons implicating a possible dysfunction in hippocampal learning. The latter was assessed using the Water Cross Maze (WCM) test (Botreau and Gisquet-Verrier, 2010). Furthermore, deficits in adult neurogenesis are thought to be potentially important in the pathology of neuropsychiatric disorders such as depression and anxiety (Lee et al., 2012; Kheirbek et al., 2012; Sahay and Hen, 2007). The forced swim test was conducted to explore whether TFAM depletion-dependent impairment of adult neurogenesis leads to depression-like behavior. An overview of all cohorts that were examined in distinct behavioral test is depicted in Figure 27.

	Rotarod	Open Field	Pre-Pulse Inhibition	Social Discrimination	Water Cross Maze	Forced Swim Test	
4 months young recombined	–	–	–	–	✕	–	
7 months adult recombined	✕	✕	✕	✕	–	–	control mice:
9 months young recombined	–	–	–	–	–	✕	CAG-CAT-EGFP x TfamloxP/loxP
1 year young recombined	✕	✕	✕	✕	–	–	cko mice:
1 year adult recombined	✕	✕	✕	✕	–	–	CAG-CAT-EGFP x GLAST::CreERT2 x TfamloxP/loxP

Figure 27 Overview of all cohorts tested in different behavioral screenings. Mice were tested either young (P14/16/18) or adult (2 months of age) Tamoxifen-treated at distinct ages between 4 months and 1 year. Littermates were used and GLAST::CreERT2 negative animals were considered treated but non-recombined control mice.

To analyze the behavior, three cohorts were screened in RR, OF, PPI and SD. For an overview of the number of mice that were tested and their corresponding body weight see Figure 28 a. Interestingly, mutant mice tended to have less weight than control mice. This difference was highly significant in adult recombined one year old female mice (WT: 28.88 ± 1.12 g versus cko: 21.61 ± 1.9 g, p = 0.007, Figure 28 b).

The time points for testing were chosen according to proliferation deficits seen in the DG of *Tfam* cko mice (4.2.1) and behavioral phenotypes seen in other known TFAM-deficient mouse models (MitoPark and MILON mice) as discussed in section 3.2.4. Note that the latter were neuron specific

TFAM depletions, induced as soon as the expression of the Cre-driver started continuing until the death of the mice. MILON mice exhibited behavioral phenotypes at the age of five to six months (Sörensen et al., 2001) and the fact that in MitoPark mice the behavioral phenotype continues to worsen with increasing age (Ekstrand et al., 2007) led to the analysis of adult (four to nine months) and aged (one year old) GLAST::CreERT2 TFAM-deficient animals.

Two cohorts, including littermate controls, were Tamoxifen-treated at the age of eight weeks and were analyzed six months or around eleven months later. To target more GLAST positive cells and thereby increasing the load of mitochondrial dysfunction in the mutant mice, one cohort was Tamoxifen-treated during postnatal week three and was analyzed either four, nine, or twelve months later. The four months time point for the WCM analysis was chosen as there was a striking decrease in proliferation in four months old TFAM-depleted mice (4.2.1), which may result in a possible deficit in hippocampus-dependent learning tasks.
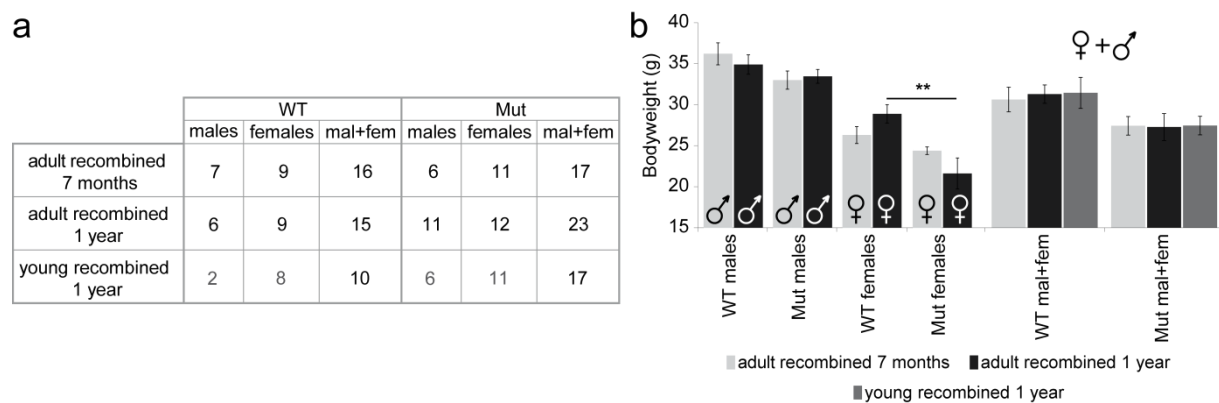
Figure 28 TFAM-depleted mice showed reduced body weight. (a) Number of tested animals in RR, OF, PPI and SD. As there were not enough WT males in the young recombined 1 year old animals these were analyzed as mixed mixed cohorts illustrated in grey numbers. (b) Overview of measured body weight of analyzed mice. Males and females separately for adult recombined cohorts. Note that the body weight is also depicted as mixed cohorts for all three groups. Mean ± s.e.m.; **p < 0.01.

4.5.1   Rotarod (RR): TFAM deficiency does not cause motor coordination defects

As shown by (Sausbier et al., 2004) cerebellar dysfunction results in impairment of the motor coordination as analyzed by RR. Taking the nearly complete recombination in Bergmann glia, which most probably also affect the adjacent Purkinje neurons, in the cerebellum of reporter positive TFAM-depleted mice (Figure 11), the question arises of whether the *Tfam* cko affects the cerebellar-dependent motor behavior.

The rotarod was used to study motor coordination of TFAM-deficient mice while taking advantage of the natural fear of falling. Usually, mice stay as long as possible on the rotating rod and are only

falling off if they cannot cope with the speed anymore. The rod is accelerating its speed from four to 40 rpm in 300 sec. Mice are tested for three consecutive trials taking five minutes each, interrupted by 15 min resting intervals. Usually mice improve throughout the different trials, while the latency to fall increases from trial to trial. There was a tendency towards an improved performance from trial 1 to trial 3 of adult recombined seven months and one year old as well as young recombined one year old cohorts tested (Figure 29 a, c, and e). None of them was significantly better than any other. Mice clinging to the rod making a passive turn was like falling, determining the end of a trial, and was counted as the number of total passive rotations throughout the whole experiment (Figure 29 b, d, and f). There was no behavioral phenotype in any of the analyzed parameters of the RR test, meaning that all mutant mice were able to perform this motor coordination test.

Taken together, TFAM depletion in astrocytes and radial glia-like stem cells does not result in motor coordination impairment.
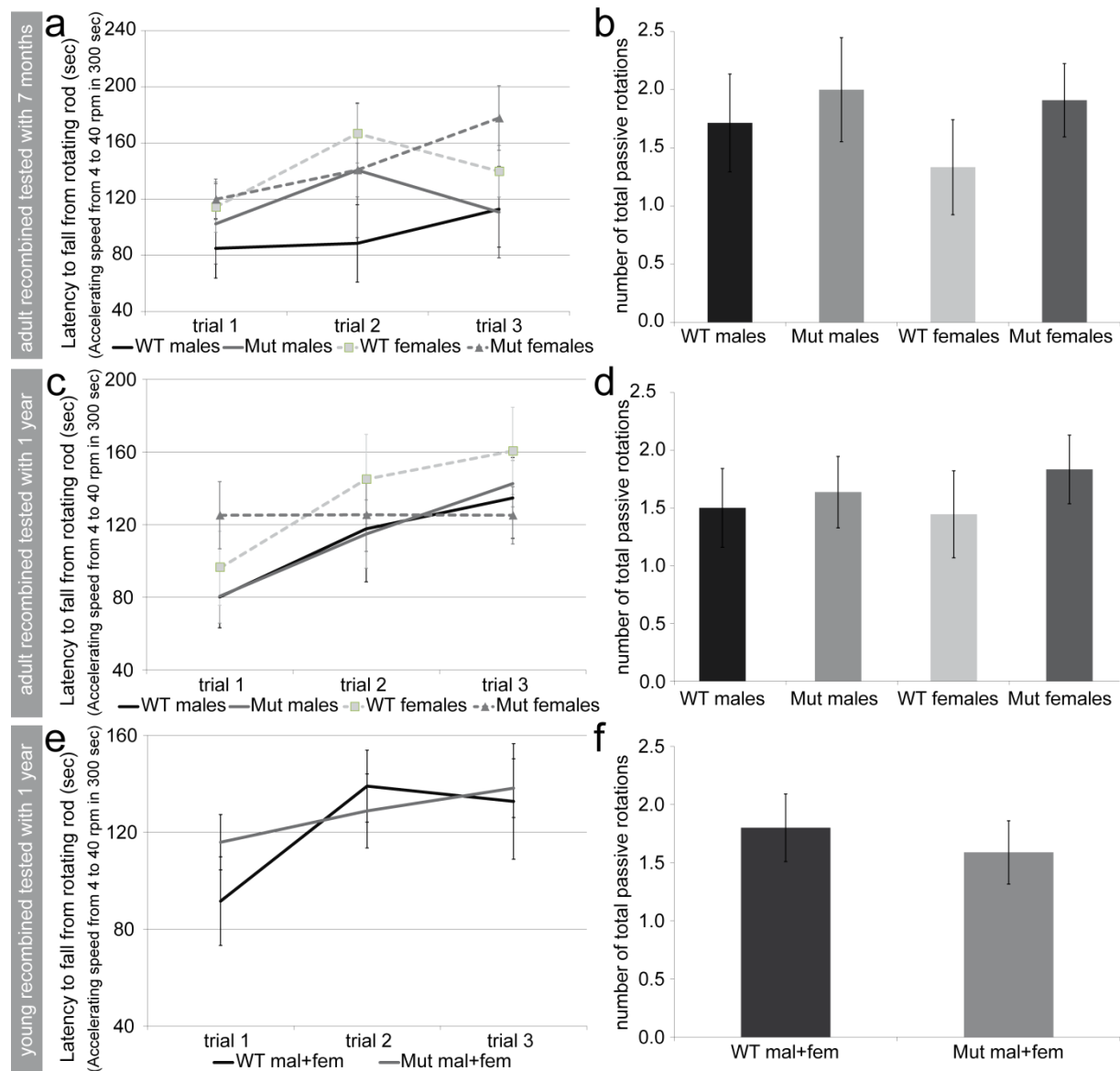
Figure 29 Rotarod testing showed no behavioral effect in TFAM-deficient mice in analyzed cohorts. (a, c, e) Depicted is the latency to fall from the rotating rod which is accelerating its speed from 4 to 40 rpm in 300 sec over the course of the experiment (trial 1, 2, and 3) as well as the total number of passive rotations during the whole experiment (b, d, e). Mean ± s.e.m.

4.5.2 No strong anxiety or locomotor deficiency detectable in TFAM-depleted mice in the Open Field (OF)

As illustrated by Figure 11 there are many regions including the cerebellum containing a lot of recombined TFAM-deficient cells, which might result in locomotor phenotypes. The open field test (OF) determines locomotor activity (distance travelled), vertical exploration (rearing activity) and anxiety-related behaviour (centre time) in a novel environment.

To examine the effect of TFAM deficiency on locomotor and general OF performance, mice were either recombined at two months of age (adult) or during postnatal week three (young). The latter

was used to increase the number of TFAM-deficient cells and thereby reach a higher level of mitochondrial dysfunction that might accelerate possible behavioral phenotypes.

Adult recombined mice that were tested at the age of seven months did not show significant differences regarding their travel distance measured over the time course of 20 min (Figure 30 a) or as total distance travelled (Figure 30 b). This was accompanied by an unchanged whole average speed (Figure 30 c). In addition, there were only minor differences in some of the other analyzed parameters like number and latency of (first) center entries, rearing frequency, or whole resting time.

Testing adult recombined mice at the age of one year did in general not show any striking differences in the travelled distance (Figure 30 d, e) and the other examined parameters. However, focusing on the female mutant mice they exhibited a significantly reduced whole arena average speed (WT: 15.49 ± 0.71 cm/sec versus cko: 13.30 ± 0.68 cm/sec, p = 0.043, Figure 30 f) as well as number of center entries (WT: 215.56 ± 16.53 versus cko: 161.69 ± 12.42, p = 0.015, data not shown). This was associated with a significantly decreased distance travelled in the center (WT: 5049.62 ± 377.5 cm versus cko: 3748.92 ± 276.65 cm, p = 0.01; data not shown). However, taking into account that there was no effect on the total distance travelled, not even during the different time intervals, these significant findings can be considered as minor effects that do not represent a strong phenotype.

Young recombined mixed cohorts of TFAM-deficient mice tested at the age of one year displayed no change in either the total distance travelled or the whole average speed (Figure 30 h, i). However, during the second five minute time bin of the total testing time of 20 min there was a clear reduction of the distance travelled (control 4930.81 ± 316.28 cm versus 4012.04 ± 179.19 cm, p = 0.011, Figure 30 g). These TFAM-depleted male and female mice also entered significantly less the center of the open field box (center entries: 171.53 ± 11.72) than equally Tamoxifen-treated siblings lacking the GLAST::CreERT2 having a non-recombined *Tfam* locus (219.70 ± 16.36, p = 0.022).

To summarize, the OF test revealed several small, mostly sex-dependent differences of mutant and WT mice. However, these differences were minor and did not include the main parameters whole average speed and total distance travelled. This led to the conclusion that TFAM deficiency does not result in a clear locomotor, exploration or anxiety-like behavioral impairment.
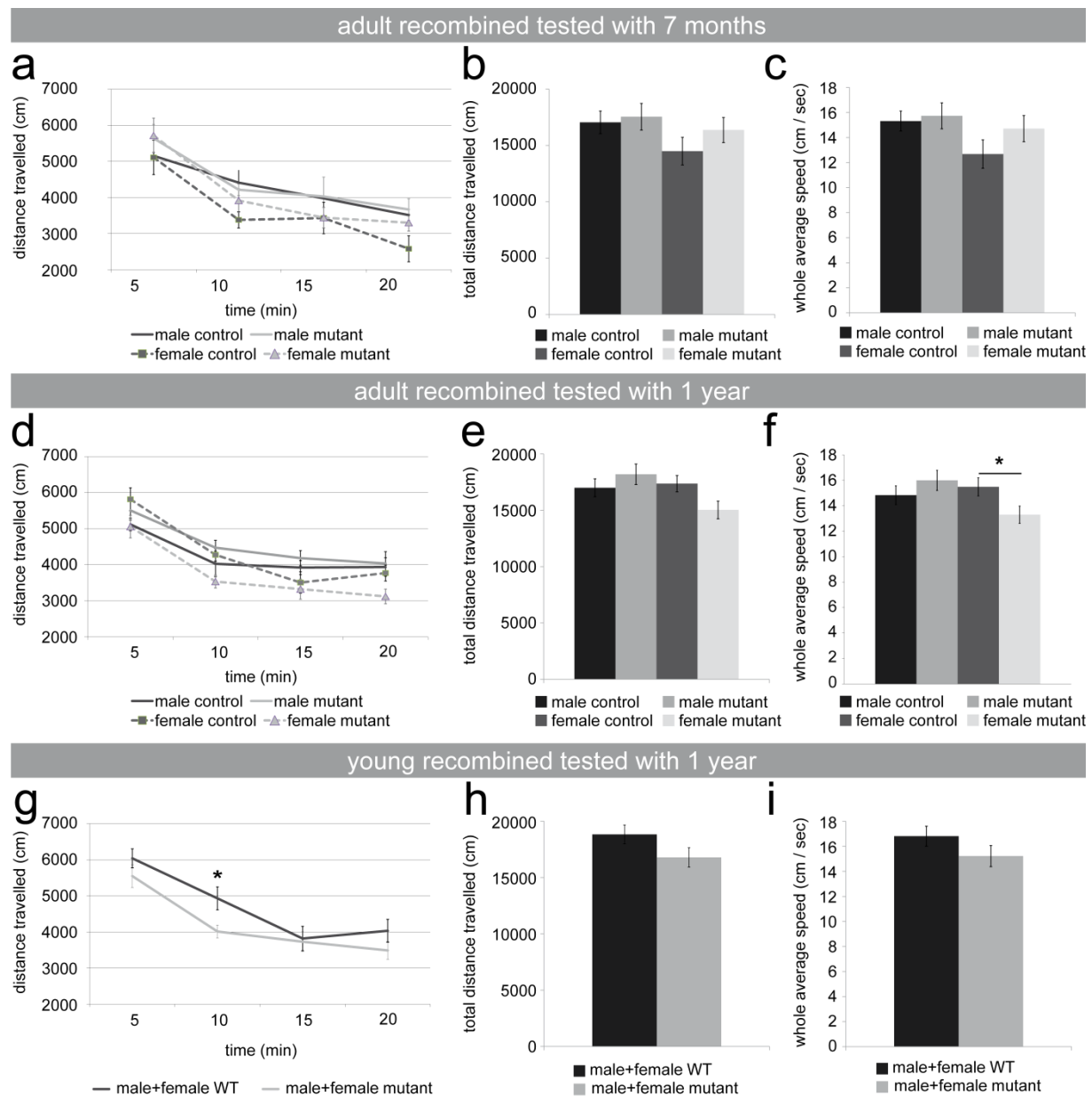
Figure 30 Open Field: TFAM-deficient mice in an anxiety related test. Three different cohorts were Tamoxifen-treated either at the age of 2 (young) or 8 (adult) weeks and were tested at the age of 1 or half a year. The adult recombined 7 months old cohort did not show any differences in either (a) the time course of distance travelled, or (b) the total distance travelled, neither in (c) the whole average speed. Analyzing an adult recombined cohort at 1 year of age revealed no changes in (d) distance travelled over the course of 20 min or (e) total distance travelled. (f) Female mutant mice were in average moving slower in the open field than control female mice. (g) Young recombined mice analyzed as a mixed cohort tested at the age of 1 year travelled significantly less in the first 10 min than control mice. No differences were observed concerning (h) total distance travelled or (i) whole average speed. Mean ± s.e.m.; *p < 0.05.

4.5.3 Pre-Pulse Inhibition (PPI) did not reveal any striking defects in basic neuronal function

PPI is based on the startle reflex, which is an involuntary reaction of an animal in response to a sudden acoustic stimulus. Under standard conditions mice show an inhibited reaction to an acoustic startle after being exposed to a non-startling pre-pulse (Marongiu et al., 2012). Therefore PPI was measured as the percentage of persisting startle reactivity after increasing pre-pulse intensities (67 to 81 dB). This behavioral test allows the analysis of basic properties of nerve function like impaired central nervous system inhibition (sensorimotor gating Braff and Geyer, 1990) including inter alia the forebrain, (Crawley et al., 2001), as one of the regions that is strongly affected by the GLAST::CreERT2 driven TFAM deficiency (compare Figure 11).

Neither the adult nor the young Tamoxifen-treated *Tfam* cko mice showed a distinct acoustic startle reactivity as depicted in Figure 31 a, c, and e. Moreover, no difference could be detected in PPI per burst (Figure 31 b, d, and f).

In summary, analyses of TFAM-deficient mice young or adult recombined at seven months or one year did not reveal any clear defects in their PPI, implying a functional neuronal network in TFAM mutant animals.
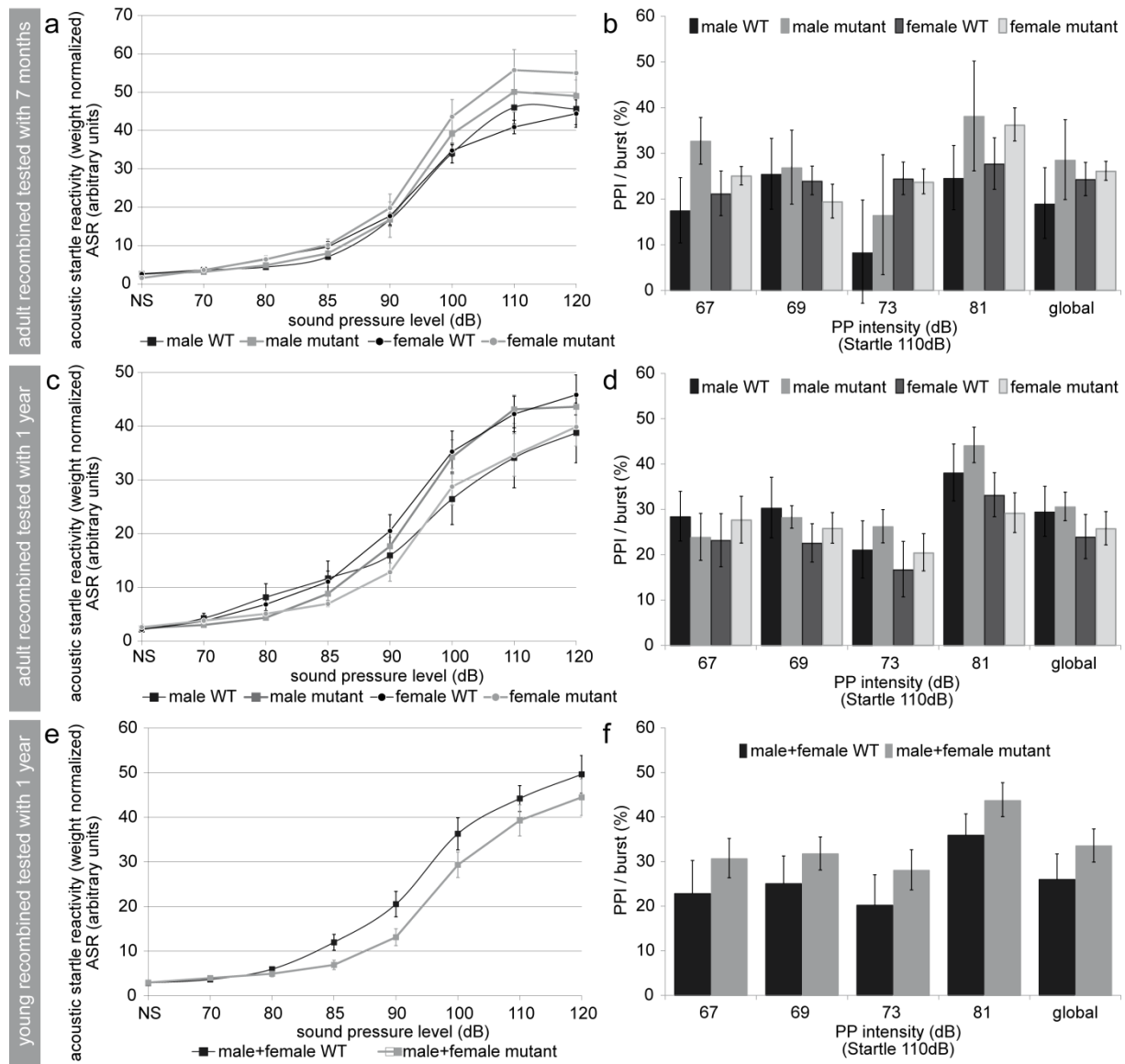
Figure 31 Acoustic startle and PPI were slightly changed in distinct cohorts. (a, c, e) The acoustic startle reactivity (ASR) measured in arbitrary units and normalized to the body weight of the mice was ascending with increasing sound pressure levels starting from 70 to 120 dB. There was no difference between the corresponding groups. (b, d, f) PPI (Pre-Pulse Inhibition) per burst in percentage depicted according to the raising PP intensity prior to a 110 dB startle showed a tendency towards a weakened PPI in the mixed 1 year old cohort, whereas no change could be observed in the adult recombined mice. Mean ± s.e.m.

4.5.4 Significant impairment of Social Discrimination (SD) capability in one year old young recombined TFAM-deficient mice

As was shown in Figure 11, one the largest fraction of recombined neurons in the GLAST::CreERT2 mouse model is generated in the SVZ and migrates into the olfactory bulb which in addition contains many recombined astrocytes. The social discrimination test is based on olfactory learning and short-term memory, employing the ability of mice to discriminate for a certain time between familiar and novel individuals (Engelmann et al., 2011; Engelmann et al., 1995).

During the sample phase mice were allowed to explore an unknown stimulus (individual). Following a fixed retention interval they were exposed to the same familiar subject as well as an unfamiliar mouse so they could choose which of them they wanted to explore more. Sniffing time was used as a measurement for exploration.
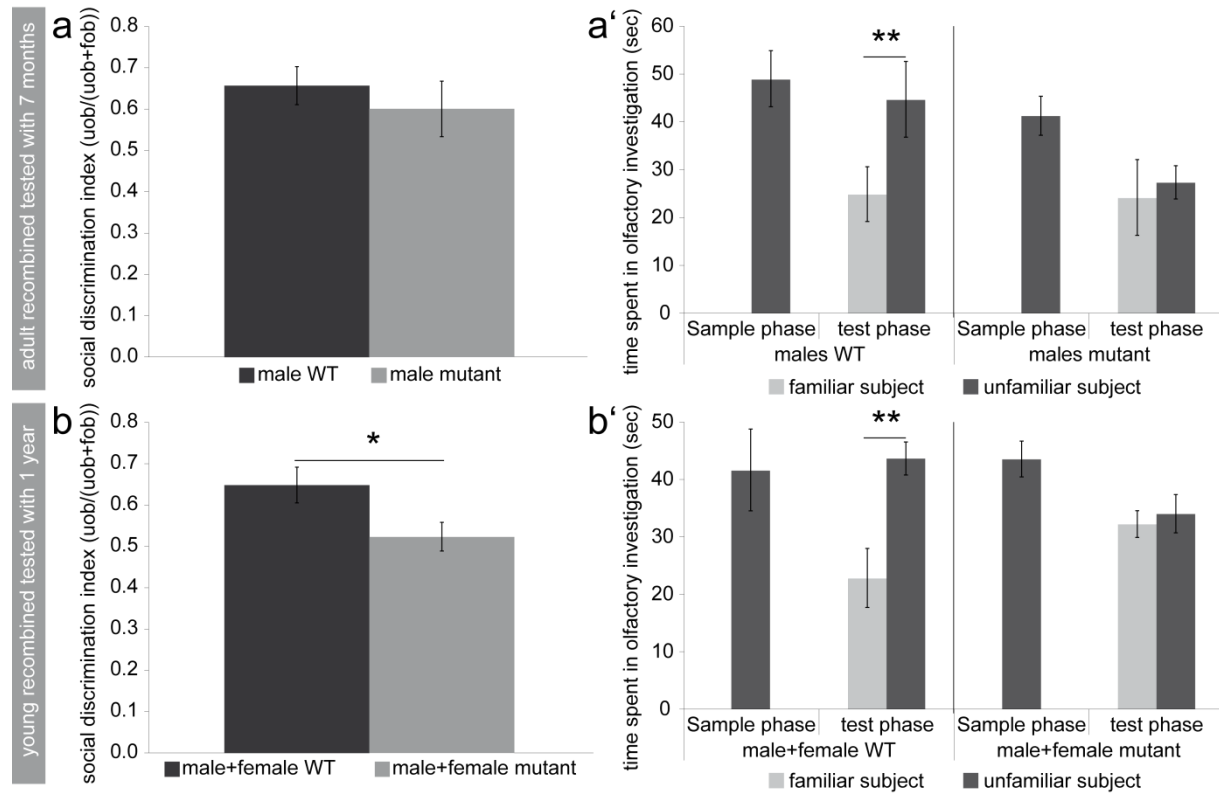
Figure 32 Social discrimination: There was a significant difference in distinguishing the familiar object (fob) from the unknown object (uob) in the young recombined mixed (males plus females) cohort at the age of 1 year. The social discrimination index is illustrating how much time the animals spent with the uob in relation to the total time that they spent sniffing at both (a, b). During the sample phase the animals get to know a former unknown mouse, that will become the fob during test phase while there is a new mouse being the uob. The time spent in olfactory investigation was measured (a', b'). (a) The adult recombined 7 months old mice did not show significant differences in their ability to recognize the uob. (a') However, the corresponding control mice spent siginificantly more time with the unknown object (only shown for the male group) therefore validating the test. (b) A significant decrease in the social discrimination index reflects a significant phenotype in the TFAM-depleted young recombined 1 year old tested mixed cohort. (b') Testvalidation. TFAM mutant mice equally investigate the uob and the fob, not being able to discriminate between both. Mean ± s.e.m.; *p < 0.05, **p < 0.01.

Functionality of the test is defined by control mice spending significantly more time sniffing the unknown object during test phase. Functionality was given in adult recombined seven months old male mice and young recombined one year old animals, but not in the female seven months old adult recombined cohort and the adult recombined one year old mice (data not shown). Illustrated in Figure 32 a' and b' are the well-performing control mice of the adult recombined male cohort. Male mutant mice showed very high variation in the social discrimination index (defined as the ratio of the

time spent at the unknown object in relation to the total sniffing time) yet in general were unable to discriminate between the known and the unknown object (Figure 32 a, a'). Therefore, only a tendency in SD impairment was seen. In the aged young recombined cohort WT mice explored the unknown object (uob) twice as long as the familiar object (fob: 22.75 ± 2.92 sec versus uob: 43.62 ± 5.24 sec, p = 0.007) whereas the mutant mice could not discriminate which one they already knew so they distributed their time equally between both objects (fob: 32.18 ± 3.39 sec versus uob: 33.99 ± 2.40 sec, p = 0.35). In this case the mutant mixed cohort showed a strong disturbance of their discrimination ability, which was reflected in a significantly lower recognition index of 0.52 ± 0.04 in contrast to the WT group 0.65 ± 0.04 (p = 0.04).

In conclusion, only the young recombined mutant mice developed an impairment of SD with age.

4.5.5 TFAM depletion in hippocampal adult-born neurons is not affecting hippocampal learning as needed in the Water Cross Maze (WCM)

The WCM is a hippocampal-dependent test as mice have to go for spatial cues rather than learning a specific body turn while showing an egocentric striatal-dependent response strategy (Botreau and Gisquet-Verrier, 2010). The hippocampal proliferation defect (4.2.1) in four months old young recombined TFAM-deficient reporter positive mice raised the possibility of a hippocampus-based behavioral phenotype (Arruda-Carvalho et al., 2011). Therefore, the same time point was chosen to determine the hippocampal-dependent learning capacity of TFAM-depleted mice.

The accuracy is essentially the most important parameter as it illustrates a general output of the WCM. As can be seen in Figure 33 d, male and female WT and cko mice reached a level of more than 83 % accuracy (indicated by the dotted line) at the end of each training period, which implied that nearly all mice directly chose the correct goal arm in the end. Between 33 % and 83 % accuracy the animals were not yet considered good learners, but also not extremely poor learners, whereas being less than 33 % accurate means they did not learn anything at all. The latter does not apply to the first day of re-training as the low accuracy on that day indicated that the animals learned very well during the first week. They remembered the platform being in the west arm, directly swimming there without success.

Figure 33 Water cross maze demonstrating very similar learning capabilities between young recombined WT and mutant mice. (a) Schematic experimental paradigm of the young Tamoxifen-treated mice that were tested at the age of 4 months and were single housed 1 week prior testing. (b) Picture of the used WCM. The testing period consisted of 5 days training, two days resting interval and 5 days of retraining. (c) The latency to reach the platform in the right arm decreased during the training period. (d) The accuracy to reach the platform was strongly improved. (e) Associated with the accuracy the number of wrong platform visits was reduced. (f) During both training periods all groups were equally good and improving learners. This parameter reflects if the mice headed first into the wrong arm directly realizing they need to go to the other side or if they did not make any mistake at all. 8 mice per group were tested. Mean ± s.e.m.

Both groups re-learned the new platform location within a short time. On the second day during re-learning, in accordance with the accuracy the latency to reach the platform decreased from around 20 sec to around 8 sec, with no significant differences between the groups as seen in the wrong platform visits. Visits of the wrong platform decreased to almost zero on day five of the training week. Both groups reached a high accuracy level at the end of the training week. This is expressed by around six wrong platform visits on the first day of the second week. Nearly all mice went to the learned west arm position of the platform that was correct during the first week, but wrong during the re-training in the second week. The second day of re-learning mice did not swim until the very

end of the arm. By predicting the possible outcome using their prefrontal cortex it was enough for them to have a look into the wrong arm to realize that they need to go to the other side and obey the new rule (Rossi et al., 2012; Pasupathy and Miller, 2005). Figure 33 f shows the percentage of accurate learners in the different groups. Only one out of eight non 100 % accurate learner was responsible for a shift of 20 % in the male cko versus WT groups on day four and five during the first week because of that small difference there was no significant change detectable.

In conclusion, four months old TFAM-deficient mice are able to discriminate spatial clues and perform well in a hippocampal-dependent learning WCM test.

4.5.6 TFAM-deficient mice do not exhibit a depression-like behavior in the Forced Swim Test (FST)

Impaired adult neurogenesis was shown to lead to an increased anxiety-like behavior in transgenic mouse models (Revest et al., 2009; Bergami et al., 2008) and might play a key role in neuropsychiatric disorders such as depression and anxiety (Lee et al., 2012; Kheirbek et al., 2012; Sahay and Hen, 2007). The FST was employed to investigate whether the TFAM-deficient mice exhibit any signs of depression-like behavior as they showed impairment of adult-born neurons (4.2.1, 4.3.1). The principle of the FST is based on the series of reactions a mouse performs if enclosed in an inescapable water filled glass cylinder. They first struggle vigorously until they surrender and start to float (Porsolt et al., 1977). A decreased latency to immobility as well as a shortened swimming period in favor of floating is judged as depression-like behavior (Mosienko et al., 2012).

The same young recombined cohorts that were tested in the WCM at the age of four months underwent the FST at the age of nine months, except for the female groups. There was no significant difference observed neither in the latency to the first floating episode (data not shown) nor in the total immobility time analyzed per minute (Figure 34), indicating that TFAM-deficient aged male mice do not have increased depression-like behavior.
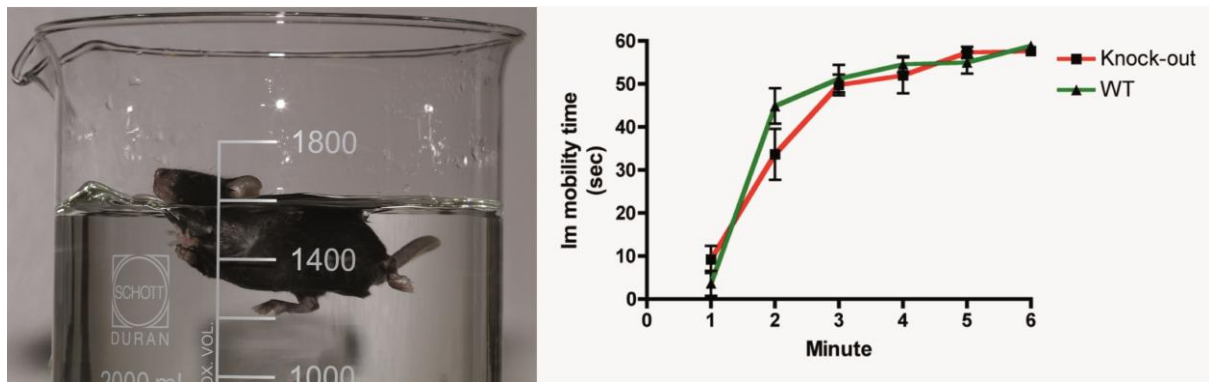
Figure 34 Forced swim test demonstrating well-performing young recombined male WT and mutant mice at the age of 9 months. Mice were observed for 6 min in tempered water, whether they were swimming or floating, while floating was counted as immobility. During the first 2 min both groups were swimming around more than they floated this ratio switched between minute 2 and 3.

5 DISCUSSION

The process of brain ageing is complex and encompassing anatomical and physiological alterations, such as neurodegeneration or a general reduction in the density of synapses and neurotransmitter receptors (Klempin and Kempermann, 2007). The continuous generation of new neurons within the subgranular zone of the adult hippocampus is important for cognitive functions and relies on maintenance, proliferation, and differentiation of adult neural stem cells. The latter three mechanisms depend on well regulated signaling pathways, like the NOTCH/RBPJk pathway, that if disturbed may result in an enhanced proliferation and differentiation of adult neural stem cells, causing a premature depletion of the stem cell pool (Ehm et al., 2010). Interestingly, the rate of adult neurogenesis declines with age (Schouten et al., 2012; Drapeau et al., 2003) and the reduced generation of adult-born neurons correlates with age-associated cognitive decline (Schouten et al., 2012). The underlying reasons and modulators are not yet fully understood.

Recent publications have strengthened the idea that different aspects of mitochondrial dysfunction contribute to ageing associated phenotypes (Troulinaki and Bano, 2012; Walton et al., 2012). Mouse models with increased mtDNA mutations were found to have a premature ageing phenotype (Edgar and Trifunovic, 2009; Kujoth et al., 2007). Conditional TFAM depletion in mice revealed hallmarks of ageing in targeted tissues, such as pancreas and heart (Falkenberg et al., 2007; Silva et al., 2000; Wang et al., 1999; Larsson et al., 1998), and progressive neurodegeneration in studies targeting neuronal cell populations (Ekstrand et al., 2007; Sörensen et al., 2001).

Adult-born neurons contributing to hippocampal-dependent cognitive functions are generated and integrated within a so-called neurogenic niche (Song et al., 2002; Mercier et al., 2002). The niche is characterized by cellular networks including astroglia (Morrens et al., 2012; Wilhelmsson et al., 2012; Masiulis et al., 2011). Astroglia in the hippocampus are of special interest since they provide the cellular origin for newly generated neurons and contribute to the neurogenic microenvironment as protoplasmic astrocytes (Morrens et al., 2012).

Astrocytes, the most abundant non-neuronal cell type in the mammalian brain (Nagai et al., 2007), are well known for their function in neurometabolic coupling, which includes the transfer from lactate, generated via glycolysis in astrocytes, to high energy demanding neurons (Magistretti, 2006). In addition to supply of neurons with nutrients, astrocytes maintain homeostasis in the brain by, e.g., the uptake of excessive neurotransmitters and providing precursors of neurotransmitters to neurons. This vast variety of functions enables astrocytes to protect neurons but also to induce neurodegeneration under certain pathological conditions. Indeed, a specific role of astrocytes during neurodegeneration and impaired neuronal function was reported for neurodegenerative disorders

like ALS, Rett syndrome (RTT), spinocerebellar atrophy, or HD (Nagai et al., 2007; Marchetto et al., 2008; Okabe et al., 2012; Custer et al., 2006; Shin et al., 2005). Moreover, it was shown that mutant SOD1-expressing astrocytes specifically increase the degeneration of motor neurons in a rodent (Nagai et al., 2007) and in a human cell culture model (Marchetto et al., 2008). Most probably this is mediated by secreted factors that induce the B-Cell Leukemia-2 associated X-protein (Bax)-dependent death machinery in neurons (Nagai et al., 2007). In a RTT mouse model of methyl-CpG–binding protein 2 (MeCP2) null mice it was found that a modified expression of astrocytic markers such as GFAP, S100β, glutamate transporters, and GS was associated with, for example, increased clearance of glutamate causing neuronal dysfunction (Okabe et al., 2012).

As the importance of astrocytes in CNS homeostasis is increasingly appreciated, and the impact of mitochondrial dysfunction in astrocytes has not been finally revealed, this study aims to investigate the effects of a dysfunctional mitochondrial electron transfer chain in astrocytes and radial glial stem cells in the adult hippocampus. This was caused by depletion of the nuclear encoded mitochondrial transcription factor A. The transgenic mice generated during this study provide a new model to gain a deeper insight into impaired mitochondrial function in a large subset of astrocytes in the adult mouse brain.

5.1   TFAM depletion and mitochondrial dysfunction in the GLAST::CreERT2 x *Tfam*[loxP/loxP] mice

An active Cre recombinase in GLAST positive cells excises the floxed exons six and seven from the nuclear *Tfam* gene. Using FACSorted reporter positive cells, indicating an active Cre, it was shown by genotyping PCR that the *Tfam* locus was recombined *in vivo* (4.1). Employing immunocytochemistry, genotyping PCR, and qRTPCR, depletion of TFAM was detected on protein, DNA, and RNA level in cultured astrocytes (4.1). In alignment with previously reported *Tfam*[loxP/loxP] transgenic mice it may be assumed that recombination of the *Tfam* locus *in vivo* is consequentially followed by reduced *Tfam* mRNA and protein, reduced mtDNA (after one to two months), mtRNA (after two to four months) and decreased activity of respiratory chain complexes I, III, and IV (after two to four months) (Ekstrand et al., 2007; Sörensen et al., 2001; Wredenberg et al., 2002).

TFAM depletion was induced to cause mitochondrial dysfunction; preliminary data suggest a reduction of the activity of respiratory chain complexes I and IV in isolated mitochondria from dissected brain tissue (including SVZ/OB) of one year old young recombined (GLAST::CreERT2 x) TFAM-depleted mice (data not shown).

TFAM depletion in cells with high oxidative phosphorylation activity results in COX (mtDNA-encoded Complex IV) negative but SDH (nuclear-encoded Complex II) positive cells (Wang et al., 1999). Here, enzymatic COX/SDH staining (Müller-Höcker, 1989; Mahad et al., 2009) revealed only a slight COX deficiency in the OB granule layer of ten months old young recombined (GLAST::CreERT2 x) TFAM-depleted mice and there was no COX deficiency detectable in any other brain region as analyzed by sagittal cryosections (data not shown).

In MILON mice, MitoPark mice or, e.g., Mlc1f-Cre x *Tfam*^{lox/loxP} myopathy mice COX negative cells were traceable as early as in three to four months old mice corresponding to the age of the onset of observed phenotypes (Sörensen et al., 2001; Ekstrand et al., 2007; Wredenberg et al., 2002). That implies either no strong respiratory chain deficiency even in ten months old GLAST::CreERT2 x *Tfam*^{loxP/loxP} mice, or the COX deficiency did not exceed a certain threshold. It was described, that a tissue-specific critical load of complex dysfunctionality is necessary to generate a biochemical defect with consequences on cellular function. Thus, cells with mitochondrial dysfunctions below this threshold will appear as histochemically normal (Schon et al., 1997; Rahman et al., 2000; Bua et al., 2006; McFarland and Turnbull, 2009; Ross et al., 2010).

Summarizing, genotyping indicated efficient *Tfam* gene recombination in astrocytes by GLAST driven Cre recombinase. The fact that COX deficiency was only observed in a region where numerous new neurons are generated from astrocytes and that astrocyte rich regions did not show a deficit suggests that astrocytes in general have a low susceptibility to mitochondrial respiratory complex dysfunctionality. Such hypothesis can be tested in future studies by further applying mitochondrial assays like the mitochondrial respiration assay (Rogers et al., 2011). This will provide more evidence for mitochondrial dysfunction in this TFAM-deficient mouse model.

5.2   Mitochondrial dysfunction in adult astrocytes is linked to ageing associated phenotypes

Mitochondrial dysfunctions involving accumulated mtDNA mutations, increased ROS production, impaired mitochondrial dynamics, and in particular reduced energy metabolism were shown to contribute to the process of ageing in several tissues and cell types, e.g., myocardium (Müller-Höcker, 1989), muscle cells (Fayet et al., 2002), or brain tissue (Cottrell et al., 2001a; Lee and Wei, 2012; Trifunovic et al., 2004). In this study, TFAM depletion as a previously demonstrated means to cause impairment in mitochondrial function was used as a tool to induce ageing related phenotypes in targeted astroglia.

In contrast to neuronal studies, TFAM depletion did not interfere with astrocyte survival at the examined time points. This resistance to mitochondrial insults can be explained by the metabolic requirements of astrocytes. Astrocytes largely rely on complete glycolysis providing neurons with high extracellular lactate for their aerobic energy generation, in addition to glucose (Aubert et al., 2007; Jakoby et al., 2012). Astroglia can store glycogen (Hertz et al., 2007). They use glycolysis and neurotransmitter turnover to produce ATP, and partially rely on diffusion of ATP since their narrow extensions cannot hold mitochondria (Hertz et al., 2007). This combination makes astrocytes less susceptible to low oxygen than neurons, and therefore less sensitive to impairment of mitochondrial metabolism (Turner and Adamson, 2011).

Astrocytes in the ageing brain develop characteristics distinct from their properties in the young adult brain (Bernal and Peterson, 2011). Thus, brain regions, such as the entorhinal cortex display a higher fraction of GFAP-positive astrocytes during ageing (Bernal and Peterson, 2011; Goss et al., 1991; Nichols et al., 1993; Morgan et al., 1997). This resembles characteristics of a mild inflammation process as seen in young adult brains, lacking other markers of reactive astrocytes such as hypertrophy, up-regulation of Vimentin, or even proliferation (Sofroniew, 2009; Sofroniew and Vinters, 2010). Interestingly, a mild version of reactive gliosis including an increase of GFAP-expressing astrocytes, was detected in the neocortex and the molecular layer of the hippocampus of young recombined TFAM-depleted mice (Figure 25), while increased expression of Vimentin (Figure 26) or proliferation (data not shown) were missing. This indicates that mitochondrial dysfunction is sufficient to reproduce a part of the structural astrocytic ageing phenotype, thereby suggesting that mitochondrial impairment might be linked to the alterations observed in astroglia in the ageing brain.

Impaired cognition, motor coordination, and changed behavior due to altered sensitivity to certain stimuli have been reported to be associated with ageing (Todorović et al., 2003; Godbout et al., 2008; Young et al., 2010; Bernardes de Jesus et al., 2012). However, TFAM-deficient mice revealed no impairment in exploration and anxiety-like behavior (OF, Figure 30, Todorović et al., 2003), sensorimotor gating (PPI, Figure 31, Young et al., 2010), or locomotion (RR, Figure 29, Bernardes de Jesus et al., 2012), indicating that TFAM-depletion from astrocytes and the ensuing mitochondrial impairment have only minor impacts on CNS plasticity and function.

The time points used for behavioral testing were chosen with respect to proliferation deficits in the DG of *Tfam* cko mice (4.2.1) and behavioral phenotypes observed by other groups studying TFAM-deficient mouse models (Dufour et al., 2008; Sörensen et al., 2001; Ekstrand et al., 2007). Neurons are highly dependent on mitochondrial integrity for function and survival (Kann and Kovács, 2007). The present results indicate that in contrast to neurons, astrocytes are by far less susceptible to mitochondrial dysfunction most likely owing to their different metabolic requirements (Turner and

Adamson, 2011; Aubert et al., 2007; Jakoby et al., 2012). The GLAST-dependent TFAM deletion did not affect neurons, except for the newly generated neurons, oligodendrocytes, and the vasculature system. It is therefore not surprising that there was only a partial overlap between phenotypes observed in the *Tfam* cko mice and in aged animals. Nevertheless, it cannot be excluded that TFAM depletion in astrocytes may have a considerable impact on CNS function at later stages than the ones examined in this study. It is possible that aged neurons will be more susceptible to surrounding TFAM-depleted astrocytes than young or middle aged neurons. Such possibility will have to be examined by studying the anatomy and function of the CNS at later stages. Irrespective of these possibilities, the present data indicate that mitochondrial dysfunction in protoplasmic astrocytes is not sufficient to elicit a major behavioral ageing phenotype and neurodegeneration, thus arguing that mitochondrial dysfunction in astrocytes contributes only marginally to CNS ageing phenotypes.

An interesting observation of this study was that the fraction of recombined astrocytes in the molecular layer of the hippocampus was strongly increased (Figure 25). This observation was remarkable because of two facts: Firstly, this increase was only observed in this region, suggesting that the response of astrocytes to TFAM depletion may be region specific, which may be in line with the merging concept, that astrocytes are not a homogenous population but have region specific properties (Molofsky et al., 2012; Yeh et al., 2009; Tsai et al., 2012). Secondly, the total density of astrocytes was unaltered, suggesting that the total number of astrocytes in a given region is tightly regulated. One potential explanation to this phenomenon could be that upon recombination TFAM-depleted astrocytes became reactive and proliferative, somehow suppressing the proliferation of non-recombined astrocytes. Overall it will be interesting to determine, how the proliferation of recombined or non-recombined astrocytes was regulated not to exceed physiological numbers of astrocytes.

5.3   TFAM depletion in astrocytes has profound impact on adult neurogenesis

In contrast to protoplasmic astrocytes, radial glial cells, which serve as neural stem cells, were strongly affected by TFAM depletion. Investigation of the proliferation capacity of neural stem cells in TFAM-deficient mice revealed a significant decrease of the proliferation rate in four months old animals (Ki67 staining, Figure 12). In addition, the survival seemed to be impaired as determined by BrdU maintaining cells in the DG of young recombined four and six months old *Tfam* cko mice (Figure 12 c-d). Thus, mitochondrial dysfunction due to TFAM depletion impedes proliferation of neural stem cells and survival of newborn neurons. These data support the idea that neural stem cells with mitochondrial dysfunction in the adult hippocampus behave in a similar way as observed in neural

stem cells in the aged hippocampus, showing declining hippocampal neurogenesis with age (Jinno, 2011; Kuhn et al., 1996).

This study found that TFAM deletion does not significantly alter the density of radial glial cells (Figure 15). Thus, TFAM depletion and the ensuing mitochondrial dysfunction does not impair the survival of stem cells but rather results in a functional depletion of stem cells, which is in line with the observation that ageing changes the proliferative activity of the stem cell pool (Lugert et al., 2010; Encinas and Sierra, 2012; Liu and Rando, 2011). Survival of the neuronal progeny, however, is strongly affected. Overall these data demonstrate, that stem cell proliferation and survival of the neuronal progeny are more susceptible to altered mitochondrial function than the stem cell pool itself. Thus, with regard to their survival following TFAM depletion radial glial cells behave similar to their protoplasmic counterparts. Overall the data also suggest that quiescent stem cells are less mitochondrial ATP-dependent than their progeny. This is reminiscent of the situation in embryonic stem cells (ESCs) (Chung et al., 2007; Facucho-Oliveira et al., 2007; St John et al., 2005). Pluripotent ESCs depend on anaerobic respiration, since they possess only few small perinuclear mitochondria (Spikings et al., 2007; Stojkovic et al., 2001; Wilding et al., 2001). The primary reason for preferential ATP production via anaerobic glycolysis is the reduction of ROS generation (Birket et al., 2011). Once ESCs start to differentiate, their mitochondrial replication and transcription factors become up-regulated, the density and distribution of mitochondria increases and their mitochondria acquire a more mature elongated morphology with an increased cristae surface (Facucho-Oliveira and St John, 2009). Assuming that neural stem cells undergo a similar transition upon differentiation, depletion of TFAM would significantly counteract the generation of functional mature mitochondria and thereby inhibiting the switch from glycolysis to aerobic respiration, which impedes differentiation and development of new neurons that have a high energetic demand.

Tfam cko mice generated significantly less neurons (Figure 14 e). This is also reminiscent of ageing, where a decreased differentiation of stem cells into neurons has been reported (Encinas et al., 2011b; Encinas and Sierra, 2012; Artegiani and Calegari, 2012). In particular newly generated cells derived from TFAM-depleted stem cells less frequently generated neurons (Figure 14 e). There was a trend towards less recombined GFP-positive cells with an astroglial fate (Figure 14 g). In contrast there was a significant increase in the non-recombined astroglial fraction (Figure 14 g).

The *in vivo* differentiation results of TFAM-depleted stem cells are partially similar to a previous report about 8-oxoguanine DNA glycosylase ko mice derived neural stem cells (Wang et al., 2011a). Those showed a differentiation shift from neurogenesis towards astrogenesis due to accumulation of mtDNA mutations at the expense of neurogenesis (Wang et al., 2011a).

The fact that TFAM-depleted stem cells differentiated less frequently into neurons may be explained by the specific metabolic requirements of neurons. Neurons have a highly oxidative metabolism (Turner and Adamson, 2011). Thus, they are prone to mitochondrial dysfunction especially since they have high energetic demands after neuronal activation (Turner and Adamson, 2011). It is therefore possible that stem cells avoid differentiating into this highly susceptible phenotype. This observation is highly interesting as it suggests that the metabolic status of stem/progenitor cells may dictate fate decisions. The current knowledge about the impact of energy metabolism on adult neural stem cell fate indicates a modifying effect of low or high energy levels on adult neurogenesis (for review see Rafalski and Brunet, 2011).

The portion of S100β positive cells derived from non-recombined stem cells was increased in *Tfam* cko mice. This might reflect a compensation for the reduced TFAM-deficient astroglial population, resulting in less neuronal progeny in favor of newly generated astrocytes. An enhanced differentiation into astroglial cells could contribute to a physiological hippocampal environment, which may support pre-existing and newly generated neurons. Astrocytes form a large syncytium via gap-junctions consisting of, e.g., connexin 43 (Cx43) hemichannels (Nagy and Rash, 2003). This enables communication between astrocytes via diffusion of small molecules such as glucose, ATP, potassium, or calcium, enabling nutrients/energy supply and signaling molecules to be distributed throughout the syncytium (Orellana et al., 2012; Sofroniew and Vinters, 2010; Kielian, 2008; Seifert et al., 2006; Nedergaard et al., 2003). Therefore, communication of TFAM WT astrocytes with TFAM-depleted astrocytes may help to maintain the astrocytic network and to compensate for dysfunctional astrocytes. This is particularly interesting as the GLAST-driven Cre recombinase is active in 60 % to 80 % of astrocytes in the brain (Mori et al., 2006), resulting in a mixed population of WT and TFAM mutant astrocytes. Inflammation studies on the other hand revealed a decrease of Cx43 protein and reduced astroglial coupling (Kielian, 2008). Therefore, it would be worthwhile to examine the extent of coupling of TFAM mutant astrocytes and non-recombined astrocytes within *Tfam* cko mice. It would be interesting to determine, if there is an increase in gap-junctions enabling the mixing of astroglial compounds (smaller than 1 kDa, Nedergaard et al., 2003), resulting in a homogenized astrocytic population. Or, on the contrary, if there is a decrease of gap-junctions to seal off recombined TFAM-deficient astrocytes from the remaining healthy astroglial fraction.

Tfam cko mice handled the hippocampus-dependent learning water cross maze task just as well as age-matched WT mice (Figure 33). On first glance this may be surprising given the fact that hippocampal neurogenesis has been found crucial for spatial learning (Dupret et al., 2008). However, it is of note that most behavioral tests that revealed a spatial learning deficit in the context of impaired neurogenesis were far more complex. This suggests that the present test might have been

too elementary to discover fine deficiencies in hippocampal learning. Recent publications demonstrated that detection of such fine deficiencies could be approached by, for example, pattern separation tasks (Sahay et al., 2011; Aimone et al., 2011). Pattern separation is a process relying on adult neurogenesis for the formation of new episodic memories that are very similar to pre-existing ones but are nevertheless represented as discrete events (Treves et al., 2008). Since adult neurogenesis is not completely abolished in the *Tfam* cko mice, but rather modified by reduction of the number of newborn neurons and most probably impaired neuronal function due to alterations in mitochondrial metabolism, it would be interesting to further investigate the precise discrimination ability of TFAM mutant mice using a pattern separation test.

TFAM-depleted mice tested during this study did not show any signs of depressive-like behavior in the FST (Figure 34). It would be interesting if their sensitivity regarding LPS is changed as reported in old mice, where exacerbated depressive-like behavior was observed upon lipopolysaccharide (LPS)-treatment (Godbout et al., 2008). It also needs to be mentioned, that the anxiety/depression like phenotype in the context of perturbed hippocampal neurogenesis is not consistently reported in the literature (Clément et al., 2002; Cryan et al., 2002; Fernandez and Gaspar, 2012; Finn et al., 2003; Leventhal et al., 2008).

Aged mice were also demonstrated to have an impairment in solving olfactory discrimination tasks as well as reduced olfactory sensitivity (Patel and Larson, 2009; Sterlemann et al., 2010). Thus, considering mitochondrial dysfunction to be one important factor in ageing (Sahin and Depinho, 2010; Bishop et al., 2010), altered SVZ neurogenesis and function was assumed to result in reduced olfaction. Young recombined one year old TFAM-depleted mice showed a significant decrease in their social discrimination capability (Figure 32). This indicates a premature impairment of the olfactory discrimination capability. Why adult recombined mice do not exhibit detectable levels of olfactory dysfunction is not yet clear, but may be related to the differences in recombination efficiency within the OB network which is largely set up during the early postnatal period (López-Mascaraque and Castro, 2002; Winpenny et al., 2011; Patel and Larson, 2009).

5.4   Additional phenotypes

A surprising observation was the fact that young recombined TFAM-deficient mice had a significantly decreased body weight at the age of eight months (data not shown) and adult recombined mice at the age of one year (Figure 28). Ageing phenotypes comprise many characteristics including a decline in body weight (Trifunovic et al., 2004; Kujoth et al., 2006). Hence, GLAST-controlled deletion of TFAM may produce premature ageing phenotypes in non-CNS organs as well. Whether these

alterations are caused by CNS deficits or by loss of TFAM in peripheral organs, remains to be determined. GLAST expression was reported to occur in young rats in peripheral organs (Berger and Hediger, 2006; Mason and Huggett, 2002) and GLAST expression outside of the murine brain was described in the spinal cord of postnatal mice up to three weeks of age (Shibata et al., 1997). However, the extent of GLAST::CreERT2 activity in young adult mice in particular in peripheral tissues is unexplored. CNS deficits have been reported to produce alterations in body weight that can be caused by perturbed function of the monitor of the cellular energy status, the AMP-activated protein kinase (AMPK) (Minokoshi et al., 2004), within the hypothalamus, a region with a high recombination rate in the studied TFAM-depleted mice (Figure 11). The AMPK interacts, for instance, with Leptin, a hormone, that has a major role in the control of body weight (Friedman and Halaas, 1998) and affects mitochondrial function (Martinez-Abundis et al., 2012), which might provide a link between mitochondrial dysfunction in the affected regions and the drop of body weight. Finally, an impaired regulation of the cellular energy status can be a cause for decreased food intake followed by a reduction in body weight. An approach to investigate the impact of TFAM depletion in peripheral organs regarding the drop of body weight could be the use of a different astrocyte-specific CreERT2 driver as, for instance, the hGFAP::CreERT2 transgenic mice (Hirrlinger et al., 2006; Ganat et al., 2006; Chow et al., 2008). Analyses of other astrocyte-specific CreERT2 transgenic mice crossed to the $Tfam^{loxP/loxP}$ might strengthen the CNS or peripheral organ hypothesis. The use of other astrocyte-specific gene promoter to drive $Tfam$ recombination, such as GFAP, S100β, Vimentin, or GS, has also limitations like targeting only a small subset of astrocytes or even being expressed in other cell types like oligodendrocytes (Mori et al., 2006). Thus, the most promising analysis to determine the cause of the loss of weight in GLAST::CreERT2 x $Tfam^{loxP/loxP}$ mice would be the examination of reporter positive cells in peripheral organs, e.g., the digestive system or fat cells (Berger and Hediger, 2006) concerning their cell viability and mitochondrial functionality.

5.5   The influence of acute and chronic TFAM depletion on the morphology of newborn neurons, their spine and mitochondrial content

TFAM-deficient newborn neurons differed significantly with respect to their morphology from WT neurons (Figure 18 d, e). This suggests, that mitochondrial dysfunction impairs dendritic maturation under physiological conditions.

Physical exercise was shown to induce proliferation (Kronenberg et al., 2006; van Praag et al., 1999), increase hippocampal dendritic maturation (Piatti et al., 2011)(Kathrin Steib, unpublished data) and mitochondrial biogenesis (Viña et al., 2009)(Kathrin Steib, unpublished data). To challenge the

Tfam cko mice or eventually rescue TFAM depletion phenotypes physical exercise, in the form of a voluntary running wheel, was added as a stimulus.

WT neurons showed a significantly increased dendritic length and complexity accompanied by a reduced amount of branch points upon physical exercise (Figure 18).

Although TFAM-depleted newborn neurons are capable of increasing their neuronal morphology under running conditions, they do not reach a level of dendritic length and complexity comparable to neurons of running WT mice. This indicates that physical exercise can only partly rescue the morphological phenotype observed upon mitochondrial dysfunction due to TFAM depletion The fact that mitochondrial mass increases upon physical activity and that TFAM-depleted neurons only showed a limited response to physical activity indicates that increasing the pool of functional mitochondria represents an important contributor to the activity-dependent development of new neurons. This would aid in deciphering, what could transduce such coupling of mitochondrial function and activity it is tempting to speculate that transcriptional programs regulating mitochondrial biogenesis may be involved (Fernandez-Marcos and Auwerx, 2011; Viña et al., 2009). PGC1α and NRF-1/-2 would interact to up-regulate nuclear encoded genes that are important for mitochondrial structures, thereby increasing mitochondrial biogenesis (Gottlieb and Gustafsson, 2011; Scarpulla, 2008). *Tfam* expression would be as well increased under WT conditions (Gottlieb and Gustafsson, 2011). However, in the *Tfam* cko mice the partial rescue needs to rely on mitochondrial functions that exclude the mtDNA encoded respiratory chain as TFAM is essential for mtDNA transcription (Scarpulla, 2008).

TFAM-deficient neurons in these experiments develop in close proximity to TFAM-depleted astrocytes. This means an additional altered microenvironment that may have side effects on the neuronal progeny of TFAM-depleted radial glial cells. To investigate acute TFAM depletion in newborn neurons in an otherwise non-TFAM-deficient background, neurons were retrovirally targeted causing Cre-recombination of the *Tfam* locus only in newly generated retrovirally labeled cells.

Acute TFAM depletion led to a significantly reduced total dendritic length and arborisation complexity three months after the Cre-transduction, but not in four or six weeks old neurons (Figure 24). The mitochondrial content in the three months old neurons was not altered.

Thus, a reduction of dendritic growth and complexity becomes apparent at a much later time point, namely at three months after birth of the targeted neurons, than in chronic TFAM-depleted newborn neurons (three weeks). Hence, the loss of TFAM affects the cells only upon abolishment of pre-existing *Tfam* mRNA and TFAM protein. Although the gene locus is recombined, remaining

Tfam mRNA and non-degraded TFAM protein may result in detectable TFAM protein levels long after recombination, as seen in the MILON mice (Sörensen et al., 2001). However, TFAM-deficient neurons show a significantly shorter and less complex morphology than WT neurons, proving that the loss of TFAM within single neurons is enough to generate a reduced dendritic arborisation complexity. This also indicates that a neurogenic niche composed of WT astrocytes cannot prevent impaired morphological development of single TFAM-deficient newborn neurons. The BrdU experiments (Figure 14) suggested that TFAM deficiency in astrocytes of the neurogenic niche may influence the behavior of stem cells and their progeny with intact TFAM. The impact of TFAM-deficient astrocytes on maturation of newborn neurons with intact mitochondria was not investigated in this study, but given that astrocytes are regulators of synaptic plasticity and that glia and neurons are metabolically coupled, it will be interesting to investigate the metabolic profile of astrocytes and neurons in *Tfam* cko mice (Kumar Jha et al., 2012; Magistretti, 2009; Figley and Stroman, 2011; Pellerin et al., 2007). The question, whether TFAM-deficient astrocytes within the neurogenic niche have a direct impact on spine formation of newly generated neurons, can be tackled by analysis of dendritic fragments closely surrounded by recombined and labeled astrocytes. This method was established by Toni et al. showing that astrocytic function has a great impact on spine formation (Nicolas Toni, Université de Lausanne, personal communication). Taking into account that differences may occur within one neuron, analyzing fragments in the same area, but where the dendritic segments were shielded by a deficient astrocyte or a healthy non-recombined one, a more detailed investigation of spine density needs to be employed to check for the effect of TFAM-deficient astrocytes on TFAM-depleted newborn neurons. This might reveal differences in spine formation in TFAM-deficient mice that have been missed ignoring the presence or absence of TFAM-depleted astrocytes in close proximity.

In *vitro* synaptogenesis relies on functional mitochondria (Dickey and Strack, 2011). Surprisingly, the spine density was unchanged in TFAM-depleted newborn neurons at the age of three or six weeks if compared to WT control neurons (Figure 21). The challenge of a voluntary running wheel was also applied to analyze the effect of physical activity on spine formation. Three weeks old WT neurons showed no increase in spine number under running conditions, but a tendency to more mature mushroom-like neurons (Figure 21). These findings are supported by data from the literature describing the same phenomenon under running conditions: no increase in spine density, but differences in the level of maturity of the synapses upon physical activity (Zhao et al., 2006; Morgenstern et al., 2008). Running conditions had no effect on the percentage of mushroom spines in TFAM-deficient neurons, but there was a trend towards an increased spine density detectable upon running (Figure 21). This tendency towards an increased amount of spines per dendritic segment might indicate that even under conditions of mitochondrial dysfunction the spine density

remains modifiable by external stimuli like running. Nevertheless, it needs to be further analyzed whether the generated spines are representing functional synapses. It was reported that silent synapses occur during CNS development while the synapses mature (Liao et al., 1999) as well as in the adult brain representing, for example, a faster way of modifiable synaptic plasticity (Lee and Dong, 2011). The latter means that pre-existing silent synapses, which contain only NMDA receptors, may be fast activated by rapid acquisition of alpha-amino-3-hydroxy-5-methyl-4-isoxazolepropionic acid (AMPA) receptors (Lee and Dong, 2011; Li and Sheng, 2003). Silent synapses might be pre- or post-synaptic silent being unable to release neurotransmitter or lacking functional receptors on their surface (for review see Atwood and Wojtowicz, 1999; Crawford and Mennerick, 2012).

The mitochondrial density within dendrites was neither altered in chronically TFAM-depleted neurons (Figure 19), nor in acute TFAM-depleted newborn neurons (Figure 24). Interestingly, three weeks old neurons of *Tfam* cko mice did also not reveal any increase of mitochondrial number or volume upon physical activity (Figure 19), in contrast to WT neurons, which can up-regulate their mitochondrial biogenesis resulting in a significantly increased mitochondrial number and volume per dendrite (Steiner et al., 2011; Safdar et al., 2011). This implies that, TFAM becomes the rate limiting factor for mitochondrial biogenesis in situations that stimulate massive biogenesis of mitochondria. Nevertheless, the mitochondrial density in six weeks old neurons in WT and Tfam cko mice was comparable under running conditions. This suggests a delayed generation of new mitochondria in TFAM mutant neurons rather than no increase in mitochondrial mass upon physical exercise. However, the functionality of the generated mitochondria needs to be further analyzed regarding, for example, the mitochondrial membrane potential.

Tfam cko mice, under non-running conditions, showed more mitochondrial volume in the soma/shaft area of three weeks old neurons without an increase in mitochondrial number or total mitochondrial volume per cell (Figure 19). This indicates larger single mitochondria. Giant mitochondria have been reported to occur during ageing, being unable to undergo physiological fusion and fission processes, they contribute to impaired mitochondrial membrane potential, accumulation of deficient mitochondria, and reduced respiratory activity (Navratil et al., 2008). In line with swollen or giant mitochondria the examination of possibly altered mitochondrial ultrastructure, e.g., cristae in *Tfam* cko mice requires further study using electron microscopy.

Since the confocal images analyzed before are static pictures of moving organelles and to some extent plastic cells, it is not yet clear, whether mitochondrial dysfunction in *Tfam* cko mice is composed of reduced mitochondrial distribution or dynamics (Dogan and Trifunovic, 2011). Therefore, it would be important to further investigate, e.g., fusion and fission processes in *ex vivo*

hippocampal slices using a live imaging setup (Cho et al., 2007; Lein et al., 2011; Kann et al., 2005), to explore hidden mitochondrial dysfunctions employing flash-frozen methods.

In conclusion, TFAM depletion leads to an impaired dendritic plasticity growth of newborn neurons, which can only be partially rescued by physical exercise. Considering the reduced survival of the neuronal progeny in *Tfam* cko mice, it might be that only the fittest cells survive, in such a small amount that they can be supported by the remaining non-recombined astrocytes within the DG.

5.6   Future directions

The present study revealed for the first time that mitochondrial dysfunction in astrocytes can partially lead to an ageing brain phenotype. In particular astrocytes with stem cell function were found to be susceptible to mitochondrial dysfunction and responded with functional deficits, whereas protoplasmic astrocytes appeared to be quite resistant. Thus, it will be interesting to compare in future studies the mitochondria-dependent metabolic requirements of these cell types and to understand, how the metabolic state affects stem cell function. A first glimpse to this question was provided by the recent study by Knobloch and colleagues (2013), who showed an intriguing dependence of radial glial stem cells on lipogenic pathways (Knobloch et al., 2013).

Furthermore, it will be interesting to study the contribution of astrocytic mitochondrial dysfunction and astrocytes during ageing in the pathological context. Thus far, the data indicates that mitochondrial function is largely dispensable for CNS plasticity and function under non-stress conditions. Astrocytes fulfill also important functions under pathological conditions. Astrocytes release growth factors (Bernal and Peterson, 2011), regulate their glucose uptake adapted to neuronal excitation and energy demand (Magistretti, 2006). They protect the brain as a part of the blood brain barrier (Attwell et al., 2010; Gordon et al., 2007) and maintain a redox homeostasis by producing antioxidants (Swanson et al., 2004; Dringen et al., 2000), thereby enhancing neuronal survival in particular after brain injuries (Slemmer et al., 2008). Reactive astroglia are key players in the scar formation process after brain injury or inflammation, secluding the affected brain region to protect healthy brain parts (Faulkner et al., 2004; Sofroniew, 2005; Voskuhl et al., 2009). It needs to be pointed out that scar formation and reactive gliosis also have their drawbacks. Scar formation for example impedes tissue repair (Wilhelmsson et al., 2006). Reactive astrocytes release cytotoxic radicals and inflammatory cytokines (Shibata and Kobayashi, 2008). Moreover, they show an increased expression of heme-oxygenase (Espada et al., 2010), a stress protein, which degrades heme causing iron overload and mitochondrial dysfunction. Thereby, neuronal function and survival is impaired. It can be said, that every disturbance of astrocytic function has a negative effect on brain

function (Nedergaard and Dirnagl, 2005), e.g., impaired brain ammonia disposal in hepatic encephalopathy (Lemberg and Fernández, 2009), decreased glutamate uptake in episodic ataxia 6 (Winter et al., 2012), or astrogliopathy in Alexander disease (Prust et al., 2011). There are many examples of astrocytic dysfunction interfering with neuronal activity and viability.

Mitochondrial biogenesis is increased upon stroke in cortical tissue (Yin et al., 2008). Considering that TFAM depletion interferes with generation of functional mitochondria, it would be interesting to examine the response of *Tfam* cko mice to a stressor like stroke (Moro et al., 2005). The normal reaction upon induced stroke in the neocortex is a strong reactive gliosis with increased glial proliferation and even migration (Shimada et al., 2012). Assuming that astrocytes can cope with TFAM deficiency under physiological conditions, they might not be able to handle an additional stressor, leading to altered astrocytic viability, causing a weaker reactive gliosis and most probably increased cell death of surrounding neurons. To additionally investigate, whether *Tfam* cko mice are more susceptible to excitotoxic stress injection of kainic acid could be used as another stressor (Sörensen et al., 2001).

Lastly and most importantly, it will be interesting to examine if signs of mitochondrial dysfunction can be detected in the ageing human brain. Thus far, studies have shown that mitochondrial dysfunction and DNA mutations occur in neurons of the aged human brain (Chakrabarti et al., 2011; Long et al., 2012; Kumar et al., 2013; Swerdlow, 2011).

Mitochondrial morphology is the most obvious parameter to examine mitochondrial dysfunction, in particular since excessive enlargement/elongation or the other extreme enhanced fragmentation is linked to mitochondrial impairment and disorders (Merkwirth et al., 2012; Duvezin-Caubet et al., 2006). Immunohistochemistry is not applicable to analyze mitochondrial morphology within the fine network of astrocytic branches and narrow extensions. To gain further insight ultrastructural electron microscopy analysis is required. This would also be a promising approach to investigate human post-mortem brain tissue, comparing young versus old humans. Besides the morphology there are several other indicators of mitochondrial dysfunction, for example, respiratory chain deficiencies measured via COX/SDH staining (Mahad et al., 2009; Wang et al., 1999; Ross et al., 2010), or deletion analysis of single genes like *Tfam* or of the whole mitochondrial genome (Taylor et al., 2003; Trifunovic et al., 2004; Bua et al., 2006; Harada and Korf, 2013). Such studies would be highly valuable to tease out the currently elusive contribution of astrocytes to brain ageing and neurodegeneration and would significantly support the validation of astrocytes as potential cellular targets in human ageing and disease.

6 MATERIALS AND METHODS

6.1 Materials

All chemicals used in this work were, if not stated otherwise, purchased from Sigma-Aldrich (Deisenhofen, Germany), Biomol (Hamburg, Germany), Biorad (Munich, Germany), Fluka (by Sigma-Aldrich, Deisenhofen, Germany), Invitrogen (Karlsruhe, Germany), Merck (Darmstadt, Germany), Roth (Karlsruhe, Germany), Riedel de Haen (Seelze, Germany), Serva (Heidelberg, Germany). Reagents for molecular biology were purchased from Applied Biosystems (Darmstadt, Germany), New England Biolabs (Frankfurt am Main, Germany), PeproTech (Hamburg, Germany), Promega (Mannheim, Germany), Roche (Mannheim, Germany) and Waters (Germany). MilliQ water was used for the generation of solutions (Millipore, Schwalbach, Germany). All restriction enzymes and their respective buffers were purchased from Fermentas (St. Leon-Rot, Germany), Roche (Mannheim, Germany) and New England Biolabs (NEB) (Frankfurt am Main, Germany).

Master-Mixes for PCR and quantitative real-time PCR were purchased from Eppendorf (Hamburg, Germany) and Agilent (Boeblingen, Germany).

6.1.1 Histological solutions

Borate buffer	Boric Acid	100	mM
	3.0915 g Boric acid in 500 ml H_2O		
	Dissolve in H_2O and adjust to pH 8.5		
Cryoprotect solution	Glycine	25	% (v/v)
	Ethylenglycol	25	% (v/v)
	Phosphate buffer	0.1	M
DAPI	6-diamidino-2-phenylindole	14.3	M
4 % PFA	Paraformaldehyd	4	% (w/v)
	NaOH	2-3	pellets
	Dissolve in 0.1 M PO_4-Buffer. Heat up to solve; pH 7.4		
Phosphate buffer 0.2 M	Sodium phosphate monobasic	0.552	% (w/v)
	Sodium phosphate dibasic	2.19	% (w/v)

Sucrose 30%	Sucrose	30	% (w/v)
	Dissolved in 0.1 M Phosphate-buffer.		
TBS (10x)	Tris	250	mM
	NaCl	1.37	M
	KCl	26	mM
	Adjust to pH 7.5		
TBS++	TBS	1	x
	normal donkey serum	3	% (v/v)
	Triton X-100	0.25	% (v/v)

6.1.2   Cell culture media and solutions

CaCl$_2$	CaCl$_2$ in H$_2$O	2	M
Dissociation solution	Trypsin (Sigma T4665)	0.13	% (w/v)
	Hyaluronidase (Sigma H3884)	0.07	% (w/v)
	dissolved in solution 1, sterile filtrated, prewarmed at 37 °C.		
HBS (2x)	NaCl	16	% (w/v)
	KCl	0.74	% (w/v)
	Na$_2$HPO$_4$ x 7 H$_2$O	0.402	% (w/v)
	Glucose	2	% (w/v)
	HEPES (Gibco 15630-1M)	10	% (w/v)
	NaOH, adjust to pH 7.05		
HEK293T cell medium	DMEM (Gibco 41966)	500	ml
	FBS (PAA A15-102)	10	% (v/v)
	Anti-anti (Gibco 15240-062-100x)	1	% (v/v)
Astrocyte medium	DMEM/F12 (GIBCO-31331)	500	ml
	Glucose	0.45	% (w/v)
	FBS (PAA A15-102)	10	% (v/v)
	Horse Serum (Gibco 26050-088)	5	% (v/v)
	B27 (Gibco 08-0085SA-50x)	2	% (v/v)

	Anti-anti (Gibco 15240-062-100x)	1	% (v/v)
	10 ng EGF and FGF per ml medium fresh every second day.		
Preparation buffer (astrocytes)	HBSS (Life Tech 1x)	50	ml
	HEPES (Gibco 15630-1M)	1	% (v/v)
Neurosphere medium	DMEM/F12 (GIBCO-31331)	500	ml
	B27 (Gibco 08-0085SA-50x)	2	% (v/v)
	Anti-anti (Gibco 15240-062-100x)	1	% (v/v)
	HEPES (Gibco 15630-1M)	1	% (v/v)
	10 ng EGF and FGF per ml medium fresh every second day.		
Solution 1 (NSC preparation)	HBSS (Life Tech 10x)	10	% (v/v)
	D-Glucose (Sigma)	1.8	% (v/v)
	HEPES (Life Tech, 1M)	1.5	% (v/v)
	pH 7.5		
Solution 2 (NSC preparation)	HBSS (Life Tech 10x)	5	% (v/v)
	Sucrose (Sigma)	30.8	% (w/v)
	pH 7.5		
Solution 3 (NSC preparation)	BSA (Sigma A4503)	4	% (w/v)
	HEPES (Life Tech, 1M)	2	% (v/v)
	EBSS (Life Tech 1x)	98	% (v/v)
	pH 7.5		

6.1.3 Molecular biology solutions

DNA-Loading dye (6 x)	Tris/HCl, pH 7.5	10	mM
	Glycerol	50 %	(v/v)
	EDTA	100	mM
	Xylencyanol	0.25 % (w/v)	
	Bromphenol blue	0.25 % (w/v)	
EtBr	Ethidiumbromide staining solution	1	µg/ml

LB medium	Bacto-Trypton	10	g/l
	Bacto-yeast extract	5	g/l
	NaCl	10	g/l
	pH 7.0; autoclaved (120°C, 20 min)		

LB agar	Bacto-Trypton	10	g/l
	Bacto-yeast extract	5	g/l
	NaCl	10	g/l
	Bacto-agar	15	g/l
	pH 7.0; autoclaved (120°C, 20 min)		

LBamp agar plates	LB agar + Ampicillin	0.1	% (m/v)

PBS (10x)	NaCl	137	mM
	KCl	2.7	mM
	Na_2HPO_4	8	mM
	KH_2PO_4	1.4	mM
	Adjust to pH 7.4		

TAE-buffer (5x)	Tris, pH 8.3	90	mM
	Acetic acid	90	mM
	EDTA	2.5	mM

6.1.4 Commercial kits (Manufacturer)

cDNA Kit SuperScript III	Invitrogen, Karlsruhe, Germany
DNA Maxi Prep	Promega, Mannheim, Germany
DNA Mini Prep/ NucleoSpin Plasmid Kit	Macherey-Nagel, Düren, Germany
PCR Master Mix	Eppendorf, Hamburg, Germany
RNeasy Kit	Qiagen, Hilden, Germany
SYBR Green ER qPCR Super Mix	ABI Prism, Applied Biosystems, CA, USA
QIAquick Gel extraction	Qiagen, Hilden, Germany
QIAquick PCR purification Kit	Qiagen, Hilden, Germany

6.1.5 Primary antibodies

antibody	species	dilution	Company
beta-galactosidase	rabbit	1:500	Cappel/MP Biomedicals, Illkirch, France
BrdU	rat	1:500	AbD Serotec, Düsseldorf, Germany
Cytochrome C	mouse	1:500	Becton Dickinson, Heidelberg, Germany
DAPI (fluorescent dye)		1:10.000	Sigma, Munich, Germany
DCX (C-18)	goat	1:250	Santa Cruz Biotechnology, Heidelberg, Germany
GFAP	rabbit	1:500	Dako, Hamburg, Germany
GFP	chicken	1:500	Aves Labs, Tigard, US-OR
Glutaminsynthetase (Mab 302)	mouse	1:500	Merck Millipore, Darmstadt, Germany
Iba1 (019-19741)	rabbit	1:500	WAKO Chemicals, Neuss, Germany
Ki67	rabbit	1:1000	Novocastra, Newcastle upon Tyne, UK
Prox1 (Ab5475)	rabbit	1:3000	Merck Millipore, Darmstadt, Germany
Sox2 (Y-17)	goat	1:1000	Santa Cruz Biotechnology, Heidelberg, Germany
TFAM	rabbit	1:500	gift of Nils-Göran Larsson, Cologne, Germany
βIII-tubulin (Tuj1)	mouse	1:2000	Sigma, Munich, Germany

6.1.6 Secondary antibodies

All secondary antibodies were purchased from Jackson ImmunoResearch Laboratories, Bar Harbor, US and Biotium, CA, US. Following fluorophore-conjugated antibodies directed against different species, according to primary antibodies, used in this work were Alexa 488, Alexa 543, Cy3, Cy5, FITC, and CF633. Dilutions of secondary antibodies were generally 1:250 or 1:1000 for CF633 (2 mg/ml).

6.1.7 Plasmids

pCAG-GFP	Expression vector, Amp^r	Zhao et al., 2006
pCAG-GFP-IRES-Cre	Expression vector, Amp^r	Jagasia et al., 2009
pCAG-GFP-IRES-mDsRed	Expression vector, Amp^r	this work
pCAG-IRES-mDsRed	Expression vector, Amp^r	Group Prof. Dr. Lie

6.1.8   Primer

Primer used for genotyping were as followed:

name	oligosequence (5' - 3' direction)
TFAM-A	CTGCCTTCCTCTAGCCCGGG
TFAM-B	GTAACAGCAGACAACTTGTG
TFAM-C	CTCTGAAGCACATGGTCAAT
R26R-R1	CACACCAGGTTAGCCTTTAAGC
R26R-D1	CAAAGTCGCTCTGAGTTGTTATC
R26R-Mutant	GCGAAGAGTTTGTCCTCA
EGFP-CAT-2	GGTACATTGAGCAACTGACTG
EGFP-AG-2	CTGCTAACCATGTTCATGCC
GLAST-CreER fwd	GAGGCACTTGGCTAGGCTCTGAGGA
GLAST-CreER rev	GAGGAGATCCTGACCGATCAGTTGG
GLAST-rerCreER1	GGTGTACGGTCAGTAAATTGGACAT

and primer for quantitative real-time PCR primer were:

name	oligosequence (5' - 3' direction)
3'UTR Tfam 1005	GCTGAGTTCTGCCTTTTGCT
3'UTR Tfam 1140	ACCACCACACAACTGTCACC
VDAC1 (Porin) mus F	GGGGATGCGAGAGTTGATAA
VDAC1 (Porin) mus R	GGAATGGGGTTTCTGCTGTA
CD68 mus 457 3'	CAATTCAGGGTGGAAGAAAG
CD68 mus 644	CTCGGGCTCTGATGTAGGTC
GFAP mus 507 3'	GCACAGGACCTCGGCACC
GFAP mus 655	TCCAGCGATTCAACCTTTCT
Vimentin mus 1148 3'	CAGATGCGTGAGATGGAAGA
Vimentin mus 1335	TCCAGCAGCTTCCTGTAGGT
nPF527 (RNaseP)	CAATCTCCAATGCCCTCAAT
nPR656 (RNaseP)	AGCCCAAACAGCAGTCCTAA
GAPDH fwd	GTGTTCCTACCCCCAATGTGT
GAPDH rev	ATTGTCATACCAGGAAATGAGCTT

6.1.9   Software

Genomatix	Genomatix Software GmbH, Munich, Germany
SPSS Statistics Standard	IBM, Ehningen, Germany
Imaris 7.5	Bitplane Scientific Software, Zurich, Switzerland
Leica Application Suite AF	Leica Microsystems, Wetzlar, Germany
NetPrimer	PREMIER Biosoft, http://www.premierbiosoft.com/netprimer/
Primer3	http://frodo.wi.mit.edu/
StepOne Real-Time PCR	Applied Biosystems, life technologies, CA, USA
Vector NTI	Invitrogen, Karlsruhe, Germany

6.2 Methods

6.2.1 Statistical analyses

Unpaired Student's t-test was used for analyses of most experiments. Before the t-test, an f-test was performed. In those cases in which the f-test resulted in a difference in the variances, a Mann-Whitney-Wilcoxon rank sum test was applied. For behavioral and cell extension analyses SPSS Statistics Standard was used for statistics in particular repeated measurements. Differences were considered statistically significant at $p < 0.05$. If not stated otherwise, all data are presented as mean ± s.e.m.

6.2.2 Mouse Analyses

All experiments were carried out in accordance with the European Communities Council Directive (86/609/EEC). The Government of Upper Bavaria approved the retroviral injections into the brain of adult mice which were carried out in accordance with protocols approved by the Institutional Animal Care Use Committee of the Salk Institute for Biological Studies (Jagasia et al., 2009).

For all experiments, mice were group housed in standard cages under a 12 h light/dark cycle with ad libitum access to water and food. C57BL/6 mice were obtained from Charles River and Harlan. $Tfam^{loxP/loxP}$ mice as described previously (Larsson et al., 1998; Wang et al., 1999) were crossed with GLAST::CreERT2 (GLAST) (Mori et al., 2006) and CAG-CAT-EGFP (EGFP) or R26R beta-galactosidase (R26R) mice (Nakamura et al., 2006).

Table 1 Mouse lines and their origin.

$Tfam^{loxP/loxP}$	conditional $Tfam$ knockout mice	Larsson et al., 1998
GLAST::CreERT2	inducible Cre recombinase activity under the GLAST promotor	Mori et al., 2006
CAG-CAT-EGFP	conditional EGFP reporter mice	Nakamura et al., 2006
R26R	conditional ß-galactosidase reporter mice	Nakamura et al., 2006

6.2.2.1 Breeding strategies

For the chronic TFAM depletion plus retroviral injections GLAST x R26R mice were used as control and GLAST x R26R x $Tfam^{loxP/loxP}$ as mutants. Littermates from GLAST x R26R x $Tfam^{loxP/+}$ parents were intra peritoneal (IP) injected with 0.5 mg Tamoxifen (Sigma) once per day at postnatal days 14, 16 and 18.

For chronic TFAM depletion plus BrdU injections GLAST x EGFP x $Tfam^{loxP/+}$ mice were used to produce GLAST x EGFP x $Tfam^{+/+}$ and $Tfam^{loxP/loxP}$ mice. The thus obtained littermates were deployed to start the following breedings. GLAST x EGFP mated with EGFP mice generated $Tfam$ Wildtype mice. GLAST x EGFP x $Tfam^{loxP/loxP}$ crossed with EGFP x $Tfam^{loxP/loxP}$ generated floxed $Tfam$ mice. Their offspring was IP injected with 0.5 mg Tamoxifen (Sigma) once per day at postnatal days 14, 16 and 18. For behavioral testings GLAST negative littermates from GLAST x EGFP x $Tfam^{loxP/loxP}$ crossed with EGFP x $Tfam^{loxP/loxP}$ breedings were used as non-recombined Tamoxifen-treated genetically close controls.

For acute TFAM depletion EGFP x $Tfam^{loxP/loxP}$ matings were utilized. These mice did not acquire any Tamoxifen treatment. They received retroviral injections in the hilus at the age of eight weeks. In the case of the TFAM-depleted newborn neurons they had been given a combination of CAG-Cre-IRES-GFP plus CAG-IRES-mitoDsRed to recombine the $Tfam$ locus and start the expression of EGFP as well as to mark the morphology of the whole cell and the mitochondria. CAG-GFP plus CAG-IRES-mitoDsRed was employed to label non-recombined newly generated neurons in EGFP x $Tfam^{loxP/loxP}$ mice.

Table 2 Mouse lines for different experimental paradigms.

GLAST::CreERT2 x R26R (x Tfam$^{loxP/loxP}$)	chronic TFAM depletion plus retroviral injections
GLAST::CreERT2 x CAG-CAT-EGFP (x Tfam$^{loxP/loxP}$)	chronic TFAM depletion plus BrdU injections
(GLAST::CreERT2) x CAG-CAT-EGFP x Tfam$^{loxP/loxP}$	behavioral testings
(CAG-CAT-EGFP x) Tfam$^{loxP/loxP}$	acute TFAM depletion via retroviral injections

6.2.2.2   Tailclip DNA-isolation and Genotyping

Tailclips were taken at the age of three weeks after weaning and directly collected into PCR-tubes. 100 µl 50 mM NaOH (400 mg/200 ml Millipore) were added before incubation at 98 °C for 20 min. The tubes were cooled down to 4 °C for 5 min prior to addition of 30 µl 1 M Tris-HCl pH 7 (15,76 g/100 ml Millipore +NaOH until pH 7). The tail DNA can be directly used for genotyping or was stored at -20 °C until use.

The right genotype was determined at weaning by PCR analyses using the genotyping PCR primer as shown in 0. 24 µl aliquots of the mastermix plus 1 µl of tail DNA were used for all genotyping PCRs. The PCR reaction mixes and conditions were as described in Table 3 till Table 6.

Table 3 Genotyping PCR for the *Tfam* locus (Mastermix for 10 reactions and PCR program)

5 PRIME Mastermix 2.5 x	100 µl	Denaturation	95 °C	5 min	
TFAM-A (10 pmol/µl)	20 µl		Denaturation	95 °C	30 s
TFAM-B (10 pmol/µl)	10 µl	35 cycles	Annealing	53 °C	30 s
TFAM-C (10 pmol/µl)	10 µl		Extension	72 °C	30 s
Ampuwa	100 µl	Final Synthesis	72 °C	5 min	

The expected size of PCR products for $Tfam^{+/+}$ was 404 bp, for $Tfam^{loxP/loxP}$ 437 bp, and for $Tfam^{-/-}$ it was 329 bp.

Table 4 EGFP genotyping PCR (Mastermix for 10 reactions and PCR program)

5 PRIME Mastermix 2.5 x	100 µl	Denaturation	95 °C	8 min	
CAT-2 (10 pmol/µl)	10 µl		Denaturation	95 °C	30 s
AG-2 (10 pmol/µl)	10 µl	40 cycles	Annealing	55 °C	30 s
Ampuwa	120 µl		Extension	72 °C	1 min
		Final Synthesis	72 °C	10 min	

As the EGFP reporter cassette was randomly inserted into the genome the genotyping primer were directed against EGFP itself resulting in just band at 300 bp in case of the existence of the EGFP gene there was no possibility to examine if mice were homo- or heterozygous.

Table 5 R26R genotyping PCR (Mastermix for 10 reactions and PCR program)

5 PRIME Mastermix 2.5 x	100 µl	Denaturation	95 °C	4 min	
D1 (10 pmol/µl)	10 µl		Denaturation	95 °C	30 s
R1 (10 pmol/µl)	5 µl	40 cycles	Annealing	50 °C	35 s
Mutant (10 pmol/µl)	5 µl		Extension	72 °C	35 s
Ampuwa	120 µl	Final Synthesis	72 °C	10 min	

The expected bands for the R26R genotyping were 253 bp for the WT locus and 300 bp for the locus including the β-galactosidase gene or eventually a mixture of both so two bands in case of the heterozygous animals.

Table 6 GLAST genotyping PCR (Mastermix for 10 reactions and PCR program)

CL	25 µl				
Q solution	50 µl	Denaturation	94 °C	2 min	
dNTPs (10mmol each)	5 µl				
CreER fwd (10 pmol/µl)	5 µl		Denaturation	94 °C	20 s
CreER rev (10 pmol/µl)	5 µl	35 cycles	Annealing	55 °C	20 s
rerCreER1 (10 pmol/µl)	5 µl		Extension	72 °C	30 s
Tag Q (U/ml)	10 µl				
Ampuwa	113 µl	Final Synthesis	72 °C	5 min	

The GLAST genotyping resulted in a 700 bp band in case of the WT or an additional one at 300 bp if an animal was heterozygous and positive for the CreERT2.

6.2.2.3 Retroviral Injections and Virusproduction

Retroviral injections using a vector that is based on the Moloney murine leukemia retrovirus allowed the transduction and therefore manipulation of single dividing cells in an otherwise largely unchanged adult hippocampal niche (Tashiro et al., 2006). For generation of the replication incompetent retrovirus particles human embryonic kidney (HEK) 293T cells were transfected with a mixture of plasmids containing capsid (CMV-VsVg), viral proteins (CMV-gag/pol) and a retroviral plasmid (CAG-vector). Supernatant was harvested four times every two days after transfection with Lipofectamine 2000 (Invitrogen) and concentrated using ultracentrifugation (Zhao et al., 2006; Tashiro et al., 2006; Jagasia et al., 2009; Mu et al., 2012). Viral titers were determined by transduction of HEK293T cells for 72 h with limiting dilution of MMLV suspension and counting of reporter expressing cell spots under a fluorescent microscope (Leica Microsystems). Titers applied were ~1×10^8 colony-forming units per ml (Zhao et al., 2006).

The *Tfam* gene was disrupted in adult floxed mice as described previously (Larsson et al., 1998) by stereotactic injection of a retrovirus coding for Cre recombinase into the adult dentate gyrus (pCAG-GFP-IRES-Cre). The Cre/loxP recombination system as described by (Kühn and Torres, 2002) was used to excise exons six and seven of the *Tfam* gene (Larsson et al., 1998). For visualization of dentate

granular cells and mitochondrial morphology pCAG-GFP, pCAG-IRES-mitoDsRed or the combination of both pCAG-GFP-IRES-mitoDsRed were injected (Mu et al., 2012; Zhao et al., 2006; Jagasia et al., 2009).

For the experiments two months old mice were anesthetized by IP injection of sleep (see Table 7 for composition). After being deeply narcotized they were clamped in a stereotactic chamber (Stoelting, Föhr Medical Instruments) to inject a volume of 0.9 µl virus (virus was diluted to 1×10^8 colony-forming units per ml with PBS prior injection) into the hilus of each hemisphere at coordinates relative to the bregma as follows: medial/lateral = ±1.6; anterior/posterior = -1.9; and dorsal/ventral from dura = -1.9. The surgery has been completed by sewing the scalp and waking up the mice on a heating plate (38 °C) by injecting the sleep antagonist awake (Table 7). Mice were sacrificed according to the distinct experiments at certain days post injection (dpi).

For running conditions mice were grouped in cages containing two animals with free access to a running wheel one week prior retroviral injections.

Table 7 Composition of anesthetics: sleep and its antagonist awake.

	Active compound	Drug name (company)	Stock (mg/ml)	Dose (mg/kg)	to inject (ml/kg)	Concentration needed (mg/ml)	Volume fractions (ml)
sleep	Fentanyl	Fentanyl (Janssen-Cilag)	0.1	0.05	10	0.005	0.25
	Midazolam	Dormicum (Roche)	5	5	10	0.5	0.5
	Medetomidine	Domitor (Pfizer)	1	0.5	10	0.05	0.25
	NaCl						Ad 5 ml
awake	Buprenorphine	Temgesic (Essex Pharma)	0.3	0.1	10	0.01	0.17
	Atipamezol	Antisedan (Pfizer)	5	2.5	10	0.25	0.25
	Flumazenil	Anexate (Hexal)	0.1	0.5	10	0.05	2.5
	NaCl						Ad 5 ml

6.2.2.4   Tamoxifen and BrdU injections

10 mg/ml Tamoxifen (Sigma) was left shaking at 4 °C in sunflower seed oil (Sigma) and 100 % Ethanol in a 10:1 ratio until completely dissolved (Erdmann et al., 2007). The solution was stored at -20 °C until use and in between usage for a maximum of four weeks. Whole litters were intraperitoneally (IP) injected once a day every second day at the age of P14, P16 and P18 using a dosage of 0.5 mg Tamoxifen in the case of the young recombined animals. The adult recombined mice received 1 mg Tamoxifen twice a day on five consecutive days at the age of two months (Mori et al., 2006; Hirrlinger et al., 2006).

For proliferation and survival studies animals were IP injected with a single dose of Bromodeoxyuridine (BrdU, 50 mg/kg body weight, Sigma-Aldrich) per day. BrdU was dissolved in 0.9 % NaCl and sterile filtrated. For proliferation BrdU was either administered once at the age of eight weeks 3 h prior perfusion or for seven consecutive days at the age of four months while mice were sacrificed one day after the last injection. Survival studies included three consecutive days of single BrdU injections at the age of eight weeks, while animals were perfused two or four months later.

To induce physical activity mice were grouped in cages containing two animals with free access to a running wheel for the indicated period of time (compare experimental setup Figure 13).

6.2.2.5   Perfusion and tissue processing

Mice were deeply anaesthetised by CO_2 and transcardially perfused at a speed of 10 ml per minute using phosphate-buffered saline (PBS, pH 7.4) for 5 min followed by 4 % Paraformaldehyd (PFA) applying the same settings. Animals were sacrificed at respective time points after distinct types of injections. Group sizes were minimal n equal three, exact numbers for each experiment are marked in the corresponding sections. Mice were decapitated, brains removed and post-fixed in 4 % PFA overnight at 4 °C. Following day brains were transferred into a 30 % sucrose solution and stored at 4 °C until usage. Brains were cut into 40 µm thick coronal or sagittal sections for general immunohistochemistry or 70 to 105 µm coronal sections for cell morphology analyses using a sliding microtome (Leica Microsystems, Wetzlar, Germany).

6.2.2.6   Immunohistochemistry

Brain sections were washed for three times 15 min in Tris-buffered saline (TBS) followed by a blocking step in TBS supplemented with 3 % normal donkey serum and 0.25 % Triton X-100 (TBS++)

for at least 1 h. Sections were then incubated in TBS++ containing the primary antibodies at the appropriate dilutions on a rotating rod at 4 °C for 48 h. After three washes in TBS and blocking in TBS++ for 30 min, sections were incubated in TBS++ containing appropriate secondary antibodies for 2 h at RT. Samples were washed three times with TBS, while the second washing step included 10 mg/ml DAPI (Sigma-Aldrich) for 10 min, and were mounted in Aqua PolyMount (Polysciences, Warrington, USA) on superfrost glass slides (Menzel-Gläser, Braunschweig, Germany). Sections were allowed to dry overnight at RT before being stored at 4 °C until usage.

For a BrdU staining the same procedure was applied except for an additional pretreatment. After the first three TBS washing steps sections were incubated with 2N HCl (9.51 ml H_2O plus 2.49 ml HCl) for 15 min slightly shaking at 37 °C followed by two rounds of 0.1 M Borate buffer for 10 min shaking at RT. Before continuing with the standard protocol in particular the TBS++ blocking step sections were thoroughly washed six times with TBS for at least 10 min each. The number of BrdU-, BrdU/S100β-, Prox1-, and green fluorescent protein (GFP)-expressing cells in the dentate gyrus was determined in every sixth 40 μm coronal section of the dorsal hippocampus. DAPI staining was used to trace the granule cell layer. Cell numbers were normalized to the analyzed granule cell layer volume. GFP+ cells were phenotyped by analyzing the coexpression with lineage-specific markers.

For GFAP immunohistochemistry cells were counted in an exemplary square in the center of the molecular layer as shown in Figure 25 c and d. Cell numbers were normalized to the counted volume. A similar square was chosen to count cells in the isocortex directly above the hippocampus.

6.2.2.7   Morphology analyses using Imaris 7.5

Confocal single plane images and *Z*-stacks were taken on a SP5 confocal microscope (Leica). For whole cell morphology at least three cells per animal and a minimum of 15 cells from more than 3 mice per group where chosen. The analyzed cells were located on the middle part of the upper arm of the dentate gyrus (DG) and were not obviously cut. Sections were 70 μm thick to guarantee penetration of the antibodies to determine the recombined cells (β-gal[+]) while having a larger population of uncut cells compared to 40 μm sections. For combined mitochondrial and morphology analyses scans, 0.3 μm stacks in a 1024 x 1024 resolution were taken with a 63 times glycerol objective.

The Imaris 7.5 software (Bitplane) allowed reconstructing virus targeted cells taking advantage of their fluorescent reporters. The "filament" tool was used to semiautomatically trace dendritic trees and thereby getting information about cell length, branch points and Scholl intersections. The "surface" tool was applied to reconstruct mitochondria and soma according to their fluorescence

intensities choosing appropriate volume thresholds. For mitochondria an additional background subtraction was selected as well as an "enabled" function to automatically separate mitochondria in close proximity. Surfaces were used to calculate mitochondrial and soma volumes and mitochondrial numbers, that were normalized either to the dendritic cell length or soma volume. Every Imaris 7.5 analysis was manually corrected if necessary.

6.2.2.8 Spine analysis and mitochondrial fragmentation or elongation analysis

Confocal 0.3 µm stacks in a 1024 x 1024 resolution were taken with a 63 times glycerol objective and an additional 5 times zoom on a SP5 confocal microscope (Leica). Spine pictures were taken from 10 individual cells per animal (3 to 4 in total) containing one dendritic arm each located in two thirds of the molecular layer. The pictures were taken including the mDsRed signal to analyze mitochondrial length. The Leica Application Suite AF was used to manually count dendritic spines and determine their morphology. A spine head larger than 0.6 µm was defined as mushroom spine. The mitochondrial length was measured using the same software and was classified into four groups. These classifications were fragmented (< 1 µm), medium (1-2 µm), medium large (2-3 µm) and tubular (> 3 µm). The percentage was determined with regard to the total counted spine or mitochondrial number.

6.2.2.9 Cell extension analysis for immature neurons

Filament tracing is a time-consuming task and is therefore limited to a small number of cells. An alternative method (cell extension method) was applied to analyze a larger cohort of neurons. The cell extension method was less time consuming and less restrictive with respect to whole intact cells, but was limited to immature neurons, as mature cells are all spanning the molecular layer reaching the hippocampal fissure. This method is based on a ratio of the maximal possible extension of a cell, which is varying according to the cell localization in the DG, and the actual extension measured from the soma to the end of the furthest reaching dendrite as depicted in Figure 35. If a neuron is spanning the whole molecular layer as far as the hippocampal fissure, like a mature neuron, the ratio would be 1:1. The smaller a cell is in relation to its maximal possible extension the smaller the ratio. Cells were preferentially analyzed in the upper arm and if an increase of cell numbers was needed also in the lower arm. Four mice per group and at least 19 to 65 cells per animal were measured. In the lower arm the natural border of the hippocampus was used to determine the maximal possible extension instead of the hippocampal fissure.
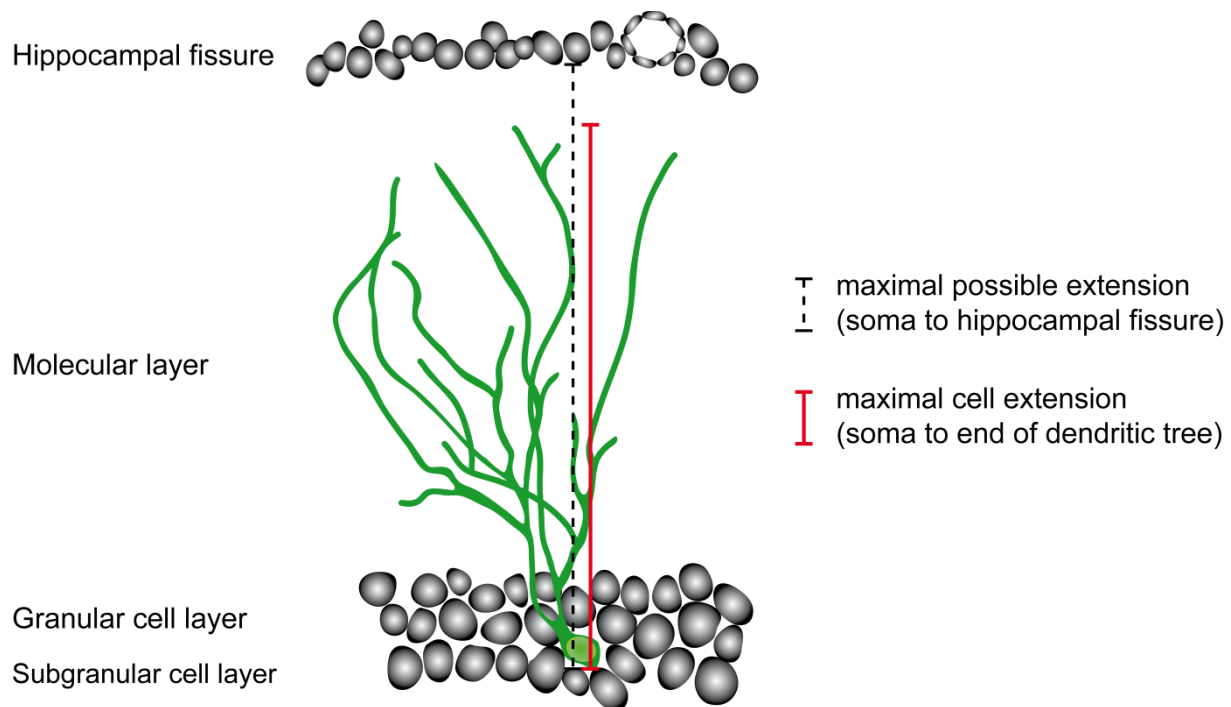
Figure 35 Schematic description of the maximum cell extension analysis. A maturing neuron (green) is depicted in the upper arm of the DG including measurement marks for the possible extension (black dotted line) and the maximal cell extension (red line).

6.2.2.10 Behavioral Analyses

All behavioral examinations were performed during the light period of the light/dark cycle, if not mentioned otherwise. Mice were housed three per cage except for the single housed mice cohorts of the WCM and FST. The RR, OF, and PPI tests were carried out following the standardized operation protocols used for behavioral screening developed by EUMORPHIA that are available at EMPReSS[1] European Mouse Phenotyping Resource or were based on these and adapted to the specifications of the used setup. For data analyses the Observer 4.1 Software (Noldus, Wageningen, The Netherlands) was used. The data are presented as mean ± s.e.m. and for statistical purposes were either two-tailed unpaired or paired Student's t-test, two-way or three-way ANOVA applied when appropriate. At least 30 min prior testing the animals were allowed to acclimate in the room where a test was conducted.

Rotarod (RR), open field (OF), PrePulseInhibition (PPI) and social discrimination (SD) were carried out in collaboration with the German Mouse Clinic and the group of Sabine Hölter Koch. Water Cross Maze (WCM) was established in the laboratory of Prof. Dr. Carsten T. Wotjak (MPI of Psychiatry) and conducted by Anupam Sah and Judith Reichel. Forced Swim Test (FST) was done in cooperation with

---

[1] [online] URL: http://www.empress.har.mrc.ac.uk/browser/ (Behaviour and cognition) [04.02.2013, 08:05]

the group of Volker Eulenburg (Friedrich-Alexander University of Erlangen-Nürnberg) and accomplished with the help of Stefanie Schuster.

We used different cohorts of CAG-CAT-EGFP (E) x $Tfam^{loxP/loxP}$ (T) / x GLAST::CreERT2 (G) mice. ET mice were used as controls for the mutant EGT mice. All except for one cohort were Tamoxifen-treated at the age of two weeks and analyzed at different time points after the recombination. Control and mutant mice coming from the same litters were chosen to diminish behavioral effects caused by slightly different genetic backgrounds or handling differences.

6.2.2.10.1 Rotarod

The used RR apparatus (LE8200 Letica, Panlab, Spain/Bioseb, France) contained a rotating rod with a diameter of 5 cm that was covered by grey insulation rubber foam and was separated into five test lanes by white plastic spacer discs. Each test lane was 5 cm wide and had a flap underneath that was functioning as a fall sensor and stopped the latency to fall. The rotating rod allowed acceleration from 40 to 400 rpm in 300 sec. At the beginning mice were placed on the constantly rotating rod (4 rpm) to see whether they were able to keep their balance and walk on the rod. If this was fine the first trial was started and the latency and the rpm at which every mouse was falling off was noted. A mouse passing a whole turn of the rod without falling off, was taken off the rod, time was stopped and a passive turn was noted. The setup was cleaned with disinfectant between the different trials. Three trials with a duration of 5 min each and a 15 min resting interval between the beginnings of consecutive trials were conducted. After all three trials each mouse was weighed and the body weight noted.

6.2.2.10.2 Open Field

The square-shaped (45.5 x 45.5 x 39.5 cm) OF box from TSE ActiMot[2] contained two pairs of light-beam strips (transmitter and receiver) arranged at right angles to determine x and y coordinates of the mouse. Two additional uni-dimensional light-barrier strips allowed for detection of rearing. The experimental room was illuminated to approximately 200 lux which resulted in 150 lux in the corners of the test arena.

---

[2] [online] URL: http://www.tse-systems.com/products/behavior/activity/actimot2.htm [19.02.2013, 10:20]

The mice were individually placed into the box facing the middle of one of the walls and observed while exploring the arena for 20 min. A disinfectant was used to clean the apparatus between test subjects.

An imaginary division of the OF box into an inner part (42 % of the total arena) and a periphery corridor (8 cm along the walls) were used to collect data concerning latency and number of center entries, percentage of time spent, speed of movement, and total distance travelled, resting and permanence time, either in the center or periphery or both. Besides these parameters rearing was recorded. Furthermore, the time course of distance travelled, rearing frequencies and additionally the percentage of time spent in the center and distance travelled was analyzed in 5 min intervals.

6.2.2.10.3 Pre-Pulse Inhibition

The PPI was assessed one week after the OF using a startle test station (Med Associates Inc., VT, USA) containing four identical sound-attenuating cubicles and a Med Associates "Advanced Startle" software. The experiments were conducted during the light cycle phase. In the beginning the animals were allowed to acclimate for 5 min without a pre-pulse stimulus followed by five bursts of white noise of 110 dB per 40 msec. The background noise used for normalisation was 65 dB. During the trials four different pre-pulse intensities of 67, 69, 73 and 81 dB were applied, each pre-pulse was presented 50 msec before the 110 dB startle pulse. These four pre-pulse intensities were organized in 10 blocks, so that each trial type was presented once per block in a random fashion with intervals varying from 20 to 30 sec.

6.2.2.10.4 Social Discrimination

Experimental mice were put in a fresh cage 2 h prior testing. Into this familiar cage an ovariectomised (OVX) female mouse was introduced and the behavior of the experimental mouse was recorded for a 4 min sampling phase before removing the OVX female again. 2 h later in addition to the known OVX female another unfamiliar OVX female was introduced in parallel. The experimental mouse was observed for another 4 min precisely monitoring the investigation behavior in relation with the known and novel conspecifics. Significantly longer sniffing of the unknown compared with the known mouse was judged as intact recognition memory. Furthermore, a recognition index reflecting the ratio of the investigation time of the novel stimulus compared to the total investigation time (familiar plus unfamiliar) was determined (Pham et al., 2010).

6.2.2.10.5 Water Cross Maze

Mice were single housed starting one week prior testing. The WCM as depicted in Figure 33 b contains four arms, which can be individually closed by using a transparent partition, additionally a platform and a shovel to get the mice out of the water. Four light sources facing the walls were indirectly illuminating the room (low lighting conditions). Extra-maze cues like dishcloth, heat lamp or a broom were kept at the very same position for the whole training period. The 23 °C warm water in the WCM was replaced every day and filled up to 11.5 cm to cover the platform. Water drops on the walls needed to be wiped dry prior testing a new mouse to avoid blurring the view, addition of extra-maze cues and a general smear.

The mice were trained in four groups of eight animals for six trials a day. A whole group was brought into the WCM room and the first animal was placed in the WCM its head orientated towards the experimentator. After scooping the animal out of the water, it was placed in its homecage next to a red light preventing a drop in body temperature.

The partition was used to block the arm opposite to the starting arm. The mice had 30 sec after being dropped into the water to reach the platform, which was located at the end of one of the other arms, and climb on it. There are three different learning protocols (free, response or place learning) for the WCM. To detect hippocampal-dependent spatial learning deficits the place learning strategy was applied. Therefore the platform was located at the far end of the west arm during the first week and at the end of the east arm during the second week. As illustrated in Figure 36 the starting position for the mice was changed irregularly during training and re-training phase pursuing the scheme depicted in Table 8. There were five days (1-5) of training during the first week followed by two days of resting and five days (6-10) of re-training during the second week.

Table 8 Place learning: Sequence of starting positions on distinct experimental days.

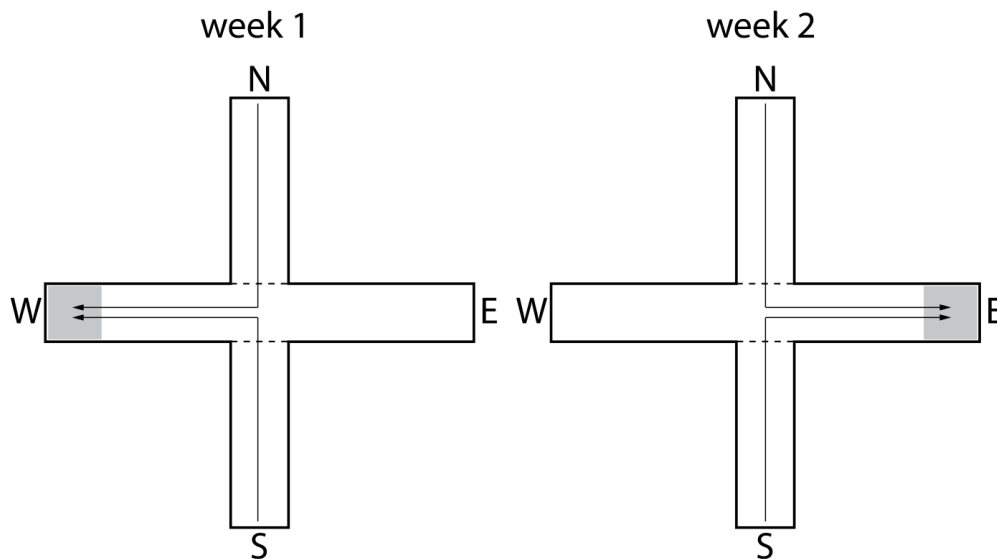| Testing days	1, 3, 5, 7, 9	2, 4, 6, 8, 10
Start position sequence	N, S, S, N, N, S	S, N, N, S, S, N

Figure 36 Spatial or place learning protocol for WCM. First week training phase finding the platform (grey square) placed in the west arm (W) starting either from the south (S) or north (N) arm, the opposite one blocked by transparent partition (dotted line). Second week representing the re-training phase using the same starting positions but locating the platform in the east arm (E). The arrows are marking the optimal way to the platform.

The time of the trials was noted to ensure equal inter-trial-intervals. The other parameters rated were "arms visited", "wrong platform visit" and "total time until platform". The latter describes the latency to reach the platform which was stated as 31 sec if the animal did not find the platform within 30 sec. For "arms visited" it was counted as soon as a mouse entered a new arm with its whole body except for the tail. If the animal reached for the outer third of the arm opposite of the platform containing arm it was scored as "wrong platform visit", while swimming back to the starting position was not. It was also noted whether an animal tried to climb up the walls, was circling or floating.

On the first day mice, that did not reach the platform, where guided using a grid to lead the animals towards the goal arm and let them sit on the platform for approximately 20 sec. All six trials were listed and scored "1" that means accurate if the mouse directly swum into the goal arm sitting on the platform within maximal 30 sec or "0" if not. If five out of six trials per day (= 83 %) could be declared correct the animal was considered an accurate performer. Each wrong platform visit was counted as "1", if an animal repeatedly reached for the outer arm of the arm opposite of the platform the visits were added up to the total number of wrong platform visits. If an animal swum into the wrong arm, but did not enter the outer third this was noted as "0" for accuracy as well as wrong platform visits.

6.2.2.10.6 Forced Swim Test

Male mice in a predefined age (9 months) that were single housed and kept under a 12 h dark and light cycle were tested shortly before the start of their dark cycle, in that case from 4 to 7 pm. A 2 l beaker glass with a diameter around 15 cm was filled with 1.6 l 26 °C warm water prior testing. The water was exchanged and temperature controlled after every fourth to fifth animal. The testing period was in total 6 min. The floating time in every minute was counted using two timers being able to save in total six individual time frames (each one for 1 min).

The 6 min period was started when placing the mouse in the water. From that moment on the time was stopped while the mouse was floating. A mouse was considered floating after not trying to escape for at least 2 sec, keeping his forepaws close to his body using one or two hind legs to stabilize itself. The first floating was not counted as it is in most cases a shock reaction of facing to be swimming in the water. Moving around a little while floating was still counted as floating until the mouse showed signs of trying to get out of the beaker. If the mouse started struggling and was still after 2 sec it was stated as struggling.

For the equipment it was important that the mice could not reach the bottom with their tale, the diameter was long enough to avoid stretching of the mouse and not too long to avoid the mouse being swimming around too much looking for a way to escape.

6.2.3   Molecular Biology Methods

6.2.3.1   RNA Isolation

RNA was isolated from dissected hippocampus or Cortex using either the RNeasy Kit (Qiagen, Hilden, Germany) according to manufacturer's protocol, or using the Trizol (Invitrogen, Karlsruhe, Germany) reagent. For the latter 100 mg of tissue was homogenized in 1 ml Trizol and either stored at -20 °C or directly incubated at RT for 5 min before adding one-fifth volume of Chloroform and vigorously vortexing the whole mixture for 15 sec. After 3 min incubation at RT the mixture was subsequently centrifuged at 14000 rcf, and 4 °C for 15 min. The aqueous phase was transferred into a new 1.5 ml Eppendorf tube and incubated for another 10 min at RT with 0.5 ml ice-cold Isopropanol per 1 ml of Trizol. Lysate was centrifuged (14000 rcf / 4 °C / 30 min) again, supernatant was discarded and the remaining pellet washed with 75 % EtOH (14000 rcf / 4 °C / 5 min) before being dried at RT for about 5 min. RNA was dissolved in RNase-free water at 55 °C, 500 rpm for 10 min and the concentration was measured using a NanoDrop Spectrophotometer (Thermo Fisher Scientific, Waltham, MA-US).

6.2.3.2   DNA Isolation and Purification

DNA isolation was performed using the NucleoSpin Plasmid Kit (Macherey-Nagel). The QIAquick Gel Extraction Kit (Qiagen) was applied to purify DNA from agarose gels and the QIAquick PCR purification Kit (Qiagen) was used for direct purification of PCR fragments. For DNA precipitation, dissolved DNA was mixed with one-tenth of 3 M NaAc (pH 4.6) (v/v) and 2.5 times 100 % EtOH (v/v), incubated at -20 °C for at least 1 h and then centrifuged at 13000 rcf at 4 °C for 30 min. DNA pellet was allowed to dry at RT for 10 min and was resuspended in an appropriate volume of ddH$_2$O. Concentrations were measured with a NanoDrop Spectrophotometer (Thermo Fisher Scientific).

6.2.3.3   cDNA Synthesis

cDNA synthesis of a minimum of ~300 ng RNA using Superscript III Kit (Invitrogen) was carried out according to manufacturer's protocol including DNase (Promega) treatment.

6.2.3.4   Quantitative real-time PCR

Quantitative real-time PCR (qRTPCR) was performed on a StepOne instrument (Applied Biosystems) using SYBR GreenER qPCR Super Mix (ABI Prism, applied biosystems, CA, USA) for detection. The qRTPCR was carried out according to manufacturer's guidelines, using 200 nM of each primer (forward and reverse) as wells as only 1 µl appropriately diluted cDNA per 20 µl reaction volume. The reaction started with a denaturation step at 95 °C for 10 min followed by 40 cycles consisting of 95 °C for 15 sec and 60 °C for 1 min. Online Software tools as NetPrimer and Primer3 were used to design and pre-analyze primer for different targets.

6.2.3.5   Transformation

DH5α or TOP10 competent cells were thawed on ice for 15 min before 90 µl of the cell suspension was transferred to 14 ml round-bottom Falcon tube. Cells were mixed with DNA and incubated on ice for 30 min. A 45 sec heat-shock was applied by incubating the tubes in a pre-warmed 42 °C water bath followed by 2 min on ice. 1 ml of LB medium was added to the cells which were allowed to recover for 1 h shaking (400 rpm) at 37 °C before being spread on Ampicillin (100 µg/ml) containing agar plates. For a fast retransformation cells were incubated with DNA for 15 min after thawing and directly plated.

6.2.3.6 Cloning of CAG GFP IRES mDsRed

DNA of interest was subcloned from other plasmids. Plasmids of interest were digested with appropriate restriction endonucleases and further cloned into a shuttle vector, which is derived from pBluescript II carrying additional restriction sites for Pme1 and Sfi1. Finally, cDNA was excised and ligated into a retroviral vector of choice in the correct orientation.

Buffers, enzymes and incubation times were as given in the manufacturers protocol (NEB). Dephosphorylation of opened vector was carried out by incubation with 5 U phosphatase (New England biolabs) at 37 °C for 30 min to prevent religation. Prior ligation fragments were purified by agarose gel electrophoresis, extracted using the QIAquick Gel Extraction Kit (Qiagen), and combined in a 3:1 ratio (DNA_{insert} : DNA_{vector}) with 400 U T4-DNA-ligase (NEB) in the appropriate buffer at 16 °C for 14 h. As negative control 1 µl of digested vector without insert was used.

6.2.4 Cell Biology Methods

6.2.4.1 Cell Culture

6.2.4.1.1 HEK293T cells

HEK293T cells were cultured in DMEM (high glucose + pyruvate) supplemented with 10 % of bovine serum albumin and 1x penicillin/streptomycin/fungizone (Anti-Anti). Cells were grown on uncoated cell culture plates and passaged by trypsination when cell density reached 70 % confluence.

6.2.4.1.2 Neurospheres (SVZ mouse adult neural stem cells)

Neurospheres were cultured from neural stem cells isolated from adult mouse brain SVZ. Mice were killed by cervical dislocation and brains immediately transferred to ice-cold DPBS. SVZs were dissected by cutting very thinly the wall of the lateral ventricle. Tissue was incubated for 15 min at 37 °C in 5 ml dissociation media. After gentle mechanical disruption by using glass pipettes, until medium became milky, incubation was continued for additional 15 min at 37 °C. Subsequently enzymatic reaction was stopped by addition of 5 ml ice-cold solution 3, cells were passed through a 70 µm strainer (Falcon Cat.: 352350) and centrifuged at 300 rcf for 10 min. Supernatant was discarded, pellet resuspended in 10 ml ice-cold solution 2 and spun down at 300 rcf for 10 min. Supernatant was removed, cells were resuspended in 2 ml ice-cold solution 3 and gently transferred on top of 12 ml of ice-cold solution 3 in a fresh 15 ml tube. After centrifugation at 400 rcf for 10 min the cell pellet was resuspended in neurosphere (NS) medium containing 10 ng/ml EGF and FGF (Peprotech). Neurospheres were grown in NS media at 37 °C and 5 % CO_2. They were passaged every

5th to 7th day after reaching a certain size (100 – 140 µm in diameter). For splitting, neurospheres were transferred to a 15 ml tube and centrifuged at 100 rcf for 5 min. Supernatant was filtrated through a 0.40 µm strainer (Falcon Cat.: 352340) and kept at 37 °C. Pellet was washed once in 1 % DPBS, resuspended in 0.5 ml accutase (Millipore SCR005) and incubated at 37 °C for 5 to 10 min. Neurospheres were dissociated by gentle trituration (20 times) through a 200 µl pipette tip on top of a 5 ml pipette. 2 ml pre-warmed neurosphere NS medium were added to stop the enzymatic reaction. Cells were centrifuged at 400 rcf for 7 min, resuspended in NS medium and cell number determined using a Neubauer counting chamber. After first passage cells were grown in 15 ml NS medium containing 20 % (v/v) of old medium (supernatant from first centrifugation). Cell density after following passages was 200.000 cells per 15 ml (medium flask).

Neurospheres were cultured for up to eight passages before new stem cells were isolated.

6.2.4.1.3   Astrocytes

Postnatal mice P5 or P6 were decapitated and the heads were sterilized with 70 % EtOH before being transferred into ice-cold astrocyte preparation buffer. The hippocampus and cortex were dissected by carefully removing all meninges. The minced tissue was centrifuged (900 g, 5 min, RT) in a 15 ml Falcon tube. The supernatant was discarded and the pellet resuspended in 10 ml of astrocyte medium using a 5 ml pipet. Usually two brains were mixed together in one medium sized flask (10 ml, 1T75) or one brain in 5 ml in a small sized flask (1T25). Medium was exchanged every four days after 2 h of shaking (200 rpm) at RT to remove unattached tissue like fast proliferating microglia cells. Cells were passaged by trypsination when cell density reached 70 % confluence.

6.2.4.2   Fluorescence-activated cell sorting (FACS)

Mice were decapitated after a fast neck fracture and the hippocampus was taken out and cut into small pieces. Tissue from one mouse was resuspended in 1 ml of enzyme mixture incubating for a maximum of 25 min in a 37 °C warm water bath, while mixing it ever 5 min in between with a flamed glass capillary. The enzyme mixture was composed of 50 µl (50 mM) EDTA and 50 µl (100 mM) L-Cysteine that were left shaking for 30 min at 4 °C to activate 2 mg Papain dissolved in 5 ml HBSS, as well as 5 mg Dispase and 2 mg DNase I and 167 µl $MgSO_4$ dissolved in additional 5 ml of HBSS that were added and sterile filtered before use.

After resuspension the tissue enzyme mix was passed through a 70 µm filter into a 50 ml Falcon tube. The filter was flushed with 2 ml of DMEM/F12 (GIBCO-31331) supplemented with 10 % FBS and the

cell suspension transferred into a 15 ml Falcon using another 3 ml medium to rinse the 50 ml tube. The suspension was centrifuged at 1000 rcf for 3 min at RT. Supernatant was discarded and the pellet resolved in 10 ml DMEM/F12 supplemented with 10 % FBS. This centrifugation step was repeated once and the cell pellet was resuspended in 5 ml DMEM / F12 supplemented with 10 % FBS and mixed with 5 ml Percoll (4.5 ml Percoll plus 0.5 ml 10x PBS) prior a 30 min centrifugation at 13.000 rpm at RT. Afterwards the myelin layer needed to be removed and the solution was filled up to 5 ml with PBS before another centrifugation at 1.000 rcf for 3 min at RT. Supernatant was discarded and the cell pellet was resuspended in 0.5 ml medium and was transferred into a 1.5 ml Eppendorf tube. The rest of the pellet was dissolved in 0.3 ml medium and was transferred into the same Eppendorf tube. Cells were passed through a 40 µm strainer and sorted according to their green fluorescent signal into a new tube. They were kept on ice and directly proceeded for DNA and RNA isolation. Flow cytometry was conducted in collaboration with Wolfgang Beisker at the institute of molecular toxicology and pharmacology at the Helmholtz Centre Munich.

7 ABBREVIATIONS

aa	Amino acid
ADP	Adenosine di phosphat
Akt	Protein kinase B
ALS	Amyotrophic lateral sclerosis
AMP	Adenosine mono phosphat
Amp	Ampicillin
AMPA	alpha-amino-3-hydroxy-5-methyl-4-isoxazolepropionic acid
ARSACS	Autosomal recessive spastic ataxia of Charlevoix-Saguenay
ATP	Adenosine tri phosphat
Bax	Bcl2 associated X-protein
Bcl2	B-Cell Leukemia-2
bHLH	Basic helix-loop-helix
bp	Base pair
BrdU	Bromodesoxy uridin
BSA	Bovine serum albumin
°C	Degrees Celsius
CaCl$_2$	Calcium Chloride
CamKII	Calmodulin kinase II
CAT	Chloramphenicol acetyltransferase
Cb	Cerebellum
cDNA	copy DNA
ChIP	Chromatin immuno precipitation
(c)ko	(conditional) knockout
CMV	Cytomegalovirus
CNS	Central nervous system
CO$_2$	Carbon dioxide
COX1	Cytochrome c oxidase subunit 1
Cre	Bacteriophage P1 recombinase
Ctx	Cortex
DAPI	4',6-Diamidino-2-phenylindol
DAT	Dopamine transporter
DCX	Doublecortin
DG	Dentate Gyrus
DNA	Desoyxribonucleic acid
Drp1	Dynamin-related protein
E.coli	Escherichia coli
EAAT1	Excitatory amino acid transporter 1
EBSS	Earle´s balanced salt solution
EDTA	Ethylendiamintetraacetat
EGF	Epthelial growth factor
(E)GFP	(enhanced) green fluorescent protein
EGTA	Ethylene glycol tetraacetic acid
ESC	Embryonic stem cell
et al.	et alteri
EtOH	Ethanol

FCS	Fetal calf serum
FGF	Fibrillary growth factor
Fis1	Fission 1
FITC	Fluorescein
FMI	FMI Föhr Medical Instruments GmbH
fob	Familiar object
FST	Forced Swim Test
g	Gram(s), gravitation
GABA	γ-Aminobutyric acid
GAPDH	Glyceraldehyd-3-phosphate dehydrogenase
GCL	Granular cell layer of DG
GDAP1	Ganglioside-induced differentiation-associated-protein 1
GFAP	Glial fibrillary acidic protein
Glast	Glutamate aspartate transporter
GS	Glutamine synthetase
h	Hours
HBSS	Hank´s balanced salt solution
HC	Hippocampus
HCl	Hydrochloride acid
HD	Huntington's disease
HEK	Human embryonic kidney cell
HEPES	4-(2-hydroxyethyl)-1-iperazineethanesulfonic acid
hGFAP	Human GFAP promoter
HMG box	High mobility group box
IL	Interleukin
i. p.	intra peritoneal
IRES	Internal ribosomal entry side
kDa	Kilo Dalton
l	Liter
Leu	Leucin
LHON	Leber's Hereditary Optic Neuropathy
LPS	Lipopolysaccharide
lux	lat. Light
LV	Lateral ventricle
M	Molar, mol
m	Milli (10-3)
MeCP2	Methyl-CpG–binding protein 2
MERRF	Myoclonus epilepsy with ragged-red fibers
MFN2	Mitofusin 2
MILON	Mitochondrial late-onset neurodegeneration
min	Minute(s)
Mitopark	Mice showing a mitochondrial dependent parkinson disease phenotype
mNSC	Neural stem cells from mouse
mTERF	Mitochondrial transcription termination factor
Mut	Mutant
n	Sample size
NaCl	Natrium chloride

NaOH	Natrium hydroxide
NRF1/ 2	Nuclear respiration factor 1 and 2
nt	Nucleotides
OB	Olfactory bulb
OF	Open Field
OH	Heavy strand origin of replication
OL	Light strand origin of replication
OPA1	Optic atrophy 1
P	Postnatal day
p	p-value for statistical analysis
P14/16/18	Postnatal day 14, 16 and 18
PARP	Poly [ADP-ribose] polymerase
PBS	Phosphate buffered saline
PCR	Polymerase chain reaction
PD	Parkinson's disease
PFA	Paraformaldehyd
PGC1α	PPARγ coactivator 1α
pH	Potentium hydrogenii
Phe	Phenylalanin
PINK1	PTEN-induced kinase 1
PolgA	mtDNA polymerase γ
POLRMT	Mitochondrial RNA polymerase
PPARγ	Peroxisome proliferator-activated receptor gamma
PPI	Pre-pulse inhibition
PTEN	Phosphatase and tensin homolog
qRTPCR	Quantitative real-time PCR
R26R	ß-galactosidase gene integrated in the Rosa26 locus
Rcf	Centrifugal force (g force)
RMS	Rostral migratory stream
RNA	Ribonucleic acid
ROS	Reactive oxygen species
RR	Rotarod
rRNA	ribosomal RNA
RT	Room temperature
RTT	Rett syndrome
s.e.m.	Standard error of the mean
SD	Social Discrimination
SGZ	Subgranularzone (part of the the DG Granular Cell layer, facing the hilus)
Sirt1	Sirtuin 1
SLC1A3	Solute carrier family 1 member 3
SOD1	Superoxide dismutase 1
SOX2	Sry-box containing gene 2
SVZ	Subventricular Zone
TAE	Tris acetate with EDTA
TBS	Tris buffered saline
TF	Transcription factor
TFAM	Mitochondrial transcription factor A

TFMB2	Mitochondrial transcription factor B2
TGF	Transforming growth factor
TNFα	Tumor necrosis factor alpha
Tris	Tris-(hydroxymethyl-) aminomethan
tRNA	transfer RNA
U	Units
UCP	Uncoupling proteins
uob	Unknown object
V	Volt
Val	Valin
(v/v)	Volume/volume
WCM	Water Cross Maze
WT	Wildtype
(w/v)	Weight/volume
x	Symbol for crosses between mouse lines
μ	Micro (10-6)

8 REFERENCES

Ables JL, Decarolis NA, Johnson MA, Rivera PD, Gao Z, Cooper DC, Radtke F, Hsieh J, Eisch AJ. 2010. Notch1 is required for maintenance of the reservoir of adult hippocampal stem cells. The Journal of neuroscience 30:10484–10492.

Ahn S, Joyner AL. 2005. In vivo analysis of quiescent adult neural stem cells responding to Sonic hedgehog. Nature 437:894–897.

Aimone JB, Deng W, Gage FH. 2011. Resolving new memories: a critical look at the dentate gyrus, adult neurogenesis, and pattern separation. Neuron 70:589–596.

Allen NJ, Barres BA. 2009. Neuroscience: Glia - more than just brain glue. Nature 457:675–677.

Almeida A, Almeida J, Bolaños JP, Moncada S. 2001. Different responses of astrocytes and neurons to nitric oxide: the role of glycolytically generated ATP in astrocyte protection. Proceedings of the National Academy of Sciences of the United States of America 98:15294–15299.

Almeida A, Cidad P, Delgado-Esteban M, Fernández E, García-Nogales P, Bolaños JP. 2005. Inhibition of mitochondrial respiration by nitric oxide: its role in glucose metabolism and neuroprotection. Journal of Neuroscience Research 79:166–171.

Altman J, Das GD. 1965. Post-natal origin of microneurones in the rat brain. Nature 207:953–956.

Alvarez-Buylla A, Garcia-Verdugo JM. 2002. Neurogenesis in adult subventricular zone. The Journal of neuroscience 22:629–634.

Alvarez V, Corao AI, Alonso-Montes C, Sánchez-Ferrero E, Mena L de, Morales B, García-Castro M, Coto E. 2008. Mitochondrial transcription factor A (TFAM) gene variation and risk of late-onset Alzheimer's disease. Journal of Alzheimer's disease 13:275–280.

Anderson S, Bankier AT, Barrell BG, Bruijn MH de, Coulson AR, Drouin J, Eperon IC, Nierlich DP, Roe BA, Sanger F, Schreier PH, Smith AJ, Staden R, Young IG. 1981. Sequence and organization of the human mitochondrial genome. Nature 290:457–465.

Araque A, Parpura V, Sanzgiri RP, Haydon PG. 1999a. Tripartite synapses: glia, the unacknowledged partner. Trends in neurosciences 22:208–215.

Araque A, Sanzgiri RP, Parpura V, Haydon PG. 1999b. Astrocyte-induced modulation of synaptic transmission. Canadian journal of physiology and pharmacology 77:699–706.

Arruda-Carvalho M, Sakaguchi M, Akers KG, Josselyn SA, Frankland PW. 2011. Posttraining ablation of adult-generated neurons degrades previously acquired memories. The Journal of neuroscience 31:15113–15127.

Artegiani B, Calegari F. 2012. Age-related cognitive decline: can neural stem cells help us? Aging (Aging) 4:176–186.

Attwell D, Buchan AM, Charpak S, Lauritzen M, Macvicar BA, Newman EA. 2010. Glial and neuronal control of brain blood flow. Nature 468:232–243.

Atwood HL, Wojtowicz JM. 1999. Silent synapses in neural plasticity: current evidence. Learning & memory 6:542–571.

Aubert A, Pellerin L, Magistretti PJ, Costalat R. 2007. A coherent neurobiological framework for functional neuroimaging provided by a model integrating compartmentalized energy metabolism. Proceedings of the National Academy of Sciences of the United States of America 104:4188–4193.

Ban T, Heymann JAW, Song Z, Hinshaw JE, Chan DC. 2010. OPA1 disease alleles causing dominant optic atrophy have defects in cardiolipin-stimulated GTP hydrolysis and membrane tubulation. Human Molecular Genetics 19:2113–2122.

Belenguer P, Pellegrini L. 2012. The dynamin GTPase OPA1: More than mitochondria? Biochimica et Biophysica Acta (BBA) - Bioenergetics.

Belluzzi O, Benedusi M, Ackman J, LoTurco JJ. 2003. Electrophysiological differentiation of new neurons in the olfactory bulb. The Journal of neuroscience 23:10411–10418.

Bergami M, Rimondini R, Santi S, Blum R, Götz M, Canossa M. 2008. Deletion of TrkB in adult progenitors alters newborn neuron integration into hippocampal circuits and increases anxiety-like behavior. Proceedings of the National Academy of Sciences of the United States of America 105:15570–15575.

Berger UV, Hediger MA. 2006. Distribution of the glutamate transporters GLT-1 (SLC1A2) and GLAST (SLC1A3) in peripheral organs. Anatomy and embryology 211:595–606.

Bernal GM, Peterson DA. 2011. Phenotypic and gene expression modification with normal brain aging in GFAP-positive astrocytes and neural stem cells. Aging Cell 10:466–482.

Bernardes de Jesus B, Vera E, Schneeberger K, Tejera AM, Ayuso E, Bosch F, Blasco MA. 2012. Telomerase gene therapy in adult and old mice delays aging and increases longevity without increasing cancer. EMBO molecular medicine 4:691–704.

Bibb MJ, van Etten RA, Wright CT, Walberg MW, Clayton DA. 1981. Sequence and gene organization of mouse mitochondrial DNA. Cell 26:167–180.

Bindoff LA, Engelsen BA. 2012. Mitochondrial diseases and epilepsy. Epilepsia 53 Suppl 4:92–97.

Birket MJ, Orr AL, Gerencser AA, Madden DT, Vitelli C, Swistowski A, Brand MD, Zeng X. 2011. A reduction in ATP demand and mitochondrial activity with neural differentiation of human embryonic stem cells. Journal of Cell Science 124:348–358.

Bishop NA, Lu T, Yankner BA. 2010. Neural mechanisms of ageing and cognitive decline. Nature 464:529–535.

Bocci T, Pecori C, Giorli E, Briscese L, Tognazzi S, Caleo M, Sartucci F. 2011. Differential motor neuron impairment and axonal regeneration in sporadic and familiar amyotrophic lateral sclerosis with SOD-1 mutations: lessons from neurophysiology. International journal of molecular sciences 12:9203–9215.

Bogenhagen D, Clayton DA. 1977. Mouse L cell mitochondrial DNA molecules are selected randomly for replication throughout the cell cycle. Cell 11:719–727.

Boldogh IR, Pon LA. 2007. Mitochondria on the move. Trends in cell biology 17:502–510.

Bonaguidi MA, Wheeler MA, Shapiro JS, Stadel RP, Sun GJ, Ming G, Song H. 2011. In vivo clonal analysis reveals self-renewing and multipotent adult neural stem cell characteristics. Cell 145:1142–1155.

Boscia F, Esposito CL, Di Crisci A, Franciscis V de, Annunziato L, Cerchia L. 2009. GDNF selectively induces microglial activation and neuronal survival in CA1/CA3 hippocampal regions exposed to NMDA insult through Ret/ERK signalling. PLoS ONE 4:e6486.

Botreau F, Gisquet-Verrier P. 2010. Re-thinking the role of the dorsal striatum in egocentric/response strategy. Frontiers in behavioral neuroscience 4:7.

Braff DL, Geyer MA. 1990. Sensorimotor gating and schizophrenia. Human and animal model studies. Archives of general psychiatry 47:181–188.

Braun K, Antemano R, Helmeke C, Büchner M, Poeggel G. 2009. Juvenile separation stress induces rapid region- and layer-specific changes in S100ss- and glial fibrillary acidic protein-immunoreactivity in astrocytes of the rodent medial prefrontal cortex. Neuroscience 160:629–638.

Broglio SP, Eckner JT, Paulson HL, Kutcher JS. 2012. Cognitive decline and aging: the role of concussive and subconcussive impacts. Exercise and sport sciences reviews 40:138–144.

Bua E, Johnson J, Herbst A, Delong B, McKenzie D, Salamat S, Aiken JM. 2006. Mitochondrial DNA-deletion mutations accumulate intracellularly to detrimental levels in aged human skeletal muscle fibers. American journal of human genetics 79:469–480.

Buffo A, Rite I, Tripathi P, Lepier A, Colak D, Horn A, Mori T, Götz M. 2008. Origin and progeny of reactive gliosis: A source of multipotent cells in the injured brain. Proceedings of the National Academy of Sciences of the United States of America 105:3581–3586.

Campbell CT, Kolesar JE, Kaufman BA. 2012. Mitochondrial transcription factor A regulates mitochondrial transcription initiation, DNA packaging, and genome copy number. Biochimica et Biophysica Acta (BBA) - Gene Regulatory Mechanisms 1819:921–929.

Carleton A, Petreanu LT, Lansford R, Alvarez-Buylla A, Lledo P. 2003. Becoming a new neuron in the adult olfactory bulb. Nature neuroscience 6:507–518.

Cassereau J, Chevrollier A, Gueguen N, Desquiret V, Verny C, Nicolas G, Dubas F, Amati-Bonneau P, Reynier P, Bonneau D, Procaccio V. 2011. Mitochondrial dysfunction and pathophysiology of Charcot-Marie-Tooth disease involving GDAP1 mutations. Experimental neurology 227:31–41.

Cerbai F, Lana D, Nosi D, Petkova-Kirova P, Zecchi S, Brothers HM, Wenk GL, Giovannini MG. 2012. The neuron-astrocyte-microglia triad in normal brain ageing and in a model of neuroinflammation in the rat hippocampus. PLoS ONE 7:e45250.

Chada SR, Hollenbeck PJ. 2003. Mitochondrial movement and positioning in axons: the role of growth factor signaling. The Journal of experimental biology 206:1985–1992.

Chakrabarti S, Munshi S, Banerjee K, Thakurta IG, Sinha M, Bagh MB. 2011. Mitochondrial Dysfunction during Brain Aging: Role of Oxidative Stress and Modulation by Antioxidant Supplementation. Aging and disease 2:242–256.

Chan DC. 2006. Mitochondria: dynamic organelles in disease, aging, and development. Cell 125:1241–1252.

Chan DC. 2012. Fusion and Fission: Interlinked Processes Critical for Mitochondrial Health. Annual review of genetics.

Chen H, Chomyn A, Chan DC. 2005. Disruption of fusion results in mitochondrial heterogeneity and dysfunction. The Journal of biological chemistry 280:26185–26192.

Cho S, Wood A, Bowlby MR. 2007. Brain slices as models for neurodegenerative disease and screening platforms to identify novel therapeutics. Current Neuropharmacology 5:19–33.

Chow LML, Zhang J, Baker SJ. 2008. Inducible Cre recombinase activity in mouse mature astrocytes and adult neural precursor cells. Transgenic research 17:919–928.

Christopherson KS, Ullian EM, Stokes CCA, Mullowney CE, Hell JW, Agah A, Lawler J, Mosher DF, Bornstein P, Barres BA. 2005. Thrombospondins are astrocyte-secreted proteins that promote CNS synaptogenesis. Cell 120:421–433.

Chung S, Dzeja PP, Faustino RS, Perez-Terzic C, Behfar A, Terzic A. 2007. Mitochondrial oxidative metabolism is required for the cardiac differentiation of stem cells. Nature clinical practice. Cardiovascular medicine 4 Suppl 1:S60-7.

Clayton DA. 1991. Nuclear gadgets in mitochondrial DNA replication and transcription. Trends in Biochemical Sciences 16:107–111.

Clelland CD, Choi M, Romberg C, Clemenson GD, Fragniere A, Tyers P, Jessberger S, Saksida LM, Barker RA, Gage FH, Bussey TJ. 2009. A functional role for adult hippocampal neurogenesis in spatial pattern separation. Science 325:210–213.

Clément Y, Calatayud F, Belzung C. 2002. Genetic basis of anxiety-like behaviour: a critical review. Brain research bulletin 57:57–71.

Comte C, Tonin Y, Heckel-Mager A, Boucheham A, Smirnov A, Auré K, Lombès A, Martin RP, Entelis N, Tarassov I. 2012. Mitochondrial targeting of recombinant RNAs modulates the level of a heteroplasmic mutation in human mitochondrial DNA associated with Kearns Sayre Syndrome. Nucleic Acids Research.

Cottrell DA, Blakely EL, Johnson MA, Borthwick GM, Ince PI, Turnbull DM. 2001a. Mitochondrial DNA mutations in disease and ageing. Novartis Foundation symposium 235:234-43; discussion 243-6.

Cottrell DA, Ince PG, Wardell TM, Turnbull DM, Johnson MA. 2001b. Accelerated ageing changes in the choroid plexus of a case with multiple mitochondrial DNA deletions. Neuropathology and applied neurobiology 27:206–214.

Crawford DC, Mennerick S. 2012. Presynaptically silent synapses: dormancy and awakening of presynaptic vesicle release. The Neuroscientist 18:216–223.

Crawley JN, Gerfen CR, Rogawski MA, Sibley DR, Skolnick P, Wray S, editors. 2001. Measurement of Startle Response, Prepulse Inhibition, and Habituation. Hoboken, NJ, USA: John Wiley & Sons, Inc.

Cryan JF, Markou A, Lucki I. 2002. Assessing antidepressant activity in rodents: recent developments and future needs. Trends in pharmacological sciences 23:238–245.

Csordás A. 2006. Mitochondrial transfer between eukaryotic animal cells and its physiologic role. Rejuvenation research 9:450–454.

Custer SK, Garden GA, Gill N, Rueb U, Libby RT, Schultz C, Guyenet SJ, Deller T, Westrum LE, Sopher BL, La Spada AR. 2006. Bergmann glia expression of polyglutamine-expanded ataxin-7 produces neurodegeneration by impairing glutamate transport. Nature neuroscience 9:1302–1311.

Deas E, Plun-Favreau H, Gandhi S, Desmond H, Kjaer S, Loh SHY, Renton AEM, Harvey RJ, Whitworth AJ, Martins LM, Abramov AY, Wood NW. 2011. PINK1 cleavage at position A103 by the mitochondrial protease PARL. Human Molecular Genetics 20:867–879.

Delatycki MB, Corben LA. 2012. Clinical features of Friedreich ataxia. Journal of child neurology 27:1133–1137.

Deng W, Saxe MD, Gallina IS, Gage FH. 2009. Adult-born hippocampal dentate granule cells undergoing maturation modulate learning and memory in the brain. The Journal of neuroscience 29:13532–13542.

D'Errico I, Dinardo MM, Capozzi O, Virgilio C de, Gadaleta G. 2005. History of the Tfam gene in primates. Gene 362:125–132.

Dickey AS, Strack S. 2011. PKA/AKAP1 and PP2A/Bβ2 regulate neuronal morphogenesis via Drp1 phosphorylation and mitochondrial bioenergetics. The Journal of neuroscience 31:15716–15726.

Dietrich MO, Andrews ZB, Horvath TL. 2008. Exercise-induced synaptogenesis in the hippocampus is dependent on UCP2-regulated mitochondrial adaptation. The Journal of neuroscience 28:10766–10771.

Divakaruni AS, Brand MD. 2011. The Regulation and Physiology of Mitochondrial Proton Leak. Physiology 26:192–205.

Dogan SA, Trifunovic A. 2011. Modelling mitochondrial dysfunction in mice. Physiological research 60 Suppl 1:S61-70.

Drapeau E, Mayo W, Aurousseau C, Le Moal M, Piazza P, Abrous DN. 2003. Spatial memory performances of aged rats in the water maze predict levels of hippocampal neurogenesis. Proceedings of the National Academy of Sciences of the United States of America 100:14385–14390.

Dringen R, Gutterer JM, Hirrlinger J. 2000. Glutathione metabolism in brain metabolic interaction between astrocytes and neurons in the defense against reactive oxygen species. European journal of biochemistry 267:4912–4916.

Du C, Fang M, Li Y, Li L, Wang X. 2000. Smac, a mitochondrial protein that promotes cytochrome c-dependent caspase activation by eliminating IAP inhibition. Cell 102:33–42.

Duffy PE, Huang YY, Rapport MM. 1982. The relationship of glial fibrillary acidic protein to the shape, motility, and differentiation of human astrocytoma cells. Experimental cell research 139:145–157.

Dufour E, Terzioglu M, Sterky FH, Sörensen L, Galter D, Olson L, Wilbertz J, Larsson N. 2008. Age-associated mosaic respiratory chain deficiency causes trans-neuronal degeneration. Human Molecular Genetics 17:1418–1426.

Dupret D, Fabre A, Döbrössy MD, Panatier A, Rodríguez JJ, Lamarque S, Lemaire V, Oliet SHR, Piazza P, Abrous DN. 2007. Spatial learning depends on both the addition and removal of new hippocampal neurons. PLoS biology (PLoS biology) 5:e214.

Dupret D, Revest J, Koehl M, Ichas F, Giorgi F de, Costet P, Abrous DN, Piazza PV. 2008. Spatial relational memory requires hippocampal adult neurogenesis. PLoS ONE 3:e1959.

Duvezin-Caubet S, Jagasia R, Wagener J, Hofmann S, Trifunovic A, Hansson A, Chomyn A, Bauer MF, Attardi G, Larsson N, Neupert W, Reichert AS. 2006. Proteolytic processing of OPA1 links mitochondrial dysfunction to alterations in mitochondrial morphology. The Journal of biological chemistry 281:37972–37979.

Echtay KS, Roussel D, St-Pierre J, Jekabsons MB, Cadenas S, Stuart JA, Harper JA, Roebuck SJ, Morrison A, Pickering S, Clapham JC, Brand MD. 2002. Superoxide activates mitochondrial uncoupling proteins. Nature 415:96–99.

Edgar D, Trifunovic A. 2009. The mtDNA mutator mouse: Dissecting mitochondrial involvement in aging. Aging (Albany NY) 1:1028–1032.

Ehm O, Göritz C, Covic M, Schäffner I, Schwarz TJ, Karaca E, Kempkes B, Kremmer E, Pfrieger FW, Espinosa L, Bigas A, Giachino C, Taylor V, Frisén J, Lie DC. 2010. RBPJkappa-dependent signaling is essential for long-term maintenance of neural stem cells in the adult hippocampus. The Journal of neuroscience 30:13794–13807.

Ehses S, Raschke I, Mancuso G, Bernacchia A, Geimer S, Tondera D, Martinou J, Westermann B, Rugarli EI, Langer T. 2009. Regulation of OPA1 processing and mitochondrial fusion by m-AAA protease isoenzymes and OMA1. The Journal of Cell Biology 187:1023–1036.

Ekstrand MI, Falkenberg M, Rantanen A, Park CB, Gaspari M, Hultenby K, Rustin P, Gustafsson CM, Larsson N. 2004. Mitochondrial transcription factor A regulates mtDNA copy number in mammals. Human Molecular Genetics 13:935–944.

Ekstrand MI, Terzioglu M, Galter D, Zhu S, Hofstetter C, Lindqvist E, Thams S, Bergstrand A, Hansson FS, Trifunovic A, Hoffer B, Cullheim S, Mohammed AH, Olson L, Larsson N. 2007. Progressive parkinsonism in mice with respiratory-chain-deficient dopamine neurons. Proceedings of the National Academy of Sciences of the United States of America 104:1325–1330.

Encinas JM, Hamani C, Lozano AM, Enikolopov G. 2011a. Neurogenic hippocampal targets of deep brain stimulation. The Journal of comparative neurology 519:6–20.

Encinas JM, Michurina TV, Peunova N, Park J, Tordo J, Peterson DA, Fishell G, Koulakov A, Enikolopov G. 2011b. Division-coupled astrocytic differentiation and age-related depletion of neural stem cells in the adult hippocampus. Cell Stem Cell 8:566–579.

Encinas JM, Sierra A. 2012. Neural stem cell deforestation as the main force driving the age-related decline in adult hippocampal neurogenesis. Behavioural brain research 227:433–439.

Engelmann M, Hädicke J, Noack J. 2011. Testing declarative memory in laboratory rats and mice using the nonconditioned social discrimination procedure. Nature Protocols 6:1152–1162.

Engelmann M, Wotjak CT, Landgraf R. 1995. Social discrimination procedure: An alternative method to investigate juvenile recognition abilities in rats. Physiology & Behavior 58:315–321.

Erdmann G, Schütz G, Berger S. 2007. Inducible gene inactivation in neurons of the adult mouse forebrain. BMC Neuroscience (BMC Neuroscience) 8:63.

Eroglu C, Barres BA. 2010. Regulation of synaptic connectivity by glia. Nature 468:223–231.

Espada S, Ortega F, Molina-Jijón E, Rojo AI, Pérez-Sen R, Pedraza-Chaverri J, Miras-Portugal MT, Cuadrado A. 2010. The purinergic P2Y(13) receptor activates the Nrf2/HO-1 axis and protects against oxidative stress-induced neuronal death. Free radical biology & medicine 49:416–426.

Espósito MS, Piatti VC, Laplagne DA, Morgenstern NA, Ferrari CC, Pitossi FJ, Schinder AF. 2005. Neuronal differentiation in the adult hippocampus recapitulates embryonic development. The Journal of neuroscience 25:10074–10086.

Facucho-Oliveira JM, Alderson J, Spikings EC, Egginton S, St John JC. 2007. Mitochondrial DNA replication during differentiation of murine embryonic stem cells. Journal of Cell Science 120:4025–4034.

Facucho-Oliveira JM, St John JC. 2009. The relationship between pluripotency and mitochondrial DNA proliferation during early embryo development and embryonic stem cell differentiation. Stem Cell reviews (Stem cell reviews) 5:140–158.

Faigle R, Song H. 2012. Signaling mechanisms regulating adult neural stem cells and neurogenesis. Biochimica et Biophysica Acta (BBA).

Falkenberg M, Gaspari M, Rantanen A, Trifunovic A, Larsson N, Gustafsson CM. 2002. Mitochondrial transcription factors B1 and B2 activate transcription of human mtDNA. Nature genetics 31:289–294.

Falkenberg M, Larsson N. 2009. Structure casts light on mtDNA replication. Cell 139:231–233.

Falkenberg M, Larsson N, Gustafsson CM. 2007. DNA replication and transcription in mammalian mitochondria. Annual Review of Biochemistry 76:679–699.

Farge G, Laurens N, Broekmans OD, van den Wildenberg SMJL, Dekker LCM, Gaspari M, Gustafsson CM, Peterman EJG, Falkenberg M, Wuite GJL. 2012. Protein sliding and DNA denaturation are essential for DNA organization by human mitochondrial transcription factor A. Nature communications 3:1013.

Faulkner JR, Herrmann JE, Woo MJ, Tansey KE, Doan NB, Sofroniew MV. 2004. Reactive astrocytes protect tissue and preserve function after spinal cord injury. The Journal of neuroscience 24:2143–2155.

Fayet G, Jansson M, Sternberg D, Moslemi AR, Blondy P, Lombès A, Fardeau M, Oldfors A. 2002. Ageing muscle: clonal expansions of mitochondrial DNA point mutations and deletions cause focal impairment of mitochondrial function. Neuromuscular disorders 12:484–493.

Feil R, Wagner J, Metzger D, Chambon P. 1997. Regulation of Cre recombinase activity by mutated estrogen receptor ligand-binding domains. Biochemical and biophysical research communications 237:752–757.

Fernandez HH. 2012. Nonmotor complications of Parkinson disease. Cleveland Clinic journal of medicine 79 Suppl 2:S14-8.

Fernandez-Marcos PJ, Auwerx J. 2011. Regulation of PGC-1 a nodal regulator of mitochondrial biogenesis. American Journal of Clinical Nutrition 93:884S.

Fernandez SP, Gaspar P. 2012. Investigating anxiety and depressive-like phenotypes in genetic mouse models of serotonin depletion. Neuropharmacology 62:144–154.

Figley CR, Stroman PW. 2011. The role(s) of astrocytes and astrocyte activity in neurometabolism, neurovascular coupling, and the production of functional neuroimaging signals. The European journal of neuroscience 33:577–588.

Filippov V, Kronenberg G, Pivneva T, Reuter K, Steiner B, Wang LP, Yamaguchi M, Kettenmann H, Kempermann G. 2003. Subpopulation of nestin-expressing progenitor cells in the adult murine hippocampus shows electrophysiological and morphological characteristics of astrocytes. Molecular and cellular neurosciences 23:373–382.

Finn DA, Rutledge-Gorman MT, Crabbe JC. 2003. Genetic animal models of anxiety. Neurogenetics 4:109–135.

Fleury C, Neverova M, Collins S, Raimbault S, Champigny O, Levi-Meyrueis C, Bouillaud F, Seldin MF, Surwit RS, Ricquier D, Warden CH. 1997. Uncoupling protein-2: a novel gene linked to obesity and hyperinsulinemia. Nature genetics 15:269–272.

Forner F, Foster LJ, Campanaro S, Valle G, Mann M. 2006. Quantitative Proteomic Comparison of Rat Mitochondria from Muscle, Heart, and Liver. Molecular & Cellular Proteomics 5:608–619.

Friedman JM, Halaas JL. 1998. Leptin and the regulation of body weight in mammals. Nature 395:763–770.

Fukuyama K, Ishikawa Y, Ogino T, Inoue H, Yamaoka R, Hirose T, Nishihira T. 2012. Mucosal necrosis of the small intestine in myopathy, encephalopathy, lactic acidosis, and stroke-like episodes syndrome. World journal of gastroenterology 18:5986–5989.

Fusté JM, Wanrooij S, Jemt E, Granycome CE, Cluett TJ, Shi Y, Atanassova N, Holt IJ, Gustafsson CM, Falkenberg M. 2010. Mitochondrial RNA polymerase is needed for activation of the origin of light-strand DNA replication. Molecular cell 37:67–78.

Galindo MF, Solesio ME, Atienzar-Aroca S, Zamora MJ, Jordán Bueso J. 2012. Mitochondrial dynamics and mitophagy in the 6-hydroxydopamine preclinical model of Parkinson's disease. Parkinson's disease 2012:131058.

Ganat YM, Silbereis J, Cave C, Ngu H, Anderson GM, Ohkubo Y, Ment LR, Vaccarino FM. 2006. Early postnatal astroglial cells produce multilineage precursors and neural stem cells in vivo. The Journal of neuroscience 26:8609–8621.

Garthe A, Behr J, Kempermann G. 2009. Adult-generated hippocampal neurons allow the flexible use of spatially precise learning strategies. PLoS ONE 4:e5464.

Geisler S, Holmström KM, Treis A, Skujat D, Weber SS, Fiesel FC, Kahle PJ, Springer W. 2010. The PINK1/Parkin-mediated mitophagy is compromised by PD-associated mutations. Autophagy 6:871–878.

Ge S, Goh ELK, Sailor KA, Kitabatake Y, Ming G, Song H. 2006. GABA regulates synaptic integration of newly generated neurons in the adult brain. Nature 439:589–593.

Ge S, Pradhan DA, Ming G, Song H. 2007. GABA sets the tempo for activity-dependent adult neurogenesis. Trends in neurosciences 30:1–8.

Ge S, Sailor KA, Ming G, Song H. 2008. Synaptic integration and plasticity of new neurons in the adult hippocampus. The Journal of physiology 586:3759–3765.

Gilkerson RW. 2009. Mitochondrial DNA nucleoids determine mitochondrial genetics and dysfunction. The international journal of biochemistry & cell biology 41:1899–1906.

Girard M, Lariviere R, Parfitt DA, Deane EC, Gaudet R, Nossova N, Blondeau F, Prenosil G, Vermeulen EGM, Duchen MR, Richter A, Shoubridge EA, Gehring K, McKinney RA, Brais B, Chapple JP, McPherson PS. 2012. Mitochondrial dysfunction and Purkinje cell loss in autosomal recessive spastic ataxia of Charlevoix-Saguenay (ARSACS). Proceedings of the National Academy of Sciences 109:1661–1666.

Godbout JP, Moreau M, Lestage J, Chen J, Sparkman NL, O' Connor J, Castanon N, Kelley KW, Dantzer R, Johnson RW. 2008. Aging exacerbates depressive-like behavior in mice in response to activation of the peripheral innate immune system. Neuropsychopharmacology 33:2341–2351.

Gordon GRJ, Mulligan SJ, Macvicar BA. 2007. Astrocyte control of the cerebrovasculature. Glia 55:1214–1221.

Goritz C, Mauch DH, Pfrieger FW. 2005. Multiple mechanisms mediate cholesterol-induced synaptogenesis in a CNS neuron. Molecular and cellular neurosciences 29:190–201.

Goss JR, Finch CE, Morgan DG. 1991. Age-related changes in glial fibrillary acidic protein mRNA in the mouse brain. Neurobiology of aging 12:165–170.

Gottlieb RA, Gustafsson ÅB. 2011. Mitochondrial turnover in the heart. Biochimica et Biophysica Acta (BBA) - Molecular Cell Research 1813:1295–1301.

Gould E. 2007. How widespread is adult neurogenesis in mammals? Nature reviews. Neuroscience 8:481–488.

Gulbransen BD, Sharkey KA. 2012. Novel functional roles for enteric glia in the gastrointestinal tract. Nature reviews. Gastroenterology & hepatology 9:625–632.

Halassa MM, Fellin T, Haydon PG. 2007a. The tripartite synapse: roles for gliotransmission in health and disease. Trends in molecular medicine 13:54–63.

Halassa MM, Fellin T, Takano H, Dong J, Haydon PG. 2007b. Synaptic islands defined by the territory of a single astrocyte. The Journal of neuroscience 27:6473–6477.

Hallberg BM, Larsson N. 2011. TFAM forces mtDNA to make a U-turn. Nature structural & molecular biology 18:1179–1181.

Hamm RJ, Pike BR, O'Dell DM, Lyeth BG, Jenkins LW. 1994. The rotarod test: an evaluation of its effectiveness in assessing motor deficits following traumatic brain injury. Journal of neurotrauma 11:187–196.

Harada S, Korf BR. 2013. Overview of molecular genetic diagnosis. Current protocols in human genetics 9:Unit9.1.

Harman D. 1972. The biologic clock: the mitochondria? Journal of the American Geriatrics Society 20:145–147.

Hastings, Gould. 1999. Erratum: rapid extension of axons into the CA3 region by adult-generated granule cells. J comp neurol 413:146-154. The Journal of comparative neurology 415:144.

Hatefi Y. 1985. The mitochondrial electron transport and oxidative phosphorylation system. Annual Review of Biochemistry 54:1015–1069.

Hebert SL, Lanza IR, Nair KS. 2010. Mitochondrial DNA alterations and reduced mitochondrial function in aging. Mechanisms of Ageing and Development 131:451–462.

Heinrich C, Blum R, Gascón S, Masserdotti G, Tripathi P, Sánchez R, Tiedt S, Schroeder T, Götz M, Berninger B. 2010. Directing astroglia from the cerebral cortex into subtype specific functional neurons. PLoS biology (PLoS biology) 8:e1000373.

Hertz L, Peng L, Dienel GA. 2007. Energy metabolism in astrocytes: high rate of oxidative metabolism and spatiotemporal dependence on glycolysis/glycogenolysis. Journal of cerebral blood flow and metabolism 27:219–249.

Higginson IJ, Gao W, Saleem TZ, Chaudhuri KR, Burman R, McCrone P, Leigh PN. 2012. Symptoms and quality of life in late stage Parkinson syndromes: a longitudinal community study of predictive factors. PLoS ONE 7:e46327.

Hinkle DA, Baldwin SA, Scheff SW, Wise PM. 1997. GFAP and S100beta expression in the cortex and hippocampus in response to mild cortical contusion. Journal of neurotrauma 14:729–738.

Hirrlinger PG, Scheller A, Braun C, Hirrlinger J, Kirchhoff F. 2006. Temporal control of gene recombination in astrocytes by transgenic expression of the tamoxifen-inducible DNA recombinase variant CreERT2. Glia 54:11–20.

Höke A, Silver J. 1994. Heterogeneity among astrocytes in reactive gliosis. Perspectives on developmental neurobiology 2:269–274.

Hollenbeck PJ, Saxton WM. 2005. The axonal transport of mitochondria. Journal of Cell Science 118:5411–5419.

Holt IJ, Lorimer HE, Jacobs HT. 2000. Coupled Leading- and Lagging-Strand Synthesis of Mammalian Mitochondrial DNA. Cell 100:515–524.

Hughes EG, Elmariah SB, Balice-Gordon RJ. 2010. Astrocyte secreted proteins selectively increase hippocampal GABAergic axon length, branching, and synaptogenesis. Molecular and cellular neurosciences 43:136–145.

Iadecola C, Nedergaard M. 2007. Glial regulation of the cerebral microvasculature. Nature neuroscience 10:1369–1376.

Imayoshi I, Sakamoto M, Ohtsuka T, Takao K, Miyakawa T, Yamaguchi M, Mori K, Ikeda T, Itohara S, Kageyama R. 2008. Roles of continuous neurogenesis in the structural and functional integrity of the adult forebrain. Nature neuroscience 11:1153–1161.

Israel MA, Yuan SH, Bardy C, Reyna SM, Mu Y, Herrera C, Hefferan MP, van Gorp S, Nazor KL, Boscolo FS, Carson CT, Laurent LC, Marsala M, Gage FH, Remes AM, Koo EH, Goldstein LSB. 2012. Probing sporadic and familial Alzheimer's disease using induced pluripotent stem cells. Nature 482:216–220.

Iwabu M, Yamauchi T, Okada-Iwabu M, Sato K, Nakagawa T, Funata M, Yamaguchi M, Namiki S, Nakayama R, Tabata M, Ogata H, Kubota N, Takamoto I, Hayashi YK, Yamauchi N, Waki H, Fukayama M, Nishino I, Tokuyama K, Ueki K, Oike Y, Ishii S, Hirose K, Shimizu T, Touhara K, Kadowaki T. 2010. Adiponectin and AdipoR1 regulate PGC-1alpha and mitochondria by Ca(2+) and AMPK/SIRT1. Nature 464:1313–1319.

Jagasia R, Steib K, Englberger E, Herold S, Faus-Kessler T, Saxe M, Gage FH, Song H, Lie DC. 2009. GABA-cAMP Response Element-Binding Protein Signaling Regulates Maturation and Survival of Newly Generated Neurons in the Adult Hippocampus. Journal of Neuroscience 29:7966–7977.

Jakoby P, Schmidt E, Ruminot I, Gutiérrez R, Barros LF, Deitmer JW. 2012. Higher Transport and Metabolism of Glucose in Astrocytes Compared with Neurons: A Multiphoton Study of Hippocampal and Cerebellar Tissue Slices. Cerebral cortex.

Jinno S. 2011. Decline in adult neurogenesis during aging follows a topographic pattern in the mouse hippocampus. The Journal of comparative neurology 519:451–466.

Jin SM, Lazarou M, Wang C, Kane LA, Narendra DP, Youle RJ. 2010. Mitochondrial membrane potential regulates PINK1 import and proteolytic destabilization by PARL. The Journal of Cell Biology 191:933–942.

Jin SM, Youle RJ. 2012. PINK1- and Parkin-mediated mitophagy at a glance. Journal of Cell Science 125:795–799.

Jones R. 2010. The roles of PINK1 and Parkin in Parkinson's disease. PLoS biology (PLoS biology) 8:e1000299.

Jonsson T, Atwal JK, Steinberg S, Snaedal J, Jonsson PV, Bjornsson S, Stefansson H, Sulem P, Gudbjartsson D, Maloney J, Hoyte K, Gustafson A, Liu Y, Lu Y, Bhangale T, Graham RR, Huttenlocher J, Bjornsdottir G, Andreassen OA, Jönsson EG, Palotie A, Behrens TW, Magnusson OT, Kong A, Thorsteinsdottir U, Watts RJ, Stefansson K. 2012. A mutation in APP protects against Alzheimer's disease and age-related cognitive decline. Nature 488:96–99.

Kang J, Tian J, Pan P, Zald P, Li C, Deng C, Sheng Z. 2008. Docking of axonal mitochondria by syntaphilin controls their mobility and affects short-term facilitation. Cell 132:137–148.

Kann O, Kovács R. 2007. Mitochondria and neuronal activity. American journal of physiology. Cell physiology 292:C641-57.

Kann O, Kovács R, Njunting M, Behrens CJ, Otáhal J, Lehmann T, Gabriel S, Heinemann U. 2005. Metabolic dysfunction during neuronal activation in the ex vivo hippocampus from chronic epileptic rats and humans. Brain 128:2396–2407.

Karalay O, Doberauer K, Vadodaria KC, Knobloch M, Berti L, Miquelajauregui A, Schwark M, Jagasia R, Taketo MM, Tarabykin V, Lie DC, Jessberger S. 2011. Prospero-related homeobox 1 gene (Prox1) is regulated by canonical Wnt signaling and has a stage-specific role in adult hippocampal neurogenesis. Proceedings of the National Academy of Sciences of the United States of America 108:5807–5812.

Karl T, Pabst R, Hörsten S von. 2003. Behavioral phenotyping of mice in pharmacological and toxicological research. Experimental and toxicologic pathology 55:69–83.

Karram K, Goebbels S, Schwab M, Jennissen K, Seifert G, Steinhäuser C, Nave K, Trotter J. 2008. NG2-expressing cells in the nervous system revealed by the NG2-EYFP-knockin mouse. Genesis 46:743–757.

Kaufman BA, Durisic N, Mativetsky JM, Costantino S, Hancock MA, Grutter P, Shoubridge EA. 2007. The mitochondrial transcription factor TFAM coordinates the assembly of multiple DNA molecules into nucleoid-like structures. Molecular biology of the cell 18:3225–3236.

Kawamoto S, Niwa H, Tashiro F, Sano S, Kondoh G, Takeda J, Tabayashi K, Miyazaki J. 2000. A novel reporter mouse strain that expresses enhanced green fluorescent protein upon Cre-mediated recombination. FEBS Letters (FEBS letters) 470:263–268.

Kazanis I. 2012. Neurogenesis in the Adult Mammalian Brain: How Much Do We Need, How Much Do We Have? Current topics in behavioral neurosciences.

Kempermann G, Gage FH. 2000. Neurogenesis in the adult hippocampus. Novartis Foundation symposium 231:220-35; discussion 235-41, 302-6.

Kempermann G, Gage FH. 2002. Genetic determinants of adult hippocampal neurogenesis correlate with acquisition, but not probe trial performance, in the water maze task. The European journal of neuroscience 16:129–136.

Kempermann G, Gast D, Gage FH. 2002. Neuroplasticity in old age: sustained fivefold induction of hippocampal neurogenesis by long-term environmental enrichment. Annals of neurology 52:135–143.

Kempermann G, Gast D, Kronenberg G, Yamaguchi M, Gage FH. 2003. Early determination and long-term persistence of adult-generated new neurons in the hippocampus of mice. Development 130:391–399.

Kempermann G, Kuhn HG, Gage FH. 1997. Genetic influence on neurogenesis in the dentate gyrus of adult mice. Proceedings of the National Academy of Sciences of the United States of America 94:10409–10414.

Kheirbek MA, Klemenhagen KC, Sahay A, Hen R. 2012. Neurogenesis and generalization: a new approach to stratify and treat anxiety disorders. Nature neuroscience 15:1613–1620.

Kielian T. 2008. Glial connexins and gap junctions in CNS inflammation and disease. Journal of neurochemistry 106:1000–1016.

Kijima K, Numakura C, Izumino H, Umetsu K, Nezu A, Shiiki T, Ogawa M, Ishizaki Y, Kitamura T, Shozawa Y, Hayasaka K. 2005. Mitochondrial GTPase mitofusin 2 mutation in Charcot-Marie-Tooth neuropathy type 2A. Human genetics 116:23–27.

Kispal G, Csere P, Prohl C, Lill R. 1999. The mitochondrial proteins Atm1p and Nfs1p are essential for biogenesis of cytosolic Fe/S proteins. The EMBO Journal 18:3981–3989.

Kitamura T, Saitoh Y, Takashima N, Murayama A, Niibori Y, Ageta H, Sekiguchi M, Sugiyama H, Inokuchi K. 2009. Adult neurogenesis modulates the hippocampus-dependent period of associative fear memory. Cell 139:814–827.

Klempin F, Kempermann G. 2007. Adult hippocampal neurogenesis and aging. European archives of psychiatry and clinical neuroscience 257:271–280.

Knobloch M, Braun SMG, Zurkirchen L, Schoultz C von, Zamboni N, Araúzo-Bravo MJ, Kovacs WJ, Karalay O, Suter U, Machado RAC, Roccio M, Lutolf MP, Semenkovich CF, Jessberger S. 2013. Metabolic control of adult neural stem cell activity by Fasn-dependent lipogenesis. Nature 493:226–230.

Koga Y, Povalko N, Nishioka J, Katayama K, Kakimoto N, Matsuishi T. 2010. MELAS and L-arginine therapy: pathophysiology of stroke-like episodes. Annals of the New York Academy of Sciences 1201:104–110.

Kohman RA, Rhodes JS. 2012. Neurogenesis, inflammation and behavior. Brain, behavior, and immunity.

Komitova M, Serwanski DR, Lu QR, Nishiyama A. 2011. NG2 cells are not a major source of reactive astrocytes after neocortical stab wound injury. Glia 59:800–809.

Kozlova M, Kentroti S, Vernadakis A. 1993. Influence of culture substrata on the differentiation of advanced passage glial cells in cultures from aged mouse cerebral hemispheres. International journal of developmental neuroscience 11:513–519.

Kriegstein A, Alvarez-Buylla A. 2009. The glial nature of embryonic and adult neural stem cells. Annual review of neuroscience 32:149–184.

Kronenberg G, Bick-Sander A, Bunk E, Wolf C, Ehninger D, Kempermann G. 2006. Physical exercise prevents age-related decline in precursor cell activity in the mouse dentate gyrus. Neurobiology of aging 27:1505–1513.

Krzisch M, Sultan S, Sandell J, Demeter K, Vutskits L, Toni N. 2013. Propofol Anesthesia Impairs the Maturation and Survival of Adult-born Hippocampal Neurons. Anesthesiology.

Kuhn HG, Biebl M, Wilhelm D, Li M, Friedlander RM, Winkler J. 2005a. Increased generation of granule cells in adult Bcl-2-overexpressing mice: a role for cell death during continued hippocampal neurogenesis. The European journal of neuroscience 22:1907–1915.

Kuhn HG, Cooper-Kuhn C, Eriksson P, Nilsson M. 2005b. Signals regulating neurogenesis in the adult olfactory bulb. Chemical senses 30 Suppl 1:i109-10.

Kuhn HG, Dickinson-Anson H, Gage FH. 1996. Neurogenesis in the dentate gyrus of the adult rat: age-related decrease of neuronal progenitor proliferation. The Journal of neuroscience 16:2027–2033.

Kühn R, Torres RM. 2002. Cre/loxP recombination system and gene targeting. Methods in molecular biology 180:175–204.

Kujoth GC, Bradshaw PC, Haroon S, Prolla TA. 2007. The role of mitochondrial DNA mutations in mammalian aging. PLoS genetics (PLoS genetics) 3:e24.

Kujoth GC, Leeuwenburgh C, Prolla TA. 2006. Mitochondrial DNA mutations and apoptosis in mammalian aging. Cancer research 66:7386–7389.

Kukat A, Trifunovic A. 2009. Somatic mtDNA mutations and aging--facts and fancies. Experimental gerontology 44:101–105.

Kumar Jha M, Jeon S, Suk K. 2012. Pyruvate Dehydrogenase Kinases in the Nervous System: Their Principal Functions in Neuronal-glial Metabolic Interaction and Neuro-metabolic Disorders. Current Neuropharmacology 10:393–403.

Kumar A, Gibbs JR, Beilina A, Dillman A, Kumaran R, Trabzuni D, Ryten M, Walker R, Smith C, Traynor BJ, Hardy J, Singleton AB, Cookson MR. 2013. Age-associated changes in gene expression in human brain and isolated neurons. Neurobiology of aging 34:1199–1209.

Kumar M, Kaur P, Saxena R, Sharma P, Dada R. 2012. Clinical characterization and mitochondrial DNA sequence variations in Leber hereditary optic neuropathy. Molecular vision 18:2687–2699.

Kutschera U, Niklas KJ. 2005. Endosymbiosis, cell evolution, and speciation. Theory in biosciences 124:1–24.

Lakatos A, Derbeneva O, Younes D, Keator D, Bakken T, Lvova M, Brandon M, Guffanti G, Reglodi D, Saykin A, Weiner M, Macciardi F, Schork N, Wallace DC, Potkin SG. 2010. Association between mitochondrial DNA variations and Alzheimer's disease in the ADNI cohort. Neurobiology of aging 31:1355–1363.

Laplagne DA, Espósito MS, Piatti VC, Morgenstern NA, Zhao C, van Praag H, Gage FH, Schinder AF. 2006. Functional convergence of neurons generated in the developing and adult hippocampus. PLoS biology (PLoS biology) 4:e409.

Larsson NG, Clayton DA. 1995. Molecular genetic aspects of human mitochondrial disorders. Annual review of genetics 29:151–178.

Larsson NG, Luft R. 1999. Revolution in mitochondrial medicine. FEBS Letters (FEBS letters) 455:199–202.

Larsson NG, Wang J, Wilhelmsson H, Oldfors A, Rustin P, Lewandoski M, Barsh GS, Clayton DA. 1998. Mitochondrial transcription factor A is necessary for mtDNA maintenance and embryogenesis in mice. Nature genetics 18:231–236.

Latoo J, Mistry M, Dunne FJ. 2012. Depression in Parkinson's disease: diagnosis and management. British journal of hospital medicine 73:331–334.

Lauro C, Cipriani R, Catalano M, Trettel F, Chece G, Brusadin V, Antonilli L, van Rooijen N, Eusebi F, Fredholm BB, Limatola C. 2010. Adenosine A1 receptors and microglial cells mediate CX3CL1-induced protection of hippocampal neurons against Glu-induced death. Neuropsychopharmacology 35:1550–1559.

Ledesma A, Lacoba M de, Rial E. 2002. The mitochondrial uncoupling proteins. Genome Biology 3:3015.1-9.

Lee BR, Dong Y. 2011. Cocaine-induced metaplasticity in the nucleus accumbens: silent synapse and beyond. Neuropharmacology 61:1060–1069.

Lee H, Wei Y. 2012. Mitochondria and aging. Advances in experimental medicine and biology 942:311–327.

Lee MM, Reif A, Schmitt AG. 2012. Major Depression: A Role for Hippocampal Neurogenesis? Current topics in behavioral neurosciences.

Legros F, Malka F, Frachon P, Lombès A, Rojo M. 2004. Organization and dynamics of human mitochondrial DNA. Journal of Cell Science 117:2653–2662.

Lein PJ, Barnhart CD, Pessah IN. 2011. Acute hippocampal slice preparation and hippocampal slice cultures. Methods in molecular biology 758:115–134.

Lemberg A, Fernández MA. 2009. Hepatic encephalopathy, ammonia, glutamate, glutamine and oxidative stress. Annals of hepatology 8:95–102.

Leventhal AM, Pettit JW, Lewinsohn PM. 2008. Characterizing major depression phenotypes by presence and type of psychomotor disturbance in adolescents and young adults. Depression and anxiety 25:575–592.

Liao D, Zhang X, O'Brien R, Ehlers MD, Huganir RL. 1999. Regulation of morphological postsynaptic silent synapses in developing hippocampal neurons. Nature neuroscience 2:37–43.

Lie DC, Dziewczapolski G, Willhoite AR, Kaspar BK, Shults CW, Gage FH. 2002. The adult substantia nigra contains progenitor cells with neurogenic potential. The Journal of neuroscience 22:6639–6649.

Lie DC, Song H, Colamarino SA, Ming G, Gage FH. 2004. Neurogenesis in the adult brain: new strategies for central nervous system diseases. Annual review of pharmacology and toxicology 44:399–421.

Lill R. 2009. Function and biogenesis of iron–sulphur proteins. Nature 460:831–838.

Litonin D, Sologub M, Shi Y, Savkina M, Anikin M, Falkenberg M, Gustafsson CM, Temiakov D. 2010. Human mitochondrial transcription revisited: only TFAM and TFB2M are required for transcription of the mitochondrial genes in vitro. The Journal of biological chemistry 285:18129–18133.

Liu L, Rando TA. 2011. Manifestations and mechanisms of stem cell aging. The Journal of Cell Biology 193:257–266.

Li Y, Aimone JB, Xu X, Callaway EM, Gage FH. 2012. Development of GABAergic inputs controls the contribution of maturing neurons to the adult hippocampal network. Proceedings of the National Academy of Sciences of the United States of America 109:4290–4295.

Li Z, Sheng M. 2003. Some assembly required: the development of neuronal synapses. Nature reviews. Molecular cell biology 4:833–841.

Lodeiro MF, Uchida A, Bestwick M, Moustafa IM, Arnold JJ, Shadel GS, Cameron CE. 2012. Transcription from the second heavy-strand promoter of human mtDNA is repressed by transcription factor A in vitro. Proceedings of the National Academy of Sciences of the United States of America 109:6513–6518.

Long J, He P, Shen Y, Li R. 2012. New evidence of mitochondria dysfunction in the female Alzheimer's disease brain: deficiency of estrogen receptor-β. Journal of Alzheimer's disease 30:545–558.

López-Mascaraque L, Castro F de. 2002. The olfactory bulb as an independent developmental domain. Cell death and differentiation 9:1279–1286.

Lugert S, Basak O, Knuckles P, Haussler U, Fabel K, Götz M, Haas CA, Kempermann G, Taylor V, Giachino C. 2010. Quiescent and active hippocampal neural stem cells with distinct morphologies respond selectively to physiological and pathological stimuli and aging. Cell Stem Cell 6:445–456.

Macauley SL, Pekny M, Sands MS. 2011. The Role of Attenuated Astrocyte Activation in Infantile Neuronal Ceroid Lipofuscinosis. Journal of Neuroscience 31:15575–15585.

Magistretti PJ. 2006. Neuron-glia metabolic coupling and plasticity. The Journal of experimental biology 209:2304–2311.

Magistretti PJ. 2009. Role of glutamate in neuron-glia metabolic coupling. The American journal of clinical nutrition 90:875S-880S.

Magrané J, Sahawneh MA, Przedborski S, Estévez ÁG, Manfredi G. 2012. Mitochondrial dynamics and bioenergetic dysfunction is associated with synaptic alterations in mutant SOD1 motor neurons. The Journal of neuroscience 32:229–242.

Mahad DJ, Ziabreva I, Campbell G, Laulund F, Murphy JL, Reeve AK, Greaves L, Smith KJ, Turnbull DM. 2009. Detection of cytochrome c oxidase activity and mitochondrial proteins in single cells. Journal of neuroscience methods 184:310–319.

Marchetto MCN, Muotri AR, Mu Y, Smith AM, Cezar GG, Gage FH. 2008. Non-cell-autonomous effect of human SOD1 G37R astrocytes on motor neurons derived from human embryonic stem cells. Cell Stem Cell 3:649–657.

Margulis L. 1975. Symbiotic theory of the origin of eukaryotic organelles; criteria for proof. Symposia of the Society for Experimental Biology:21–38.

Marín-Burgin A, Mongiat LA, Pardi MB, Schinder AF. 2012. Unique processing during a period of high excitation/inhibition balance in adult-born neurons. Science 335:1238–1242.

Marongiu MF, Poddie D, Porcu S, Manchinu MF, Castelli MP, Sogos V, Bini V, Frau R, Caredda E, Collu M, Ristaldi MS, D'Adamo P. 2012. Reversible Disruption of Pre-Pulse Inhibition in Hypomorphic-Inducible and Reversible CB1-/- Mice. PLoS ONE 7:e35013.

Marques O, Outeiro TF. 2012. Alpha-synuclein: from secretion to dysfunction and death. Cell death & disease 3:e350.

Martinez-Abundis E, Rajapurohitam V, Haist JV, Gan XT, Karmazyn M. 2012. The obesity-related peptide leptin sensitizes cardiac mitochondria to calcium-induced permeability transition pore opening and apoptosis. PLoS ONE 7:e41612.

Martin LJ. 2012. Biology of mitochondria in neurodegenerative diseases. Progress in molecular biology and translational science 107:355–415.

Masiulis I, Yun S, Eisch AJ. 2011. The interesting interplay between interneurons and adult hippocampal neurogenesis. Molecular neurobiology 44:287–302.

Mason DJ, Huggett JF. 2002. Glutamate transporters in bone. Journal of musculoskeletal & neuronal interactions 2:406–414.

Mason HA, Ito S, Corfas G. 2001. Extracellular signals that regulate the tangential migration of olfactory bulb neuronal precursors: inducers, inhibitors, and repellents. The Journal of neuroscience 21:7654–7663.

Mauch DH, Nägler K, Schumacher S, Göritz C, Müller EC, Otto A, Pfrieger FW. 2001. CNS synaptogenesis promoted by glia-derived cholesterol. Science 294:1354–1357.

McBride HM, Neuspiel M, Wasiak S. 2006. Mitochondria: more than just a powerhouse. Current biology 16:R551-60.

McFarland R, Turnbull DM. 2009. Batteries not included: diagnosis and management of mitochondrial disease. Journal of internal medicine 265:210–228.

McKinney RA. 2010. Excitatory amino acid involvement in dendritic spine formation, maintenance and remodelling. The Journal of physiology 588:107–116.

Melov S, Schneider JA, Coskun PE, Bennett DA, Wallace DC. 1999. Mitochondrial DNA rearrangements in aging human brain and in situ PCR of mtDNA. Neurobiology of aging 20:565–571.

Mercier F, Kitasako JT, Hatton GI. 2002. Anatomy of the brain neurogenic zones revisited: fractones and the fibroblast/macrophage network. The Journal of comparative neurology 451:170–188.

Merkwirth C, Martinelli P, Korwitz A, Morbin M, Brönneke HS, Jordan SD, Rugarli EI, Langer T. 2012. Loss of prohibitin membrane scaffolds impairs mitochondrial architecture and leads to tau hyperphosphorylation and neurodegeneration. PLoS genetics (PLoS genetics) 8:e1003021.

Miller RH, Raff MC. 1984. Fibrous and protoplasmic astrocytes are biochemically and developmentally distinct. The Journal of neuroscience 4:585–592.

Ming G, Song H. 2005. Adult neurogenesis in the mammalian central nervous system. Annual review of neuroscience 28:223–250.

Minokoshi Y, Alquier T, Furukawa N, Kim Y, Lee A, Xue B, Mu J, Foufelle F, Ferré P, Birnbaum MJ, Stuck BJ, Kahn BB. 2004. AMP-kinase regulates food intake by responding to hormonal and nutrient signals in the hypothalamus. Nature 428:569–574.

MITCHELL P. 1961. Coupling of phosphorylation to electron and hydrogen transfer by a chemi-osmotic type of mechanism. Nature 191:144–148.

Miura T, Katakura Y, Yamamoto K, Uehara N, Tsuchiya T, Kim EH, Shirahata S. 2001. Neural stem cells lose telomerase activity upon differentiating into astrocytes. Cytotechnology 36:137–144.

Molofsky AV, Krencik R, Krenick R, Ullian EM, Ullian E, Tsai H, Deneen B, Richardson WD, Barres BA, Rowitch DH. 2012. Astrocytes and disease: a neurodevelopmental perspective. Genes & development 26:891–907.

Monden Y, Mori M, Kuwajima M, Goto T, Yamagata T, Momoi MY. 2012. Late-onset Leigh syndrome with myoclonic epilepsy with ragged-red fibers. Brain & development.

Morgan TE, Rozovsky I, Goldsmith SK, Stone DJ, Yoshida T, Finch CE. 1997. Increased transcription of the astrocyte gene GFAP during middle-age is attenuated by food restriction: implications for the role of oxidative stress. Free radical biology & medicine 23:524–528.

Morgenstern NA, Lombardi G, Schinder AF. 2008. Newborn granule cells in the ageing dentate gyrus. The Journal of physiology 586:3751–3757.

Mori T, Buffo A, Götz M. 2005. The novel roles of glial cells revisited: the contribution of radial glia and astrocytes to neurogenesis. Current topics in developmental biology 69:67–99.

Mori T, Tanaka K, Buffo A, Wurst W, Kühn R, Götz M. 2006. Inducible gene deletion in astroglia and radial glia-A valuable tool for functional and lineage analysis. Glia 54:21–34.

Moro MA, Almeida A, Bolaños JP, Lizasoain I. 2005. Mitochondrial respiratory chain and free radical generation in stroke. Free radical biology & medicine 39:1291–1304.

Morrens J, van Den Broeck W, Kempermann G. 2012. Glial cells in adult neurogenesis. Glia 60:159–174.

Morris RL, Hollenbeck PJ. 1995. Axonal transport of mitochondria along microtubules and F-actin in living vertebrate neurons. The Journal of Cell Biology 131:1315–1326.

Mosienko V, Bert B, Beis D, Matthes S, Fink H, Bader M, Alenina N. 2012. Exaggerated aggression and decreased anxiety in mice deficient in brain serotonin. Translational Psychiatry 2:e122.

Mu L, Berti L, Masserdotti G, Covic M, Michaelidis TM, Doberauer K, Merz K, Rehfeld F, Haslinger A, Wegner M, Sock E, Lefebvre V, Couillard-Despres S, Aigner L, Berninger B, Lie DC. 2012. SoxC Transcription Factors Are Required for Neuronal Differentiation in Adult Hippocampal Neurogenesis. Journal of Neuroscience 32:3067–3080.

Müller-Höcker J. 1989. Cytochrome-c-oxidase deficient cardiomyocytes in the human heart--an age-related phenomenon. A histochemical ultracytochemical study. The American journal of pathology 134:1167–1173.

Nadege B, Patrick L, Rodrigue R. 2009. Mitochondria: from bioenergetics to the metabolic regulation of carcinogenesis. Frontiers in Bioscience Volume:4015–4034.

Nagai M, Re DB, Nagata T, Chalazonitis A, Jessell TM, Wichterle H, Przedborski S. 2007. Astrocytes expressing ALS-linked mutated SOD1 release factors selectively toxic to motor neurons. Nature neuroscience 10:615–622.

Nagy JI, Rash JE. 2003. Astrocyte and oligodendrocyte connexins of the glial syncytium in relation to astrocyte anatomical domains and spatial buffering. Cell communication & adhesion 10:401–406.

Nakamura K, Greenwood A, Binder L, Bigio EH, Denial S, Nicholson L, Zhou XZ, Lu KP. 2012. Proline isomer-specific antibodies reveal the early pathogenic tau conformation in Alzheimer's disease. Cell 149:232–244.

Nakamura T, Colbert MC, Robbins J. 2006. Neural crest cells retain multipotential characteristics in the developing valves and label the cardiac conduction system. Circulation research 98:1547–1554.

Nakashiba T, Cushman JD, Pelkey KA, Renaudineau S, Buhl DL, McHugh TJ, Rodriguez Barrera V, Chittajallu R, Iwamoto KS, McBain CJ, Fanselow MS, Tonegawa S. 2012. Young dentate granule cells mediate pattern separation, whereas old granule cells facilitate pattern completion. Cell 149:188–201.

Narendra D, Tanaka A, Suen D, Youle RJ. 2008. Parkin is recruited selectively to impaired mitochondria and promotes their autophagy. The Journal of Cell Biology 183:795–803.

Navratil M, Terman A, Arriaga EA. 2008. Giant mitochondria do not fuse and exchange their contents with normal mitochondria. Experimental cell research 314:164–172.

Neary JT, Kang Y, Willoughby KA, Ellis EF. 2003. Activation of extracellular signal-regulated kinase by stretch-induced injury in astrocytes involves extracellular ATP and P2 purinergic receptors. The Journal of neuroscience 23:2348–2356.

Nedergaard M, Dirnagl U. 2005. Role of glial cells in cerebral ischemia. Glia 50:281–286.

Nedergaard M, Ransom B, Goldman SA. 2003. New roles for astrocytes: redefining the functional architecture of the brain. Trends in neurosciences 26:523–530.

Newsholme P, Gaudel C, Krause M. 2012. Mitochondria and diabetes. An intriguing pathogenetic role. Advances in experimental medicine and biology 942:235–247.

Nichols NR, Day JR, Laping NJ, Johnson SA, Finch CE. 1993. GFAP mRNA increases with age in rat and human brain. Neurobiology of aging 14:421–429.

Nimchinsky EA, Sabatini BL, Svoboda K. 2002. Structure and function of dendritic spines. Annual review of physiology 64:313–353.

Nolte C, Matyash M, Pivneva T, Schipke CG, Ohlemeyer C, Hanisch UK, Kirchhoff F, Kettenmann H. 2001. GFAP promoter-controlled EGFP-expressing transgenic mice: a tool to visualize astrocytes and astrogliosis in living brain tissue. Glia 33:72–86.

Oberheim NA, Takano T, Han X, He W, Lin JHC, Wang F, Xu Q, Wyatt JD, Pilcher W, Ojemann JG, Ransom BR, Goldman SA, Nedergaard M. 2009. Uniquely hominid features of adult human astrocytes. The Journal of neuroscience 29:3276–3287.

Okabe Y, Takahashi T, Mitsumasu C, Kosai K, Tanaka E, Matsuishi T. 2012. Alterations of gene expression and glutamate clearance in astrocytes derived from an MeCP2-null mouse model of Rett syndrome. PLoS ONE 7:e35354.

Olichon A, Guillou E, Delettre C, Landes T, Arnauné-Pelloquin L, Emorine LJ, Mils V, Daloyau M, Hamel C, Amati-Bonneau P, Bonneau D, Reynier P, Lenaers G, Belenguer P. 2006. Mitochondrial dynamics and disease, OPA1. Biochimica et Biophysica Acta (BBA) 1763:500–509.

Oliveira JMA. 2010. Nature and cause of mitochondrial dysfunction in Huntington's disease: focusing on huntingtin and the striatum. Journal of neurochemistry 114:1–12.

Orellana JA, Bernhardi R von, Giaume C, Sáez JC. 2012. Glial hemichannels and their involvement in aging and neurodegenerative diseases. Reviews in the neurosciences 23:163–177.

Ortinski PI, Dong J, Mungenast A, Yue C, Takano H, Watson DJ, Haydon PG, Coulter DA. 2010. Selective induction of astrocytic gliosis generates deficits in neuronal inhibition. Nature neuroscience 13:584–591.

Owens DF, Kriegstein AR. 2002. Is there more to GABA than synaptic inhibition? Nature reviews. Neuroscience 3:715–727.

Pamplona R. 2011. Mitochondrial DNA damage and animal longevity: insights from comparative studies. Journal of aging research 2011:807108.

Parisi MA, Clayton DA. 1991. Similarity of human mitochondrial transcription factor 1 to high mobility group proteins. Science 252:965–969.

Park CB, Larsson N. 2011. Mitochondrial DNA mutations in disease and aging. The Journal of Cell Biology 193:809–818.

Pasupathy A, Miller EK. 2005. Different time courses of learning-related activity in the prefrontal cortex and striatum. Nature 433:873–876.

Patel RC, Larson J. 2009. Impaired olfactory discrimination learning and decreased olfactory sensitivity in aged C57Bl/6 mice. Neurobiology of aging 30:829–837.

Patzko A, Shy ME. 2012. Charcot-Marie-Tooth disease and related genetic neuropathies. Continuum (Minneap Minn) 18:39–59.

Peitz M, Pfannkuche K, Rajewsky K, Edenhofer F. 2002. Ability of the hydrophobic FGF and basic TAT peptides to promote cellular uptake of recombinant Cre recombinase: a tool for efficient genetic engineering of mammalian genomes. Proceedings of the National Academy of Sciences of the United States of America 99:4489–4494.

Pekny M, Nilsson M. 2005. Astrocyte activation and reactive gliosis. Glia 50:427–434.

Pellerin L, Bouzier-Sore A, Aubert A, Serres S, Merle M, Costalat R, Magistretti PJ. 2007. Activity-dependent regulation of energy metabolism by astrocytes: an update. Glia 55:1251–1262.

Perea G, Navarrete M, Araque A. 2009. Tripartite synapses: astrocytes process and control synaptic information. Trends in neurosciences 32:421–431.

Peretto P, Merighi A, Fasolo A, Bonfanti L. 1997. Glial tubes in the rostral migratory stream of the adult rat. Brain research bulletin 42:9–21.

Petrak LJ, Harris KM, Kirov SA. 2005. Synaptogenesis on mature hippocampal dendrites occurs via filopodia and immature spines during blocked synaptic transmission. The Journal of comparative neurology 484:183–190.

Pham TT, Giesert F, Röthig A, Floss T, Kallnik M, Weindl K, Hölter SM, Ahting U, Prokisch H, Becker L, Klopstock T, Hrabé Angelis M de, Beyer K, Görner K, Kahle PJ, Vogt Weisenhorn DM, Wurst W. 2010. DJ-1-deficient mice show less TH-positive neurons in the ventral tegmental area and exhibit non-motoric behavioural impairments. Genes, Brain and Behavior 9:305–317.

Piatti VC, Davies-Sala MG, Espósito MS, Mongiat LA, Trinchero MF, Schinder AF. 2011. The timing for neuronal maturation in the adult hippocampus is modulated by local network activity. The Journal of neuroscience 31:7715–7728.

Piatti VC, Espósito MS, Schinder AF. 2006. The timing of neuronal development in adult hippocampal neurogenesis. Neuroscientist 12:463–468.

Pleasure SJ, Collins AE, Lowenstein DH. 2000. Unique expression patterns of cell fate molecules delineate sequential stages of dentate gyrus development. The Journal of neuroscience 20:6095–6105.

Porsolt RD, Bertin A, Jalfre M. 1977. Behavioral despair in mice: a primary screening test for antidepressants. Archives internationales de pharmacodynamie et de thérapie 229:327–336.

Pratt AJ, Getzoff ED, Perry JJP. 2012. Amyotrophic lateral sclerosis: update and new developments. Degenerative neurological and neuromuscular disease 2012:1–14.

Prust M, Wang J, Morizono H, Messing A, Brenner M, Gordon E, Hartka T, Sokohl A, Schiffmann R, Gordish-Dressman H, Albin R, Amartino H, Brockman K, Dinopoulos A, Dotti MT, Fain D, Fernandez R, Ferreira J, Fleming J, Gill D, Griebel M, Heilstedt H, Kaplan P, Lewis D, Nakagawa M, Pedersen R, Reddy A, Sawaishi Y, Schneider M, Sherr E, Takiyama Y, Wakabayashi K, Gorospe JR, Vanderver A. 2011. GFAP mutations, age at onset, and clinical subtypes in Alexander disease. Neurology 77:1287–1294.

Prut L, Belzung C. 2003. The open field as a paradigm to measure the effects of drugs on anxiety-like behaviors: a review. European journal of pharmacology 463:3–33.

Rafalski VA, Brunet A. 2011. Energy metabolism in adult neural stem cell fate. Progress in neurobiology 93:182–203.

Rahman S, Lake BD, Taanman JW, Hanna MG, Cooper JM, Schapira AH, Leonard JV. 2000. Cytochrome oxidase immunohistochemistry: clues for genetic mechanisms. Brain 123 Pt 3:591–600.

Rajaraman S, Choi J, Cheung P, Beaudry V, Moore H, Artandi SE. 2007. Telomere uncapping in progenitor cells with critical telomere shortening is coupled to S-phase progression in vivo. Proceedings of the National Academy of Sciences of the United States of America 104:17747–17752.

Rajeswari MR. 2012. DNA triplex structures in neurodegenerative disorder, Friedreich's ataxia. Journal of biosciences 37:519–532.

Rantanen A, Jansson M, Oldfors A, Larsson NG. 2001. Downregulation of Tfam and mtDNA copy number during mammalian spermatogenesis. Mammalian genome 12:787–792.

Rao MS, Shetty AK. 2004. Efficacy of doublecortin as a marker to analyse the absolute number and dendritic growth of newly generated neurons in the adult dentate gyrus. The European journal of neuroscience 19:234–246.

Revest J, Dupret D, Koehl M, Funk-Reiter C, Grosjean N, Piazza P, Abrous DN. 2009. Adult hippocampal neurogenesis is involved in anxiety-related behaviors. Molecular psychiatry 14:959–967.

Robel S, Berninger B, Götz M. 2011. The stem cell potential of glia: lessons from reactive gliosis. Nature reviews. Neuroscience 12:88–104.

Rogers GW, Brand MD, Petrosyan S, Ashok D, Elorza AA, Ferrick DA, Murphy AN. 2011. High throughput microplate respiratory measurements using minimal quantities of isolated mitochondria. PLoS ONE 6:e21746.

Rossi MA, Hayrapetyan VY, Maimon B, Mak K, Je HS, Yin HH. 2012. Prefrontal cortical mechanisms underlying delayed alternation in mice. Journal of neurophysiology 108:1211–1222.

Ross JM, Öberg J, Brené S, Coppotelli G, Terzioglu M, Pernold K, Goiny M, Sitnikov R, Kehr J, Trifunovic A, Larsson N, Hoffer BJ, Olson L. 2010. High brain lactate is a hallmark of aging and caused by a shift in the lactate dehydrogenase A/B ratio. Proceedings of the National Academy of Sciences of the United States of America 107:20087–20092.

Rötig A, Lonlay P de, Chretien D, Foury F, Koenig M, Sidi D, Munnich A, Rustin P. 1997. Aconitase and mitochondrial iron-sulphur protein deficiency in Friedreich ataxia. Nature genetics 17:215–217.

Rouault TA, Tong W. 2005. Iron-sulphur cluster biogenesis and mitochondrial iron homeostasis. Nature reviews. Molecular cell biology 6:345–351.

Rubio-Perez JM, Morillas-Ruiz JM. 2012. A review: inflammatory process in Alzheimer's disease, role of cytokines. ScientificWorldJournal 2012:756357.

Saaltink D, Håvik B, Verissimo CS, Lucassen PJ, Vreugdenhil E. 2012. Doublecortin and doublecortin-like are expressed in overlapping and non-overlapping neuronal cell population: implications for neurogenesis. The Journal of comparative neurology 520:2805–2823.

Safdar A, Little JP, Stokl AJ, Hettinga BP, Akhtar M, Tarnopolsky MA. 2011. Exercise increases mitochondrial PGC-1alpha content and promotes nuclear-mitochondrial cross-talk to coordinate mitochondrial biogenesis. The Journal of biological chemistry 286:10605–10617.

Sahay A, Hen R. 2007. Adult hippocampal neurogenesis in depression. Nature neuroscience 10:1110–1115.

Sahay A, Scobie KN, Hill AS, O'Carroll CM, Kheirbek MA, Burghardt NS, Fenton AA, Dranovsky A, Hen R. 2011. Increasing adult hippocampal neurogenesis is sufficient to improve pattern separation. Nature 472:466–470.

Sahin E, Depinho RA. 2010. Linking functional decline of telomeres, mitochondria and stem cells during ageing. Nature 464:520–528.

Sausbier M, Hu H, Arntz C, Feil S, Kamm S, Adelsberger H, Sausbier U, Sailer CA, Feil R, Hofmann F, Korth M, Shipston MJ, Knaus H, Wolfer DP, Pedroarena CM, Storm JF, Ruth P. 2004. Cerebellar ataxia and Purkinje cell dysfunction caused by Ca2+-activated K+ channel deficiency. Proceedings of the National Academy of Sciences of the United States of America 101:9474–9478.

Saxe MD, Battaglia F, Wang J, Malleret G, David DJ, Monckton JE, Garcia ADR, Sofroniew MV, Kandel ER, Santarelli L, Hen R, Drew MR. 2006. Ablation of hippocampal neurogenesis impairs contextual fear conditioning and synaptic plasticity in the dentate gyrus. Proceedings of the National Academy of Sciences of the United States of America 103:17501–17506.

Scarpulla RC. 2008. Transcriptional paradigms in mammalian mitochondrial biogenesis and function. Physiological reviews 88:611–638.

Scemes E, Giaume C. 2006. Astrocyte calcium waves: what they are and what they do. Glia 54:716–725.

Schmidt-Hieber C, Jonas P, Bischofberger J. 2004. Enhanced synaptic plasticity in newly generated granule cells of the adult hippocampus. Nature 429:184–187.

Schon EA, Bonilla E, DiMauro S. 1997. Mitochondrial DNA mutations and pathogenesis. Journal of bioenergetics and biomembranes 29:131–149.

Schon EA, Przedborski S. 2011. Mitochondria: the next (neurode)generation. Neuron 70:1033–1053.

Schouten M, Buijink MR, Lucassen PJ, Fitzsimons CP. 2012. New Neurons in Aging Brains: Molecular Control by Small Non-Coding RNAs. Frontiers in neuroscience 6:25.

Schwarz TJ, Ebert B, Lie DC. 2012. Stem cell maintenance in the adult mammalian hippocampus: A matter of signal integration? Developmental Neurobiology 72:1006–1015.

Seifert G, Schilling K, Steinhäuser C. 2006. Astrocyte dysfunction in neurological disorders: a molecular perspective. Nature reviews. Neuroscience 7:194–206.

Seo AY, Joseph A, Dutta D, Hwang JCY, Aris JP, Leeuwenburgh C. 2010. New insights into the role of mitochondria in aging: mitochondrial dynamics and more. Journal of Cell Science 123:2533–2542.

Seri B, García-Verdugo JM, McEwen BS, Alvarez-Buylla A. 2001. Astrocytes give rise to new neurons in the adult mammalian hippocampus. The Journal of neuroscience 21:7153–7160.

Sherratt HS. 1991. Mitochondria: structure and function. Revue neurologique 147:417–430.

Shibata N, Kobayashi M. 2008. [The role for oxidative stress in neurodegenerative diseases]. Brain and nerve 60:157–170.

Shibata T, Yamada K, Watanabe M, Ikenaka K, Wada K, Tanaka K, Inoue Y. 1997. Glutamate transporter GLAST is expressed in the radial glia-astrocyte lineage of developing mouse spinal cord. The Journal of neuroscience 17:9212–9219.

Shihabuddin LS, Horner PJ, Ray J, Gage FH. 2000. Adult spinal cord stem cells generate neurons after transplantation in the adult dentate gyrus. The Journal of neuroscience 20:8727–8735.

Shimada IS, LeComte MD, Granger JC, Quinlan NJ, Spees JL. 2012. Self-renewal and differentiation of reactive astrocyte-derived neural stem/progenitor cells isolated from the cortical peri-infarct area after stroke. The Journal of neuroscience 32:7926–7940.

Shin J, Fang Z, Yu Z, Wang C, Li S, Li X. 2005. Expression of mutant huntingtin in glial cells contributes to neuronal excitotoxicity. The Journal of Cell Biology 171:1001–1012.

Shi P, Wei Y, Zhang J, Gal J, Zhu H. 2010. Mitochondrial dysfunction is a converging point of multiple pathological pathways in amyotrophic lateral sclerosis. Journal of Alzheimer's disease 20 Suppl 2:S311-24.

Shi Y, Dierckx A, Wanrooij PH, Wanrooij S, Larsson N, Wilhelmsson LM, Falkenberg M, Gustafsson CM. 2012. Mammalian transcription factor A is a core component of the mitochondrial transcription machinery. Proceedings of the National Academy of Sciences of the United States of America.

Shors TJ, Miesegaes G, Beylin A, Zhao M, Rydel T, Gould E. 2001. Neurogenesis in the adult is involved in the formation of trace memories. Nature 410:372–376.

Siciliano G, Mancuso M, Pasquali L, Manca ML, Tessa A, Iudice A. 2000. Abnormal levels of human mitochondrial transcription factor A in skeletal muscle in mitochondrial encephalomyopathies. Neurological sciences 21:S985-7.

Silva JP, Köhler M, Graff C, Oldfors A, Magnuson MA, Berggren PO, Larsson NG. 2000. Impaired insulin secretion and beta-cell loss in tissue-specific knockout mice with mitochondrial diabetes. Nature genetics 26:336–340.

Slemmer JE, Shacka JJ, Sweeney MI, Weber JT. 2008. Antioxidants and free radical scavengers for the treatment of stroke, traumatic brain injury and aging. Current medicinal chemistry 15:404–414.

Snyder JS, Kee N, Wojtowicz JM. 2001. Effects of adult neurogenesis on synaptic plasticity in the rat dentate gyrus. Journal of neurophysiology 85:2423–2431.

Sofroniew MV. 2005. Reactive astrocytes in neural repair and protection. The Neuroscientist 11:400–407.

Sofroniew MV. 2009. Molecular dissection of reactive astrogliosis and glial scar formation. Trends in neurosciences 32:638–647.

Sofroniew MV, Vinters HV. 2010. Astrocytes: biology and pathology. Acta neuropathologica 119:7–35.

Solá S, Morgado AL, Rodrigues CMP. 2013. Death receptors and mitochondria: Two prime triggers of neural apoptosis and differentiation. Biochimica et Biophysica Acta (BBA) 1830:2160–2166.

Sologub M, Litonin D, Anikin M, Mustaev A, Temiakov D. 2009. TFB2 is a transient component of the catalytic site of the human mitochondrial RNA polymerase. Cell 139:934–944.

Song H, Kempermann G, Overstreet Wadiche L, Zhao C, Schinder AF, Bischofberger J. 2005. New neurons in the adult mammalian brain: synaptogenesis and functional integration. The Journal of neuroscience 25:10366–10368.

Song H, Stevens CF, Gage FH. 2002. Astroglia induce neurogenesis from adult neural stem cells. Nature 417:39–44.

Sörensen L, Ekstrand M, Silva JP, Lindqvist E, Xu B, Rustin P, Olson L, Larsson NG. 2001. Late-onset corticohippocampal neurodepletion attributable to catastrophic failure of oxidative phosphorylation in MILON mice. The Journal of neuroscience 21:8082–8090.

Soriano P. 1999. Generalized lacZ expression with the ROSA26 Cre reporter strain. Nature genetics 21:70–71.

Spelbrink JN, Li FY, Tiranti V, Nikali K, Yuan QP, Tariq M, Wanrooij S, Garrido N, Comi G, Morandi L, Santoro L, Toscano A, Fabrizi GM, Somer H, Croxen R, Beeson D, Poulton J, Suomalainen A, Jacobs HT, Zeviani M, Larsson C. 2001. Human mitochondrial DNA deletions associated with mutations in the gene encoding Twinkle, a phage T7 gene 4-like protein localized in mitochondria. Nature genetics 28:223–231.

Spikings EC, Alderson J, St John JC. 2007. Regulated mitochondrial DNA replication during oocyte maturation is essential for successful porcine embryonic development. Biology of reproduction 76:327–335.

St John JC, Ramalho-Santos J, Gray HL, Petrosko P, Rawe VY, Navara CS, Simerly CR, Schatten GP. 2005. The expression of mitochondrial DNA transcription factors during early cardiomyocyte in vitro differentiation from human embryonic stem cells. Cloning Stem Cells 7:141–153.

Steiner B, Klempin F, Wang L, Kott M, Kettenmann H, Kempermann G. 2006. Type-2 cells as link between glial and neuronal lineage in adult hippocampal neurogenesis. Glia 54:805–814.

Steiner JL, Murphy EA, McClellan JL, Carmichael MD, Davis JM. 2011. Exercise training increases mitochondrial biogenesis in the brain. Journal of applied physiology 111:1066–1071.

Sterlemann V, Rammes G, Wolf M, Liebl C, Ganea K, Müller MB, Schmidt MV. 2010. Chronic social stress during adolescence induces cognitive impairment in aged mice. Hippocampus 20:540–549.

Stojkovic M, Machado SA, Stojkovic P, Zakhartchenko V, Hutzler P, Gonçalves PB, Wolf E. 2001. Mitochondrial distribution and adenosine triphosphate content of bovine oocytes before and after in vitro maturation: correlation with morphological criteria and developmental capacity after in vitro fertilization and culture. Biology of reproduction 64:904–909.

Strooper B de, Voet T. 2012. Alzheimer's disease: A protective mutation. Nature 488:38–39.

Suh H, Consiglio A, Ray J, Sawai T, D'Amour KA, Gage FH. 2007. In vivo fate analysis reveals the multipotent and self-renewal capacities of Sox2+ neural stem cells in the adult hippocampus. Cell Stem Cell 1:515–528.

Suhonen JO, Peterson DA, Ray J, Gage FH. 1996. Differentiation of adult hippocampus-derived progenitors into olfactory neurons in vivo. Nature 383:624–627.

Surmeier DJ, Guzman JN, Sanchez-Padilla J, Goldberg JA. 2010. What causes the death of dopaminergic neurons in Parkinson's disease? Progress in brain research 183:59–77.

Swanson RA, Ying W, Kauppinen TM. 2004. Astrocyte influences on ischemic neuronal death. Current molecular medicine 4:193–205.

Swerdlow RH. 2011. Brain aging, Alzheimer's disease, and mitochondria. Biochimica et Biophysica Acta (BBA) 1812:1630–1639.

Tashiro A, Zhao C, Gage FH. 2006. Retrovirus-mediated single-cell gene knockout technique in adult newborn neurons in vivo. Nature Protocols 1:3049–3055.

Tatsuta T, Langer T. 2008. Quality control of mitochondria: protection against neurodegeneration and ageing. The EMBO Journal 27:306–314.

Taylor RW, Barron MJ, Borthwick GM, Gospel A, Chinnery PF, Samuels DC, Taylor GA, Plusa SM, Needham SJ, Greaves LC, Kirkwood TBL, Turnbull DM. 2003. Mitochondrial DNA mutations in human colonic crypt stem cells. The Journal of clinical investigation 112:1351–1360.

Terkawi AS, Wani TM, Al-Shuaibi KM, Tobias JD. 2012. Anesthetic considerations in Leigh disease: Case report and literature review. Saudi journal of anaesthesia 6:181–185.

Todorović C, Dimitrijević M, Stanojević S, Kovacević-Jovanović V, Miletić T, Laban O, Radulović J. 2003. Correlation between age-related changes in open field behavior and plaque forming cell response in DA female rats. The International journal of neuroscience 113:1259–1273.

Toni N, Laplagne DA, Zhao C, Lombardi G, Ribak CE, Gage FH, Schinder AF. 2008. Neurons born in the adult dentate gyrus form functional synapses with target cells. Nature neuroscience 11:901–907.

Toni N, Teng EM, Bushong EA, Aimone JB, Zhao C, Consiglio A, van Praag H, Martone ME, Ellisman MH, Gage FH. 2007. Synapse formation on neurons born in the adult hippocampus. Nature neuroscience 10:727–734.

Tozuka Y, Fukuda S, Namba T, Seki T, Hisatsune T. 2005. GABAergic excitation promotes neuronal differentiation in adult hippocampal progenitor cells. Neuron 47:803–815.

Treves A, Tashiro A, Witter MP, Moser EI. 2008. What is the mammalian dentate gyrus good for? Neuroscience 154:1155–1172.

Trifunovic A, Hansson A, Wredenberg A, Rovio AT, Dufour E, Khvorostov I, Spelbrink JN, Wibom R, Jacobs HT, Larsson N. 2005. Somatic mtDNA mutations cause aging phenotypes without affecting reactive oxygen species production. Proceedings of the National Academy of Sciences of the United States of America 102:17993–17998.

Trifunovic A, Larsson N. 2002. Tissue-specific knockout model for study of mitochondrial DNA mutation disorders. Methods in enzymology 353:409–421.

Trifunovic A, Larsson N. 2008. Mitochondrial dysfunction as a cause of ageing. Journal of internal medicine 263:167–178.

Trifunovic A, Wredenberg A, Falkenberg M, Spelbrink JN, Rovio AT, Bruder CE, Bohlooly-Y M, Gidlöf S, Oldfors A, Wibom R, Törnell J, Jacobs HT, Larsson N. 2004. Premature ageing in mice expressing defective mitochondrial DNA polymerase. Nature 429:417–423.

Troulinaki K, Bano D. 2012. Mitochondrial deficiency: a double-edged sword for aging and neurodegeneration. Frontiers in genetics 3:244.

Tsai H, Li H, Fuentealba LC, Molofsky AV, Taveira-Marques R, Zhuang H, Tenney A, Murnen AT, Fancy SPJ, Merkle F, Kessaris N, Alvarez-Buylla A, Richardson WD, Rowitch DH. 2012. Regional astrocyte allocation regulates CNS synaptogenesis and repair. Science 337:358–362.

Tümpel S, Rudolph KL. 2012. The role of telomere shortening in somatic stem cells and tissue aging: lessons from telomerase model systems. Annals of the New York Academy of Sciences 1266:28–39.

Turner DA, Adamson DC. 2011. Neuronal-astrocyte metabolic interactions: understanding the transition into abnormal astrocytoma metabolism. Journal of neuropathology and experimental neurology 70:167–176.

Uitti RJ, Baba Y, Wszolek ZK, Putzke DJ. 2005. Defining the Parkinson's disease phenotype: initial symptoms and baseline characteristics in a clinical cohort. Parkinsonism & Related Disorders 11:139–145.

van Praag H. 2005. Exercise Enhances Learning and Hippocampal Neurogenesis in Aged Mice. Journal of Neuroscience 25:8680–8685.

van Praag H, Christie BR, Sejnowski TJ, Gage FH. 1999. Running enhances neurogenesis, learning, and long-term potentiation in mice. Proceedings of the National Academy of Sciences of the United States of America 96:13427–13431.

van Praag H, Schinder AF, Christie BR, Toni N, Palmer TD, Gage FH. 2002. Functional neurogenesis in the adult hippocampus. Nature 415:1030–1034.

Viña J, Gomez-Cabrera MC, Borras C, Froio T, Sanchis-Gomar F, Martinez-Bello VE, Pallardo FV. 2009. Mitochondrial biogenesis in exercise and in ageing. Advanced drug delivery reviews 61:1369–1374.

Vinet J, van Weering HRJ, Heinrich A, Kälin RE, Wegner A, Brouwer N, Heppner FL, van Rooijen N, Boddeke HWGM, Biber K. 2012. Neuroprotective function for ramified microglia in hippocampal excitotoxicity. Journal of neuroinflammation 9:27.

Vives V, Alonso G, Solal AC, Joubert D, Legraverend C. 2003. Visualization of S100B-positive neurons and glia in the central nervous system of EGFP transgenic mice. The Journal of comparative neurology 457:404–419.

Voskuhl RR, Peterson RS, Song B, Ao Y, Morales LBJ, Tiwari-Woodruff S, Sofroniew MV. 2009. Reactive astrocytes form scar-like perivascular barriers to leukocytes during adaptive immune inflammation of the CNS. The Journal of neuroscience 29:11511–11522.

Wallace DC. 2005. A mitochondrial paradigm of metabolic and degenerative diseases, aging, and cancer: a dawn for evolutionary medicine. Annual review of genetics 39:359–407.

Wallace DC, Singh G, Lott MT, Hodge JA, Schurr TG, Lezza AM, Elsas LJ, Nikoskelainen EK. 1988. Mitochondrial DNA mutation associated with Leber's hereditary optic neuropathy. Science 242:1427–1430.

Walton NM, Shin R, Tajinda K, Heusner CL, Kogan JH, Miyake S, Chen Q, Tamura K, Matsumoto M. 2012. Adult neurogenesis transiently generates oxidative stress. PLoS ONE 7:e35264.

Wang J, Silva JP, Gustafsson CM, Rustin P, Larsson N. 2001. Increased in vivo apoptosis in cells lacking mitochondrial DNA gene expression. Proceedings of the National Academy of Sciences 98:4038–4043.

Wang J, Wilhelmsson H, Graff C, Li H, Oldfors A, Rustin P, Brüning JC, Kahn CR, Clayton DA, Barsh GS, Thorén P, Larsson NG. 1999. Dilated cardiomyopathy and atrioventricular conduction blocks induced by heart-specific inactivation of mitochondrial DNA gene expression. Nature genetics 21:133–137.

Wang W, Esbensen Y, Kunke D, Suganthan R, Rachek L, Bjørås M, Eide L. 2011a. Mitochondrial DNA damage level determines neural stem cell differentiation fate. The Journal of neuroscience 31:9746–9751.

Wang X, Schwarz TL. 2009. Imaging axonal transport of mitochondria. Methods in enzymology 457:319–333.

Wang X, Winter D, Ashrafi G, Schlehe J, Wong YL, Selkoe D, Rice S, Steen J, LaVoie MJ, Schwarz TL. 2011b. PINK1 and Parkin target Miro for phosphorylation and degradation to arrest mitochondrial motility. Cell 147:893–906.

Weiner MW, Veitch DP, Aisen PS, Beckett LA, Cairns NJ, Green RC, Harvey D, Jack CR, Jagust W, Liu E, Morris JC, Petersen RC, Saykin AJ, Schmidt ME, Shaw L, Siuciak JA, Soares H, Toga AW, Trojanowski JQ. 2012. The Alzheimer's Disease Neuroimaging Initiative: a review of papers published since its inception. Alzheimer's & dementia 8:S1-68.

Werth JL, Thayer SA. 1994. Mitochondria buffer physiological calcium loads in cultured rat dorsal root ganglion neurons. The Journal of neuroscience 14:348–356.

Wilding M, Dale B, Marino M, Di Matteo L, Alviggi C, Pisaturo ML, Lombardi L, Placido G de. 2001. Mitochondrial aggregation patterns and activity in human oocytes and preimplantation embryos. Human reproduction 16:909–917.

Wilhelmsson U, Bushong EA, Price DL, Smarr BL, van Phung, Terada M, Ellisman MH, Pekny M. 2006. Redefining the concept of reactive astrocytes as cells that remain within their unique domains upon reaction to injury. Proceedings of the National Academy of Sciences of the United States of America 103:17513–17518.

Wilhelmsson U, Faiz M, Pablo Y de, Sjöqvist M, Andersson D, Widestrand A, Potokar M, Stenovec M, Smith PLP, Shinjyo N, Pekny T, Zorec R, Ståhlberg A, Pekna M, Sahlgren C, Pekny M. 2012. Astrocytes negatively regulate neurogenesis through the Jagged1-mediated notch pathway. Stem Cells 30:2320–2329.

Winpenny E, Lebel-Potter M, Fernandez ME, Brill MS, Götz M, Guillemot F, Raineteau O. 2011. Sequential generation of olfactory bulb glutamatergic neurons by Neurog2-expressing precursor cells. Neural development 6:12.

Winter N, Kovermann P, Fahlke C. 2012. A point mutation associated with episodic ataxia 6 increases glutamate transporter anion currents. Brain 135:3416–3425.

Wredenberg A, Wibom R, Wilhelmsson H, Graff C, Wiener HH, Burden SJ, Oldfors A, Westerblad H, Larsson N. 2002. Increased mitochondrial mass in mitochondrial myopathy mice. Proceedings of the National Academy of Sciences of the United States of America 99:15066–15071.

Xie L, Zhu X, Hu Y, Li T, Gao Y, Shi Y, Tang S. 2008. Mitochondrial DNA oxidative damage triggering mitochondrial dysfunction and apoptosis in high glucose-induced HRECs. Investigative ophthalmology & visual science 49:4203–4209.

Xu S, Zhong M, Zhang L, Wang Y, Zhou Z, Hao Y, Zhang W, Yang X, Wei A, Pei L, Yu Z. 2009. Overexpression of Tfam protects mitochondria against beta-amyloid-induced oxidative damage in SH-SY5Y cells. The FEBS journal 276:3800–3809.

Yakes FM, van Houten B. 1997. Mitochondrial DNA damage is more extensive and persists longer than nuclear DNA damage in human cells following oxidative stress. Proceedings of the National Academy of Sciences of the United States of America 94:514–519.

Yeh T, Lee DY, Gianino SM, Gutmann DH. 2009. Microarray analyses reveal regional astrocyte heterogeneity with implications for neurofibromatosis type 1 (NF1)-regulated glial proliferation. Glia 57:1239–1249.

Yen M, Wang A, Wei Y. 2006. Leber's hereditary optic neuropathy: a multifactorial disease. Progress in retinal and eye research 25:381–396.

Yin W, Signore AP, Iwai M, Cao G, Gao Y, Chen J. 2008. Rapidly increased neuronal mitochondrial biogenesis after hypoxic-ischemic brain injury. Stroke 39:3057–3063.

Youle RJ, Karbowski M. 2005. Mitochondrial fission in apoptosis. Nature reviews. Molecular cell biology 6:657–663.

Youle RJ, van der Bliek AM. 2012. Mitochondrial fission, fusion, and stress. Science 337:1062–1065.

Young JW, Wallace CK, Geyer MA, Risbrough VB. 2010. Age-associated improvements in cross-modal prepulse inhibition in mice. Behavioral neuroscience 124:133–140.

Yuste R, Bonhoeffer T. 2004. Genesis of dendritic spines: insights from ultrastructural and imaging studies. Nature reviews. Neuroscience 5:24–34.

Zeviani M, Moraes CT, DiMauro S, Nakase H, Bonilla E, Schon EA, Rowland LP. 1998. Deletions of mitochondrial DNA in Kearns-Sayre syndrome. 1988. Neurology 51:1525 and 8 pages following.

Zhang C, Zou Y, He W, Gage FH, Evans RM. 2008. A role for adult TLX-positive neural stem cells in learning and behaviour. Nature 451:1004–1007.

Zhao C, Deng W, Gage FH. 2008. Mechanisms and functional implications of adult neurogenesis. Cell 132:645–660.

Zhao C, Teng EM, Summers RG, JR, Ming GL, Gage FH. 2006. Distinct Morphological Stages of Dentate Granule Neuron Maturation in the Adult Mouse Hippocampus. Journal of Neuroscience 26:3–11.

9 APPENDIX

Acknowledgements

Erklärung

Ich erkläre an Eides statt, dass ich die der Fakultät Wissenschaftszentrum Weihenstephan für Ernährung, Landnutzung und Umwelt der Technischen Universität München zur Promotionsprüfung vorgelegte Arbeit mit dem Titel:

The effect of mitochondrial dysfunction on astrocytes and radial glia like stem cells in the adult hippocampus

am Lehrstuhl für Genetik unter der Anleitung und Betreuung durch

Univ.-Prof. Dr. W. Wurst

ohne sonstige Hilfe erstellt und bei der Abfassung nur die gemäß § 6 Abs. 5 angegebenen Hilfsmittel benutzt habe.

Ich habe die Dissertation in dieser oder ähnlicher Form in keinem anderen Prüfungsverfahren als Prüfungsleistung vorgelegt.

Ich habe den angestrebten Doktorgrad **noch nicht** erworben und bin **nicht** in einem früheren Promotionsverfahren für den angestrebten Doktorgrad endgültig gescheitert.

Die Promotionsordnung der Technischen Universität München ist mir bekannt.

München den,……………   ……………………………

Curriculum vitae

Name	Birgit Ebert
Geburtsdatum	15.05.1983
Geburtsort	Berlin-Buch
Nationalität	deutsch

Doktorarbeit

10/2008 01/2013 Promotion am Helmholtz Zentrum München
Institut für Entwicklungsgenetik
Univ.-Prof. Dr. W. Wurst
Arbeitsgruppe „Adulte Neurale Stammzellen und Neurogenese"
Thema der Dissertation: *The effect of mitochondrial dysfunction on astrocytes and radial glia like stem cells in the adult hippocampus*

Studium

10/2003 – 07/2008 Studium der Biologie an der Universität Leipzig
Diplomarbeit über: Herstellung von HIV-Immunotypen
(Univ.-Prof. Dr. Christian Jassoy)
Abschluss mit Diplom im Juli 2008

Auslandsjahr

09/2002 – 06/2003 Cast Member im Bereich Handel im Disneyland Paris

Schule

08/1995 – 06/2002 Paulus-Praetorius-Gymnasium, Bernau bei Berlin
09/1992 – 07/1995 Grundschule Marienwerder
09/1989 – 07/1992 Grundschule Berlin-Buch

Publikationen

Schwarz TJ, **Ebert B,** and Lie DC (2012) Stem cell maintenance in the adult mammalian hippocampus: a matter of signal integration? Devel Neurobio 72 (7), 1006-1015.

Manuskripte in Vorbereitung

Ebert B, Steib K, Jagasia R, Götz M, Larsson N, and Lie DC (2013) Impact of mitochondrial dysfunction on stem cell activity and neurogenesis in the adult hippocampus (*in preparation*)

Ebert B, Jagasia R, Götz M, Larsson N, Redecker C, and Lie DC (2013) Mitochondrial dysfunction in astrocytes causes ageing-associated phenotypes (*in preparation*)

Steib K, **Ebert B**, Jagasia R, Lie DC (2013) Mitochondria modify development of stem cell-derived neurons in the adult mammalian hippocampus (*in preparation*)